TARGETING VULNERABILITIES THROUGH INHIBITING THE VALOSIN-CONTAINING PROTEIN (VCP/p97) IN OVARIAN CANCER

By

Prabhakar Bastola

B.S., Truman State University, 2011

Submitted to the graduate degree program in Pharmacology and the Graduate Faculty of the University of Kansas Medical Center in partial fulfillment of the requirement for the degree of Doctor of Philosophy.

Co-Chairperson: Wen-Xing Ding, Ph.D.

Co-Chairperson: Jeremy Chien, Ph.D.

Bruno Hagenbuch, Ph.D.

Tiangang Li, Ph.D.

Joseph D. Fontes, Ph.D.

Date Defended: 04-27-2018

The dissertation committee for Prabhakar Bastola certifies that this is the approved version of the following dissertation:

TARGETING VULNERABILITIES THROUGH INHIBITING THE VALOSIN-CONTAINING PROTEIN (VCP/p97) IN OVARIAN CANCER

Co-Chairperson: Wen-Xing Ding, Ph.D.

Co-Chairperson: Jeremy Chien, Ph.D.

Date Approved: 04-28-2018

Abstract

Ovarian cancer is the fifth leading cause of cancer-related death among women and the deadliest of all gynecological cancers. Treatment failure is a major contributing factor in ovarian cancer-related mortality. Advances in the development of new agents that target critical pathways in cancer may provide better options to overcome treatment failure. One of the molecular mechanisms that can be targeted for ovarian cancer therapy is the protein quality control. Components of the protein quality control, such as heat shock proteins, the ubiquitin-proteasome system, the unfolded protein response and autophagy, regulate protein homeostasis. Protein quality control also provides phenotypic stability by buffering cryptic genetic variations that could potentially reduce the fitness of cancer cells. This concept was best illustrated by studies that genetically or pharmacologically inhibited heat-shock protein 90, and reported variations in the phenotype following the disruption of heat shock protein 90.

This dissertation investigates the therapeutic efficacy of targeting valosin-containing protein (VCP), an important component of the protein quality control, in ovarian cancer.

VCP or p97, a member of the ATPase Associated with diverse cellular Activities-ATPase (AAA-ATPase) protein family, has been associated with various cellular functions including endoplasmic reticulum associated degradation, the ubiquitin proteasome system, golgi membrane reassembly, autophagy, DNA repair and cell division making it an important regulator of the protein quality control. Recent studies identified VCP and the ubiquitin proteasome system as synthetic lethal targets in ovarian cancer. This dissertation describes the preclinical activity of VCP inhibitors in ovarian cancer. Results presented in this dissertation show that quinazoline-based VCP inhibitors initiate Gap 1 (G1) cell cycle arrest, attenuate cap-dependent protein translation and induce programmed cell death via the intrinsic and the extrinsic modes of apoptosis.

Mechanistic studies point to the unresolved unfolded protein response as a mechanism by which VCP inhibitors contribute to cytotoxicity. These results support an emerging concept that the unfolded protein response pathway may be targeted in ovarian cancer as a source of vulnerability. Since prolonged induction of the unfolded protein response results in CCAAT/enhancer binding protein homologous protein (CHOP) mediated cell death, we tested the hypothesis that VCP inhibitors act synergistically with compounds that enhance CHOP expression. Here, we show that VCP inhibitors act synergistically with salubrinal, an inhibitor of growth arrest and DNA-damage-inducible 34 (GADD34), by enhancing CHOP expression in ovarian cancer cell lines. Our results provide a proof-of-concept that VCP inhibitors can be used as a single agent and can be synergized with compounds that enhance CHOP expression to induce cell death.

While the synergistic effects observed between VCP inhibitors and GADD34 inhibitor provides an *in vitro* proof-of-concept, these results have little clinical relevance because salubrinal is not a clinical candidate. Therefore, we identified mifepristone, an FDA approved steroidal progesterone antagonist, to act synergistic with VCP inhibitors across several ovarian cancer cell lines. Combination treatment between clinically achievable doses of mifepristone and oral VCP inhibitor- CB-5083 show an atypical increase in the unfolded protein response, a significant decrease in colony formation as well as an increase in caspase activity. Mechanistic studies upon mifepristone treatment point towards the inhibition of activating transcription factor 6 (ATF6) branch and the activation of heme- regulated inhibitor (HRI) kinase pathway as two plausible mechanisms contributing towards the synergistic effect.

Oral VCP inhibitor- CB-5083 is currently in Phase I clinical trials because it shows therapeutic effects in multiple tumor xenograft models; however, the mechanism of resistance to CB-5083 is unknown. Here, we characterize the molecular mechanism of resistance to CB-5083.

Using incremental exposure to CB-5083, we established CB-5083- resistant ovarian cancer cells that show 5 to 6-fold resistance *in vitro* compared to parental cells. Genomic and complementary DNA sequencing of the *VCP* coding region revealed a pattern of co-selected mutations: (1) missense mutations at codon 470 in one copy resulting in increased ATPase activity; and (2) nonsense or frameshift mutations at codon 606 or codon 616 in another copy causing the loss of allele-specific expression. Unbiased molecular docking studies show codon 470 as a putative binding site for CB-5083. Furthermore, the analysis of somatic mutations in cancer genomes from the cancer genome atlas (TCGA) indicate that codon 616 is frequently mutated in human cancers. Thus, identification of these mutations associated with *in vitro* resistance to VCP inhibitors may be useful as potential theranostic markers while screening for patients to enroll in clinical trials. VCP has emerged as a viable therapeutic target for several cancer types, and therefore targeting such hyperactive VCP mutants should aid in improving the therapeutic outcome in cancer patients.

Overall, this dissertation 1) provides a proof-of-concept that VCP can be targeted in ovarian cancer, 2) proves that VCP inhibitors can act synergistically with other compounds that modulate the protein quality control, 3) identified a clinically relevant drug combination (CB-5083 and mifepristone) that should be investigated further, 4) unearths a novel mechanism of resistance towards the oral VCP inhibitor, CB-5083, in ovarian cancer cells.

Acknowledgements

I would like to take this opportunity to express my heartfelt gratitude to my mentor Dr. Jeremy Chien for allowing me to work on such an exciting project. I deeply appreciate all your support and cannot thank you enough for your contributions towards this dissertation. I am very grateful for your time and efforts that you took to discuss projects from its inception to completion. Your mentorship has allowed me to be an independent thinker and has helped me understand how to approach scientific problems.

I am thankful to all the past and present members of my dissertation committee, Dr. Roy Jensen, Dr. Wen-Xing Ding, Dr. Bruno Hagenbuch, Dr. Tiangang Li and Dr. Joseph D Fontes for their time, excellent suggestions and overall support to this dissertation.

I would like to thank the Pharmacology graduate committee and administrative staffs for always keeping me in track and monitoring my progress during graduate school. Similarly, I would like to thank the IGPBS program and the Cancer Biology department for all the support.

I would like to thank Derek Oien, Cristabelle Desouza, Pingping Fang, Kay Minn and all past members in the Chien laboratory for keeping an excellent work environment in the lab. I duly enjoyed each and every Happy Hour that I was able to attend. Also, each of you have made numerous contributions to this dissertation through your suggestions in lab meetings. Special thanks to Megan Cooley and Kay Minn for showing me essential lab techniques when I first joined the Chien Lab.

I would like to thank my mom Mrs. Madhu Maya Bastola for all her love and unflinching support. Words cannot describe all that you have done for me. Also, I would like to thank my sister

Prabha Bastola and brother-in-law Prabhat Bhandari for their encouragement and support. Special thanks to my relatives- Babina and Shiva in Virginia for being my family away from home.

I would like to thank all my friends and excellent teachers from New Light English Boarding School (Lekhnath, Nepal), SOS Hermann Gmeiner School (Pokhara, Nepal), Truman State University (Kirksville, Missouri) and University of Kansas Medical Center. Special thanks to friends, Keshav, Sarjan, Binaya, Ravin, Ujwal, Sudeep, Manisha, Vijay, Rijosh, Gaurav, Bhupendra, Request, Sansar, Chuanwu, Pramod, Lokendra, Zainab, Younshim and Stephen for being awesome individuals.

I would like to thank KU Endowment, KUCC Pilot Award and Department of Defense # W81XW-17-1-0078 for providing necessary funding for this research.

Table of contents

Chapter 1: Introduction and background

Chapter 2: Materials and methods

List of figures

List of tables

List of abbreviations

%	=	Percent
^{0}C	=	Degree Celsius
μM	=	Micromolar
μl	=	Microliter
Å	=	Angstrom (10^{-10} meter)
aa	=	Amino acid
AAA-ATPase	=	ATPase Associated with diverse cellular Activities- Adenosine Triphosphatase
ATF3	=	Activating Transcription Factor 3
ATF4	=	Activating Transcription Factor 4
ATF6	=	Activating Transcription Factor 6
ATF6α	=	Activating Transcription Factor 6 alpha
ATP	=	Adenosine Triphosphate
β-Actin	=	Beta-Actin
BCA Assay	=	Bicinchoninic Acid Assay
Bcl2	=	B-cell Lymphoma 2
Bcr-Abl	=	Breakpoint Cluster Region- Abelson fusion gene
BiP	=	Binding immunoglobulin Protein
BRCA1	=	Breast Cancer 1, Early Onset
BRCA2	=	Breast Cancer 2, Early Onset

CA-125	=	Cancer Antigen 125
CB	=	CB-5083
CCNE1	=	Cyclin E1
cDNA	=	Complementary Deoxyribonucleic Acid
CETSA	=	Cellular Thermal Shift Assay
CHOP	=	CCAAT/enhancer binding protein Homologous Protein
CI	=	Combination Index
CNA	=	Copy Number Alteration
CO_2	=	Carbon Dioxide
CRISPR	=	Clustered Regular Interspaced Short Palindromic Repeats
DBeQ	=	N^2,N^4-Dibenzyl quinazoline-2,4-diamine
DDIT3	=	DNA Damage-Inducible Transcript 3
DMEM	=	Dulbecco's Modified Eagle Medium
DMSO	=	Dimethyl Sulfoxide
DNA	=	Deoxyribonucleic Acid
DR5	=	Death Receptor 5
EDTA	=	Ethylenediaminetetraacetic acid
eIF2α	=	eukaryotic Initiation Factor 2 alpha
EIF3B	=	Eukaryotic translation Initiation Factor 3 Subunit B
EIF3CL	=	Eukaryotic translation Initiation Factor 3 subunit C-like protein

ER	=	Endoplasmic Reticulum
ERAD	=	Endoplasmic Reticulum Associated Degradation
ERSE	=	Endoplasmic Reticulum Stress response Element
ER stress	=	Endoplasmic Reticulum stress
FDA	=	Food and Drug Administration
FDR	=	False Discovery Rate
FIGO	=	International Federation of Gynecology and Obstetrics
FLT3	=	Fms-Like Tyrosine kinase 3
FOXM1	=	Forkhead box protein M1
fs*	=	Frameshift Deletion
GADD34	=	Growth Arrest and DNA-Damage-inducible 34
GCN2	=	General Control Nonderepressible 2
GI_{50}	=	Half maximal Growth
GM	=	Geldanamycin
Grp78	=	Glucose-Regulated Protein 78
H_20	=	Dihydrogen Monoxide (Water)
HDAC	=	Histone Deacetylase
HDAC6	=	Histone Deacetylase 6
HGSOC	=	High-Grade Serous Ovarian Cancer
HR	=	Homologous Recombination

HRI	=	Heme-Regulated Inhibitor
HRP	=	Horseradish Peroxidase
HSPs	=	Heat Shock Proteins
Hsp90	=	Heat-shock protein 90
HTS	=	High Throughput Screening
IC_{50}	=	half maximal Inhibitory Concentration
IER3IP1_1	=	Immediate-Early Response 3-Interacting Protein 1_1
IKKB	=	Inhibitor of nuclear factor Kappa B Kinase subunit beta
IRE1α	=	Inositol- Requiring Enzyme 1 alpha
JAK2	=	Janus Kinase 2
KDa	=	KiloDalton
MAPK	=	Mitogen-Activated Protein kinase
ml	=	Milliliter
mM	=	Millimolar
MMLV	=	Moloney Murine Leukemia Virus
mRNA	=	Messenger Ribonucleic Acid
mTOR	=	mechanistic Target of Rapamycin
mTORC1	=	mechanistic Target of Rapamycin Complex 1
mTORC2	=	mechanistic Target of Rapamycin Complex 2
MSS	=	Multimodal Screening

NADH	=	Nicotinamide Adenine Dinucleotide-Hydrogen
NFkB	=	Nuclear Factor Kappa B
NOD	=	Non-Obese Diabetic
OS	=	Overall Survival
PARP	=	Poly-ADP-Ribose Polymerase
PBS	=	Phosphate-Buffered Saline
PCR	=	Polymerase Chain Reaction
PERK	=	Protein kinase R-like Endoplasmic Reticulum Kinase
PFS	=	Progression-Free Survival
PI3K	=	Phosphoinositide 3-Kinase
PKR	=	Protein Kinase R
PLCO	=	Prostate, Lung, Colorectal and Ovarian
PQC	=	Protein Quality Control
PSMA1	=	Proteasome Subunit Alpha 1
PSMD1	=	Proteasome 26S Subunit, Non-ATPase 1
PVDF	=	Polyvinylidene Difluoride
RB	=	Retinoblastoma gene
RIDD	=	Regulated IRE1-Dependent Decay
RNA	=	Ribonucleic Acid
RNase	=	Ribonuclease

RPMI	=	Roswell Park Memorial Institute
Rpn	=	Regulatory Particle of Non-ATPase
RPS17	=	Ribosomal Protein S17
Rpt	=	Regulatory Particle of Triple-ATPase
RT-PCR	=	Reverse Transcriptase-Polymerase Chain Reaction
S1P	=	Site-1 Protease
S2P	=	Site-2 Protease
SAR	=	Structure-Activity Relationship
SCID	=	Severe Combined Immunodeficiency
SDS-PAGE	=	Sodium Dodecyl Sulfate-Polyacrylamide Gel Electrophoresis
SEM	=	Standard Error of the Mean
shRNA	=	short hairpin Ribonucleic Acid
SILAC	=	Stable Isotope Labeling by/with Amino acids in Cell culture
siRNA	=	small interfering Ribonucleic Acid
SNRPD1	=	Small Nuclear Ribonucleoprotein D1
SRB	=	Sulforhodamine B
STR	=	Short Tandem Repeat
TBS	=	Tris-Buffered Saline
TCA	=	Trichloroacetic acid
TCEP	=	Tris (2-carboxyethyl) phosphine hydrochloride

TCGA	=	The Cancer Genome Atlas
TIMM23B	=	Translocase of Inner Mitochondrial Membrane 23 homolog B
TN	=	Tunicamycin
TP53	=	Tumor Protein 53
Ub	=	Ubiquitin
UBL	=	Ubiquitin-Like protein
UCH37	=	Ubiquitin Carboxyl-terminal Hydrolase 37
UKCTOCS	=	United Kingdom Collaboration Trial of Ovarian Cancer
UPR	=	Unfolded Protein Response
USP14	=	Ubiquitin Specific Protease 14
USS	=	Ultrasound Screening
UTR	=	Untranslated Region
VCP	=	Valosin-Containing Protein
VEGF	=	Vascular Endothelial Growth Factor
XBP1	=	X-box Binding Protein-1

Chapter 1: Introduction and background

1.1. Ovarian Cancer

1.1.1 Ovarian Cancer incidence and subtypes

Ovarian cancer is the most lethal gynecological malignancy responsible for 14,000 deaths per year in the United States. Currently, it accounts for 2.5% of all female cancer cases, but 5% of all female cancer deaths (Siegel et al., 2018). According to the National Cancer Institute, ovarian cancer is defined as the cancer that forms in the tissues of the ovary. Once seen as a single disease derived from the ovarian surface epithelium, it is now well recognized to be a heterogeneous disease with multiple origins (Levanon et al., 2008). Based on the cell types, ovarian cancer can be divided into three groups- epithelial, germ cell, and sex cord-stromal. Epithelial ovarian cancer accounts for more than 90% of all ovarian cancer cases, while germ cell and sex cord-stromal ovarian cancer account for 3% and 2% of cases, respectively (Figure 1.1) (Siegel et al., 2018). Germ cell ovarian cancers originate from the germ cells of the ovary, whereas the sex cord-stromal ovarian cancers originate from the other supportive cells in the ovarian follicles. While the origins of germ cell and sex cord-stromal ovarian cancer are well understood, the origins of epithelial ovarian cancer have been long debated.

Recent advances in the understanding of epithelial ovarian cancer suggest it can be categorized into four distinct diseases that originate outside the ovary. Epithelial ovarian cancer can be subdivided into serous (52%), endometrioid (10%), mucinous (6%) and clear cell tumors (6%) (Figure 1.1). Growing evidence suggests that serous carcinomas originate from the epithelial cells of the fallopian tube and subsequently spread to the ovaries. Similarly, endometrioid and clear cell tumors may originate in the endometrium (lining of the uterus), while mucinous tumors may originate in the ovaries or fallopian tube-peritoneal junction. Endometrioid, mucinous and clear cell tumors are classified as Type I tumors based on their slow-growing phenotype, while more

than 90% of all serous tumors are classified as Type II carcinomas. Type II carcinomas are considered high-grade and defined by the frequent involvement of both ovaries, aggressive phenotype, late-stage diagnosis, and poor prognosis.

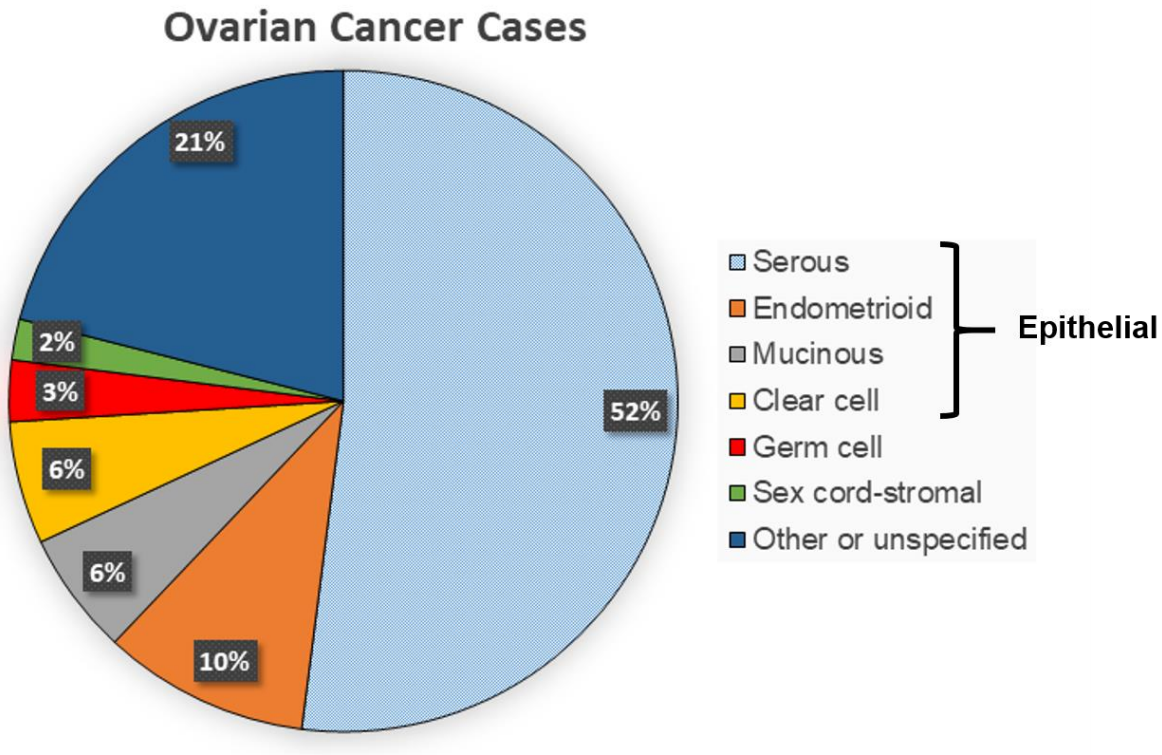

Figure 1.1. The distribution of ovarian cancer by subtypes. The pie chart represents the distribution of ovarian cancer cases by subtypes in the United States. Serous, endometrioid, mucinous and clear cells can be grouped under the epithelial ovarian cancer. Other or unspecified subtype include very low occurring ovarian tumors as well as undifferentiated tumors that are hard to categorize based on the histological phenotype. Source: North American Association of Central Cancer Registries (NAACCR), 2017.

1.1.2 Symptoms and screening modalities in ovarian cancer

The majority of ovarian cancer cases are diagnosed at an advanced stage because of the lack of specific symptoms and reliable screening tests. Common symptoms of ovarian cancer include abdominal bloating, indigestion, nausea, loss of appetite, increased abdominal girth and tiredness. Such non-specific symptoms have made the diagnosis of ovarian cancer quite challenging.

The two most commonly used screening modalities in ovarian cancer are the transvaginal ultrasound and the cancer antigen 125 blood test. The transvaginal ultrasound is performed by placing an ultrasound wand into the vagina. It uses sound waves to detect tumors in the uterus, fallopian tubes, and ovaries. The sound waves can detect tumor mass; however, it cannot determine if a mass is malignant or benign. Cancer antigen 125 is a protein marker that can be detected in the blood sample. Patients with ovarian cancer usually have elevated levels of cancer antigen 125 in their bloodstream. Since cancer antigen 125 levels often drop with decreased ovarian tumor mass, this biomarker has been used to monitor the effects of treatment. Although both these tests are extensively used in clinics, results from randomized clinical trials accessing the efficacy of cancer antigen 125 and transvaginal ultrasound on ovarian cancer mortality have been mixed (Buys et al., 2011; Jacobs et al., 2016).

1.1.3 Staging ovarian cancer

International Federation of Gynecology and Obstetrics (FIGO) staging system is the most accepted system used to stage the ovarian tumors upon diagnosis. Updated in 2014, this system now includes four stages (Prat and Oncology, 2015) which are as follow:

1) Stage I- Tumor confined to the ovaries.

2) Stage II- Tumor involves one or both ovaries with pelvic extension or primary peritoneal cancer.
3) Stage III- Tumor involves one or both ovaries with cytologically or histologically confirmed spread to the peritoneum outside the pelvis and metastasis to the retroperitoneal lymph nodes.
4) Stage IV- Distant metastases excluding peritoneal metastases.

1.1.4 Treating ovarian cancer

Ovarian cancer is a highly heterogeneous disease even though the treatment regimen remains fairly homogenous. The main treatment modalities for ovarian cancer include debulking surgery followed by chemotherapy. Recently, a few targeted therapies have been approved by the Food and Drug Administration (FDA) for ovarian cancer.

1) Optimal debulking surgery: This surgery technique includes removing all tumors larger than 1 cm (Altman et al., 2012). This often includes removing the uterus (hysterectomy) or both ovaries and fallopian tubes (bilateral salpingo-oophorectomy).
2) Adjuvant chemotherapy: Chemotherapy for ovarian cancer generally includes a combination of two drugs given intravenously 3-6 times at an interval of 3-4 weeks between treatments. Currently, the standard chemotherapy regimen includes a combination of a platinum compound such as cisplatin or carboplatin and a taxane agent such as paclitaxel or docetaxel (Akin et al., 2014; Sharma et al., 2009).
3) Targeted therapy: Targeted therapies are drugs or other agents that are developed to target specific molecules in cancer cells. Molecularly targeted therapies attack cancer cells while doing little or no damage to normal cells. In recent years, multiple targeted therapies were approved by the FDA for ovarian cancer treatment. These targeted therapies include the

angiogenesis inhibitor bevacizumab (McClung and Wenham, 2016; Pujade-Lauraine et al., 2014) and PARP inhibitors olaparib, rucaparib, and niraparib (Bamford and Webster, 2017). Clinical trials are on the way to investigate the effectiveness of these agents in combination with standard chemotherapy.

1.1.5 Survival rates for ovarian cancer

Survival of patients with ovarian cancer is largely dependent on the stage at which the tumor is first diagnosed. Although the overall 5-year survival rate for ovarian cancer is 45%, it jumps up to 92% for cases that are diagnosed at Stage I. Unfortunately, approximately 70% of ovarian cancer cases are diagnosed at Stage III and IV, where the 5-year survival rate drastically drops to 39% and 17%, respectively. These statistics highlight the importance of early detection in improving patient outcome. Similarly, newer therapeutic agents for the advanced disease may improve the overall survival rate.

1.1.6 Challenges in improving patient outcome

One of the challenges in improving the outcome of patients with ovarian cancer is the lack of early screening. Several high-profile early screening trials have investigated the feasibility and efficacy of using cancer antigen 125 and transvaginal ultrasound for the early detection of ovarian cancer. The Prostate, Lung, Colorectal, and Ovarian (PLCO) trial investigated the potential benefit of using cancer antigen 125 and transvaginal ultrasound in improving the outcome of patients with ovarian cancer. The trial enrolled 78,216 healthy women aged 55 to 74 years between 1993 and 2001. From the original enrollment, 39,105 women were placed in the intervention group, while 39,111 women were placed in the usual care group. In the intervention group, annual screening with cancer antigen 125 was performed for 6 years and transvaginal ultrasound was performed for 4 years. The usual care group did not receive these tests. The trial found that simultaneous

screening with the cancer antigen 125 and the transvaginal ultrasound did not reduce overall ovarian cancer mortality (Buys et al., 2011).

Similarly, UK Collaborative Trial of Ovarian Cancer Screening (UKCTOCS) performed a large-scale randomized controlled trial to investigate the efficacy of cancer antigen 125 or transvaginal ultrasound on ovarian cancer mortality. The study enrolled 202,638 healthy women between 50 to 74 years among 13 National Health Service Trust centers in the United Kingdom. Participants were randomly stratified into three groups: the multimodal screening group, the transvaginal ultrasound group and the no-screening group, in a 1:1:2 ratio. The multimodal screening participants received an annual screening for cancer antigen 125, while the transvaginal ultrasound screening participants received the annual transvaginal ultrasound. Participants in the no-screening group did not receive these tests. After a median follow-up of 11.1 years, the trial reported similar ovarian cancer incidence as well as similar overall ovarian cancer mortality rates among all three groups. However, when ovarian cancer mortality rates were analyzed for subjects who were in the trial for a longer period of 7-14 years, the study reported 23% reduction in mortality for the multimodal screening group and 21% reduction in mortality for the transvaginal ultrasound group compared to the no-screening group (Jacobs et al., 2016). These results indicate that early detection screens that employed the cancer antigen 125 and the transvaginal ultrasound can reduce ovarian cancer-related mortality in a long-term setting.

Additional challenges in improving the outcome of patients with ovarian cancer are tumor recurrence after chemotherapy (relapse) and acquired resistance to existing chemotherapy. Although 60-70% of ovarian cancer cases are diagnosed at Stage III and Stage IV, the cancer is responsive to the standard platinum-based chemotherapy in 70%-80% of cases. Unfortunately, most patients eventually relapse with a median progression-free survival of 18 months (Rubin et

al., 1999). Relapsed patients can often be subjected to the same treatment. However, after multiple rounds of chemotherapy, the tumor can acquire resistance to conventional chemotherapies. This clinical fact outlines the rationale for developing novel therapeutics for treating ovarian cancer in relapse and resistant settings. In the subsequent sections, I will discuss molecular characteristics of high-grade serous ovarian cancer, which constitutes 70% of all ovarian cancer cases, and I will present a molecular basis for targeting protein homeostasis to develop new targeted agents that exploit vulnerabilities in this disease.

1.1.7 Molecular characteristics of high-grade ovarian tumors

Although high-grade serous ovarian cancer displays a heterogeneous phenotype, there are some common features observed in this disease. Missense or nonsense mutations in the tumor suppressor gene *TP53* is observed in nearly all ovarian serous carcinomas (Table 1.1) (TCGA, 2011). These mutations result in the loss of functional p53 (protein product of *TP53*), which is now well accepted as an early driver mutation in Type II ovarian carcinomas, including high-grade serous ovarian cancer. This observation makes restoring the function of wild-type p53 one of the therapeutic strategies (Muller and Vousden, 2014). Furthermore, studies have now indicated that certain missense mutations in *TP53* can yield variants of p53 protein with novel functions that can promote tumorigenesis (Dittmer et al., 1993; Oren and Rotter, 2010). These reports indicate some hotspot missense mutations in *TP53* to be oncogenic (Oren and Rotter, 2010; Parrales et al., 2016); therefore, inhibiting p53 in such scenarios could be effective. Several small-molecule inhibitors have been shown to selectively either reactivate the loss-of-function p53 (p53 activating compounds) or degrade gain-of-function p53 (p53 deactivating compounds). p53 activating compounds include CP-31398, STIMA-1, and PRIMA-1, while p53 deactivating compounds include Hsp90 inhibitors and pan HDAC inhibitors (Parrales and Iwakuma, 2015). Recently,

Parrales *et al*. (2016) reported the degradation of tumor-promoting mutant p53 by statins. The treatment with statins resulted in a reduction of growth in tumors displaying the gain-of-function p53 mutations (Parrales et al., 2016). These compounds might be effective in improving the therapeutic outcome of patients with high-grade serous ovarian cancer.

Next, germline mutations in tumor suppressor genes Breast Cancer 1, Early Onset (*BRCA1)* and Breast Cancer 2, Early Onset *(BRCA2)* are observed in 7.77% and 7.13% of ovarian serous carcinomas cases, respectively (Table 1.1) with up to 50% of patients displaying defects in the homologous recombination (HR) repair pathway (Konstantinopoulos et al., 2015; TCGA, 2011). Poly (ADP-ribose) polymerase (PARP) inhibitors, which target the homologous recombination repair pathway, have also emerged as effective agents for targeting breast and ovarian cancer that harbor mutations in *BRCA1* or *BRCA2*. Other frequently reported alterations in high-grade serous ovarian cancer include upregulation of oncogenic pathways driven by *NOTCH, PI3K, RAS/MEK* and *FOXM1* (Mukhopadhyay et al., 2010; TCGA, 2011). A few studies have reported the therapeutic efficacies of targeting the altered oncogenic pathways in high-grade serous ovarian cancer in preclinical models (Cheaib et al., 2015; Zhang et al., 2014).

Most mutated genes in ovarian serous carcinomas		
Gene	**Number of mutations**	**Frequency**
TP53	585	91.76%
TTN	126	17.43%
BRCA1	49	7.77%
BRCA2	47	7.13%
USH2A	40	6.34%
CSMD3	37	5.86%
FAT3	39	5.86%
MUC16	40	5.71%
LRP2	33	4.75%
HMCN1	31	4.60%

Table 1.1. Top 10 mutated genes in ovarian serous carcinomas. Data Source: cBioPortal Cancer Genomics. Datasets: Ovarian Serous Cystadenocarcinoma (TCGA, Nature 2011) & Ovarian Serous Cystadenocarcinoma (TCGA, Provisional). Total samples analyzed = 631.

Additionally, defects in the retinoblastoma (RB) pathway, either due to the amplification of cyclin E1 (*CCNE1*) or the loss of retinoblastoma, are observed in 30% of high-grade serous ovarian cancer cases (Etemadmoghadam et al., 2013). In cyclin E1-amplified ovarian cancer cells, knocking down cyclin E1 caused cell cycle arrest and cell death (Etemadmoghadam et al., 2010), further highlighting the significance of targeting the amplified cyclin E1. Although cyclin E1-amplified high-grade serous ovarian cancer cell lines are resistant to cisplatin, they are sensitive to proteasome inhibitor bortezomib (Etemadmoghadam et al., 2013). These results indicate that cyclin E1 amplification presents a vulnerability in a subset of high-grade serous ovarian cancer.

Copy number alterations (CNA) are observed in almost all high-grade serous ovarian carcinomas. Copy number alterations result in the abundance or reduction of transcripts within the affected regions and cause genomic instability (TCGA, 2011). To better understand the genomic landscapes of cancer, Ciriello *et al.* (2013) initiated a study to look for genetic and epigenetic alterations in 12 different cancer types including ovarian cancer (Ciriello et al., 2013). The study

was geared towards identifying unique signatures in these tumors based on their genetic and epigenetic profiles from the Cancer Genome Atlas (TCGA) datasets. The study divided these 12 cancer types into two mutually exclusive classes: mutation class (M class) and copy number class (C class). Cancer driven by point mutations (M class) included kidney clear-cell carcinomas (KIRC), glioblastoma (GBM), colorectal carcinoma and uterine carcinomas. In contrast, almost all high-grade serous ovarian cancer and breast cancer samples were classified in the copy number class (C class) because their genomic signature is predominated by copy number alterations. Several other studies have also concluded that copy number alterations are a hallmark of the high-grade serous ovarian cancer (Kuo et al., 2009; TCGA, 2011).

Copy number alterations observed in the high-grade serous ovarian cancer can be viewed as a vulnerability. The increase or the decrease in transcripts from the copy number-affected regions can place a severe strain on the biological processes, such as transcription, translation, post-translation modifications, and degradation of proteins etc. The increase in RNA transcripts resulting from copy number alterations can cause transcriptomic stress, and the resulting increase in protein load can cause proteotoxic stress (Deshaies, 2014). Similarly, a decrease in RNA transcripts can also result in alterations in the steady state of the proteome by disrupting the overall protein homeostasis. Therefore, copy number alterations present a vulnerability which can be targeted by modulating protein quality control mechanisms in high-grade serous ovarian cancer. In the subsequent sections, I will discuss the phenomenon of protein homeostasis, describe protein quality control pathways, and identify specific targets in these pathways that are currently being explored in cancer therapeutics.

1.2. Protein homeostasis

Inside a cell, proteins are responsible for carrying out biochemical and cellular functions that are essential for sustaining a cellular life. Normal cellular functions are highly reliant on the steady state of the proteome maintained through dynamic regulation between protein synthesis and degradation, a process known as protein homeostasis or proteostasis. Dysregulation of protein homeostasis is the basis of most prominent disorders, including cancer. In their seminal reviews, Hanahan & Weinberg outlined hallmarks that allow non-malignant cells to acquire a neoplastic state ultimately resulting in cancer (Hanahan and Weinberg, 2000; Hanahan and Weinberg, 2011). It is now well accepted that these hallmarks are manifested through dysregulation in the protein dynamics pre-dominantly via overexpression of oncoproteins and/or downregulation of tumor suppressor proteins caused by epigenetic alterations. Furthermore, in copy number-driven cancer, such as the high-grade serous ovarian cancer, cancer cells possess additional alterations such as chromosomal duplications, aneuploidy and copy number alterations, which can further create an imbalance in protein homeostasis. The resulting stress manifested by the imbalances in protein homeostasis is called proteotoxic stress.

1.3. Protein quality control

Protein quality control includes pathways that ensure protein homeostasis either by facilitating the proper folding of misfolded or unfolded proteins or by targeting such proteins for degradation. Components of the protein quality control include 1) the unfolded protein response pathway, 2) the adaptive chaperone pathway regulated through heat shock proteins (HSPs), 3) ubiquitin proteasome system and 4) autophagy. The unfolded protein response and heat shock proteins are primarily responsible for the proper folding of unfolded or misfolded proteins (Figure 1.2). The increased levels of intracellular misfolded or unfolded proteins reduce cellular fitness, therefore

these pathways can also trigger the degradation of misfolded or unfolded proteins through the ubiquitin proteasome system and autophagy (Figure 1.2).

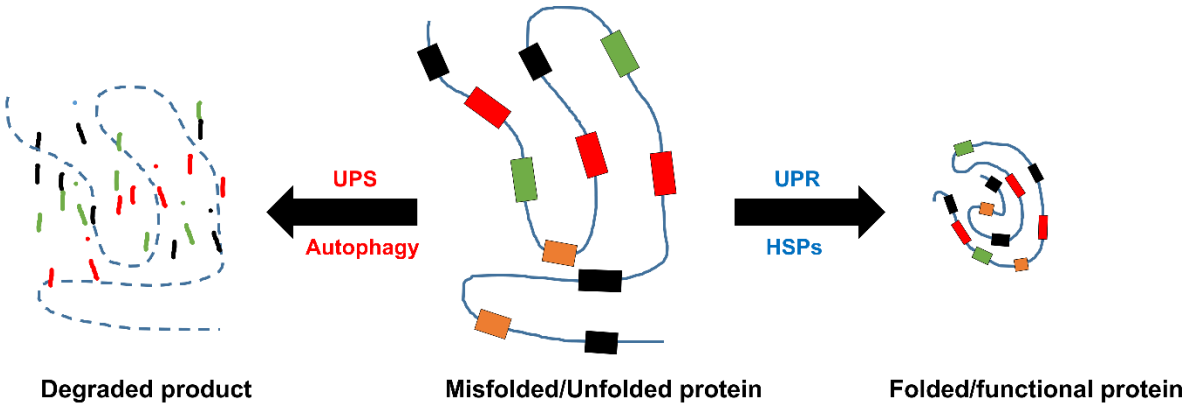

Figure 1.2. Fate of the unfolded/misfolded protein. Misfolded or unfolded protein can be refolded into its proper configuration through chaperone-mediated heat shock proteins (HSPs) or the unfolded protein response (UPR) pathway. Failure to properly fold the protein can trigger the degradation of this protein either by the ubiquitin proteasome system (UPS) or autophagy.

The unfolded protein response is a physiological response observed through the phosphorylation of two endoplasmic reticulum transmembrane proteins inositol requiring enzyme 1 (IRE1) and protein kinase R-like endoplasmic reticulum kinase (PERK), as well as through the cleavage of endoplasmic reticulum transmembrane protein activating transcription factor 6 (ATF6) (Walter and Ron, 2011). Several studies have now confirmed that cancer cells have elevated levels of unfolded protein response due to hypoxia, nutrient deprivation, copy number alterations, and mutations (Wang et al., 2010a). The unfolded protein response induces the expression of endoplasmic reticulum resident chaperones such as the glucose-regulated protein 78 (GRP78) and the glucose-regulated protein 94 (GRP94), as well as reduces protein translation. These events aid to resolve the stress response and enhance cellular fitness.

Another prominent protein quality control mechanism includes the chaperone network regulated mediated by the heat-shock proteins. By masking the effects of cryptic genetic variation, heat-shock protein 90 (Hsp90) serves as a capacitor of genetic variation while allowing phenotypic stability (Queitsch 2002; Rutherford 1998). This property of Hsp90 determines the adaptive value of genetic variations and influences the evolution of genomes (Jarosz and Lindquist, 2010). The Hsp90 complex has been shown to be upregulated in several tumor types (Barrott and Haystead, 2013; Zagouri et al., 2012). In cancer, Hsp90 allows for the proper functioning of essential oncoproteins and tumor suppressor proteins. Cancer is a heterogeneous disease, and overexpression of Hsp90 masks the defective and deleterious phenotype ultimately increasing cancer fitness.

Additionally, protein quality control mechanisms include prominent protein degradation pathways such as the ubiquitin proteasome system and autophagy, which can reduce protein load by degrading misfolded and unfolded proteins into small peptides or individual amino acids (Figure 1.2). Cancer cells display increase proteotoxic stress which makes them heavily reliant on the protein quality control mechanisms for survival and proliferation: a phenomenon known as non-oncogenic addiction. This addictive phenotype provides the rationale for targeting components of the protein quality control in cancer (Figure 1.3). In the subsequent sections, I will discuss prominent components of the protein quality control.

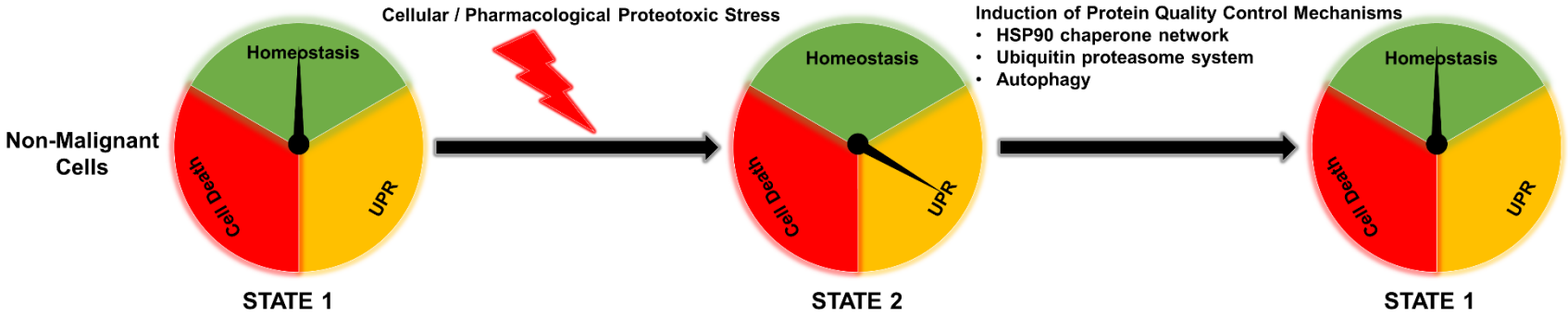

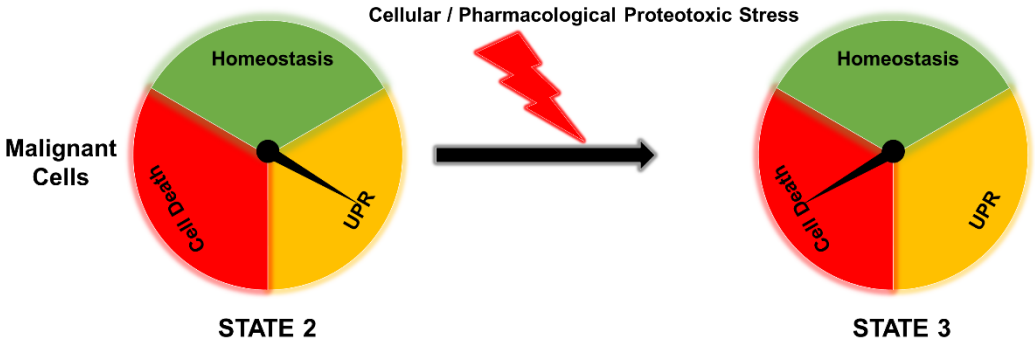

Induced State of Protein Quality Control Mechanisms
- HSP90 chaperone network
- Ubiquitin proteasome system
- Autophagy

Figure 1.3. Rational for targeting protein quality control in cancer. Non-malignant cells are at protein homeostasis with basal activity of the unfolded protein response (UPR). Cellular stressors such as the reactive oxygen species (ROS), calcium dysregulation, glucose imbalance, nutrient deprivation and increased misfolded or unfolded proteins can increase proteotoxic stress. Similarly, pharmacological agents, such as proteasome inhibitors, VCP inhibitors, and other inhibitors targeting the protein quality control mechanisms, enhance the proteotoxic stress. Non-malignant cells cope with these stresses by inducing the unfolded protein response, as well as other quality control pathways such as the heat-shock protein 90 (Hsp90) network, the ubiquitin proteasome system and autophagy, which are predominantly adaptive (State 2). Activation of protein quality control mechanisms allows the restoration of protein homeostasis in non-malignant cells. (State 1). In contrast, poor vascularization combined with genomic insults means that malignant cells already have a higher level of the unfolded protein response as well as the activation of protein quality control pathways (State 2); therefore, further cellular or pharmacological stress in malignant cells triggers cell death (State 3).

1.4. Emerging therapeutic targets in the protein quality control pathways

Several targets in the protein quality control pathways have been actively pursued in cancer therapeutics. In this chapter, I will discuss the prominent components of the protein quality control pathway, primarily focusing on the targets of emerging therapeutics for cancer treatment.

1.4.1. The unfolded protein response

Folding and maturation of secretory and membrane proteins takes place in the endoplasmic reticulum. A series of physiologically conserved signaling pathways, commonly referred to as the unfolded protein response monitor the condition of the endoplasmic reticulum and fine tunes its performance to match the protein folding capacity. The activation of the unfolded protein response increases endoplasmic reticulum space to match the increase in workload, increases the expression of endoplasmic reticulum-resident chaperones and transiently decreases protein synthesis. The unfolded protein response is triggered by changes in three transmembrane endoplasmic reticulum proteins that mediate the three branches of the unfolded protein response. These three branches include the inositol-requiring enzyme 1 alpha (IRE1α) branch, the protein kinase R-like

endoplasmic reticulum kinase (PERK) branch, and the activating transcription factor 6 (ATF6) branch. In the subsequent subsections, I will briefly discuss all three branches of the unfolded protein response.

1.4.1.1. Inositol-requiring enzyme 1 alpha (IRE1α) branch

IRE1 was first identified through inositol auxotroph selection where mutant IRE1 yeast strains required a high concentration of inositol for growth (Nikawa and Yamashita, 1992). Subsequent studies identified IRE1 as a transmembrane endoplasmic reticulum kinase, which was activated upon the induction of the unfolded protein response (Shamu and Walter, 1996). In mammalian cells, glucose-regulated protein 78 (GRP78/BiP), an endoplasmic reticulum-resident chaperone, binds and inactivates IRE1α (the IRE1 homolog implicated in unfolded protein response) under normal conditions. The unfolded proteins in the endoplasmic reticulum recruit GRP78 away from IRE1α, which allows for the activation of IRE1α through oligomerization and autophosphorylation. Activated IRE1α is a bifunctional endoribonuclease and kinase (Walter and Ron, 2011). The endoribonuclease activity of IRE1α includes the splicing of X-box binding protein-1 (XBP1) messenger RNA (Figure 1.4). Spliced XBP1 messenger RNA is translated into XBP1 transcription factor, which upregulates the expression of endoplasmic reticulum chaperones and other unfolded protein response target genes (Figure 1.4) (Oslowski and Urano, 2011; Walter and Ron, 2011).

Activation of IRE1α can attenuate protein translation through the RNAse activity known as regulated IRE1-dependent decay (RIDD) (Maurel et al., 2014), which is largely considered to be pro-survival. Paradoxically, the RIDD-dominant pathway promotes cell death in diabetes. How the IRE1 RNase activity differentially affects XBP1 splicing and transcriptional reset in different

cell types remains to be elucidated. Early evidence showed that perturbation of the unfolded protein response sensitized multiple myeloma towards proteasome inhibitors providing a rationale to identify inhibitors against specific branches of the unfolded protein response, including IRE1α. Several compounds have been shown to inhibit IRE1α. These include 1) STF-083010, 2) salicylaldehydes [3-Ethoxy-5,6-dibromosalicylaldedyde (3ETH) and 3-methoxy-6-bromosalicyaldehyde], 3) MKC-3946 and 4) toyocamycin (Chien et al., 2014; Mimura et al., 2012; Papandreou et al., 2011; Ri et al., 2012). STF-083010 was identified by screening compounds using a reporter gene assay in cells that blocked bortezomib-induced X-box binding protein-1 (XBP1) splicing. Subsequent *in vivo* studies showed that once-weekly intraperitoneal treatment of STF-083010 (30mg/kg) for two weeks significantly reduced subcutaneous multiple myeloma tumor xenografts in NOD/SCID/IL2Ry null mice (Papandreou et al., 2011). Mouse studies with another IRE1α inhibitor, 3ETH showed that intraperitoneal injection of 3ETH (20mg/kg) given three times a week for four weeks reduced human pancreatic cancer xenografts in NOD/SCID mice (Chien et al., 2014). Similarly, intraperitoneal treatment of MKC-3946 (100mg/kg) inhibited tumor burden *in vivo* in a multiple myeloma mouse xenograft model (Volkmann et al., 2011). Likewise, in SCID mice, the intraperitoneal injection of 3-methoxy-6-bromosalicyaldehyde (50mg/kg) prevented tunicamycin-induced XBP1 splicing in the liver, kidney, and spleen (Mimura et al., 2012). Lastly, intraperitoneal injection of toyocamycin (0.5mg/kg) showed a reduction in multiple myeloma xenograft with further reduction in the combination with 1mg/kg bortezomib (Ri et al., 2012). These results provide a rationale for the initiation of clinical trials of IRE1α inhibitors in several cancer types.

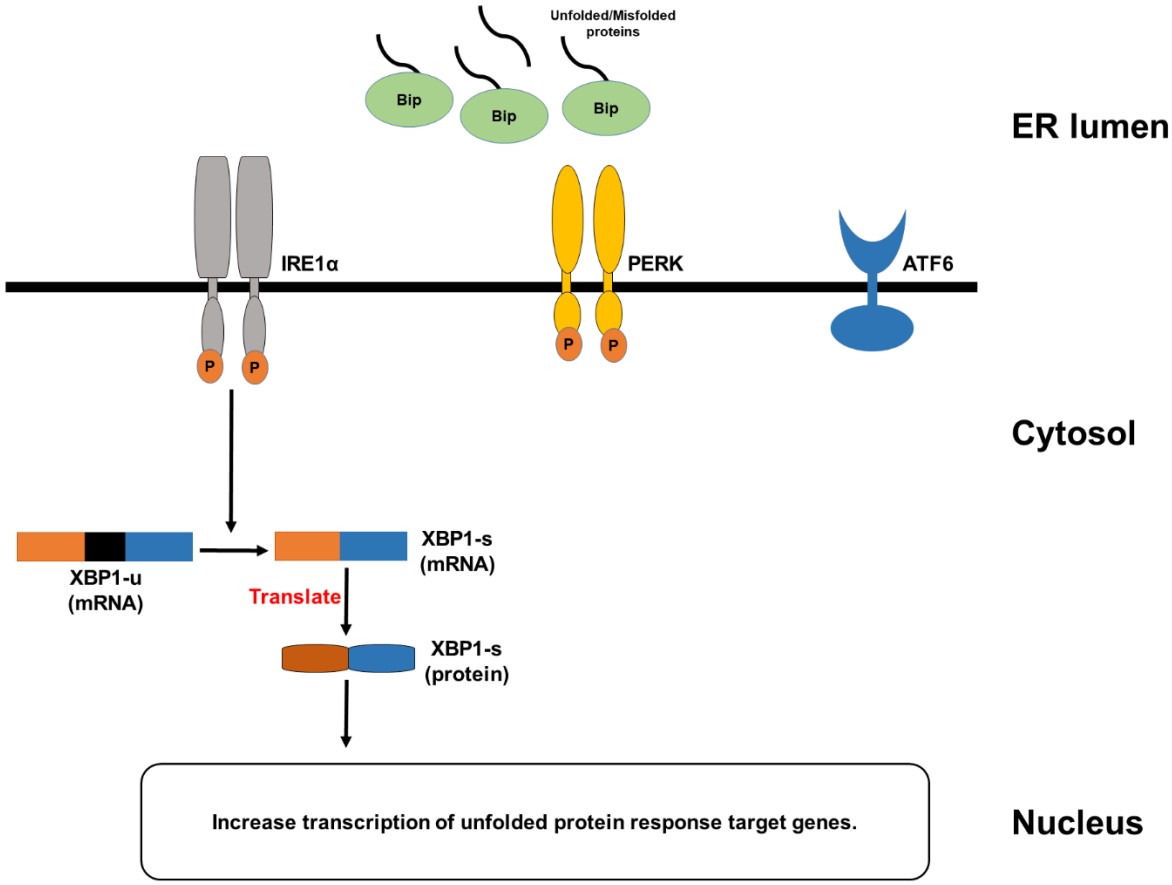

Figure 1.4. Schematic diagram representing the Inositol-requiring enzyme 1 alpha (IRE1α) branch of the unfolded protein response pathway. Increased unfolded/misfolded proteins in the endoplasmic reticulum recruit Bip (Grp78) away from IRE1α, allowing the oligomerization and autophosphorylation of IRE1α. Activated IRE1α acts as an endoribonuclease splicing X-box binding protein-1 (XBP1). Spliced XBP1 can then be translated into XBP1 protein, which is an active transcription factor responsible for inducing a subset of unfolded protein response genes mediating endoplasmic reticulum-associated degradation (ERAD) and endoplasmic reticulum biogenesis.

1.4.1.2. Protein kinase R-like endoplasmic reticulum kinase (PERK) branch

Similar to the IRE1, PERK is also an endoplasmic reticulum-resident transmembrane kinase, which can dimerize and trans-autophosphorylate upon the induction of the unfolded protein response. Activated PERK phosphorylates downstream eukaryotic initiation factor 2α (eIF2α) (Figure 1.5). This event decreases the 5' cap-dependent protein translation and increases the

expression of activating transcription factor 4 (ATF4) and CCAAT/enhancer binding protein homologous protein (CHOP) (Figure 1.5). ATF4 and CHOP are transcription factors that primarily induce expression of pro-survival genes aiding to resolve the unfolded protein response. However, a prolonged activation of the PERK branch induce cell death. Therefore PERK branch can modulate the pro-survival and pro-apoptotic response in cells based on the level of the unfolded protein response. This feature has allowed several groups to target different components of the PERK branch.

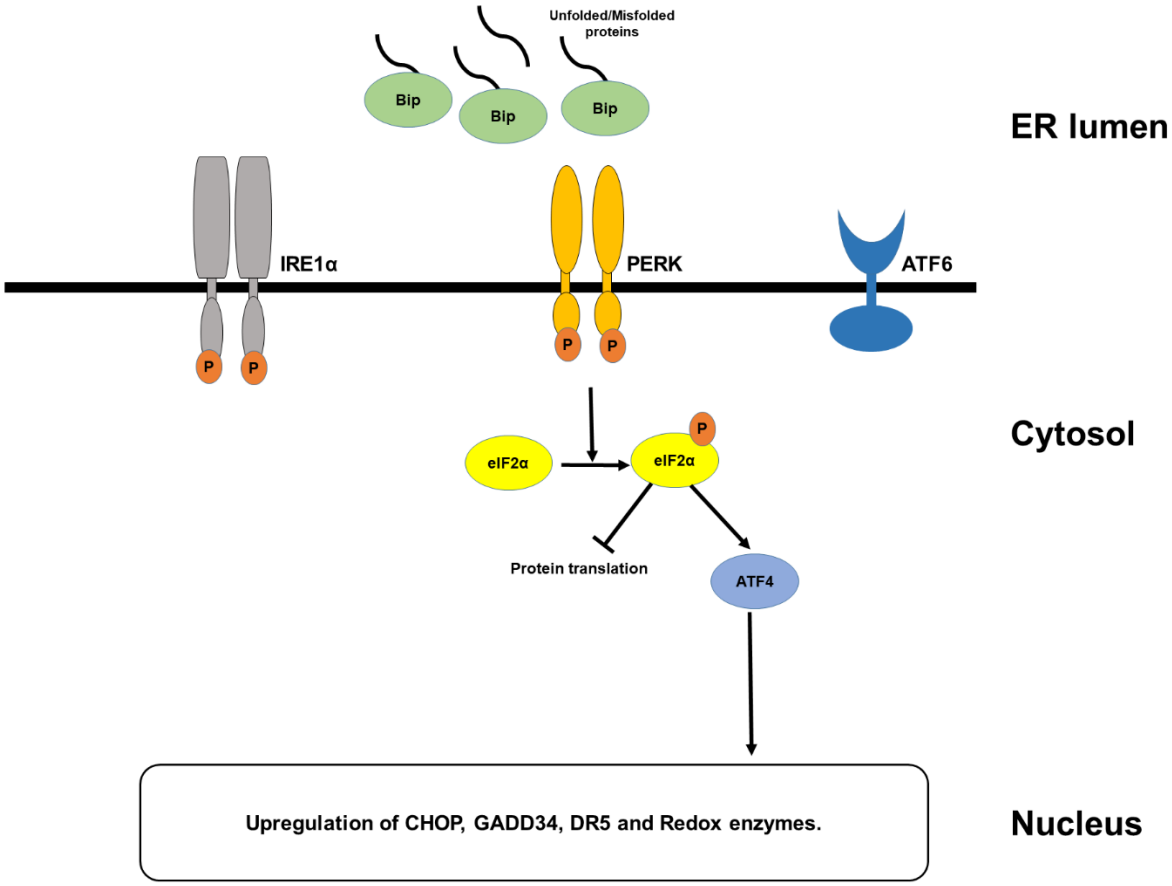

Figure 1.5. Schematic diagram representing the Protein kinase R-like endoplasmic reticulum kinase (PERK) branch of the unfolded protein response pathway. Increased unfolded/misfolded proteins in the endoplasmic reticulum recruit Bip (Grp78) away from PERK allowing the oligomerization and autophosphorylation of PERK. Activated PERK phosphorylates eukaryotic initiation factor 2α (eIF2α). Phosphorylated eIF2α promotes the translation of activating

transcription factor 4 (ATF4), while lowering global protein synthesis. ATF4 is a transcription factor that can upregulate the expression of another transcription factor CCAAT/Enhancer-binding protein homologous protein (CHOP). Both ATF4 and CHOP together can upregulated growth arrest and DNA damage-inducible protein-34 (GADD34), which can dephosphorylate phospho-eIF2α. Other outputs of the PERK branch include genes involved in antioxidant response and cell death.

Two PERK inhibitors, GSK2656157 and GSK2606414, have been shown to reduce tumor growth in several pancreatic and multiple myeloma mouse models (Atkins et al., 2013; Axten et al., 2012). Unfortunately, administration of GSK2656157 caused pancreatic toxicity. Furthermore, both PERK inhibitors were later described as potent receptor-interacting protein kinase 1 (RIPK1) inhibitors, raising questions on the conclusions of previously published studies using these compounds (Rojas-Rivera et al., 2017). Another compound, integrated stress response inhibitor (ISRIB) has been shown to modulate eIF2α phosphorylation (Sidrauski et al., 2015). ISRIB has been investigated as a potential candidate for enhancing memory retention in neurodegenerative diseases (Halliday et al., 2015). Salubrinal, an inhibitor of growth arrest and DNA damage-inducible protein 34 (GADD34), prolongs the phosphorylation of eIF2α. Salubrinal has been shown to prevent cartilage degradation in osteoarthritis (He et al., 2013) as well as provide a neuroprotective role in cerebral ischemia (Anuncibay-Soto et al., 2016). The modulation of the pro-survival and pro-apoptotic responses through the PERK branch presents an exciting opportunity to develop therapeutic agents for several human disorders including cancer.

1.4.1.3. Activating transcription factor 6 (ATF6) branch

ATF6, an endoplasmic reticulum-localized transmembrane protein, is translocated to the Golgi upon induction of the unfolded protein response (Figure 1.6). Golgi contains two specific proteases: Site-1 Protease (S1P) and Site-2 Protease (S2P) that sequentially cleave ATF6 to release the cytosolic ATF6 fragment (ATF6-N). ATF6-N is a transcription factor that translocates to the

nucleus, where it induces the expression of proteins that resolve the unfolded protein response (Figure 1.6). ATF6 is the least studied branch of the unfolded protein response, due to the lack of reliable antibodies and compounds pertaining to the ATF6 branch. Recently, two back-to-back publications have independently identified several activators and an inhibitor of ATF6. Plate *et al.* (2016) employed a three-tiered screening strategy to identify several compounds from a 644,951 small molecule library that could specifically activate ATF6. The study showed that treatment with compounds 132 and 263 induced ATF6 processing and its nuclear localization (Plate et al., 2016). In an independent screening study, Gallagher *et al.* (2016) used a cell line stably expressing the endoplasmic reticulum stress response element (ERSE) luciferase reporter to screen 106,281 compounds that could inhibit thapsigargin-induced activation of ATF6α, the isoform associated with the unfolded protein response. The study identified Ceapins as specific inhibitors of ATF6α as well as showed that treatment with Ceapin A7 sensitized cells towards unfolded protein response-mediated cytotoxicity *in vitro* (Gallagher et al., 2016). Further studies need to be performed to investigate the efficacy of these agents in targeting cancer *in vivo*.

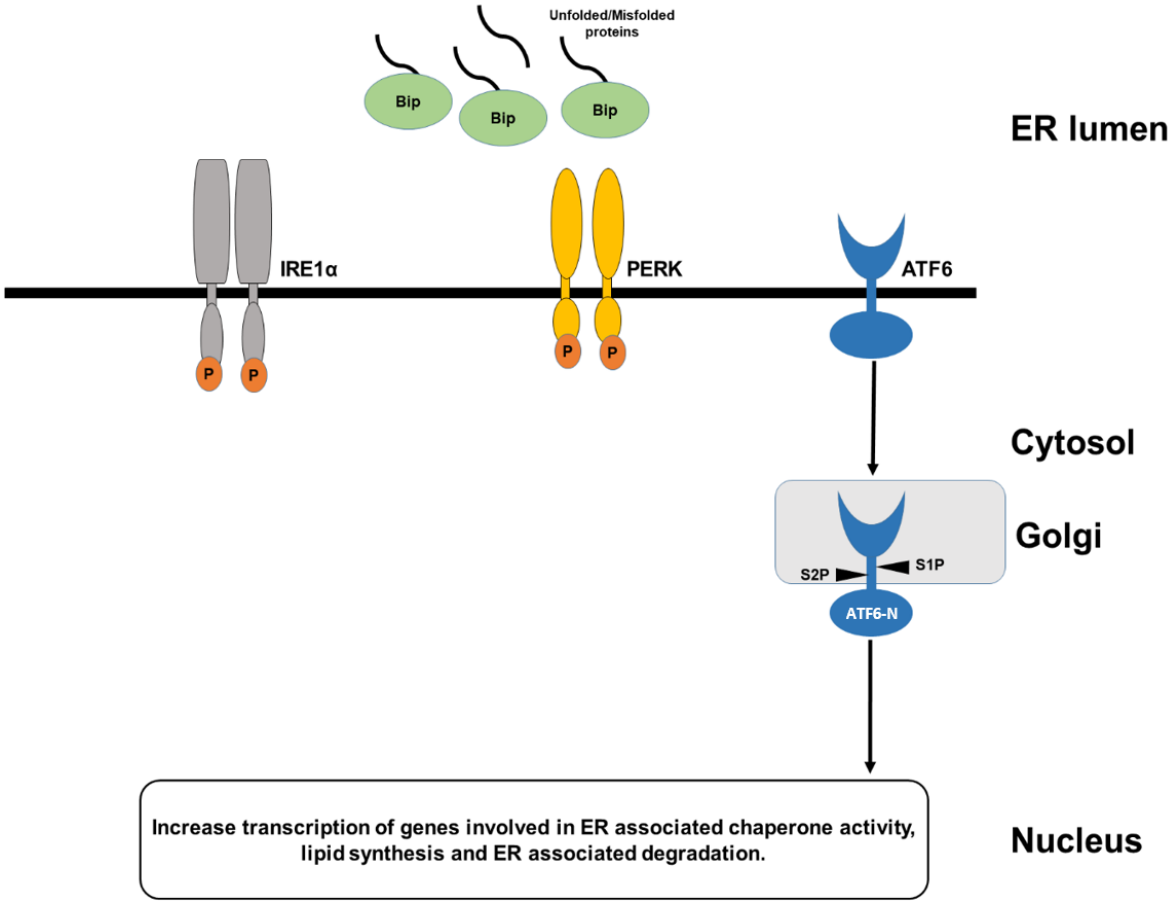

Figure 1.6. Schematic diagram representing the Activating transcription factor 6 (ATF6) branch of the unfolded protein response pathway. Activating transcription factor 6 (ATF6) is a transmembrane protein. Induction of the unfolded protein response results in the translocation of ATF6 to the Golgi where it is cleaved first by the luminal Site 1 Protease (S1P) and then the intra-membrane Site 2 Protease (S2P) releasing the cytoplasmic portion of ATF6 (ATF6-N). Activated ATF6 upregulates a subset of unfolded protein response genes associated with chaperone activity, lipid synthesis, and endoplasmic reticulum-associated degradation.

1.4.2. Heat-shock proteins (HSPs)

Heat-shock proteins (HSPs) are an ancient defense system that acts through molecular chaperones allowing for the proper folding of misfolded proteins as well as targeting the damaged proteins for degradation. In mammalian cells, heat-shock proteins are important contributors in the protein quality control. Heat-shock proteins belong to six highly conserved classes: 1) heat-shock protein 33 (Hsp33), 2) heat-shock protein 60 (Hsp60), 3) heat-shock protein 70 (Hsp70), 4) heat-shock protein 90 (Hsp90), 5) heat-shock protein 100 (Hsp100) and the class of small heat-shock proteins (sHSPs). Cancer cells are more dependent on heat-shock proteins (HSPs) for survival, which has led to the development of several inhibitors targeting different heat-shock proteins. Next, I will discuss the molecular chaperone HSP90, which has been extensively studies in cancer therapeutics.

1.4.2.1. Heat-shock protein 90 (Hsp90)

Hsp90 is a molecular chaperone that is essential for the proper folding of several client proteins, allowing these proteins to acquire a functionally active form. Hsp90 aids in maintaining proteostasis by buffering its protein substrates from several stressors such as heat shock (sudden change in temperature), oxidative stress, and proteotoxic stress. Seminal studies performed in the Lindquist laboratory have established Hsp90 as a capacitor for phenotypic variation and morphological evolution (Queitsch et al., 2002; Rutherford and Lindquist, 1998). The studies showed that robust Hsp90 activity allows for the proper functioning of metastable proteins ensuring normal growth and development (canalization). Furthermore, they showed that pharmacological inhibition of Hsp90 released these genetic variations (Rutherford and Lindquist, 1998), which manifested through defects in the phenotype (Queitsch et al., 2002). These findings have been further elaborated in the context of carcinogenesis, where robust Hsp90 expression has

been shown to stabilize key oncoproteins. In tumor cells, Hsp90 acts as a buffering system against destabilizing oncogenic mutations in oncoproteins such as *BCR-ABL, FLT3,* and *JAK2* (Ho et al., 2012) increasing the dependence of tumor cells on Hsp90. Among breast cancer patients, the high Hsp90 expression has been associated with decreased survival (Pick et al., 2007). Such evidence strengthened the idea for targeting the Hsp90 complex in tumors.

Several Hsp90 inhibitors have been tested in the preclinical and clinical settings. The first Hsp90 inhibitor identified was the benzoquinone ansamycin geldanamycin (GM) (Whitesell et al., 1994); however, it displayed low solubility and bioavailability (Supko et al., 1995). A derivative of GM, 17-allylamino- 17 demethoxygeldanamycin (17-AAG) entered clinical trials for several malignancies, but showed limited success due to poor pharmacokinetics and susceptibility to rapid drug resistance mechanisms (Neckers and Workman, 2012). Two more GM analogs, alvespimycin and retaspimycin have been pursued as clinical candidates for cancer therapeutics (Butler et al., 2015). Additional Hsp90 inhibitors that are currently in clinical trials include luminespib, onalespib, ganestespib (Butler et al., 2015).

1.4.3. Autophagy

Autophagy is an evolutionarily conserved lysosomal mediated catabolic process that degrades cytoplasmic components. Autophagy is responsible for the degradation of proteins, protein aggregates, and damaged organelles. It is primarily an adaptive mechanism allowing cells to mitigate external stresses such as nutrient deprivation, and internal stresses such as increased proteotoxic stress. Many studies have focused on targeting autophagy for cancer therapeutics. Because the mammalian target of rapamycin (mTOR) pathway regulates autophagy, pharmacologic agents that modulate the mTOR pathway have been pursued to affect autophagy pathway.

1.4.3.1. Mechanistic target of rapamycin (mTOR)

mTOR is a serine/threonine protein kinase that plays a major role in eukaryotic signaling pathways by sensing external environmental conditions. mTOR belongs to the phosphoinositide 3-kinase (PI3K) family of protein kinases comprising of two protein complexes: mTOR complex 1 (mTORC1) and mTOR complex 2 (mTORC2) (Zarogoulidis et al., 2014). mTORC1, consisting of mTOR, Raptor, and mLST8, regulates critical cellular anabolic and catabolic functions based on several environmental stimuli (Dunlop and Tee, 2009). Major cellular functions associated with mTORC1 are ribosomal biosynthesis, protein synthesis, and metabolism of lipids, nucleotide and glucose (Saxton and Sabatini, 2017). Similarly, inhibition of mTORC1 can induce autophagy (Saxton and Sabatini, 2017). mTORC2, consisting of mTOR, mLST8, and Rictor, has been primarily shown to function as an effector of insulin/PI3K-AKT pathway (Sarbassov et al., 2005). Both mTORC1 and mTORC2 have been implicated in tumorigenesis. mTORC1 lies downstream of highly mutated oncogenic pathways (PI3K/AKT as well as MAPK pathways), leading to hyperactive mTORC1 in cancers, while mTORC2 helps to activate AKT resulting in increased proliferation (Saxton and Sabatini, 2017). Therefore, targeting both mTOR complexes has been proposed as a plausible idea in cancer therapeutics.

mTOR was identified as a direct target of a compound called rapamycin, which showed remarkable antifungal, immunosuppressive and anti-cancer effect. Rapalogs (rapamycin derivatives) temsirolimus and everolimus have been approved for the treatment of breast and renal cell carcinomas (Meng and Zheng, 2015). Although, these rapalogs were effective in the pre-clinical models, barring few extraordinary responders the clinical effects of rapalogs have been largely underwhelming (Saxton and Sabatini, 2017). Such lack of effect may be due to the incomplete inhibition of mTOR by rapalogs (Kang et al., 2013). Similarly, the upregulation of the

tumor-promoting PI3K/Akt pathway upon rapalog treatment could be responsible for the poor clinical outcome (Mackenzie and Elliott, 2014). Additionally, rapalog treatment can activate autophagy by inhibiting mTORC1 partially mitigating the cytotoxic effects of these compounds. Recently, second-generation mTOR inhibitors that target mTOR by inhibiting the ATP-competitive catalytic activity have been shown to be effective in multiple cancer types and are in clinical trials (Zhou and Huang, 2012).

1.4.4. Ubiquitin proteasome system

The ubiquitin proteasome system is the principal cellular protein degradation pathway responsible for degrading 80-90% of the entire proteome (Lilienbaum, 2013). The ubiquitin proteasome system consists of three ubiquitin proteins, E1, E2, and E3, which orchestrate the attachment of polyubiquitin (primarily through ubiquitin poly-lysine 48 linkages) to protein substrates degraded by the proteasome (Figure 1.7). In the subsequent subsections, I will discuss three prominent cancer therapeutic targets in the ubiquitin proteasome system that have emerged in recent years.

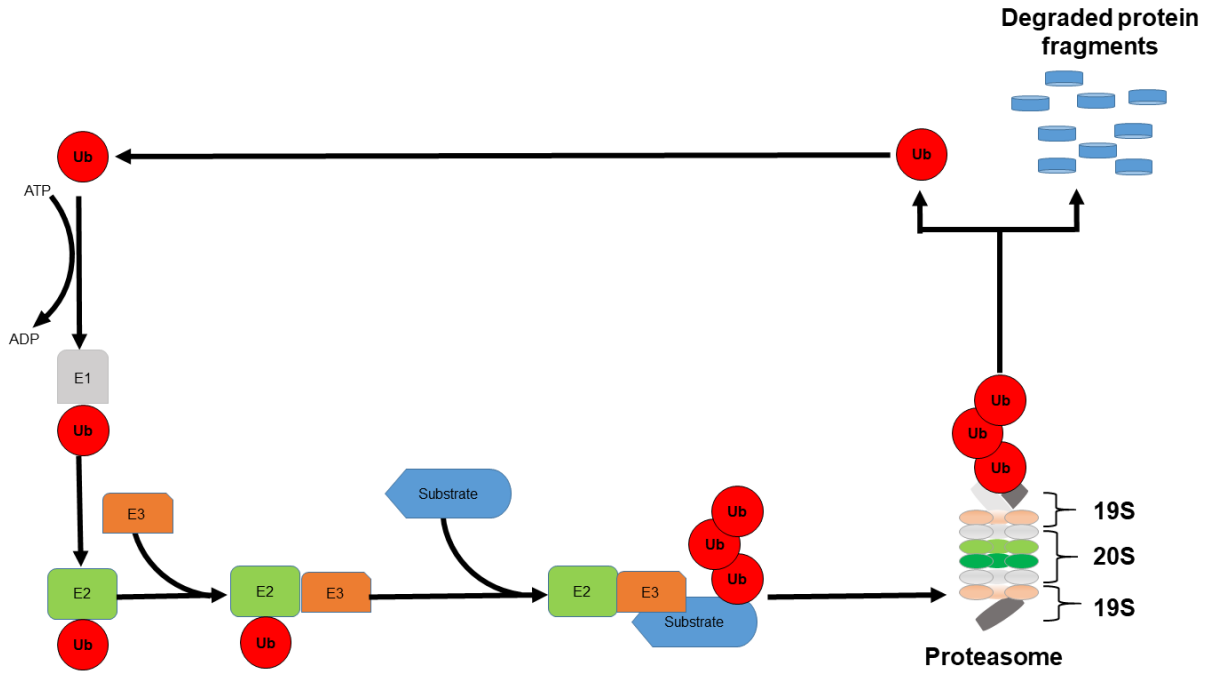

Figure 1.7. Schematic representation of the ubiquitin proteasome system. Ubiquitin (Ub) is activated by ubiquitin activating protein (E1) and subsequently conjugated to the ubiquitin conjugating enzyme (E2). Ubiquitin is then tagged to the substrate protein directly or indirectly by the E3 ubiquitin ligase. Polyubiquitinated tag at lysine 48 marks the substrate for degradation by the proteasome.

1.4.4.1. Proteasome

There are two types of proteasome, constitutive proteasome (Cp) and immunoproteasome (Ip). Cp, commonly referred to as proteasome, is a large protein complex consisting of two subcomplexes: one 20S catalytic core and one or two 19S regulatory particle(s). The 20S catalytic core consists of seven α subunits (α1- α7) and seven β subunits (β1- β7). In the Cp, β1, β2, and β5 subunits in the 20S core are responsible for peptide cleavage. The second form of proteasome, referred to as Ip, is predominately expressed in cells of hematopoietic origins, where β1, β2, and β5 subunits are substituted with iβ1, iβ2 and iβ5 subunits, respectively (Winter et al., 2017).

The 19S regulatory particle can be further subdivided into two groups: a regulatory particle of non-ATPase (Rpn) subunits and a regulatory particle of triple-ATPase (Rpt) subunits. Polyubiquitinated substrate protein docks at the ubiquitin receptor proteins Rpn10 and Rpn13, which allow for the attachment of substrate proteins to the 19S regulatory particle. Deubiquitin enzymes, Rpn11, Uch37 and Usp14, then detach the polyubiquitin from the substrate (Lee et al., 2011), allowing the substrate to enter the 20S core. Specific ATPases Rpt1-6 further drive the substrate inside the 20S core that is responsible for substrate cleavage (Deshaies, 2014).

Bortezomib (Velcade), a β5 subunit inhibitor of the 20S proteasome, was the first proteasome inhibitor to be granted FDA approval for use in multiple myeloma (Kane et al., 2003) and later in mantle cell lymphoma (Raedler, 2015). *In vitro* treatment with bortezomib has been shown to cause cell death via two separate mechanisms (Drexler et al., 2000; Lopes et al., 1997). Firstly, bortezomib treatment inhibits the degradation of inhibitor of nuclear factor kappa B kinase subunit beta (IKKβ), which then inhibits nuclear factor kappa beta (NFκB). Activation of NFκB is a pro-survival response, therefore inhibition of NFκB by IKKβ results in cell death (Hideshima et al., 2002). Secondly, treatment with proteasome inhibitors attenuates the degradation of misfolded and unfolded proteins inducing the unfolded protein response-mediated cell death (Fribley and Wang, 2006). Carfilzomib, another FDA-approved proteasome inhibitor, has been shown to display a similar mode of action with efficacy in patients with relapsed or refractory multiple myeloma (Dimopoulos et al., 2016). Although these two proteasome inhibitors show excellent efficacy in hematological malignancies, the studies performed on solid tumors so far have been underwhelming (Aghajanian et al., 2009; Aghajanian et al., 2005; Ramirez et al., 2008).

Several explanations have been provided for the lack of efficacy in solid tumors, most of which are focused on the physiology of cancer while some on the pharmacology of the drugs.

Hematological cancers such as multiple myeloma have elevated levels of nuclear factor kappa B (NFκB), therefore stabilization of inhibitor of nuclear factor kappa B kinase subunit beta (IKKβ) upon the treatment of proteasome inhibitors show significant effects in these cancers compared to solid tumors. Likewise, another explanation for this peculiarity is based on the cellular physiology of both multiple myeloma and mantle cell lymphoma. These cancers originate from antibody-producing cells which make them highly reliant on the endoplasmic reticulum and ubiquitin proteasome system for survival. Therefore, inhibition of proteasome and subsequent induction of unfolded protein response make them more vulnerable than other cancer types. Lastly, the lack of efficacy with proteasome inhibition could be due to drug pharmacology. Several *in vitro* studies have shown effective cytotoxicity by proteasome inhibitors in several solid cancer cell lines including ovarian cancer (Caravita et al., 2006; Miyamoto et al., 2013); however, numerous clinical trials have failed to show efficacy in patients (Huang et al., 2014). This could be due to inefficient drug penetration as well as fast clearance of proteasome inhibitors in patients. Intravenous administration of bortezomib has been shown to have a mean half-life of 8.68-14.8 hours in plasma (Papandreou et al., 2004). Other pharmacological agents targeting proteasome as well as other targets within the ubiquitin proteasome system could be effective in solid tumors (Anderson et al., 2015; Deshaies, 2014; Du and Mei, 2013; Gentile et al., 2015; Soucy et al., 2009).

1.4.4.2. NEDD8-activating enzyme E1 (NAE1)

Following the discovery of the ubiquitin pathway, similar pathways called ubiquitin-like protein pathways were identified. NEDD8 is a ubiquitin-like protein, which is activated by the NEDD8 activating enzyme (Ubiquitin E1 like protein). NEDD8 is then transferred to the ubiquitin-conjugating enzyme E2 M (UBE2M) and subsequently to its respective substrates. Culin-ring ligases, a class of E3 ubiquitin ligases, are one of the prominent enzymes that associate with

NEDD8, where NEDD8 binding is required for the activity of several culin-ring ligases. MLN4924 (Pevonedistat) has been identified as a potent and selective inhibitor of NEDD8 activating enzyme E1. Treatment with MLN4924 reduced NEDD8 attachment to its substrates, blocked approximately 20% of ubiquitin proteasome system-mediated protein degradation and caused cell cycle arrest, ultimately resulting in programmed cell death. Anti-tumor activity of MLN4924 has been observed in different solid tumor mouse xenograft models (Soucy et al., 2009). Such results have prompted multiple clinical trials of MLN4924 as a single agent or in combination with existing chemotherapies in mesothelioma, acute myeloid leukemia, chronic myelomonocytic leukemia and acute myelogenous leukemia.

1.4.4.3. Valosin-containing protein (VCP)

Valosin-containing protein (VCP), also known as p97, is a member of **A**TPases **A**ssociated with diverse cellular **A**ctivities- ATPase (AAA-ATPase) family of proteins that are involved in diverse cellular functions including the endoplasmic reticulum-associated degradation (ERAD), the ubiquitin proteasome system, mitochondria-associated degradation, handling aggregates, autophagy and chromatin-associated degradation (Meyer et al., 2012), making it a prominent regulator of protein quality control. VCP forms a homo-hexameric structure, each monomer consisting of an N-terminal domain, a D1 and a D2-ATPase domain and a short C-terminal domain (Figure 1.8) (Banerjee et al., 2016; Zhang et al., 2000). As a ubiquitin-segregase, VCP binds to its substrates facilitating the extraction of these substrates from the endoplasmic reticulum (DeLaBarre et al., 2006; Ye et al., 2001), mitochondria (Kim et al., 2013) and from protein complexes (Beskow et al., 2009) to target the substrates for degradation via proteasomes. Similarly, increasing evidence have now shown that VCP regulates the clearance of stress granules (Buchan et al., 2013) as well as aids in the substrate degradation via lysosomes (Ju et al., 2009).

VCP interacts with specific cofactors allowing for such diverse functions in the cell. The family of cofactors and their interactions with VCP are extensively discussed in these reviews (Hänzelmann and Schindelin, 2017; van den Boom and Meyer, 2017). Because of its prominent role in protein quality control and the clinical evidence showing an association between elevated VCP expression and poor prognosis in cancer (Tsujimoto et al., 2004a; Valle et al., 2011) and tumor recurrence (Yamamoto et al., 2003), several groups have developed inhibitors against this protein (Figure 1.9).

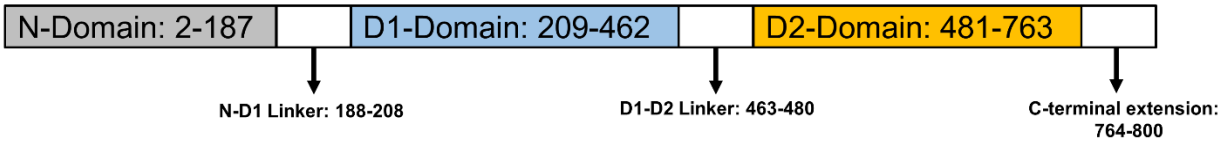

Figure 1.8. Diagram of the valosin-containing protein (VCP/p97). Monomeric VCP comprises of an N-terminal domain (aa: 2-187), D1 ATPase domain (aa: 209-462), D2 ATPase domain (aa: 481-763) domain, and a short C-terminal extension (aa 764-800). N-terminal domain interacts with substrates and cofactors while D1 and D2 ATPase domains hydrolyze ATP.

Eayarestatin 1 (Eer1) was first identified as a potent inhibitor of the ERAD that negatively affected VCP-mediated deubiquitination (Wang et al., 2008). Eer1 was shown to directly interact with VCP causing a conformational change resulting in a dysfunctional protein (Wang et al., 2010b). Subsequently, the Deshaies laboratory set out to identify specific and potent VCP inhibitors using luciferase-based high-throughput screening (HTS) assay. The screening identified N^2,N^4-dibenzyl quinazoline-2,4-diamine (DBeQ) as a selective inhibitor (Chou et al., 2011) and

later structural-activity relationship (SAR) studies identified ML240 and ML241 as potent D2 ATPase-specific VCP inhibitors (Chou et al., 2013). Although these compounds displayed increased specificity towards VCP, they lacked proper pharmacological properties for *in vivo* use. Cleave Biosciences later developed an orally bioavailable VCP inhibitor CB-5083 using ML240 as the starting compound. An oral dose of CB-5083 (100mg/kg) inhibited tumor growth in nude mice bearing different cancer xenografts (Anderson et al., 2015).

Additionally, Magnaghi *et al*. (2013) screened one million compounds using an NADH-coupled assay to measure the ATPase activity. This resulted in the identification of NMS-859 as a covalent inhibitor and NMS-873 as a non-ATP-competitive allosteric inhibitor of VCP (Magnaghi et al., 2013). UPCDC-30245 was identified as yet another VCP inhibitor related to previously identified allosteric phenyl indole-based VCP inhibitors (Alverez et al., 2015; Banerjee et al., 2016) (Figure 1.9). Sorafenib (Yi et al., 2012), rheoemodin (Kang et al., 2014) and Syk inhibitors III (Chou and Deshaies, 2011) were also identified as VCP inhibitors. Recently, the alcohol-abuse drug disulfiram was shown to inhibit VCP segregase function through the inhibition of VCP cofactor NPL4 (Skrott et al., 2017). With a prominent role in the protein quality control, targeting VCP clinically could be efficacious against multiple cancer types as well as other disorders such as inclusion body myopathy, Paget disease of the bone, and frontotemporal dementia, where mutations in VCP have been associated with the disease etiology.

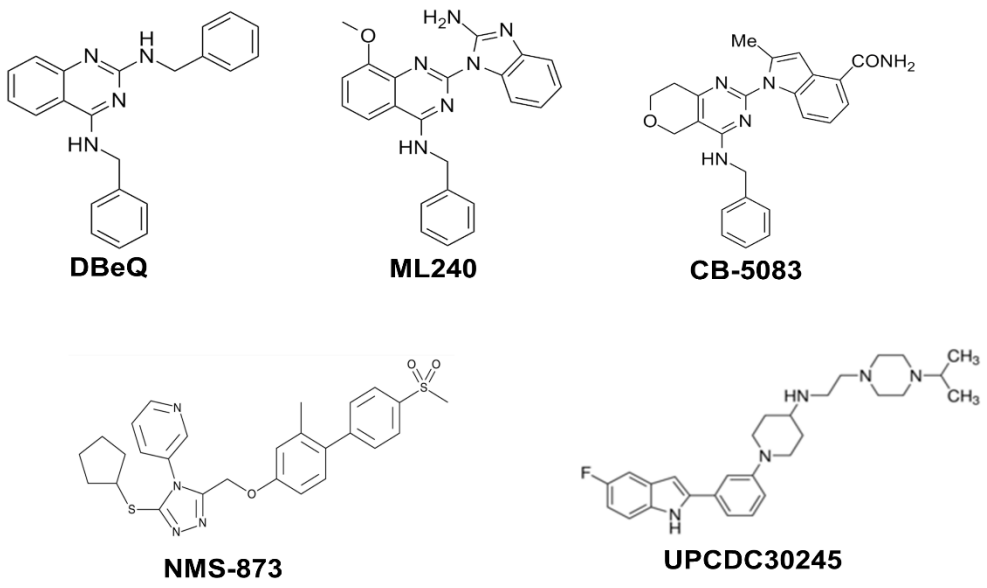

Figure 1.9. Commonly used valosin-containing protein inhibitors (VCP inhibitors). Chemical structures of commonly used VCP inhibitors (Source- PubChem).

1.5. Central hypothesis and aims

Identifying and targeting non-oncogenic pathways has been actively pursued in several tumor types including ovarian cancer (Nagel et al., 2016). In support of this concept, several genome-wide genetic screens with short hairpin RNAs (shRNAs) identified components of protein quality control as targets of vulnerability in ovarian cancer (Cheung et al., 2011; Marcotte et al., 2012; Nijhawan et al., 2012). In particular, VCP was identified as one of the lineage-specific essential genes in ovarian cancer cell lines compared to non-ovarian cancer cell lines (Cheung et al., 2011). Moreover, VCP was also identified as an essential gene in cyclin E1-overexpressed ovarian cancer cells (Etemadmoghadam et al., 2013). Recently, several groups have shown that VCP inhibitors are effective in pan-cancer cell lines with clinical candidate CB-5083 showing efficacy in multiple mouse xenograft models (Anderson et al., 2015). Based on these studies, I proposed the central hypothesis that **VCP represents a vulnerable target in ovarian cancer and can be targeted by a single agent or a combination with other agents that inhibit protein quality control pathways.** To address this central hypothesis, I proposed the following three Specific Aims:

1.5.1 Specific Aim 1: To investigate the therapeutic effects of VCP inhibitors in ovarian cancer cells.

VCP plays a prominent role in various cellular processes including endoplasmic reticulum-associated degradation (ERAD), DNA damage repair, cell cycle regulation and autophagy (Yamanaka et al., 2012). Furthermore, VCP inhibitors have emerged in recent years as a potential therapeutic option in different malignancies (Anderson et al., 2015). Through my study, I will investigate the potential therapeutic efficacy of VCP inhibitors, with a special focus on the clinical lead CB-5083 in ovarian cancer. I will characterize the mode of cell death, cell cycle regulation and changes in unfolded protein response pathway following the treatment with VCP inhibitors.

1.5.2 Specific Aim 2: To identify compounds that induce synergistic cytotoxicity with VCP inhibitors.

VCP inhibitors induce cytotoxicity in different cancer lines *in vitro* and *in vivo* (Anderson et al., 2015; Chou et al., 2011; Chou et al., 2014). However, the effects of these compounds in combination with other agents that modulate the unfolded protein response in ovarian cancer cells have not been characterized. I will determine the potential synergistic cytotoxicity between VCP inhibitors and compounds known to modulate the unfolded protein response and define the molecular mechanisms that contribute to synergistic drug interactions between VCP inhibitors and other agents that modulate the unfolded protein response and cell death pathways.

1.5.3 Specific Aim 3: To define the mechanism of resistance towards VCP inhibitors.

Development of drug-resistant cell lines through prolonged drug treatment *in vitro* allows modeling the molecular mechanism of resistance that could be seen in the clinics. Similarly, studying the molecular mechanisms contributing to cellular resistance to VCP inhibitors helps to define the on-target and off-target effects of the drugs. CB-5083 is an oral VCP inhibitor currently in Phase I clinical trials. The compound shows favorable pharmacodynamic effects in several *in vitro* and *in vivo* studies. Although missense mutations in the *VCP* coding region have been reported to contribute to CB-5083 resistance, the mechanism of resistance in ovarian cancer is not yet defined. Therefore, I will identify and characterize potential mechanisms of resistance towards the oral VCP inhibitor CB-5083 by employing an intermittent and a continuous dosing scheme to establish CB-5083 resistant ovarian cancer cells and investigate molecular mechanisms contributing to CB-5083 resistance. Finally, I will investigate new strategies that could be used to target CB-5083 resistant cell lines.

Chapter 2: Materials and methods

Portions of this chapter are reproduced from the following publications with permission where required.

- **Bastola P**, Neums L, Schoenen FJ, Chien J (2016) VCP inhibitors induce endoplasmic reticulum stress, cause cell cycle arrest, trigger caspase-mediated cell death and synergistically kill ovarian cancer cells in combination with salubrinal. Molecular Oncology 10, 1559-1574. PMID: 27729194

- **Bastola P**, Wang F, Schaich M, Gan T, Freudenthal B, Chou TF, Chien J (2017) Specific mutations in D1-D2 linker region of VCP/p97 enhance ATPase activity and confer resistance to VCP inhibitors. Cell Death Discovery 3, 17065. PMID: 29367883

2.1. Reagents

DBeQ, ML240, and ML241 were provided by Dr. Frank Schoenen at the University of Kansas (Chou et al., 2013). Salubrinal (CML0951), mifepristone (M8046), UPCDC30245 (SML1674) and tunicamycin (11089-65-9) were purchased from Sigma-Aldrich. CB-5083 (S8101), STF-083010 (S7771), bortezomib (S1013) and NMS-873 (S7285) were purchased from Selleckchem. DBeQ, ML240, ML241, NMS-873, UPCDC30245, STF-083010, bortezomib and CB-5083 were dissolved in dimethyl sulfoxide (DMSO) at the concentration of 50 mM. Salubrinal was dissolved at the concentration of 20 mM in DMSO, and tunicamycin was dissolved at the concentration of 10 mM in DMSO. Dissolved compounds were aliquoted and stored at -80°C. Stocks were thawed at room temperature and dissolved in appropriate media at selected concentrations immediately before use.

2.2. Cell lines and cell culture

Ovarian cancer cell lines OVCAR10, SKOV3, OVCAR5, and RMG1 were cultured in 1:1 mixture of MCDB 105 (Sigma-Aldrich, M6395) and Medium 199 (Sigma-Aldrich, M5017), 5% fetal bovine serum (Sigma-Aldrich, F0926), and 1% streptomycin/penicillin (Sigma-Aldrich, P0781). OVCAR8, OVSAHO parental and OVSAHO resistant cells were maintained in RPMI (Sigma-Aldrich, R8758), 10% fetal bovine serum and 1% streptomycin/penicillin. PERK-MEF$^{-/-}$ (ATCC, CRL-2976) and GCN2-MEF$^{-/-}$ (ATCC, CRL-2978) were cultured in DMEM, 0.1 mM non-essential amino acids (Fisher, MT25025CL), 0.05 nM 2-mercaptoethanol (Sigma-Aldrich, M3148), 10% fetal bovine serum, and 1% streptomycin/penicillin. HEK-293T cells were cultured in RPMI, 10% fetal bovine serum, and 1% streptomycin/penicillin. All cell lines were kept in a humidified incubator at 37°C with 5% CO_2. All cell lines were subjected to cell line identity confirmation with short tandem repeat (STR) genotyping.

2.3. Sulforhodamine B (SRB) assays and drug synergy studies

Sulforhodamine B assays were performed as previously described (Vichai and Kirtikara, 2006) with the following modifications. Briefly, two different density of cells (3000/well and 5000/well) were seeded in 96-well plates and cultured in 200 µl/well of appropriate growth media. The next day, cells were treated with different concentrations of compounds for 72 hours unless otherwise specified. After treatment, cells were fixed with 10% trichloroacetic acid (Sigma-Aldrich, T6399) at 4°C overnight. Fixed cells were then washed with running water and stained with 0.057% (weight/volume) sulforhodamine B (Sigma-Aldrich-230162) stain prepared in 1% acetic acid solution (Sigma-Aldrich, BP2401) at room temperature for 45 minutes. Excess stain was discarded, and cells were washed with 1% acetic acid solution. Stained cells were dissolved in 10 mM tris-buffered saline (TBS, pH 10), and fluorescence measurements were taken at Excitation 488 nm and Emission 585 nm using a fluorescence plate reader. Dose-response curves were fitted, and half-growth inhibition (GI_{50}) values were determined with GraphPad Prism (ver. 6) using four parameters setting. All dose-response curves were constrained to 100% at the top and greater than 0% at the bottom.

Synergy was determined by calculating the combination indexes (CIs) obtained from the fluorescence measurements. Combination indexes were calculated by dividing the expected effect by the observed effect. The expected values assume additive effects between two drugs. N represents the total number of combination indexes (CIs) determined from 16 different drug combinations in duplicates that produced 20-80% effect from three independent experiments. An example of synergy calculation is shown in Figure 2.1.

Combination index was calculated using the formula:

$CI = (D_1 + (D_2 * (1-D_1)))/ D_{observed}$

where, CI= Combination index

D_1 = average fraction affected by Drug 1,

D_2 = average fraction affected by Drug 2, and

$D_{observed}$ = average fraction affected by Drug 1 + Drug 2

Salubrinal (μM) \ DBeQ(μM)	0	1	2	3	5
	Average Effect				
0	0.02	0.02	0.14	0.18	0.55
5	0.05	0.03	0.26	0.31	0.66
10	0.04	0.08	0.31	0.40	0.64
15	0.11	0.22	0.43	0.52	0.74
20	0.21	0.41	0.58	0.64	0.74

Fraction affected (0.2-0.8)

Combination index (CI)				
		0.71	0.71	0.87
		0.56	0.52	0.88
	0.59	0.54	0.51	0.81
	0.54	0.54	0.54	0.86

n=14

Figure 2.1. An example of combination index (CI) calculation.

2.4. Clonogenic Assay

500-1000 cells/well were seeded in 6-well plates using the appropriate media. The next day, the culture media was replaced with media containing appropriate compounds, and cells were treated for 48 hours. Following the treatment, media was gently aspirated, and the wells were gently washed twice with phosphate-buffered saline (PBS, pH 7.0) and replaced with regular growth media. Cells were then allowed to grow in the incubator for 6-10 additional days while replacing media every 48 hours. Once the colonies were visible, media was aspirated, and 1 ml of crystal violet solution (0.5% crystal violet dye, 50% methanol, and 50% deionized distilled H_20)

was added to each well. The cells were stained with crystal violet solution for 30 minutes and then washed with water. In some experiments, crystal violet staining was substituted with sulforhodamine B staining as described in the Methods for sulforhodamine B assay. Sulforhodamine B staining allows dual quantitation of surviving cells by counting stained colonies and by measuring the fluorescence of extracted sulforhodamine B. The plates were then air-dried and pictures were taken using the Bio-Rad Imager System. Colonies were counted using BioRad Quantity One version 4.6.9 software. Clonogenic survival was determined relative to vehicle-treated cells and shown in bar graphs using GraphPad Prism (ver. 6).

2.5. Puromycin Incorporation Assay

Puromycin incorporation assay was performed as previously described (Schmidt et al., 2009), with the following modification. 0.5 x 10^6 cells per well were seeded in 6-well plates and cultured in 2 mL of appropriate growth media. The next day, growth media were substituted with media containing different concentrations of vehicle or compounds. The plates were placed in a humidified incubator at 37°C with 5% CO_2 for 5.5 hours, after which 2 μL of 1 mM puromycin solution (Goldbio, P-600) was added to each well and incubated for additional 30 minutes. Cells were collected, lysed and equal volumes were subjected to Western blotting according to the established protocol (please refer to section 2.12). Blots were incubated with antibodies against puromycin (Millipore, MABE343) and β-actin (Sigma-Aldrich, A1978).

2.6. Cellular Thermal Shift Assay (CETSA)

Cellular Thermal Shift Assay (CETSA) was performed as previously described (Jafari et al., 2014), with the following modifications. Briefly, 1 x 10^6 cells were seeded in 10 cm cell culture plates with appropriate growth media. The next day, regular growth media was replaced with culture media containing various concentrations of DBeQ and ML240 for 2 hours. Cells were

trypsinized, and cell pellets were collected following centrifugation. Cell pellets were dissolved in 100 µl phosphate-buffered saline (PBS) pH 7.0 and subjected to heat treatment at 57°C. Following heat treatment, proteins were precipitated using freeze-thaw in liquid nitrogen. Cells were then subjected to centrifugation at 20,000xg at 4^0C, and soluble fractions were analyzed by Western blot. Blots were incubated with antibodies against the valosin-containing protein (Santa Cruz, 20799) and β-actin (Sigma-Aldrich, A1978).

2.7. Transient small interfering RNA (siRNA) knockdown

0.5 x 10^6 cells per well were seeded in 6-well plates using appropriate growth media without antibiotics. The next day, small interfering RNAs (siRNAs) were transfected using Oligofectamine reagent (Life Technologies, 12252-011) according to the manufacturer's protocol. Non-targeting scrambled small interfering RNA was transfected in parallel as a negative control. Predesigned siRNAs for the valosin-containing protein (VCP), heme-regulated inhibitor (HRI), protein kinase R (PKR) and scrambled siRNAs were purchased from Integrated DNA Technology (IDT). Growth arrest and DNA damage-inducible protein 34 (GADD34) siRNA were purchased from Santa Cruz Biotechnology (sc-37414). Cells were collected at 48 hours after transfection, and whole cell lysates were subjected to Western blotting according to the established protocol (please refer to section 2.12). Targeting efficiency of each siRNA was evaluated based on the relative reduction in the expression of targeted protein after transfection compared to negative control using densitometry analysis. β-actin was used as the loading control.

2.8. Caspase 3 activity assay

0.5 X 10^6 cells/well were seeded in 6-well plates using the appropriate culture media. The next day, cells were treated with appropriate compounds in culture media. Cells were scrapped and collected at different time points following the treatment. Cells were lysed in caspase buffer:

20 mM PIPES, 100 mM NaCl, 1 mM EDTA, 0.1%(w/v) CHAPS, 10% sucrose, 10 mM DTT pH 7.2. Protein concentration was determined using BCA Assay. 20 μg protein was combined with 2 μL of 2 mM DEVD-Afc (kindly provided by Dr. Wen-Xing Ding's laboratory at the University of Kansas Medical Center) in 96-well flat-bottom plate (Falcon, 3296). Appropriate volumes of caspase buffer were added to make 200 μl/well. The plate was covered and incubated at 37°C. After 2 hours, fluorescence measurements were taken using a plate reader at Excitation 400 nm (nanometer) and Emission 510 nm (nanometer). Cleavage of the dye-quenched peptide by active caspase 3 releases the quencher and produces fluorescence. Fluorescence measurements were analyzed using GraphPad Prism (version 6).

2.9. Analysis of VCP expression from RNA sequencing datasets

RNA sequencing datasets (RNAseqV2 level3) from high-grade serous ovarian cancer were downloaded from the cancer genome atlas (TCGA) Research Network Data Portal (http://tcga_data.nci.nih.gov/tcga). The clinical data associated with these samples were downloaded from cBioPortal (http://www.cbioportal.org/data_sets.jsp). The sensitive samples (55 samples) were defined as being disease free for over 24 months while the resistant samples (95 samples) were defined as being disease-free for less than 12 months. From the data, normalized expression was extracted for the gene *VCP* and plotted in R with the R package 'caroline' using the plot function 'violins' (version 0.7.6. https://CRAN.Rproject.org/package.org/package-=caroline). A bin-width of h=1650 for the kernel density estimation was used for the plots. Welch's Two Sample t-test was used to calculate the p-value.

2.10. Cell Cycle Analysis

1 X 10^6 cells per plate were seeded in 10 cm cell culture plates with the appropriate culture media. The next day, cells were incubated with culture media containing the vehicle or appropriate

compounds for 18 hours. Cells were then trypsinized and cell pellets were collected in a 15 mL centrifuge tubes. Pellets were washed twice with ice-cold phosphate-buffered saline (pH 7.0). Cells were then fixed in 2ml of ice-cold phosphate-buffered saline and 95% ice-cold ethanol (Fisher, BP2818500) mixed at 1:1 ratio for 1 hour. Fixed cells were twice washed with cold phosphate-buffered saline. Finally, the pellets were resuspended in 0.1% sodium citrate solution containing RNase A (Invitrogen, AM2269) and propidium iodide solution (Sigma-Aldrich, P4170) for 30 minutes at 37^0C. Cell cycle profile for each treatment condition was then analyzed using flow cytometer based on previously established protocols at the University of Kansas Medical Center Flow Cytometry Core.

2.11. Annexin V apoptotic assay

0.3 X 10^6 cells per well were seeded in 6-well plates using the appropriate culture media and were allowed to incubate overnight. Cells were then treated with culture media containing vehicle or the compounds of interest for the indicated time. After treatment, cells were trypsinized and centrifuged at 1500 rpm for 5 minutes. Cell pellets were resuspended in Annexin V Binding Buffer containing propidium iodide (BioLegend, 640914). Annexin V and propidium iodide staining was determined by flow cytometry according to the manufacturer's protocol.

2.12. Western blot and antibodies

Cells were scrapped and collected at the end of each experiment for western blotting. Proteins were extracted in 2X Laemmli Buffer (Bio-Rad, 161-0737) containing protease inhibitor (Roche, 05892970001) and phosphatase inhibitor (Fisher, 78440). Equal volumes of samples were loaded (unless otherwise specified) in SDS-PAGE and electroblotted onto polyvinylidene difluoride PVDF membranes. Blotted membranes were incubated in 5% nonfat dry milk prepared in tris-buffered saline with 0.5% Tween-20 (TBS-T) solution for 1 hour at room temperature and

were incubated with appropriate primary antibodies prepared in 3% bovine serum albumin in TBS-T solution overnight at 4°C. Membranes were then washed with TBS-T solution and incubated with appropriate horseradish peroxidase (HRP)-conjugated secondary antibodies prepared in 3% bovine serum albumin in TBS-T solution for 1 hour at room temperature. Immunocomplexes on the blots were visualized by the Super Signal West Femto (Pierce, 34096) and recorded by Bio-Rad imager (ChemiDoc™ MP Imaging System).

Primary antibodies used for Western blotting included IRE1α (cst-3294S), phospho-IRE1α (Novus, nb100-2323), CHOP (cst,5554S), ATF4 (cst,11815S), phospho-eIF2α (Abcam, ab32157), VCP (sc,20799), PARP (cst,9542), Caspase 3 (cst,9665P), Cleaved Caspase 3 (cst,9661S), Caspase 9 (cst,9508P), Caspase 8 (sc,81656), puromycin (EMD Millipore, MABE343), β-actin (Sigma-Aldrich, A1978), GADD34 (sc,8327), VCP (sc, 20799) Bip/Grp78 (cst,3177S), p21 (sc,397), p27(cst,3686S), Cyclin D1 (sc,20044), and Cyclin E (sc,247), PERK (cst,3192S), ATF6 (cst, 65880), DYKDDDDK (cst,2368), XBP-1s (cst, 12782) . Secondary antibodies included HPR-linked anti-rabbit IgG (cst-7074) and HPR-linked anti-mouse IgG (cst-7076). Densitometry analyses were performed using ImageJ, and graphs were plotted using GraphPad Prism (ver. 6).

2.13. Genomic DNA extraction, PCR and Sanger sequencing

$1x10^6$ cells were collected from parental and resistant cell lines. Genomic DNA was extracted from each sample using Qiagen DNA purification kit (Qiagen, 69506). Following the genomic DNA extraction, segments of the *VCP* gene (exon 11-16) were amplified by polymerase chain reaction (PCR) using Q5 High-Fidelity DNA polymerase (M0491S) with specific primers. A complete list of all genomic DNA primers used for this study is provided in Table 2.1. Following PCR amplification, amplicon length was evaluated using DNA gel electrophoresis.

For Sanger sequencing, all PCR products were first purified using Qiagen PCR purification kit (Qiagen, 28104). For each sample, 5 µl of 5 µM sequencing primer (one of the PCR primers used for amplification) were mixed with 10 µl of PCR-purified product. The resulting mixtures were sent for Sanger sequencing at Genewiz. All Sanger sequencing results were analyzed using Sequencher (version 5.0, Gene Codes).

Primers	Forward primer 5'-3'	Reverse primer 5'-3'	Amplicon
Ex-11&12	TGGGTCTTTGAGGCAGCATA	TGACTCACCCTGGACCAAGT	449
Ex-13	TAATGGAGGGGATGCTTCTG	GCCCTCAGGCAAATCAATAC	339
Ex-14	CATGCTGGTTTCGGATTTCT	GCCTGAGGACTCATGCAAGT	498
Ex-15	GGGTTGGTCTAAAGGGAAGG	TCTCCATGATTGGCACATCT	375
Ex-16	TTTCCAGAGTGCATTGACAAGT	TTTGGTGTAGGTCCCCAAAG	399

Table 2.1. List of sequencing primers for exons 11-16 (VCP-gene).

2.14. RNA extraction, quantitative RT-PCR and cDNA sequencing

$1x10^6$ cells from each experimental conditions were harvested by centrifugation after washing with phosphate-buffered saline. RNA extraction was performed using Trizol reagent (Invitrogen, 15596-028) according to the manufacturer's protocol. One microgram of total RNA was reverse transcribed using a random primer (5 µM) and MMLV reverse transcriptase (Invitrogen) according to the manufacturer's protocol.

Complementary DNA was subjected to polymerase chain reaction (PCR) with specific primer pairs spanning exon 7 to 3' untranslated region (UTR) of *VCP* (Table 2.2) and the resulting amplicon was purified using PCR purification kit (Qiagen, 28104). Purified amplicons were sequenced by Sanger sequencing at Genewiz as described in Section 2.13. The results analyzed using Sequencher (ver 5.0, Gene Codes).

Primers	Forward primer 5-3	Reverse primer 5-3	Amplicon
VCP cDNA	CAATTGGTGTGAAGCCTCCT	AGAAACCCCCTGTCCAGAGT	1886

Table 2.2. Primers used to sequence complementary DNA (VCP-gene).

For quantitative reverse transcription-polymerase chain reaction (qRT-PCR), 0.5% of the complementary DNA (cDNA) was mixed with Qiagen RT^2 SYBR Green Fluor qPCR Mastermix (Qiagen, 330513). qRT-PCR was performed based on the manufacturer's protocol. The list of primers used for qRT-PCR is provided in Table 2.3.

Primers	Forward primer 5-3	Reverse primer 5-3	Amplicon
VCP	ATGCCATCGCTCCCAAAAGA	TGTCAAAGCGACCAAATCGC	174
18S	GCCCGAAGCGTTTACTTTGA	TCCATTATTCCTAGCTGCGGTATC	81

Table 2.3. List of primers used for quantitative reverse transcriptase polymerase chain reaction (q-RT-PCR).

2.15. Kaplan-Meier plots

Kaplan-Meier plotter was used to analyze the clinical association between VCP expression and outcome of patients with ovarian cancer (Gyorffy et al., 2012). The Affymetrix Probe ID 208648_at corresponding to VCP was used in the analysis. The latest version of the dataset (2015 version) includes progression-free survival and overall survival data from 1306 patients and 1582 patients, respectively. For the progression-free survival, a total of 1306 patients were included in the analysis. The median cutoff value for VCP expression is 778 (expression values range from 9 to 4128). For the overall survival, a total of 1582 patients were included in the analysis. The median cutoff value for VCP expression is 823 (expression values range from 9 to 6440). The dataset includes 1144 patients with serous histologic subtype and 36 patients with endometrioid subtype of epithelial ovarian cancer. The remaining cases are not annotated.

2.16. Determining IC_{50} values of VCP inhibitors in ATPase assays

ATPase activity assays were performed as previously described (Chou et al., 2014). Inhibition of human valosin-containing protein (25 nM monomer) was carried out in assay buffer (50 mM Tris pH 7.4, 20 mM $MgCl_2$, 1 mM EDTA, 0.5 mM TCEP) containing 0.01% Triton X-100 and 200 μM ATP. 8-dose titration was used to determine half inhibitory concentration (IC_{50}) of each compound in inhibiting the ATPase activity, which was determined by the addition of Biomol Green Reagent (Enzo Life Sciences, BML-AK111).

2.17. Molecular Docking

All molecular docking experiments were carried out with AutoDock Vina (Trott and Olson, 2010). The structure of valosin-containing protein (VCP) was acquired from the protein data bank (PDB code 5FTK), and modified by removing the bound ADP and solvent molecules, and converted to a monomeric form for the case of CB-5083, and hexameric form for the case of NMS-

873 (Banerjee et al., 2016). Auto-DockTools 4.2 was utilized to add polar hydrogens and Gasteiger charges and to position a 30 x 30 x 30 $Å^3$ search box that included both E470 and the active site (Morris et al., 2009). Structure coordinates of compounds of interest were built using Phenix and then converted to a .pdbqt format with Auto-DockTools 4.2, allowing full ligand flexibility (Adams et al., 2010). Default Autodock Vina settings were utilized for the analysis of binding modes, except that exhaustiveness was raised to 100. Measurements and figures were made in PyMol (Schrodinger, 2015).

2.18. Analysis of somatic mutations in tumor samples from the Cancer Genome Atlas (TCGA) database

The database was assessed through the cbioportal website (Gao et al., 2013). All sequencing studies (53 published and unpublished studies) from the cancer genome atlas (TCGA) were selected. The search for *VCP* gene indicates a total of 139 mutations (111 missense and 28 truncating mutations) in 79 samples. Thirteen samples have two mutations per sample, and the majority of these mutations have differences in variant allele frequencies, suggestive of independent or separate mutations.

2.19. RNA-sequencing analysis

OVSAHO parental and resistant cells were seeded in 6-well plates (0.5 X 10^6 cells/well). The next day, cells were either treated with vehicle (DMSO) or 5 μM CB-5083 for 6 hours. Each treatment condition was performed in triplicate. Cells were scraped and collected by centrifugation. Cells were then washed twice with phosphate-buffered saline (pH 7.0), and 1 ml Trizol reagent (Invitrogen, 15596-028) was added to each sample. Total RNA was extracted using the Trizol reagent according to the manufacturer's protocol. One microgram of total RNA was used to prepare sequencing library using Illumina TruSeq RNA Sample Preparation Kit v2 based on the

manufacturer's protocol. RNA sequencing was performed using Illumina HiSeq 4000 by the Genome Sequencing Core at Mayo Clinic, Rochester, Minnesota.

Sequences produced by Illumina sequencing in the FASTQ format were imported in CLCBio Genomics WorkBench (ver. 9) and mapped to the human reference genome (hg19). Reads mapping to annotated genes were counted and differentially expressed genes between two groups were determined by DESeq2. False discovery rate (FDR) cutoff value of 0.001 and absolute fold change of ≥1.5 were used to identify differentially expressed genes with high levels of statistical significance between two groups. To identify genes induced or suppressed by CB-5083, a separate analysis was performed in parental cells and CB-5083 resistant cells. For pathway analysis, differentially upregulated or downregulated genes were analyzed using Metascape webtool.

2.20. Transient plasmid transfection

0.5 X 10^6 cells/well were seeded in 6-well plates in RPMI media with 10% fetal bovine serum without penicillin & streptomycin. Cells were then allowed to incubate overnight in 37˚C humidified incubator containing 5% CO_2. The following day, p3XFlag-ATF6 plasmid was transfected using Oligofectamine reagent (Life Technologies, 122520-011) based on the provided manufacturer's protocol. Twenty-four hours later, media was aspirated and indicated compounds were added for the indicated time. p3XFLAG-ATF6 was a gift from Ron Prywes (Addgene, plasmid#11975) (Chen et al., 2002). DYKDDDDK (cst,2368) antibody was used to detect Flag tag and β-actin was used as loading control.

Chapter 3: Understanding and enhancing the cytotoxicity of VCP inhibitors in ovarian cancer

Portions of this chapter are reproduced from the following publication with permission where required.

- **Bastola P**, Neums L, Schoenen FJ, Chien J (2016) VCP inhibitors induce endoplasmic reticulum stress, cause cell cycle arrest, trigger caspase-mediated cell death and synergistically kill ovarian cancer cells in combination with salubrinal. Molecular Oncology 10, 1559-1574. PMID: 27729194

3.1. Introduction

Ovarian cancer affected 239,000 women worldwide in 2012 (Ferlay et al., 2015) and it is the leading cause of death from gynecologic cancer in the United States. Current standard-of-care for advanced-stage ovarian cancer includes debulking surgery followed by adjuvant combination chemotherapy consisting of a platinum agent and a taxane agent (Chien et al., 2013). Although the combination therapy is effective and the initial response rate is over 70%, the majority of patients with advanced disease experience recurrence (Chien et al., 2013). With subsequent re-challenge with platinum-based chemotherapy, most will acquire resistance to chemotherapy and succumb to the disease.

Therefore, it is imperative that novel therapeutic agents be developed to treat ovarian cancer and to extend the effectiveness of platinum-based chemotherapy. Recent advances in cancer therapeutics indicate that genetic defects in cancer can be exploited by synthetic lethality with chemical inhibitors. Synthetic lethality is a concept first reported in Drosophila genetics to describe the lethality of flies arising from a combination of mutations in two or more genes (Nijman, 2011). This concept was extended as an approach to target cancer-specific mutations to cause lethality in cancer cells and not in normal cells. For example, mutations in BRCA1 and BRCA2 homology recombination (HR) repair genes are common in ovarian and breast carcinomas, and cancer cells harboring these mutations are extremely sensitive to PARP1 inhibition as a result of synthetic lethality (Bryant et al., 2005; Farmer et al., 2005). Accordingly, cancer cells harboring mutations in HR repair genes can be selectively killed by PARP1 inhibitors which cause reduced toxicity to normal cells (Underhill et al., 2011).

Several studies have associated valosin-containing protein (VCP) with various cellular functions including endoplasmic reticulum-associated degradation (ERAD), Golgi membrane

reassembly, autophagy and cell division (Deshaies, 2014; Meyer et al., 2002; Seguin et al., 2014). VCP is involved in the extraction of unfolded proteins from the endoplasmic reticulum. Upon extraction, these proteins undergo proteasome-mediated degradation. Cancer cells harbor a plethora of mutations which result in an increased load of unfolded proteins required for degradation. Accordingly, VCP and components of the proteasomal degradation pathway are essential for cancer cell survival and thus present a target of vulnerability in the cancer cell that could be exploited for cancer therapy.

Several groups have recently developed specific inhibitors against VCP (Alverez et al., 2015; Alverez et al., 2016; Bursavich et al., 2010; Chou et al., 2011; Chou et al., 2014; Chou et al., 2013; Fang et al., 2015; Gui et al., 2016; Magnaghi et al., 2013; Polucci et al., 2013; Wijeratne et al., 2016), these efforts were reviewed and summarized elsewhere (Chapman et al., 2015). Among these specific inhibitors, DBeQ was initially developed as a reversible inhibitor of VCP/p97 that compromises protein homeostasis through impairment of both ubiquitin-proteasome system and autophagic protein clearance. DBeQ targets both D1 and D2 ATPase domains of VCP (Fang et al., 2015). In contrast, ML240, which was derived from the scaffold of DBeQ, targets the D2 ATPase domain (Fang et al., 2015). Another VCP inhibitor NMS-873 is a potent noncovalent, non-ATP-competitive, allosteric inhibitor of VCP and activates unfolded protein response, inhibits autophagy, and induces cell death (Magnaghi et al., 2013). Finally, a derivative of ML240 was further developed by Cleve Biosciences to produce orally bioavailable active compound CB-5083 that shows promising pre-clinical activities (Anderson et al., 2015). Consequently, CB-5083 is currently in two Phase I clinical trials (NCT02243917 and NCT02223598) sponsored by Cleave Biosciences.

Since VCP is identified as an essential gene in ovarian cancer cell lineages and also in Cyclin E1-overexpressed cisplatin-resistant ovarian cancer cell lines, we tested the potential cytotoxic activities of quinazoline-based VCP inhibitors, DBeQ, ML240, and its clinical lead CB-5083 in ovarian cancer cell lines. Moreover, we also determine the potential synergistic drug interactions between VCP inhibitors and salubrinal, an agent that enhances the expression of CHOP (also known as DDIT3, DNA Damage-Inducible Transcript 3).

3.2. Results

3.2.1 DBeQ and ML240 are effective in reducing cell viability in ovarian cancer cells

We used Sulforhodamine B (SRB) assay to determine the extent of cytotoxicity induced by DBeQ and ML240 in four ovarian cancer cell lines, namely OVCAR10, OVCAR8, SKOV3, and OVCAR5. Our results indicate that the half-maximal inhibition (GI_{50}) for DBeQ ranges from 2.6±0.9 μM – 4.6±2.01 μM; while for ML240, it ranges from 0.97±0.46 μM – 2.01±0.92 μM (Figure 3.1A-3.1C) in ovarian cancer cell lines. These results suggest that VCP inhibitors are cytotoxic towards ovarian cancer cells. ML240 displays higher levels of cytotoxicity compared to DBeQ in all the tested cell lines.

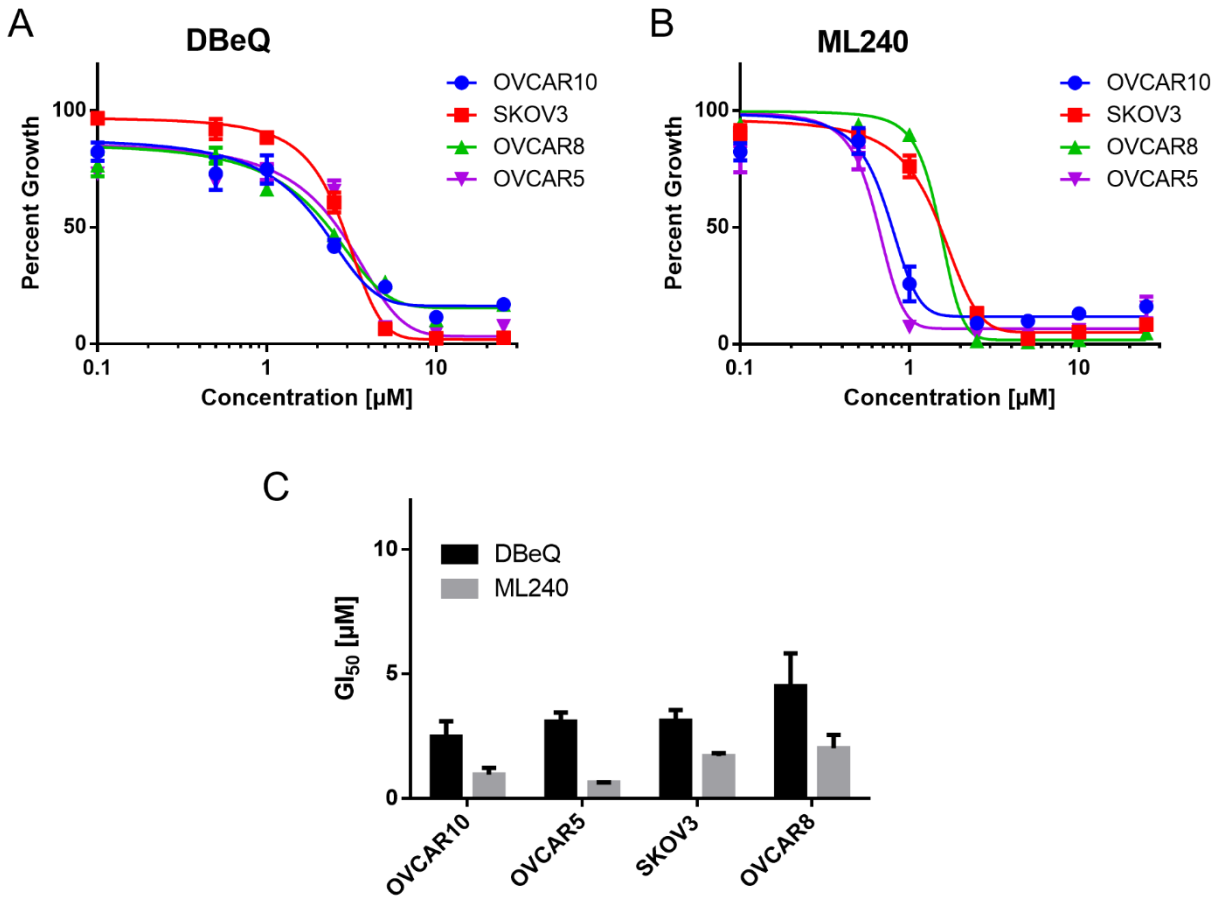

Figure 3.1. DBeQ and ML240 show increased cytotoxicity towards ovarian cancer cells. (A&B) OVCAR10, SKOV3, OVCAR8 and OVCAR5 cells were treated with vehicle (DMSO) as well as different concentrations of DBeQ and ML240 ranging up to 25 μM for 72 hours in 96-well plates. Dose-response curves were generated using GraphPad Prism using four parameters nonlinear regression (curve fit). Curves were constrained on top (100%) and bottom (less than 10%). (C) The GI_{50} for DBeQ and ML240 were shown as Mean + SEM from 3 biological replicates for all ovarian cancer cell lines. Each data point in the dose-response curve was generated from three technical replicates.

3.2.2 VCP inhibitors effectively interact and inhibit cellular VCP

Next, we compared the mean GI_{50} from several ovarian cancer cell lines with their relative VCP protein expression. A moderate positive correlation was observed between the mean GI_{50} and relative protein expression with both DBeQ (r=0.59) and ML240 (r=0.45) (Figure 3.3A, 3.3C & 3.3D). These data are consistent with the previous report indicating a positive correlation between VCP expression and GI_{50} for oral VCP inhibitor- CB-5083 (Anderson et al., 2015). Since VCP protein expression showed moderated correlation with GI_{50} for VCP inhibitors in ovarian cancer cell lines, we tested the extent to which VCP knockdown enhances the effect of VCP inhibitors. Our results indicate 50% (siVCP-1), 80% (siVCP-2), and 85% (siVCP-1+2) knockdown efficiency from three independent transient transfections (Figure 3.2A, 3.2B & 3.3B). Following transient knockdown, cells were plated for cell viability studies. Our results show a significant reduction in GI_{50} for DBeQ and ML240 following VCP knockdown (Figure 3.2C-3.2E). Moreover, VCP inhibitors display a greater reduction of GI_{50} with siVCP-2 and siVCP-1+2, consistent with higher VCP knockdown efficiencies (Figure 3.2E). These results suggest that VCP is a target of DBeQ and ML240. Furthermore, we examined cell growth following transient knockdown of VCP. Our results show a significant reduction in cell growth with siVCP-2 and siVCP1+2 (Figure 3.2F). These results provided the first functional validation of the previous studies identifying VCP as an essential gene in ovarian cancer survival (Cheung et al., 2011; Etemadmoghadam et al., 2013).

Cellular Thermal Shift Assay (CETSA) has been used as an effective tool to assess the binding of compounds to intended cellular targets. The assay analyzes the changes in the *in vitro* thermal stability of candidate cellular proteins by compounds of interest (Jafari et al., 2014). Initially, we used different temperatures following the incubation of DBeQ and ML240 for heat treatment and determined that 57^{o}C destabilized VCP (data not shown). Next, we evaluated the

thermal stability of VCP with different concentrations of DBeQ and ML240 at 57^{o}C. Here, we show a shift in the thermal stability of VCP at 57^{o}C following 2-hours incubation of cells with DBeQ and ML240 at concentrations ranging between 0.1μM- 5 μM, indicating the target engagement (Figure 3.2G-3.2H).

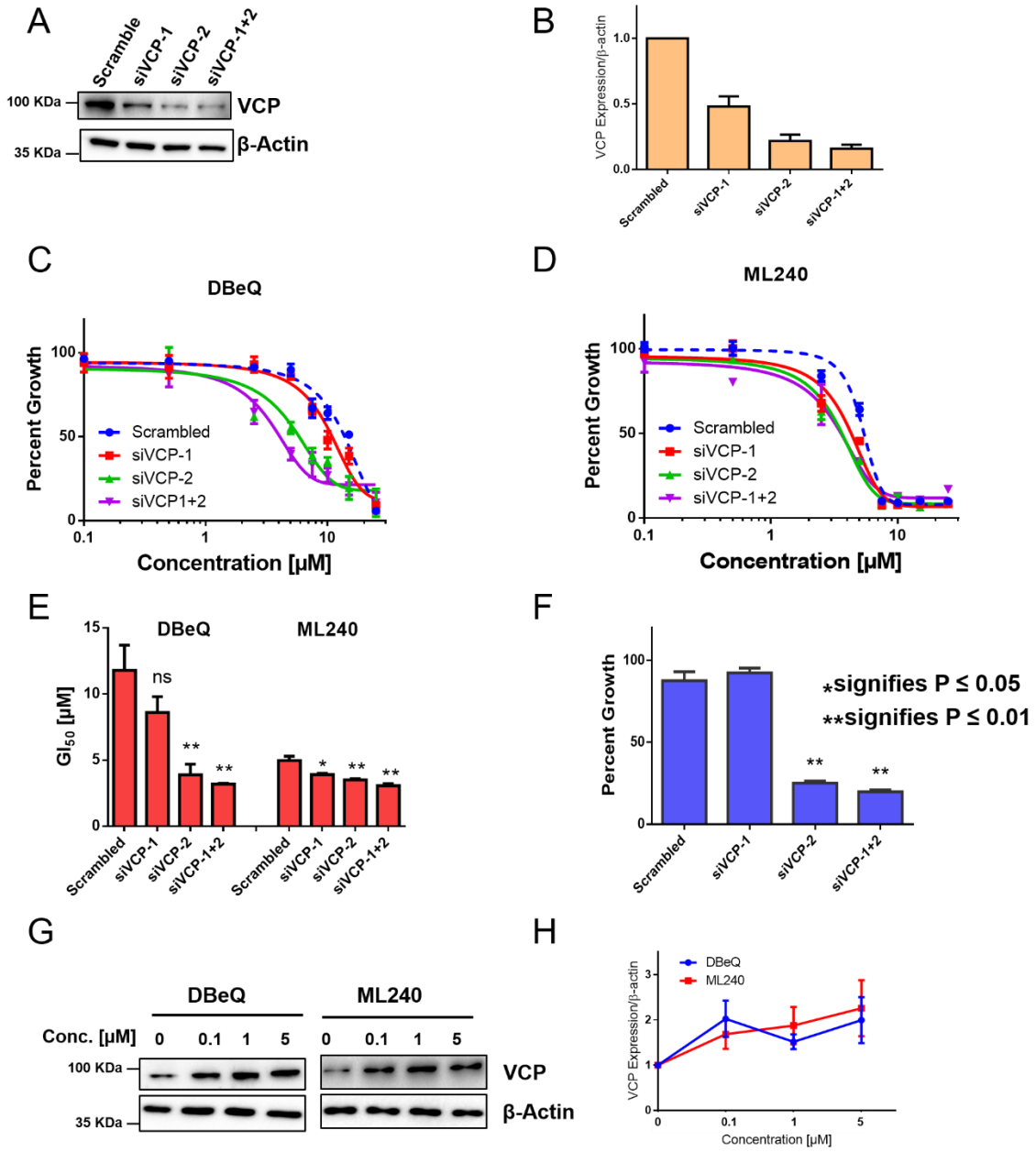

Figure 3.2. DBeQ and ML240 bind to cellular VCP/p97. (A) SKOV3 cells were transfected with two different siRNAs targeting VCP (siVCP-1 and siVCP-2), and one non-targeting scrambled small interfering RNA. Whole cell lysates following transient transfection were used to visualize the knockdown efficiencies by Western blot analysis. (B) Densitometry analysis was performed using ImageJ to observe the relative VCP expression following three independent siRNA transfections (biological replicates). SKOV3 cells transfected with scramble or VCP siRNAs were treated with different concentrations of (C) DBeQ and (D) ML240 up to 25 μM for 6 hours in 96-

well format and were allowed to recover under normal media for 6 additional days. Cell viability was measured using Sulforhodamine B (SRB) Assay. Dose-response curves were generated using GraphPad Prism using four parameters nonlinear regression (curve fit). Curves were constrained on top (100%) and bottom (less than 10%). (E) Values represent Mean + SEM GI_{50} measurements following VCP inhibition based on three biological replicates. P-values were calculated based on the student's t-test. (F) Values represent Percent growth ± SEM from three technical replicate experiments following transient knockdown of VCP followed by 6 additional days of recovery in normal media. (G) SKOV3 cells were treated with DBeQ or ML240 at concentrations between 0.1-5 µM for 2 hours. Cells were subjected to heat-shock treatment at 57°C. Soluble fractions were then subjected to Western blot analyses. (H) Values represent the relative thermal stability of VCP at 57°C at different concentrations of DBeQ or ML240 in three technical replicates.

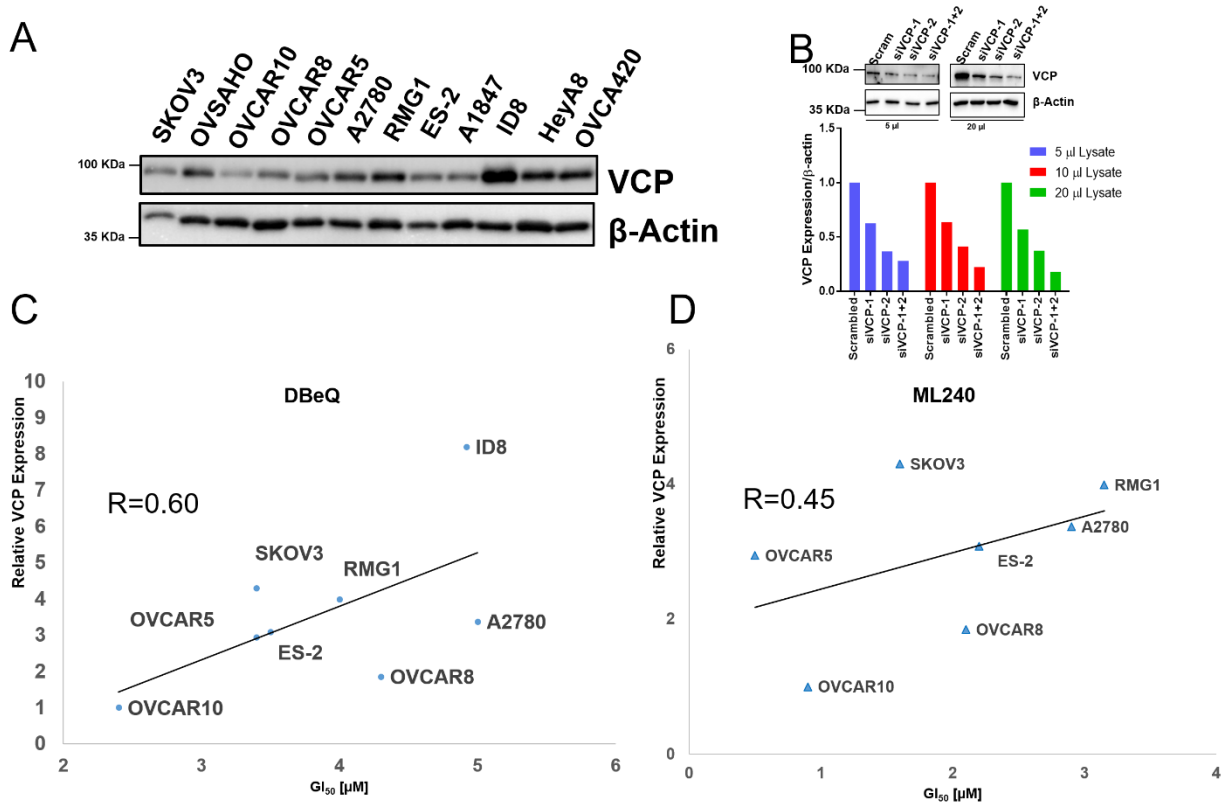

Figure 3.3. VCP protein expression correlates with VCP inhibitor cytotoxicity. (A) Whole cell lysates were generated from 12 different ovarian cancer cell lines. 40 µg of total protein from each sample was subjected to immunoblotting and probed with antibodies against VCP and β-actin. Representative immunoblot from two technical replicates. (B) Representative titration blots from Figure 3.2A generated by loading half (5 µL) and twice (20 µl) the volume of total protein loaded in Figure 3.2A (10 µL). Graphs represent relative VCP expression following transient knockdown of VCP upon loading 5 µL, 10 µL and 20 µL of whole cell lysates. Relative expression was measured using ImageJ. Graphs display the correlation between VCP protein expression and mean GI_{50} values with (C) DBeQ and (D) ML240 treatments in different ovarian cancer cell lines.

3.2.3 VCP inhibitors cause G1 cell cycle arrest

Given the well-established role of VCP in the cell cycle (Cao et al., 2003; Zhang et al., 1999), we performed cell cycle analysis to observe any changes in cell cycle distribution following the treatment with VCP inhibitors. We observed an increase in G1 and a decrease in S and G2/M phases with 5 μM DBeQ as well as an increase sub G0 phase with 10 μM DBeQ (Figure 3.4A). Similarly, we saw a reduction in S phase and an increase in sub G0 phase with ML240 treatment (Figure 3.4B). Furthermore, oral VCP inhibitor- CB-5083 treatment increased G1 and reduced S phase (Figure 3.4C). These results suggest that VCP inhibitors cause G1 cell cycle arrest followed by cell death. Next, we analyzed the expression of several cell cycle regulators that are substrates of the ubiquitin proteasome system following the treatment with VCP inhibitors. We observed variable accumulation of p21, p27, Cyclin D1, and Cyclin E with DBeQ, ML240, and CB-5083 treatments (Figure 3.4D). Overall, our results indicate that inhibition of VCP results in increased accumulation of cell cycle regulators that are substrates of the ubiquitin proteasome system.

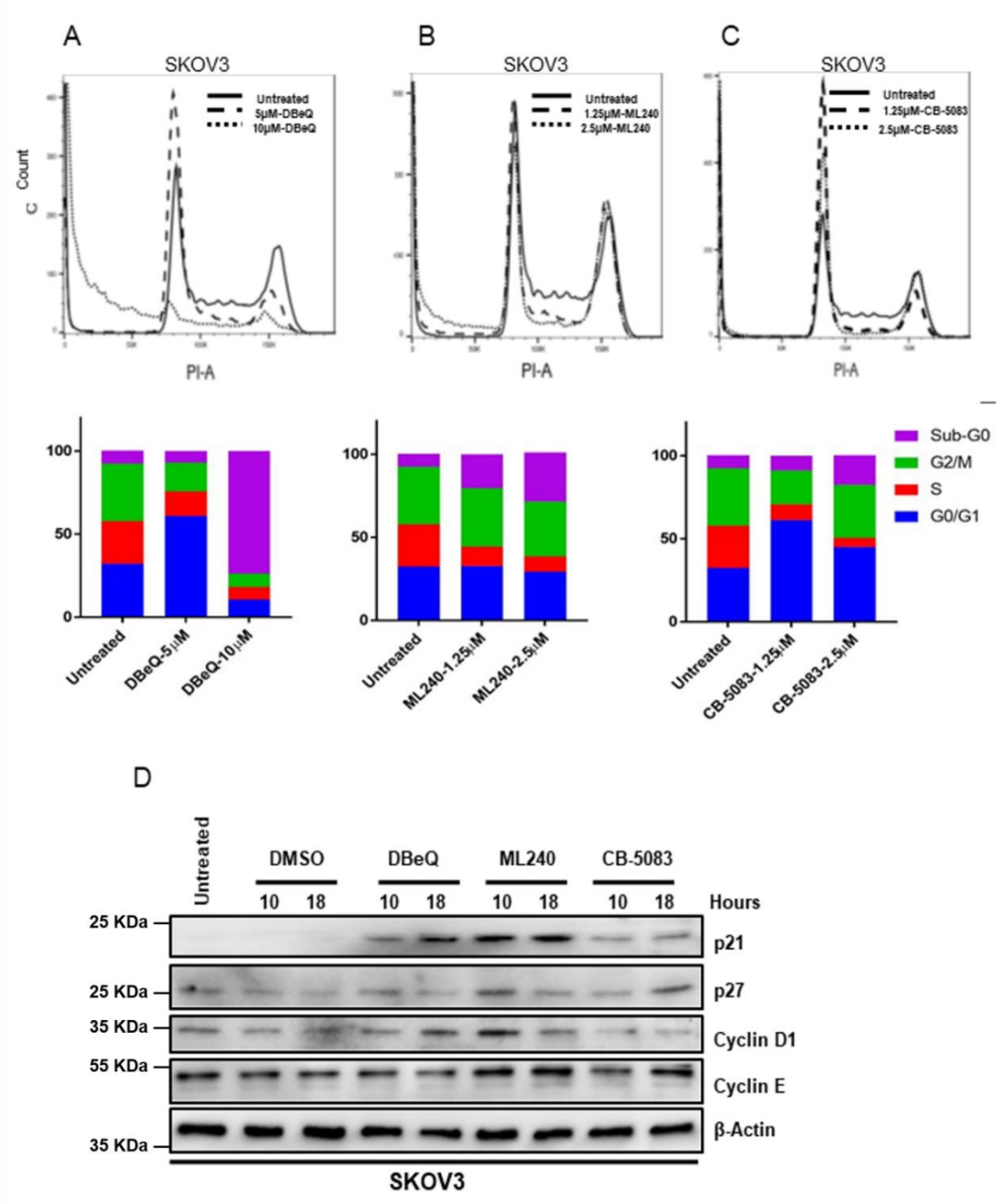

Figure 3.4. Treatment with VCP inhibitors causes G1 arrest. (A-C) Propidium iodide (PI) staining was performed on SKOV3 cells treated with DBeQ [5 μM and 10 μM], ML240 [1.25 μM and 2.5 μM] and CB-5083 [1.25 μM and 2.5 μM] for 18 hours. Bar graphs represent cells in each stage of the cell cycle following VCP inhibitor treatment for 18 hours. (D) SKOV3 cells were incubated with DMSO (vehicle), 5 μM DBeQ, 1.25 μM ML240 or 1.25 μM CB-5083 for 10 or 18 hours. Whole cell lysates were analyzed using Western blot. Representative image from at least two technical replicates for each antibody.

3.2.4 VCP inhibitors induce cell death via the apoptotic pathway

Previous studies have shown that DBeQ and ML240 induce the activation of caspases and apoptosis in non-ovarian cancer cell lines (Chou et al., 2011; Chou et al., 2013). We, therefore, analyzed the extent of apoptosis following the treatment with DBeQ or ML240 in ovarian cancer cells using Annexin V staining. We incubated SKOV3 cells with DBeQ [10 μM] or ML240 [5μM] for 6 hours followed by Annexin V and DAPI staining. Our results show a significant increase in Annexin V & DAPI positive cells following DBeQ and ML240 treatment (Figure 3.5A). Activation of procaspases is one the hallmarks of caspase-mediated apoptotic cell death. Here, we used immunoblotting to determine PARP cleavage and activation of initiator caspases as well as effector caspases. Our results indicate the PARP cleavage at 6-hour time point with DBeQ [10 μM] and ML240 [5 μM] treatment, which is consistent with the Annexin V-DAPI staining (Figure 3.5B). We also observed the cleavage of Caspase 9 and Caspase 8 following the treatment with VCP inhibitors. Caspase 9 activation was observed at a much earlier time point (6 hours) while caspase 8 activation was observed only at 24 hours following DBeQ and ML240 treatment (Figure 3.5B).

The activity of Caspase 3 was determined by the Caspase 3 activity assay. Our result indicates a significant increase in Caspase 3 activity with DBeQ [10 μM] and ML240 [5 μM] at 6-hour time point (Figure 3.5C). We observed a 2.5-fold increase in Caspase 3 activity at 24 hours with DBeQ and a 10-fold increase with ML240 (Figure 3.5C). Overall, our results are consistent with previous studies indicating caspase-mediated apoptosis by these inhibitors (Chou et al., 2011; Chou et al., 2013). Furthermore, we show that ML240 treatment results in a similar mode of cell death with higher caspase 3 activity compared to DBeQ.

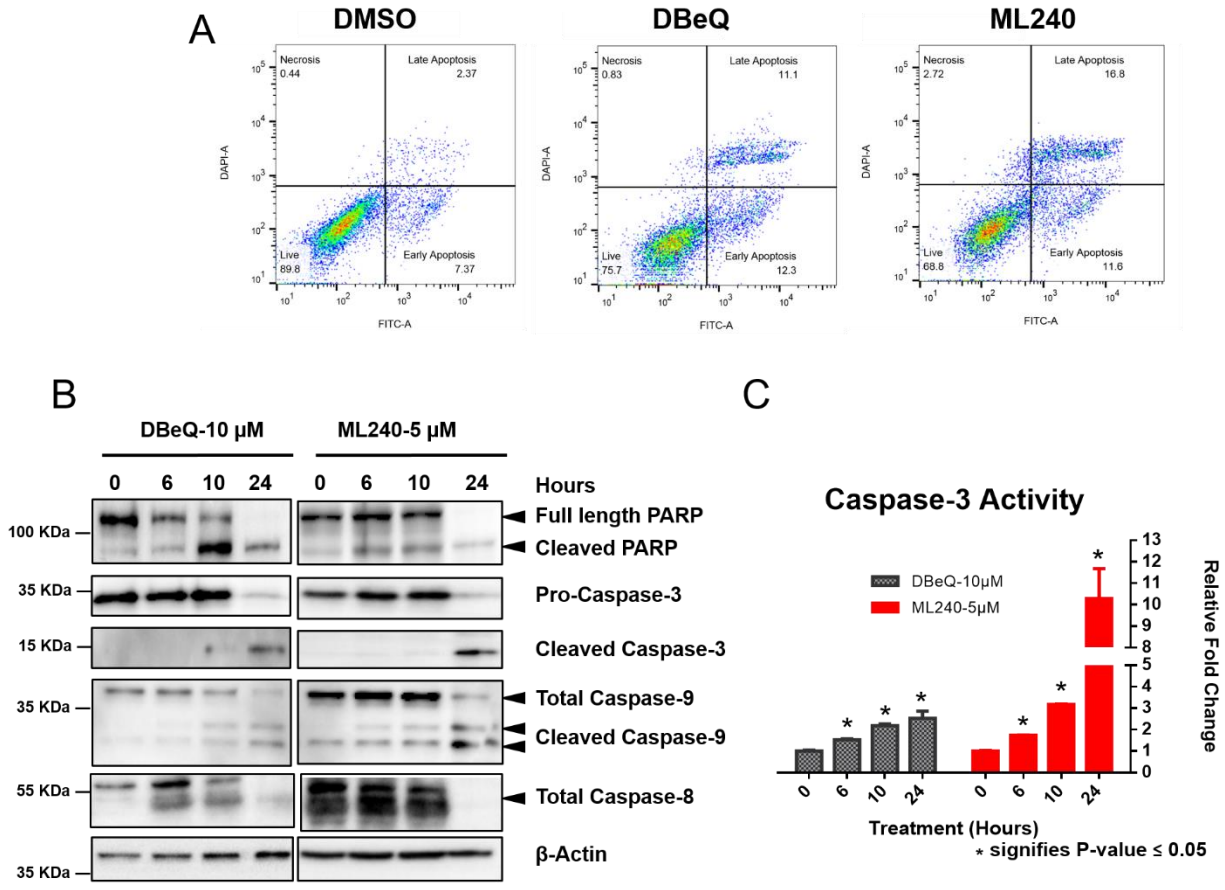

Figure 3.5. Incubation with DBeQ and ML240 induces caspase-mediated apoptosis. (A) Annexin-V/DAPI staining was performed following 6 hours of DMSO (vehicle), 10 µM DBeQ or 5 µM ML240 treatment using SKOV3 cells. (B) OVCAR10 cells were treated with 10 µM DBeQ or 5 µM ML240 for 0, 6, 10 and 24 hours. Whole cell lysates were analyzed using Western blot. Experiment B was replicated in SKOV3 cell lines. C) OVCAR10 cells were treated with 10 µM DBeQ or 5 µM ML240 for 0, 6, 10 and 24 hours. The values indicate fluorescence taken from three technical replicates. The caspase activity is represented as fold change of untreated group and plotted as Mean + SEM. P-values were calculated based on the student's t-test.

3.2.5 VCP inhibitors trigger the unfolded protein response (UPR)

Inhibition of VCP can impede the extraction of unfolded proteins from the endoplasmic reticulum (ER) and induce the unfolded protein response (UPR) (Sano and Reed, 2013). Unfolded protein response is executed via changes in three transmembrane ER proteins: IRE1α, PERK, and ATF6α (Oslowski and Urano, 2011). Previous studies have shown activation of the PERK branch with DBeQ treatment (Auner et al., 2013; Chou et al., 2011). Recently, CB-5083 treatment has been shown to activate all three branches of the unfolded protein response (Anderson et al., 2015). We decided to perform a detailed analysis comparing the effects of VCP inhibitors in the unfolded protein response pathway. SKOV3 cells were treated with DBeQ [10 μM], ML240 [5 μM] and CB-5083 [2.5 μM] up to 48 hours. Tunicamycin [2 μM], an inhibitor of N-acetylglucosamine transferase, was used as a positive control to observe the activation of the unfolded protein response. Our results indicate an increase in phospho-IRE1α by 3 hours with VCP inhibitors marking the activation of the IRE1α branch (Figure 3.6A-3.6C). We also observed an increase in the expression of CHOP and ATF4 between 3-12 hours marking the activation of the PERK branch (Figure 3.6A & 3.6C). We were unable to determine the status of the ATF6α. This lack of immunoreactivity may be due to the low basal expression of ATF6α in SKOV3 cells. Tunicamycin treatment showed a similar increase in the expression of phospho-IRE1α, CHOP, and ATF4 (Figure 3.6D). Phosphorylation of PERK upon ER stress results in the phosphorylation of eIF2α at serine 51, which has been shown to decrease cap-dependent protein translation (Harding et al., 1999). The decrease in cap-dependent protein translation reduces the protein load and allow cells to resolve ER stress (Rutkowski and Kaufman, 2004). To observe changes in cap-dependent protein translation, we treated SKOV3 cells with different concentrations of DBeQ and ML240 up to 10 μM for 5.5 hours and pulsed the cells with 1 μM puromycin for 30 minutes. Incorporated puromycin was visualized using monoclonal puromycin antibody. Results show a marked decrease

in puromycin incorporation following the treatment with VCP inhibitors (Figure 3.6E). Collectively, these results suggest that VCP inhibitors trigger the unfolded protein response through IRE1α and PERK. Similarly, increased PERK phosphorylation and poly-ubiquitination of proteins following CB-5083 treatment have been reported (Anderson et al., 2015). In line with CB-5083, treatment with DBeQ and ML240 showed enhanced accumulation of poly-ubiquitinated proteins (Figure 3.7A-3.7B).

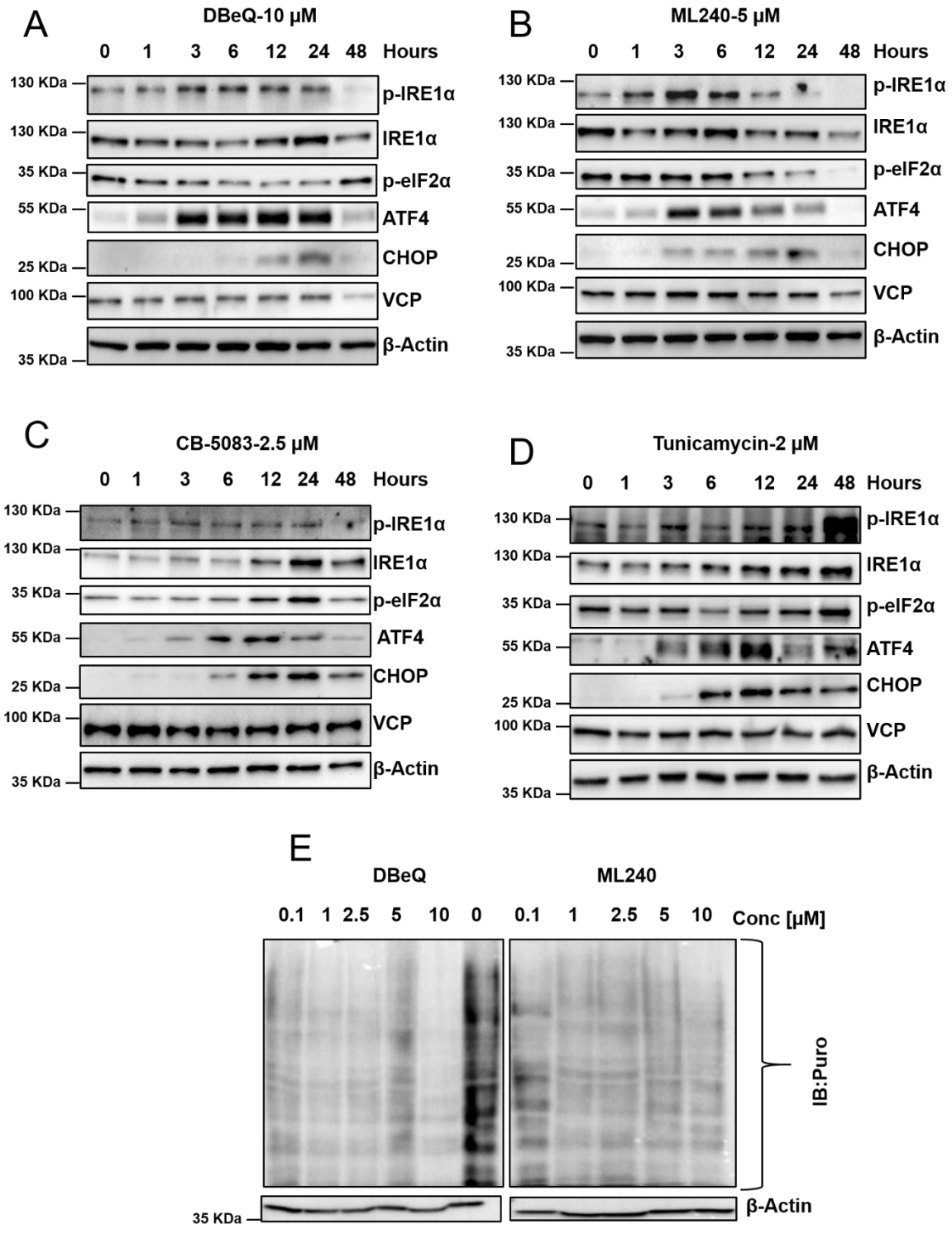

Figure 3.6. Incubation with VCP inhibitors results in the activation of unfolded protein response (UPR). SKOV3 cells were incubated with (A) 10 µM DBeQ, (B) 5 µM ML240, (C) 2.5 µM CB-5083 and (D) 2 µM Tunicamycin (positive control) for 0, 1, 3, 6, 12, 24 and 48 hours. Whole cell lysates were subjected to Western blot analysis and probed for unfolded protein

response related proteins. (E) SKOV3 cells were treated with different concentrations of DBeQ or ML240 for 6 hours and pulsed with puromycin for 30 mins. Whole cell lysates were analyzed for incorporated puromycin by Western blot. The results for both DBeQ and ML240 were obtained from the same blot that was later spliced together to remove the molecular weight marker. DMSO (0 μM) sample served as the control for both drugs. Same results were replicated using OVCAR10 ovarian cancer cell line.

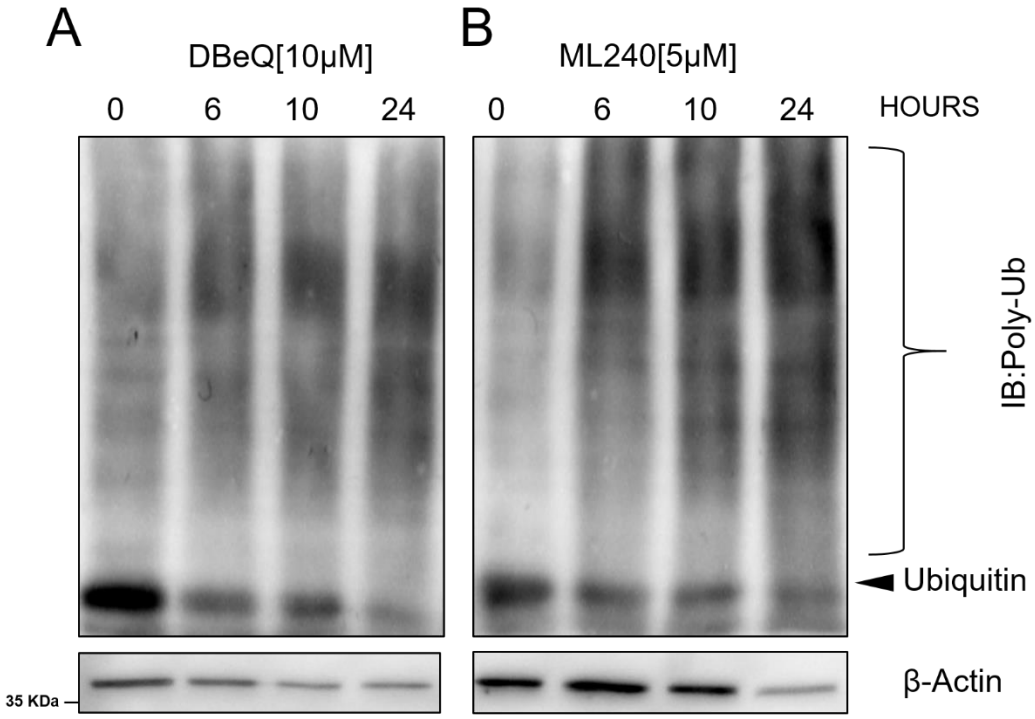

Figure 3.7. Incubation with VCP inhibitors display increased poly-ubiquitination. OVCAR10 cells were incubated with (A) DBeQ [10 μM] and (B) ML240 [5 μM] for 0, 6, 10 and 24 hours. Whole cell lysates were subjected to Western blot analysis with antibodies against ubiquitin, while β-actin was used as loading control.

3.2.6 VCP inhibitors synergize with salubrinal

Endoplasmic reticulum stress (ER stress) response is an adaptive, pro-survival mechanism; however, prolonged ER stress activates pro-apoptotic genes that contribute to cell death (Oslowski and Urano, 2011). ER stress induces CHOP expression through PERK-mediated pathway (Harding et al., 2000), and CHOP induces the expression of pro-apoptotic gene (PUMA and DR5) and decreases the expression of anti-apoptotic gene (BCL2) (Cazanave et al., 2010; Ghosh et al., 2012; McCullough et al., 2001; Yamaguchi and Wang, 2004). Therefore, we reasoned that VCP inhibitors might act synergistically with compounds that induce CHOP expression. Salubrinal, a selective inhibitor of eIF2α dephosphorylation, was first identified as a compound that reduced ER stress-induced apoptosis (Boyce et al., 2005). Since then, subsequent studies have shown that salubrinal enhances cell death via the induction of CHOP expression (Koizumi et al., 2012; Teng et al., 2014). To assess the potential synergistic effect between VCP inhibitors and Salubrinal, we investigated four high-grade serous ovarian cancer cell types namely; OVCAR10, OVCAR5, OVCAR8 and OVSAHO and two clear cell serous ovarian cancer cell types namely; RMG1 and SKOV3. These cells were treated with different concentrations of VCP inhibitors (DBeQ, ML240, and CB-5083) and Salubrinal for 72 hours. For this study, we used varying concentrations below the GI_{50} for DBeQ, ML240, and Salubrinal. For CB-5083, we used different concentrations all below the pharmacologically achievable dose (Anderson et al., 2015). Our results show synergistic effects between DBeQ and Salubrinal as well as CB-5083 and Salubrinal in all the tested ovarian cancer cell lines (Figure 3.9A-3.9B). Similar effects were observed with ML240 and Salubrinal combinations performed in OVSAHO and OVCAR8 cell lines (Figure 3.8A).

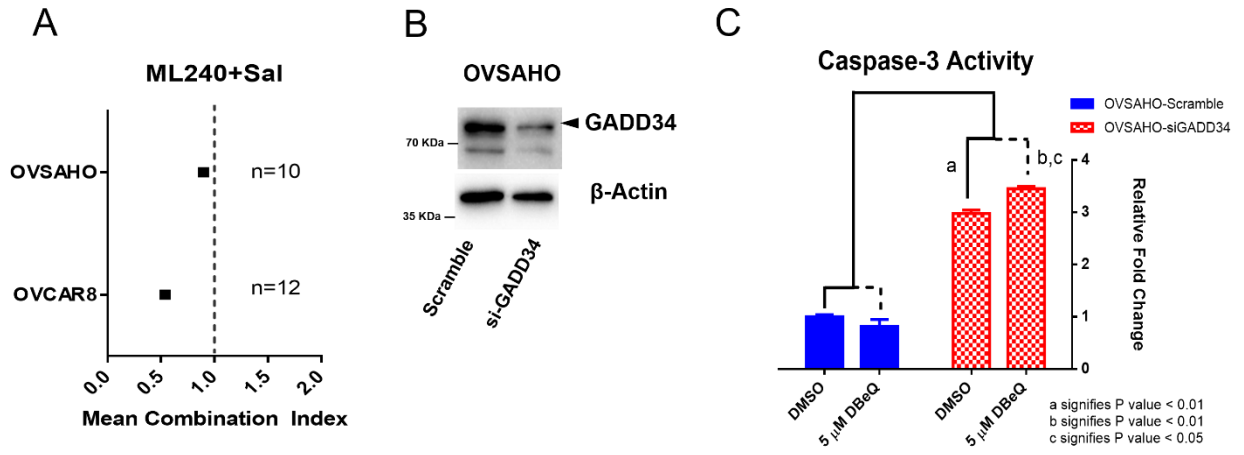

Figure 3.8. GADD34 inhibition sensitizes ovarian cancer cells towards VCP inhibitors. (A) Two high-grade serous cell ovarian cancer cell lines, OVCAR8 and OVSAHO, were incubated with different combinations of ML240 and Salubrinal. The error bars display 95% confidence interval of the mean combination index (CI) for the combinations resulting in inhibition of growth between 20-80% from two biological replicate experiments. CI values less than 1 indicate synergy while values equal to or more than 1 represent additive and antagonistic effect respectively. (B) OVSAHO cells were transfected with siRNA targeting GADD34. Whole cell lysates were collected 48 hours post-transfection and subjected to immunoblotting in order to analyze the knockdown efficiency of GADD34 siRNA. (C) Scrambled and GADD34 siRNA knockdown OVSAHO cells were subjected to 5 μM DBeQ treatment for 48 hours. The values indicate fluorescence taken from two technical replicate. The caspase activity is represented in terms of fold change and plotted as Mean + SEM. P-value is calculated based on the student's t-test. 'a' = P-value between scrambled and GADD34 knockdown cells in DMSO treatment, 'b' = P-value between scrambled and GADD34 knockdown cells in 5 μM DBeQ treatment, 'c' = P-value between DMSO treatment and 5 μM DBeQ treatment in GADD34 knockdown cells.

Next, we analyzed the short-term effect of VCP inhibitors in combination with Salubrinal. We treated OVSAHO cells with vehicle (DMSO), DBeQ, CB-5083 as well as combinations DBeQ+Salubrinal and CB-5083+Salubrinal. After treatments, cell death was analyzed using Annexin V/PI assay. With 8 hours of treatment, we observed a mean cell death of 45.56 % with DBeQ and 55.23% with DBeQ+Salubrinal (Figure 3.9C). At the same time point, we only observed a modest increase in cell death with CB-5083 as well as the CB-5083+Salubrinal treatment (Figure 3.9C). Hence, we decided to evaluate cell death with 8 hours of treatment followed by 16 hours in regular media. At 8+16 hours, our results indicate only a slight increase in cell death following Salubrinal treatment alone, while DBeQ, CB-5083 as well as their combinations with Salubrinal all resulted in a significant increase in cell death (Figure 3.9D). Together, our results indicate increased cytotoxicity with long-term (72 hours) as well as short-term (8 hours and 8+16 hours) treatment following the combination of VCP inhibitors and Salubrinal.

To further validate the results from the synergistic and cell death studies, we performed clonogenic assays in two high-grade serous ovarian cancer cell lines: OVCAR10 and OVSAHO. Clonogenic assays show a significant reduction in colony formation with the combination of DBeQ and Salubrinal as well as CB-5083 and Salubrinal further strengthening the combinational effect achieved with VCP inhibitors and Salubrinal (Figure 3.10A-3.10D). Furthermore, siRNA-mediated knockdown of GADD34 in OVSAHO cells resulted in enhanced caspase-3 activation. We observed a significant increase in caspase 3 activity only in GADD34 knockdown cells following DBeQ treatment (Figure 3.8B-3.8C). Overall, our results provide an *in vitro* proof-of-principle that inhibiting GADD34 in ovarian cancer could be one of the therapeutic strategies when developing combination therapies for VCP inhibitors.

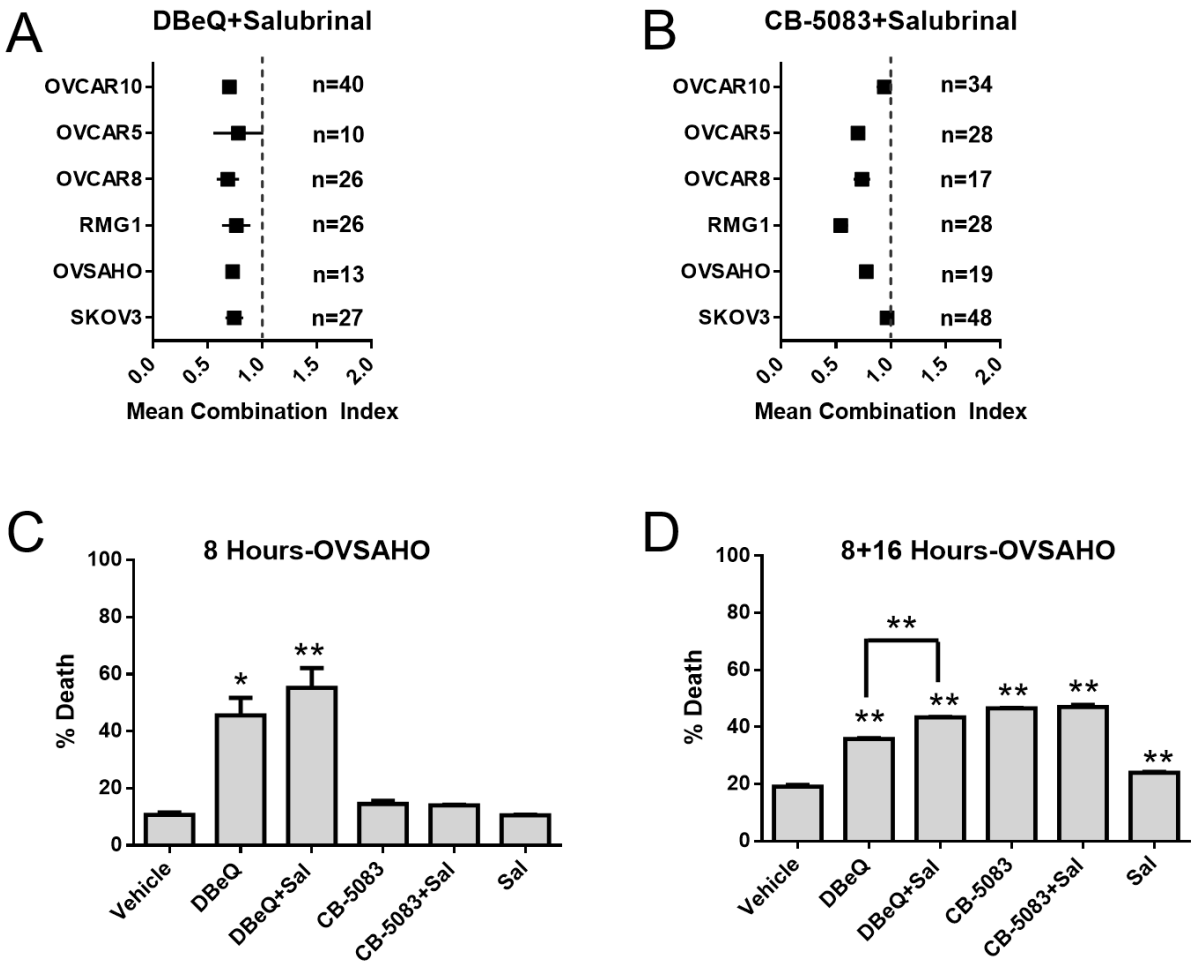

Figure 3.9. VCP inhibitors synergize with Salubrinal. Several high-grade serous ovarian cancer cell types namely; OVCAR10, OVCAR5, OVSAHO, and OVCAR8 as well as clear cell ovarian cancer cell types; SKOV3 and RMG1 were treated with different combinations of (A) DBeQ plus salubrinal and (B) CB-5083 plus salubrinal for 72 hours in 96 well format. The error bars in the figures represent 95% confidence interval of the mean combination index (CI) from 3 biological replicates with several combinations of drugs that resulted in growth inhibition between 20-80%. N represents the total number of CIs determined from 16 drug combinations in duplicates that produced 20-80% effect from three independent experiments. CI values less than 1 indicate synergy while values equal to or more than 1 represent additive and antagonistic effect respectively. OVSAHO cells were incubated with DBeQ [15 μM], CB-5083 [5 μM], salubrinal [20 μM] and combinations for (C) 8 hours and (D) 8 hours with drug followed by 16 hours in regular media. Cells were then subjected to Annexin V/PI staining and percent cell death was calculated by adding the cells in Q1, Q2 and Q4 quadrants following flow cytometry. Mean percent death ± SEM were plotted using GraphPad Prism from three biological replicate experiments and p-values were calculated using the student's t-test. Symbols '*' and '**' signify p-values less than or equal to 0.05 and 0.01 respectively.

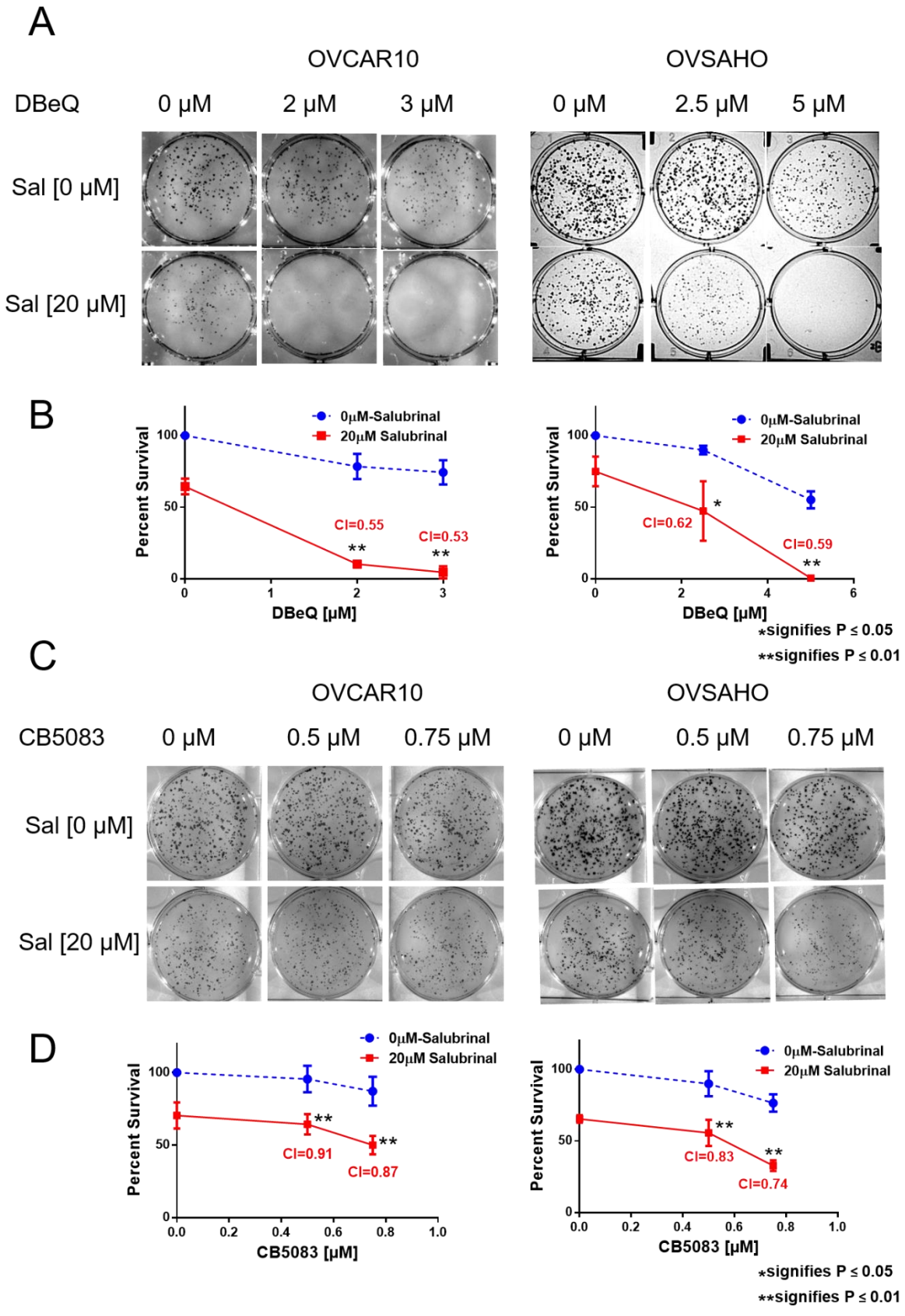
A
OVCAR10
OVSAHO
DBeQ
0 μM
2 μM
3 μM
0 μM
2.5 μM
5 μM
Sal [0 μM]
Sal [20 μM]
B
0μM-Salubrinal
20μM Salubrinal
Percent Survival
DBeQ [μM]
CI=0.55
CI=0.53
CI=0.62
CI=0.59
*signifies P ≤ 0.05
**signifies P ≤ 0.01
C
OVCAR10
OVSAHO
CB5083
0 μM
0.5 μM
0.75 μM
0 μM
0.5 μM
0.75 μM
Sal [0 μM]
Sal [20 μM]
D
0μM-Salubrinal
20μM Salubrinal
Percent Survival
CB5083 [μM]
CI=0.91
CI=0.87
CI=0.83
CI=0.74
*signifies P ≤ 0.05
**signifies P ≤ 0.01

Figure 3.10. VCP inhibitors and salubrinal combination diminishes clonogenic survival. Representative clonogenic assay performed in OVCAR10 and OVSAHO cell lines with (A) vehicle (DMSO), DBeQ, salubrinal, a combination of DBeQ plus salubrinal and (C) vehicle (DMSO), CB-5083, salubrinal, a combination of CB-5083 plus salubrinal treated for 48 hours in 6-well plates. (B&D) Percent survival based on the number of colonies formed from 3 biological replicates. Combination Indexes (CIs) were calculated using the mean number of colonies formed from three biological replicates. P-values were calculated using the student's t-test.

3.2.7 The combination of VCP inhibitors and salubrinal results in enhanced unfolded protein response

To further dissect the mechanism behind the synergistic effect observed with DBeQ and Salubrinal, we treated OVCAR10 cells with a sub-lethal dose of DBeQ [3 μM], a sub-lethal dose of Salubrinal [20 μM] and the combination of DBeQ and Salubrinal up to 48 hours. Increased expression of ATF4 and CHOP was observed within 3-6 hours in all three treatment conditions (Figure 3.11A-3.11C). We observed decreased Grp78 expression by 24 hours with DBeQ and Salubrinal alone which indicate a decrease in the endoplasmic reticulum stress response (Figure 3.11A-3.11B). However, an enhanced expression of Grp78 was observed with the combination at 24 hours indicating an increase in the endoplasmic reticulum stress response (Figure 3.11C). We also observed activation of caspase 3 (cleaved form) at 48 hours with DBeQ and Salubrinal combination suggesting that increased endoplasmic reticulum stress response triggered apoptosis (Figure 3.11C). Similarly, when lysates from different treatment conditions were analyzed, we saw enhanced CHOP expression with DBeQ and Salubrinal combination (Figure 3.11D). Taken together, these data suggest that GADD34 inhibition enhances the endoplasmic reticulum stress response induced by VCP inhibitors resulting in enhanced CHOP expression that triggers apoptosis in ovarian cancer cells.

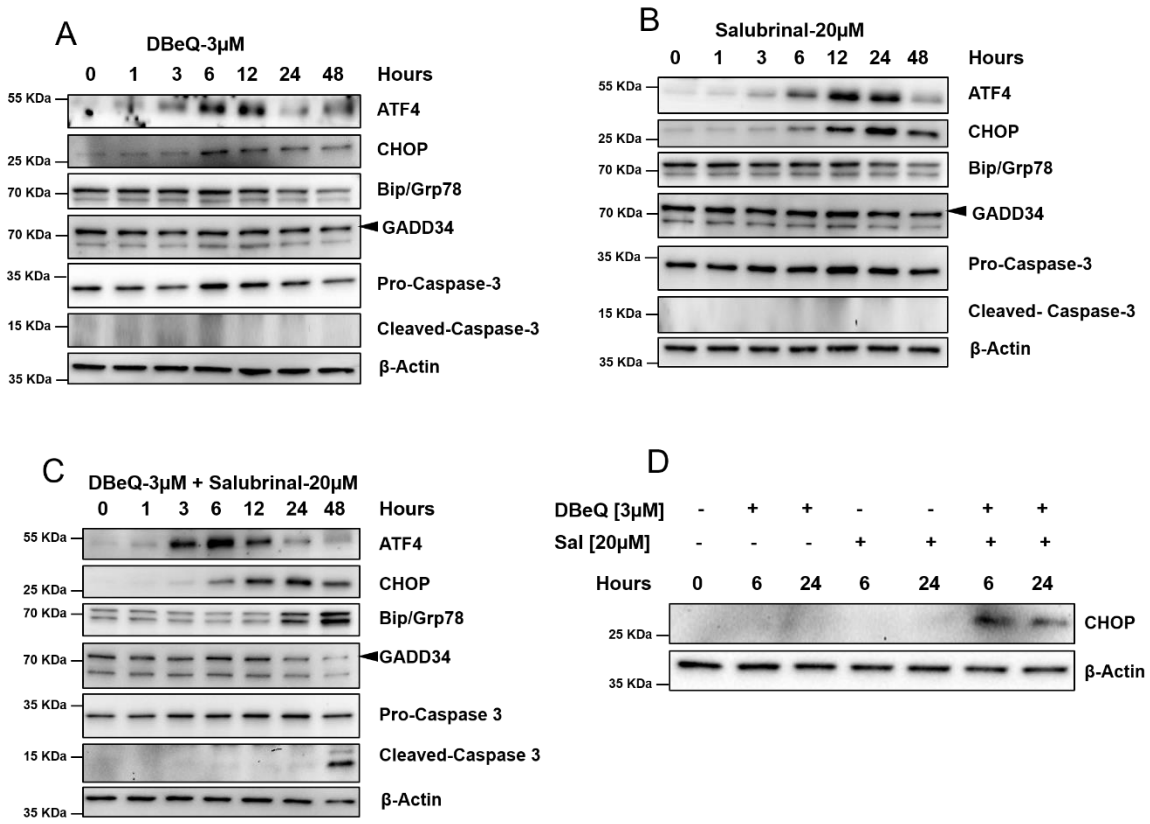

Figure 3.11. Enhanced unfolded protein response following DBeQ and Salubrinal combination results in caspase-mediated apoptosis. OVCAR10 cells were incubated with (A) sub-lethal dose of DBeQ [3 μM], (B) sub-lethal dose of salubrinal [20 μM], (C) Combination of DBeQ [3 μM] and salubrinal [20 μM] for 1, 3, 6, 12, 24, and 48 hours. Whole cell lysates were subjected to Western blot analysis and probed with the above antibodies, (D) OVCAR10 cells were treated with DBeQ [3 μM], Salubrinal [20 μM] and combination for 6 hours and 24 hours. Whole cell lysates were then subjected to immunoblotting and probed with antibodies against CHOP. β-Actin was used as a loading control. Similar results were obtained in OVSAHO ovarian cancer cell line.

3.2.8 Lower VCP expression in ovarian cancer is associated with poor outcome in patients with ovarian cancer

Since elevated expression of VCP is associated with poor prognosis in various cancer types (Tsujimoto et al., 2004b; Yamamoto et al., 2004; Yamamoto et al., 2003), we determined the association between VCP expression and clinical outcome in patients with ovarian cancer. Surprisingly, Kaplan-Meier analyses of 1648 ovarian tumor samples, provided by the online Kaplan-Meier (KM) plotter (Gyorffy et al., 2012), indicate that lower expression of VCP is associated with shorter progression-free survival (PFS) and overall survival (OS) in ovarian cancer (Figure 3.12A and 3.12B). To further understand this puzzling clinical outcome association, we analyzed the ovarian carcinoma RNA-sequencing datasets from the cancer genome atlas (Cancer Genome Atlas Research Network, 2011). We compared *VCP* gene expression in tumor samples collected from high-grade serous ovarian cancer patients that were either sensitive or resistant to the platinum-based chemotherapy. Our results show a significant reduction of *VCP* expression in tumor samples that were collected from patients with resistance to chemotherapy (p-value =0.01532) (Figure 3.12C). Taken together, these results indicate that ovarian carcinomas with lower expression of *VCP* are associated with poor response to platinum-based chemotherapy, poor progression-free survival, and poor overall survival. Although these results are in contrast to previously reported studies in other cancer types, the result is highly relevant to ovarian cancer because our results point to the clinical potential of using VCP inhibitors in the setting of platinum resistance given that these tumors have lower levels of *VCP* expression and are likely more sensitive to VCP inhibitors.

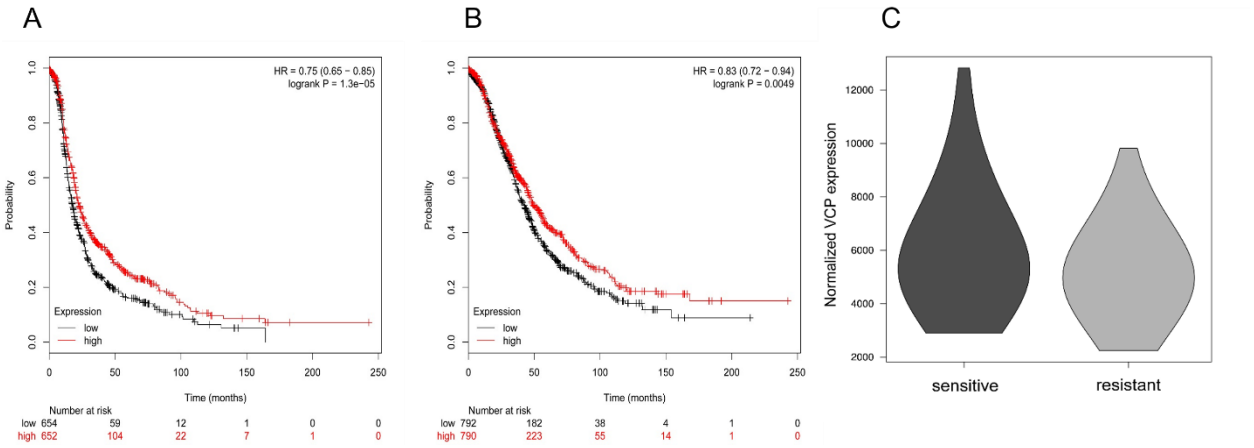

Figure 3.12. **Association between VCP expression and clinical outcome.** (A) Lower expression of VCP in ovarian carcinomas is associated with early disease recurrence (progression-free survival). (B) Lower expression of VCP in ovarian carcinomas is associated with poor overall survival. (C) RNA sequencing dataset representing high-grade serous ovarian cancer patient samples that are sensitive (n=55) and resistant (n=95) to established chemotherapy was downloaded from the TCGA Research Network Data Portal. VCP gene expression between the two datasets was compared using violin plot. p-value = 0.01532, Welch's two-sample t-test.

3.3. Discussion

In this chapter, we provided evidence that ovarian cancer cells are sensitive to VCP inhibitors. In particular, cells with lower levels of cellular VCP are more sensitive to the inhibitors. These results are consistent with prior studies indicating a strong inverse correlation between VCP expression and sensitivity to VCP inhibitors (Anderson et al., 2015). In addition, we provided evidence that VCP inhibitors interact with VCP and confer thermal stability to VCP. Collectively, these results demonstrate drug-target interactions and further support the view that lower levels of cellular VCP require a lower amount of compounds to inhibit the activity, and that on-target inhibition of VCP by these agents contributes to cytotoxicity. These results are potentially significant given that VCP expression is significantly lower in high-grade serous carcinomas collected from patients with chemotherapy-resistant ovarian cancer.

To define the molecular mechanisms associated with cytotoxicity induced by VCP inhibitors, we determined the proportion of cells in different phases of cell cycle following drug treatment. We observed that VCP inhibitors induced G1 arrest, as evident by a decrease in S-phase proportion following 18 hours of drug treatment. Subsequent to G1 arrest, we observed an increase in sub-G0 population and a concomitant decrease in G1 population, suggesting that these compounds induce cell death in the G1 population. VCP has been shown to be involved in ubiquitin-mediated degradation of cell cycle regulator Cyclin E (Dai and Li, 2001). We showed that treatment with VCP inhibitors resulted in the accumulation of Cyclin E, Cyclin D1, p21, and p27. Since we used a p53 null cell line, the accumulation of p21 was independent of p53. We observed activation of caspase-8 and caspase-9, and increased the activity of caspase-3, indicating that both extrinsic and intrinsic apoptotic pathways are activated by VCP inhibitors. These results are consistent with a recent report indicating that VCP inhibitor, CB-5083, induces cell death via DR5- and CHOP-dependent pathway (Anderson et al., 2015).

ML240 has been shown to bind selectively to the D2 domain and inhibit the D2-ATPase activity of VCP; while DBeQ inhibits the activity in both D1 and D2 domains (Chou et al., 2014). Similarly, CB-5083 which was derived from the scaffold of ML240 is a specific inhibitor of the D2 domain of VCP (Zhou et al., 2015). Our results indicate that inhibition of D2-ATPase is sufficient to cause the cytotoxic effect in ovarian cancer cells. In addition, specific inhibition of D2-ATPase domain of VCP with ML240 may be attributed to the lower GI_{50} values across all the tested cell lines.

In addition, we provided evidence that VCP inhibitors can be combined with agents that modify endoplasmic reticulum stress (ER stress) to enhance cytotoxic activities of VCP inhibitors (Figure 3.13). Our results indicate that VCP inhibitors induce the unfolded protein response and

that cytotoxicity of VCP inhibitors can be enhanced by Salubrinal, a GADD34 inhibitor that prolongs the phosphorylation of eIF2α. Although the transient phosphorylation of eIF2α is a critical adaptive response to endoplasmic reticulum stress (ER stress), resulting in a decrease in cap-dependent translation to lower protein load, sustained phosphorylation of eIF2α, in the presence of upstream ER stress, could induce CHOP and CHOP-dependent apoptosis (Marciniak et al., 2004). Consistent with this hypothesis, we observed drug synergies between VCP inhibitors and salubrinal. It is important to note that recent studies by Parzych *et al.* reported that Guanabenz, a GADD34 inhibitor, decreases cell death induced by DBeQ (Parzych et al., 2015). In our studies, we found that salubrinal, another GADD34 inhibitor, enhances the effect of DBeQ and CB-5083 in several ovarian cancer cell lines. Unlike Parzych *et al.* studies which determined the cytotoxic effect at 8 hours of treatment with one combined dose, our studies determined both the short-term and the long-term effect of the several combined doses for VCP inhibitors and Salubrinal. We observed synergistic activities of the combined drugs across several concentrations in both short-term and long-term assays in several ovarian cancer cell lines. Therefore, the differences in the outcome of these two studies may be attributable to the differences in cell models, the exposure time, and the differences in off-target effects of salubrinal and guanabenz.

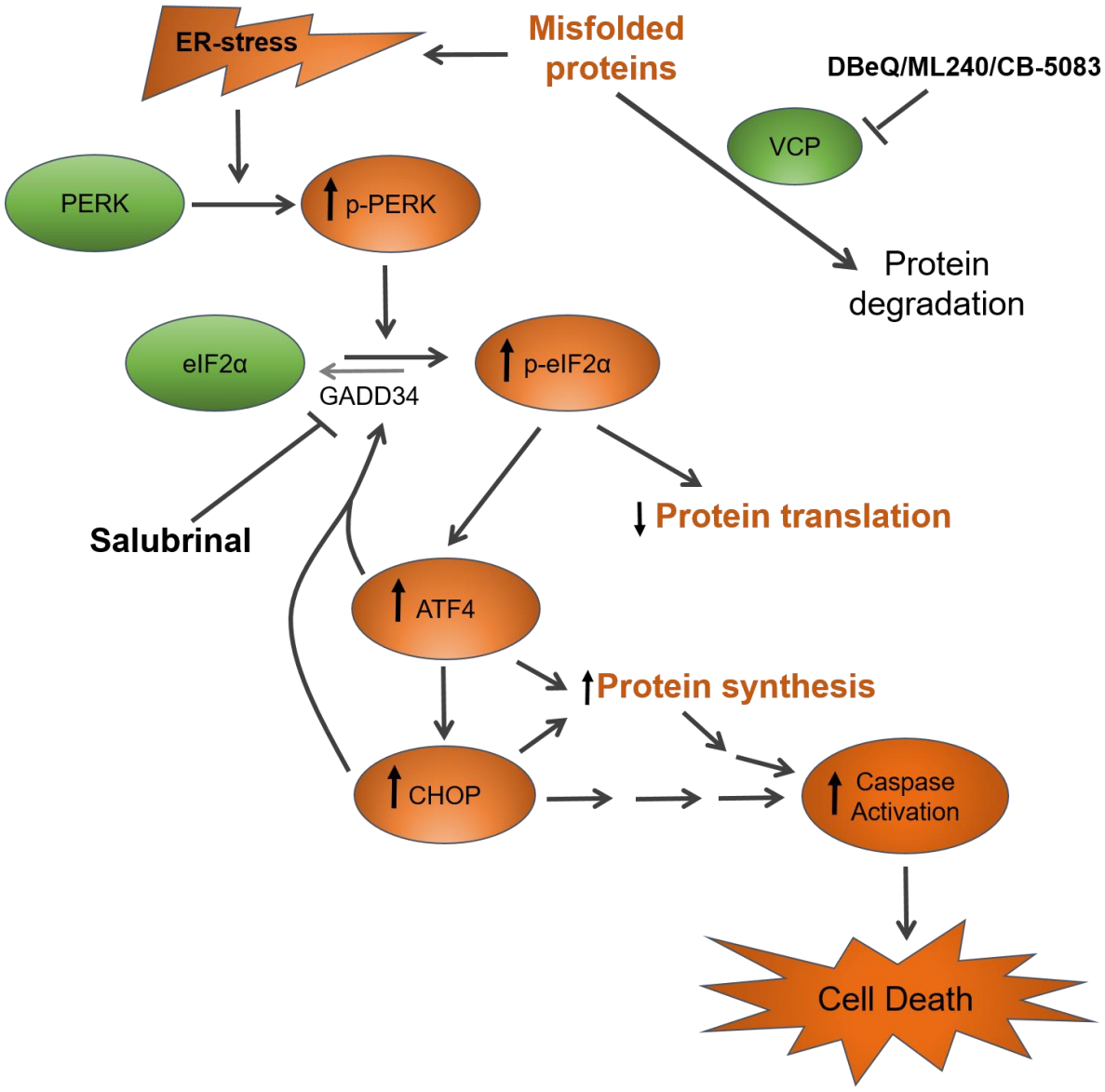

Figure 3.13. Proposed mechanism of action with the combination of VCP inhibitors and Salubrinal. DBeQ, ML240, and CB-5083 induce ER stress and activate PERK pathway. In the presence of upstream ER stress, activated by VCP inhibitors, PERK phosphorylates eIF2α and attenuates cap-dependent translation, which lower protein load to restore protein homeostasis. However, the presence of sustained ER stress (either by continuous exposure to ER stress activating agents) or unresolved ER stress (due to inhibition of GADD34 by salubrinal) can enhance or prolong the pro-apoptotic expression of CHOP and contribute to caspase-mediated apoptosis.

Prolonged endoplasmic reticulum stress (ER stress) and subsequent cell death is an important mechanism of action of drugs that target the ubiquitin-proteasome system. Bortezomib was the first compound successful in targeting the ubiquitin proteasome system in clinical settings; however, it has not been very effective against solid tumors (Huang et al., 2014). The failure to elicit similar effect has been attributed to the lack of prolonged suppression of proteasome *in vivo* in solid tumor (Deshaies, 2014). VCP inhibitors provide an exciting avenue for the development of novel chemotherapy in all tumors with enhanced unfolded protein load. In addition, identifying compounds that prolong the ER stress and enhance the cytotoxic effect of VCP inhibitors may be useful as a combination treatment strategy in solid tumors. Our results provide a proof-of-principle that VCP inhibitors and the ER stress pathways could be targeted in combination with the ER stress-prolonging agent Salubrinal for enhanced cytotoxicity.

Recently, several groups have identified the pathway involved in protein homeostasis as a target of vulnerability in ovarian cancer. For example, Cheung et al. used 102 cancer cell lines and performed genome-scale synthetic lethal screen with short hairpin RNAs (shRNAs) (Cheung et al., 2011). In this study, VCP was identified as one of the 22 putative essential genes in ovarian cancer cells. In addition, in their follow-up studies, Hahn and Bowtell groups identified VCP as one of the essential genes in Cyclin E1-overexpressing, cisplatin-resistant ovarian cancer cells (Etemadmoghadam et al., 2013). Finally, Marcotte & Brown et al. identified several components of protein homeostasis, such as SNRPD-1, PSMD1, PSMA1, PSMB2, RPS17, and EIF3B, as essential genes in several cancer cell lines (Marcotte et al., 2012). Therefore, results from our study indicating that VCP/p97, a component of protein homeostasis, can be targeted by DBeQ, ML240, and CB-5083 and that these agents induce ER stress and apoptosis in ovarian cancer cells are highly relevant for advancing VCP inhibitors as potential therapeutics for ovarian cancer.

Given that pharmacodynamics and pharmacokinetics of CB-5083, which is orally bioavailable, are already demonstrated, and that CB-5083 is well-tolerated in mice, it would be important to further develop this agent for additional preclinical and clinical studies. In addition, since VCP inhibitors induce ER stress, attenuate protein translation, increase ubiquitylation of proteins, it would be important to determine the similarity and differences in the mechanism of cell death induced by these agents compared to proteasome inhibitors, such as bortezomib. In particular, bortezomib and heat-shock protein 90 (Hsp90) inhibitors also cause proteotoxic stress, and their mechanisms of action include lowering BRCA1 expression and enhancing sensitivity to PARP inhibitors and cisplatin (Johnson et al., 2013; Neri et al., 2011; Stecklein et al., 2012). Therefore, it would be important to determine the extent to which VCP inhibitors enhances sensitivity to conventional and emerging chemotherapeutics.

Chapter 4: Atypical activation of the unfolded protein response by mifepristone enhances cytotoxicity towards VCP inhibitors

4.1. Introduction

Ovarian Cancer is the most lethal gynecological malignancy accounting for approximately 14,080 deaths in 2017. Currently, the standard treatment regimen includes surgical debulking followed by a taxane and platinum combination chemotherapy. The combination treatment regimen shows 70%-80% initial response rate (Berkenblit and Cannistra, 2005). However, upon completion of chemotherapy, half of the patients with advanced disease will experience relapse within 18-22 months of remission (Armstrong, 2002). Only a small fraction of patients with advanced disease (10-15%) achieved long-term remission with the standard chemotherapy (Armstrong, 2002). The primary cause of relapse and eventual treatment failure is the preexisting intratumor heterogeneity and cellular phenotypic plasticity driven by genetic and epigenetic alterations (Lambrechts et al., 2016). The preexisting tumor heterogeneity and plasticity at the time of treatment afford some cancer cells with proper adaptive response to chemotherapy to persist during the treatment, and these cells contribute to disease recurrence. In fact, the majority of patients who achieved a complete clinical response to the first-line chemotherapy will show residual disease on second-look laparotomy or will eventually relapse due to persistent disease (Armstrong, 2002).

After multiple rounds of chemotherapy, persistent tumor clones will expand and acquire additional genetic alterations that contribute to the acquired resistance. Therefore, it is critical to identify novel therapeutic targets and agents to treat this disease. Recently, several targeted therapies gained FDA approval in ovarian cancer. An open-labeled Phase III trial (AURELIA) evaluated the efficacy of adding bevacizumab (anti-vascular endothelial growth factor antibody) to chemotherapy in platinum-resistant ovarian cancer patients. The trial reported a significant increase in median progression-free survival (3.4 months with chemotherapy versus 6.7 months

with chemotherapy plus bevacizumab) and a non-significant increase in overall survival (13.3 months with chemotherapy versus 16.6 months with chemotherapy plus bevacizumab) (Husain et al., 2016; Pujade-Lauraine et al., 2014). Similarly, a randomized Phase III clinical trial (SOLO2), performed on platinum-sensitive relapsed patients with Breast Cancer 1, Early Onset *(BRCA1)* or Breast Cancer 2, Early Onset *(BRCA2)* mutation, analyzed the efficacy of single-agent olaparib (PARP inhibitor) versus placebo. The study reported median progression-free survival of 5.5 months for placebo versus 19.1 months for olaparib treatment in these women (Ledermann et al., 2014). These trials including other clinical trials (Ledermann, 2016; Mirza et al., 2016) paved the way for the FDA approval of bevacizumab and three PARP inhibitors, namely olaparib, rucaparib, and niraparib for the treatment of ovarian cancer. The clinical successes of these targeted therapies outline the relevance of developing novel therapeutic approaches in ovarian cancer.

Several studies have attempted to identify novel therapeutic targets and pathways in ovarian cancer. Marcotte *et al*. (2012) performed a genome-wide synthetic lethal screen with short hairpin RNAs (shRNAs) in 72 cancer cell lines, including 15 ovarian cancer cell lines. The study identified genes targeting the ubiquitin proteasome system- proteasome subunit alpha 1 (*PSMA1*) and proteasome subunit beta 2 (*PSMB2*) to be synthetically lethal (Marcotte et al., 2012). Similarly, Cheung *et al*. (2011) performed a separate genome-wide short hairpin RNA screening in 102 cell lines, including 25 ovarian cancer cell lines that identified valosin-containing protein (*VCP/p97*), an important component of protein quality control, as one of the 22 putative genes essential in ovarian cancer cells (Cheung et al., 2011). Another study identified VCP to be essential in lineage-specific cyclin E1 (CCNE1) amplified ovarian cancer (Etemadmoghadam et al., 2013).

Protein quality control includes adaptive pathways such as the unfolded protein response (UPR) and the chaperone activity of heat shock proteins (HSPs) that aid in the folding of misfolded and unfolded proteins. Additionally, protein quality control incorporates degradative pathways such as the ubiquitin proteasome system and autophagy that degrade unwanted or misfolded proteins into small peptides or individual amino acids. Oncogenic insults such as increased mutational burden, copy number alterations, chromosomal duplications/deletions and oncogene-induced oxidative stress manifest a higher burden in protein quality control, making cancer cells more reliant on these mechanisms for survival and proliferation, a phenomenon known as non-oncogenic addiction. Because cancer cells are addicted to or highly reliant on the protein quality control pathways, it is therefore imperative that targeting components of the protein quality control would be beneficial in cancer therapeutics. This idea led to the development of agents that target elements of the protein quality control mechanism for cancer therapy such as bortezomib and carfilzomib (Chen et al., 2011; Kuhn et al., 2007). Targeting protein quality control mechanisms can be extended further in designing effective drug combinations. Restorative and destructive components of the protein quality control pathway could be selectively modulated to elevate the cytotoxic effect mediated by a single agent. An example of targeting the restorative component of the protein quality control pathway includes heat-shock protein 90 (Hsp90) inhibitors. Interestingly, Hsp90 serves as a capacitor of phenotypic variations and morphologic evolution, determines the adaptive properties of genetic variations, and therefore affect the evolution of genomes (Queitsch et al., 2002; Rutherford and Lindquist, 1998). Similarly, Hsp90 expression in cancer cells is expected to modify the adaptive properties of somatic genetic variations and facilitates the evolution of cancer genomes. Therefore, targeting components of protein quality control represent a novel approach to inhibit the molecular mechanisms contributing to the

evolution of cancer genomes. In this chapter, I set out to explore the possibility of targeting multiple components of protein quality control with clinical drug candidates.

In Chapter 3, we have shown that quinazoline-based VCP inhibitors, such as DBeQ and ML240, produce dose-dependent cytotoxicity (Figure 3.1A-3.1C). Although these compounds are specific and potent VCP inhibitors, they lacked proper pharmacological properties. Using the pharmacophore from ML240, Anderson *et al*. (2015) identified an oral VCP inhibitor, CB-5083. The study reported enhanced biochemical inhibition towards VCP, increased *in vitro* cytotoxicity in several cancer types as well as pronounced *in vivo* efficacy in multiple mouse tumor xenograft models with CB-5083 (Anderson et al., 2015). The results prompted the initiation of two first-in-class Phase I clinical trials of CB-5083 in hematological cancers and solid tumors. In our current study, we investigated the *in vitro* efficacy of CB-5083 in ovarian cancer and identified new strategies to enhance the cytotoxic effect of VCP inhibitors.

To enhance the cytotoxic effect of VCP inhibitors, we decided to focus on compounds that modulate the unfolded protein response. Several inhibitors have been identified over the years that regulate specific branches of the unfolded protein response (discussed in Section 1.3.1) (Atkins et al., 2013; Papandreou et al., 2011; Ri et al., 2012). However, none of these compounds has gained FDA approval. Mifepristone (RU-486) is an FDA-approved oral progesterone receptor antagonist, and it has been used in the clinic for ending early term pregnancy. Over the years, several additionally targets for mifepristone have been identified including the glucocorticoid receptor (Baulieu, 1989) and the nuclear receptor subfamily 1 (Kretschmer and Baldwin, 2005). Multiple studies have focused on the anti-cancer effect of mifepristone in meningioma (Grunberg et al., 2006), triple negative breast cancer (Liu et al., 2016) and ovarian cancer (Goyeneche et al., 2007). Additionally, several studies have now reported that a clinically achievable dose of mifepristone

induces the unfolded protein response (Dioufa et al., 2010; Goyeneche et al., 2007; Zhang et al., 2016). However, the mechanism resulting in the induction of the unfolded protein response is unknown. Here, we show that a clinically achievable dose of mifepristone is synergistic with VCP inhibition in ovarian cancer cells. Furthermore, we report that mifepristone treatment inhibits the activating transcription factor 6 (ATF6) branch of the unfolded protein response and activates the activating transcription factor 4 (ATF4) through activation of the heme-regulated inhibitor (HRI) kinase pathway. Our results identify a plausible mechanism of the unfolded protein response with mifepristone and establish a clinically relevant drug combination based on targeting protein quality control.

4.2. Results

4.2.1 CB-5083 treatment induces cytotoxicity in ovarian cancer cells

We previously observed the dose-dependent cytotoxic effect of VCP inhibitors DBeQ and ML240 in a panel of ovarian cancer cell lines (Figure 3.1A-3.1C). However, the cytotoxic effect of the oral VCP inhibitor CB-5083 in these cells was unknown. Therefore, we performed the sulforhodamine B (SRB) assay to analyze cell viability following the treatment with incremental doses of CB-5083 up to 25 μM for 72 hours in high-grade serous ovarian cancer cell lines OVCAR10, OVCAR8, OVSAHO, and OVCAR5 as well as in clear cell ovarian cancer cell lines RMG1 and SKOV3. Consistent with other compounds in its class, CB-5083 treatment showed a dose-dependent cytotoxicity (Figure 4.1A- 4.1F) with half-maximal growth inhibition (GI_{50}) ranging from 0.46±0.07 μM to 0.94±0.23 μM (Figure 4.1G). These GI_{50} values are comparable to previously reported half-maximal growth inhibition values in the lung carcinoma cell line A459 and the colon carcinoma cell line HCT116 (Anderson et al., 2015). Our results suggest that CB-5083 can effectively inhibit *in vitro* cell growth in high-grade serous and clear cell ovarian cancer.

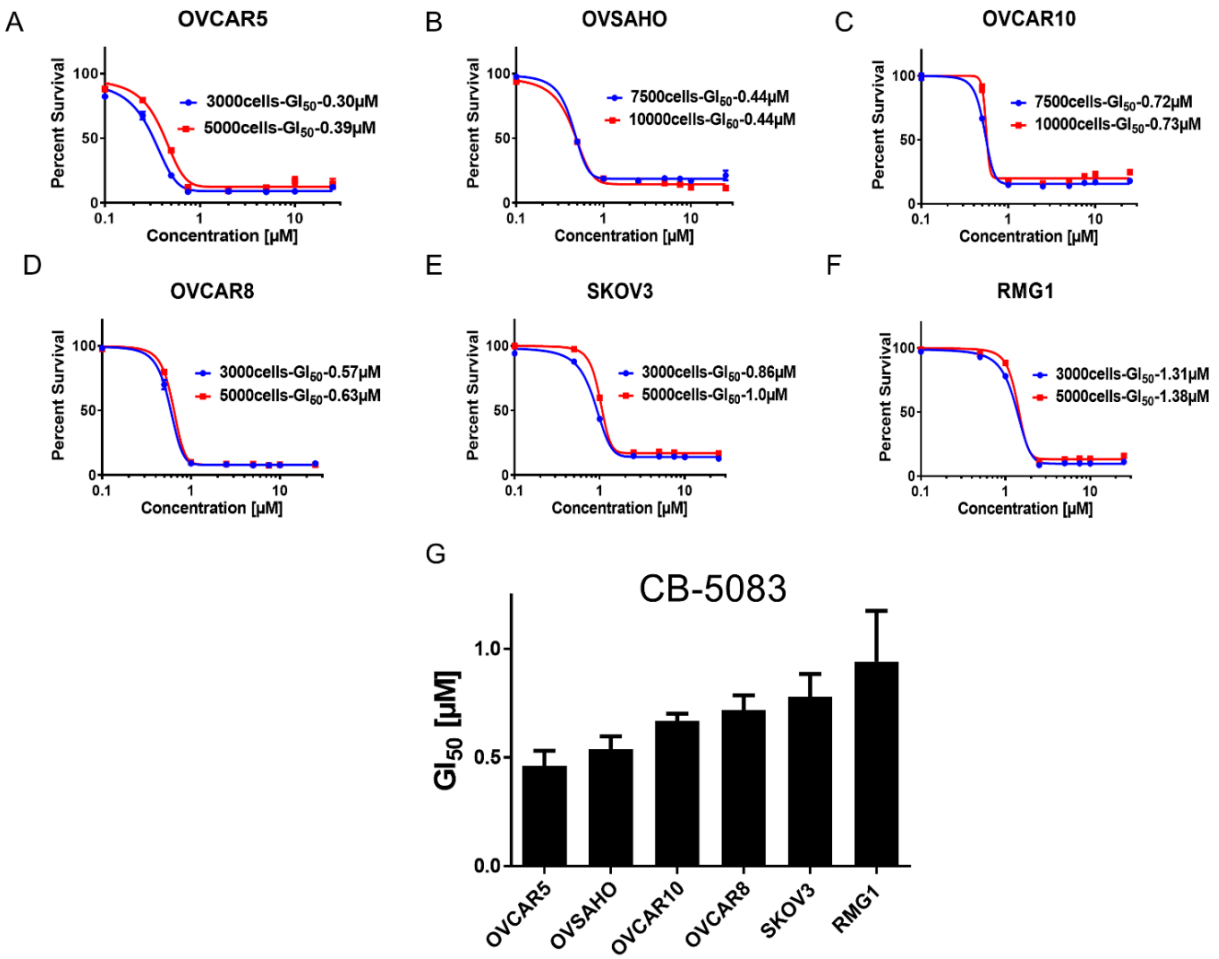

Figure 4.1. CB-5083 treatment is cytotoxic in ovarian cancer cell lines. (A-F) Ovarian cancer cells lines, namely, OVCAR5, OVSAHO, OVCAR10, OVCAR8, SKOV3, and RMG1 were treated with increasing doses of CB-5083 ranging from 0.1 μM to 25 μM for 72 hours. Dose-response curves were generated using GraphPad Prism based on the four parameters nonlinear regression. The curves were constrained at the top (100%) and the bottom (>0%). Every point in the dose-response curve represents Mean ± SEM taken from three technical replicates for all cell lines. (G) The bar graph represents Mean GI_{50} + SEM taken from four biological replicates in all cell lines.

4.2.2 VCP inhibitors show synergistic cytotoxicity with clinically achievable doses of mifepristone

Treatment with VCP inhibitors results in the induction of the unfolded protein response-mediated apoptosis (Anderson et al., 2015). Hence, we attempted to identify compounds that could produce synergistic cytotoxic effects with VCP inhibitors so that these compounds could be considered as potential clinical candidates for combination therapy with VCP inhibitors. In Chapter 3, we reported that inhibition of Growth Arrest and DNA Damage-inducible 34 (GADD34) by salubrinal results in synergistic cytotoxicity with VCP inhibitors, including CB-5083, in several ovarian cancer cell lines. Although the demonstration of synergy between VCP inhibitors and salubrinal provided proof-of-concept that multiple agents inhibiting the protein quality control pathway can be combined to achieve synergy, the clinical relevance is not prominent because salubrinal is not a clinical candidate. Several studies have now indicated that treatment with mifepristone (RU-486), an anti-progesterone receptor inhibitor, results in the induction of the unfolded protein response (Dioufa et al., 2010; Zhang et al., 2016); however, the molecular mechanism contributing to the unfolded protein response by mifepristone is not well characterized. Given that mifepristone is an FDA-approved drug, we decided to test the potential synergistic cytotoxicity between CB-5083 and mifepristone and to investigate the molecular mechanisms contributing to a potential synergy.

We performed sulforhodamine B (SRB) assays in the panel of ovarian cancer cell lines tested in Figure 4.1 with clinically achievable concentrations of CB-5083 (0.1 μM - 1 μM) and mifepristone (5 μM - 20 μM). Our results indicate that most cell lines show a synergistic effect between these two compounds (Figure 4.2A). The synergistic effects were also observed when CB-5083 was substituted with other VCP inhibitors DBeQ and NMS-873 suggesting that mifepristone enhances the cytotoxic effect of VCP inhibitors in ovarian cancer cells (Figure 4.2B-

4.2C). RMG1 cells showed the strongest synergistic effects among the cell lines we tested, hence we used this cell line for subsequent studies to investigate the molecular mechanisms contributing to the synergistic effect produced by CB-5083 and mifepristone.

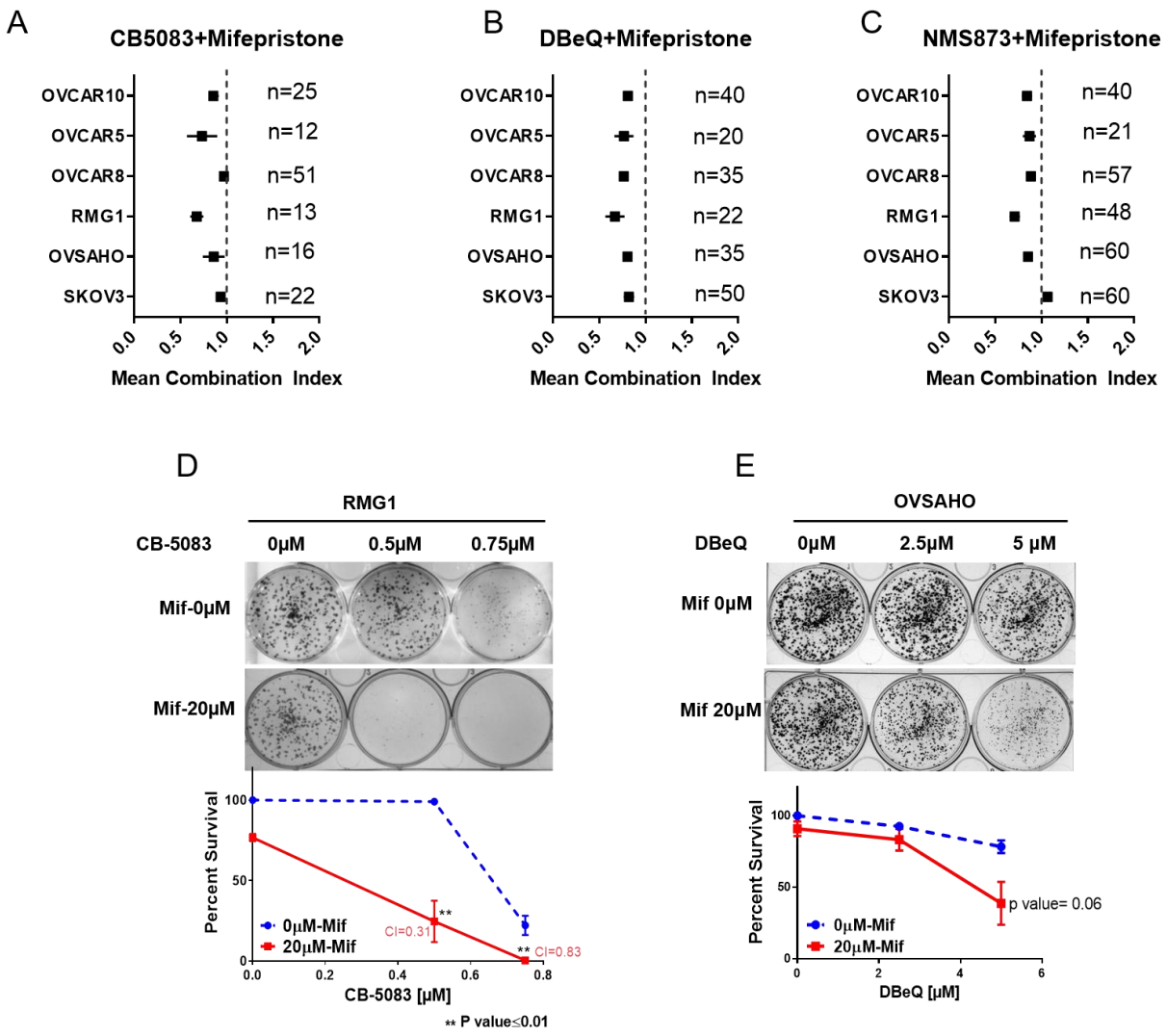

Figure 4.2. Mifepristone produces synergistic cytotoxicity with VCP inhibitors. A) High-grade serous ovarian cancer cell lines OVCAR10, OVCAR5, OVCAR8, and OVSAHO as well as clear cell ovarian cancer cell lines RMG1 and SKOV3 were treated with different combinations of mifepristone (between 5-20 μM) and CB-5083 (between 0.25-1 μM). Combination indexes (CIs)

were calculated at all such combinations that yielded an effect between 20-80%. Each data point is shown as the mean CI of all calculated combinations and 95% confidence interval. "n" represents a total number of CIs calculated from the combinations that produced the combined effect of 20-80% from three biological replicates. Mean combination index (CI) less than 1 indicates synergy. B) Same as A, but treated with different combinations of mifepristone (between 5-20 μM) and DBeQ (between 1-7.5 μM). C) Same as A, but treated with different combinations of mifepristone (between 5-20 μM) and NMS-873 (between 1-2.5 μM). (D) For the colony formation assay, RMG1 cells were treated with the indicated concentrations of CB-5083 and mifepristone for 48 hours followed by 6-8 days of recovery in regular media. Mean percent survival ± SEM was calculated based on a number of colonies from three biological replicates. (E) Similarly, OVSAHO cells treated with indicated concentrations of DBeQ and mifepristone for 48 hours followed by 6-8 days of recovery in regular media. Percent survival was calculated based on the number of colonies from three biological replicates. P values were calculated using the two-tailed student's t-test.

To further corroborate our synergistic studies, we performed colony formation assays in RMG1 cells treated with vehicle (DMSO), CB-5083, mifepristone, or the combination of CB-5083 and mifepristone. Our results indicate that single-agent treatment with 0.5 μM CB-5083 or 20 μM mifepristone only shows a modest reduction in colony formation, while the combined treatment significantly suppresses colony formation (Figure 4.2D). Similar results were observed with 0.75 μM CB-5083 and 20 μM mifepristone (Figure 4.2D) as well as with the combination of DBeQ and mifepristone (Figure 4.2E). To understand the potential mechanism of cell death with CB-5083 and mifepristone, we treated RMG1 with vehicle (DMSO), single agents CB-5083 or mifepristone, or the combination of CB-5083 and mifepristone for 12 hours or 24 hours. We observed a reduction in full-length PARP and total caspase 3 starting at 12 hours as well as a robust induction of cleaved caspase 3 at 24 hours (Figure 4.3A). Similarly, caspase activity assays showed a threefold increase in activity at 18 hours with the combination of CB-5083 and mifepristone (Figure 4.3C). These results indicate that the combination is significantly more effective in inducing caspase-mediated cell death than a single agent.

Given that both CB-5083 and mifepristone have been shown to induce the unfolded protein response, we decided to check two prominent unfolded protein response markers, namely glucose-regulated protein 78 (Grp78) and C/EBP homologous protein (CHOP) and a marker of proteasome inhibition poly-ubiquitinated proteins. We expected the combination to show an increase of both unfolded protein response markers and poly-ubiquitin. We observed a robust induction of both Grp78 and CHOP in cells treated with the combination or CB-5083 alone but not in cells treated with mifepristone alone (Figure 4.3A-4.3B). Moreover, we observed cleaved caspase 3 in cells treated with the combination but not in cells treated with a single agent. Consistent with previous studies, we observed the increase in poly-ubiquitinated proteins following CB-5083 treatment (Anderson et al., 2015). At the tested concentration, mifepristone by itself did not affect the levels of poly-ubiquitinated proteins but attenuated the levels of poly-ubiquitinated proteins induced by CB-5083. Therefore, we concluded that mifepristone modulates the unfolded protein response, but it has no effect on the ubiquitin proteasome system.

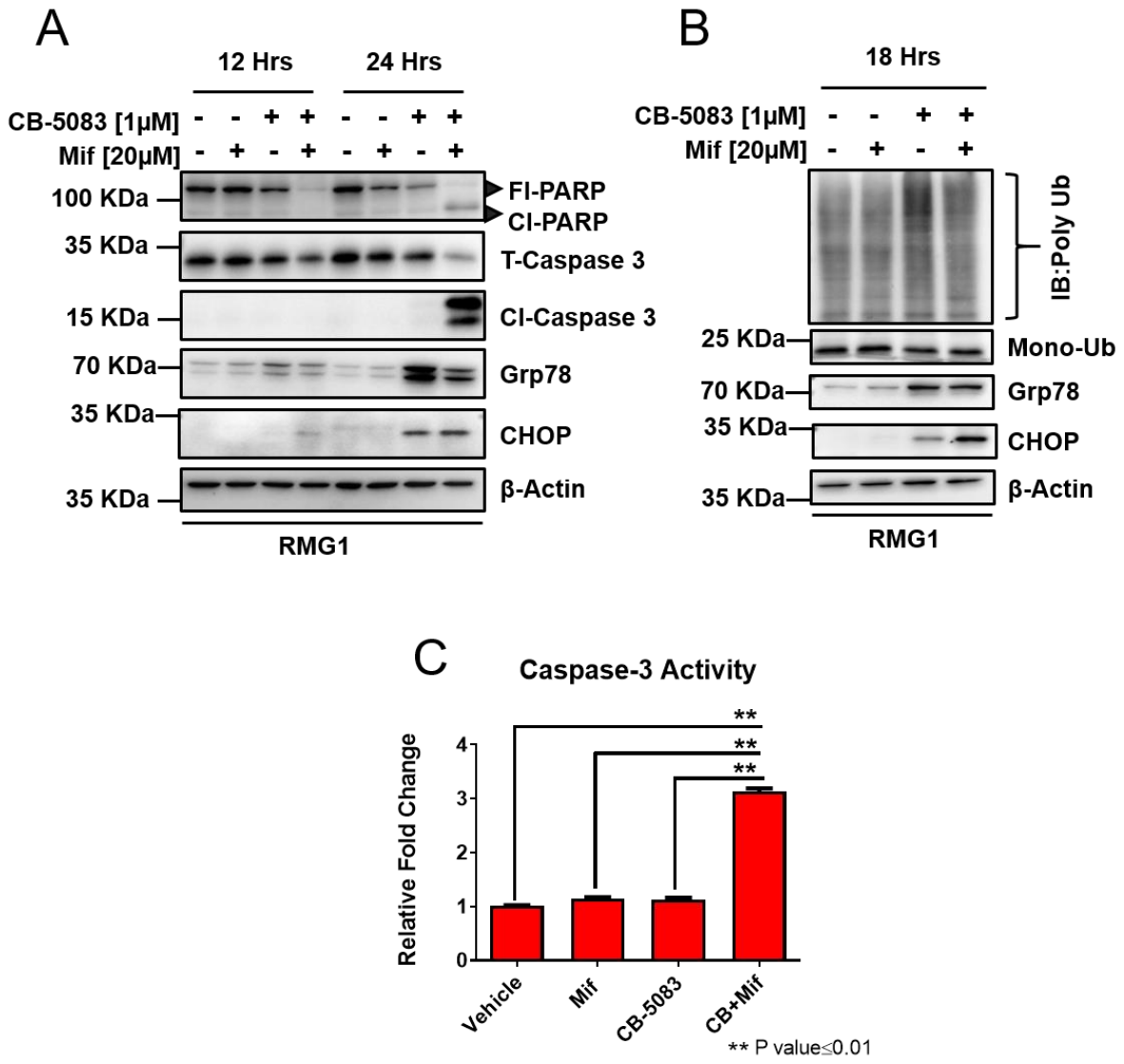

Figure 4.3. CB-5083 and mifepristone combination results in apoptosis. (A) RMG1 cells were incubated with vehicle (DMSO), CB-5083 (1 μM), mifepristone (20 μM) and combination (CB-5083 and mifepristone). Cells were harvested at 12 and 24 hours. Whole cell lysates were subjected to immunoblots and probed with the indicated antibodies. (B) Whole cell lysates were collected after 18 hours of treatment, subjected to immunoblot, and probed with the indicated antibodies. (C) 20 μg of total protein from each sample was subjected to caspase activity assay. The bar graph represents relative activity at each condition relative to vehicle (DMSO) treatment from two biological replicates. P values were calculated using the two-tailed student t-test. Similar results were reproduced using ID8 mouse ovarian cancer cell lines.

4.2.3 Mifepristone treatment shows atypical modulation of the unfolded protein response

To investigate the effect of mifepristone on the unfolded protein response, we first incubated RMG1 cells with a clinically achievable dose of mifepristone (20 μM) and harvested cells at different time-points between 1-24 hours. Similarly, we harvested samples incubated with different doses of mifepristone (5-80 μM) for 18 hours. Subsequently, whole cell lysates were tested with antibodies against all three branches of the unfolded protein response. 20 μM mifepristone treatment did not show any difference in full-length ATF6 (ATF6-FL) (Figure 4.4A-4.4B). High doses of mifepristone (40 μM - 80 μM) do seem to decrease the expression of full-length ATF6; however, this may be due to cell death observed at these high doses when treated for 18 hours (Figure 4.4B). Hence, we performed cell viability assays in RMG1 to calculate half-maximal growth inhibition (GI_{50}) upon mifepristone treatment. GI_{50} values for mifepristone were 26.4 μM and 27.9 μM (Figure 4.4C).

Next, with 20 μM mifepristone treatment, we observed an induction of ATF4 at 24 hours and slight inhibition of p-IRE1α starting at 1 hour (Figure 4.4A). In Figure 4.4B, induction of ATF4 was observed starting at 20 μM followed by CHOP induction at 40 μM. We observed a robust inhibition of p-IRE1α and induction of total IRE1α with increasing dose of mifepristone (Figure 4.4B). In both these experiments, we were unable to detect the induction of Grp78 by mifepristone (Figure 4.4A & Figure 4.4B).

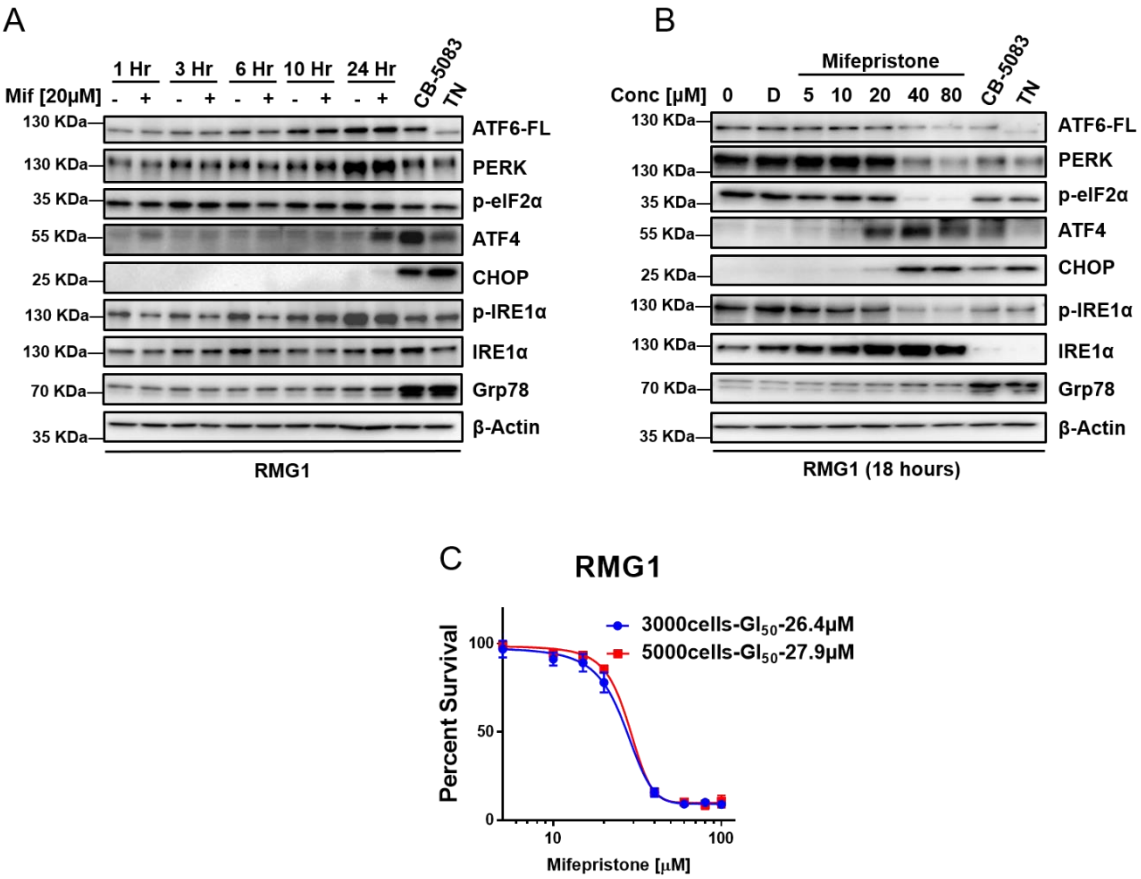

Figure 4.4. Mifepristone shows atypical modulation of the unfolded protein response. A) RMG1 cells were incubated with vehicle (DMSO) or 20 μM of mifepristone and samples were harvested at 1, 3, 6, 10 and 24 hours. Whole cell lysates were subjected to immunoblotting and probed with the antibodies for several proteins in the unfolded protein response pathway. 2.5 μM of CB-5083 and 2 μM of TN (Tunicamycin) treated for 24 hours were analyzed as positive controls. β-Actin was used a loading control. B) RMG1 cells were incubated with media (0), DMS0 (D), different doses of mifepristone (between 5 μM - 80 μM), 2.5 μM of CB-5083 and 2 μM of tunicamycin (TN). All samples were incubated for 18 hours, and protein lysates were immunoblotted with several antibodies for proteins in the unfolded protein response pathway. β-Actin was used a loading control. Both A&B experiments were reproduced at least in two biological replicate experiments. C) RMG1 cells were treated with incremental doses of mifepristone up to 100 μM for 72 hours. Dose-response curves were generated with the GraphPad Prism using four parameters nonlinear regression and the curves were constrained at top (100%) and bottom (>0%). Every point in the dose-response curve represents Mean ± SEM taken from three technical replicates.

Expression of Grp78, an ER chaperone protein, increases upon the induction of unfolded proteins via the activity in IRE1 branch and ATF6 branch of the unfolded protein response. The induction of Grp78 serves as an adaptive response to aid in the folding of misfolded and unfolded protein in the endoplasmic reticulum allowing cells to resolve the unfolded protein response. Therefore, we reasoned that mifepristone may be exerting an inhibitory effect on IRE1 or ATF6 branch (or both), which would inhibit the expression of Grp78 and attenuate the adaptive response when it is combined with VCP inhibitors, thereby resulting in enhanced cytotoxicity. To test the potential inhibitory effect of mifepristone on IRE1α, we treated RMG1 cells with increasing dose of mifepristone combined with 2 μM tunicamycin, an N-linked glycosylation inhibitor, to robustly induce all three branches of the unfolded protein response. As our control, we performed a similar experiment with STF-083010 (IRE1α inhibitor). Our results indicate that both mifepristone and STF-83010 caused a dose-dependent attenuation of Grp78 (Figure 4.5A-4.5B). Although increasing doses of STF-083010 caused a dose-dependent attenuation of spliced XBP1 (XBP1s), the expression of spliced XBP1 did not change with mifepristone treatment (Figure 4.5A-4.5B). Next, we treated RMG1 cells with increasing doses of CB-5083 (between 1 - 2.5 μM) for 6 hours. We observed an increased in spliced XBP1 (s-XBP1) expression starting at 2.5 μM of CB-5083 (Figure 4.5C). Once again, we did not observe the attenuation of spliced XBP1 (s-XBP1) with the addition of 20 μM mifepristone (Figure 4.5C). These results indicate that mifepristone does not block the endonuclease activity of IRE1 kinase.

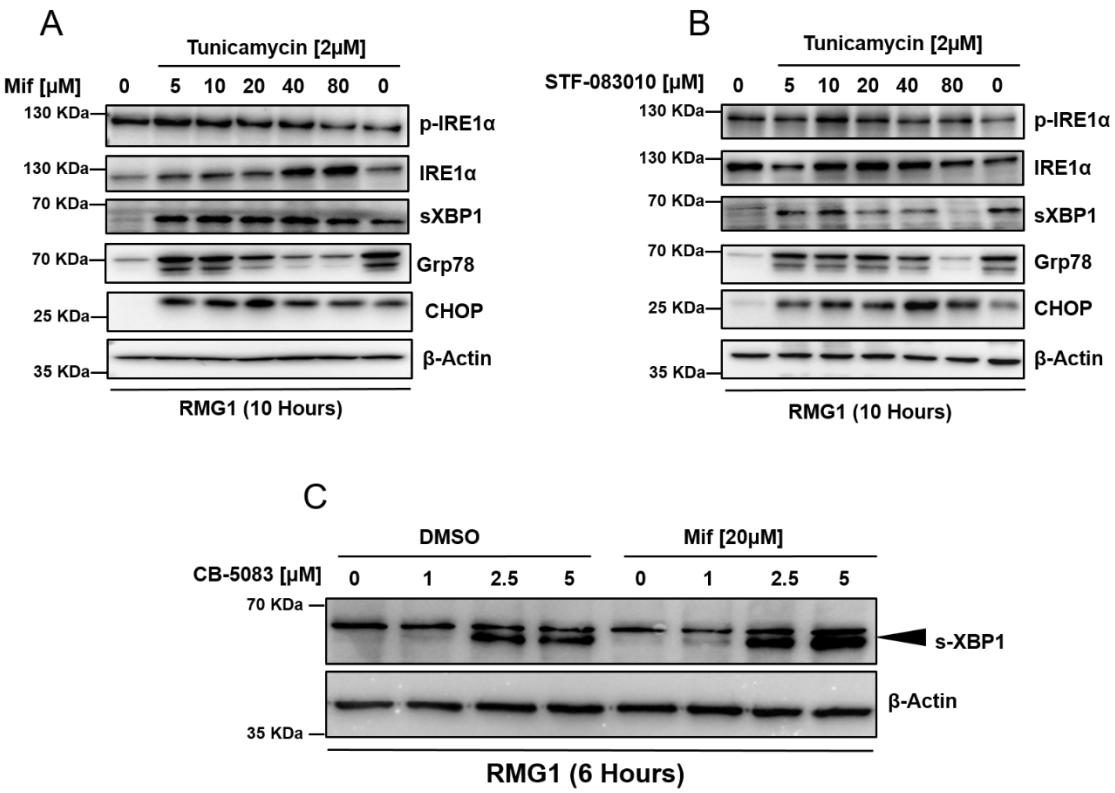

Figure 4.5. Mifepristone treatment does not inhibit IRE1α endonuclease activity. A) RMG1 cells were incubated with increasing doses of mifepristone (5 μM – 80 μM) with 2 μM of tunicamycin for 10 hours. Cells were harvested and proteins were subjected to immunoblotting to analyze the indicated proteins. B) RMG1 cells were incubated with increasing doses of IRE1α inhibitor- STF-083010 (5 μM – 80 μM) with 2 μM of tunicamycin for 10 hours. C) RMG1 cells were incubated with increasing doses of CB-5083 (1 μM – 5 μM) with or without mifepristone (20 μM) for 6 hours. Cells were harvested and proteins were subjected to immunoblotting to analyze the indicated proteins. β-Actin was used a loading control. All experiments were performed in three biological replicates.

Mifepristone (RU-486) was developed as an anti-progesterone inhibitor and later it was shown to be a potent inhibitor of glucocorticoid receptor. To investigate the potential role of progesterone and glucocorticoid receptors, we used two different cell lines, one lacking progesterone receptor (MDA-MB-468) (Subik et al., 2010) and another lacking glucocorticoid receptor (IGROV1) (Stringer-Reasor et al., 2015). We treated MDA-MB-468 cells with 10-40 µM mifepristone, or CB-5083 (1 µM), or a combination of CB-5083 (1 µM) and mifepristone (20 µM). We observed induction of ATF4 and CHOP by mifepristone, indicating that it induces unfolded protein response (Figure 4.6A). Moreover, we observed synergistic cytotoxicity between mifepristone and CB-5083 in these cells (Figure 4.6B). Similarly, glucocorticoid receptor-negative IGROV1 ovarian cancer cells displayed enhanced cytotoxicity to DBeQ and mifepristone (Figure 4.6C). These results indicate that the unfolded protein response mediated through mifepristone is independent of glucocorticoid and progesterone receptor activity.

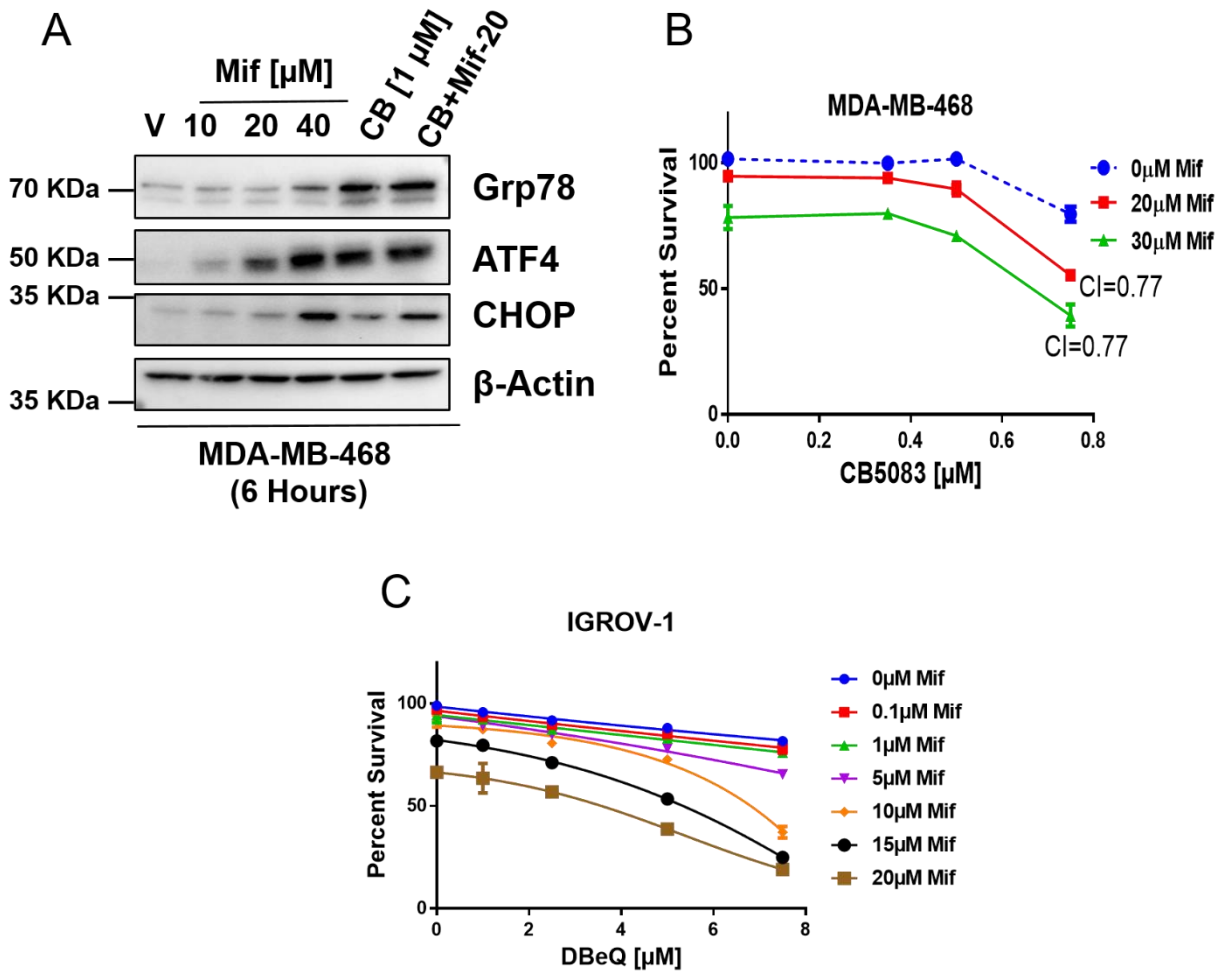

Figure 4.6. Mifepristone activates the unfolded protein response independent of glucocorticoid, estrogen and progesterone receptor inhibition. A) Triple-negative breast cancer cell line (MDA-MB-468) were incubated with indicated compounds for 6 hours. Whole cell lysates were then subjected to immublotting with antibodies for indicated proteins. β-Actin was used a loading control. B) MDA-MB-468 cells were treated with different concentrations of CB-5083 up to 0.75 μM and different concentration of mifepristone (20 μM and 30 μM) for 72 hours. Cell viability was measured using the SRB assay and dose-response curves were plotted with GraphPad Prism. CI stands for combination index. C) IGROV1 cells were treated with indicated concentrations of DBeQ and mifepristone for 72 hours. Cell viability was measured using SRB assay and dose response curves were generated using GraphPad Prism. All experiments were performed in three biological replicates.

In addition to IRE1 branch, ATF6 branch also induces Grp78 expression through the binding of nuclear ATF6 (ATF6-N) to endoplasmic reticulum stress-responsive element (ERSE) (Baumeister et al., 2005). To investigate the potential effect of mifepristone on ATF6 branch, we incubated the lysates generated from previous studies (see Fig 4.5C) with ATF6 antibody. We saw cleavage of full-length ATF6 (ATF6-FL) with 2.5 μM and 5 μM of CB-5083, however this cleavage was blocked with the addition of 20 μM mifepristone (Figure 4.7A).

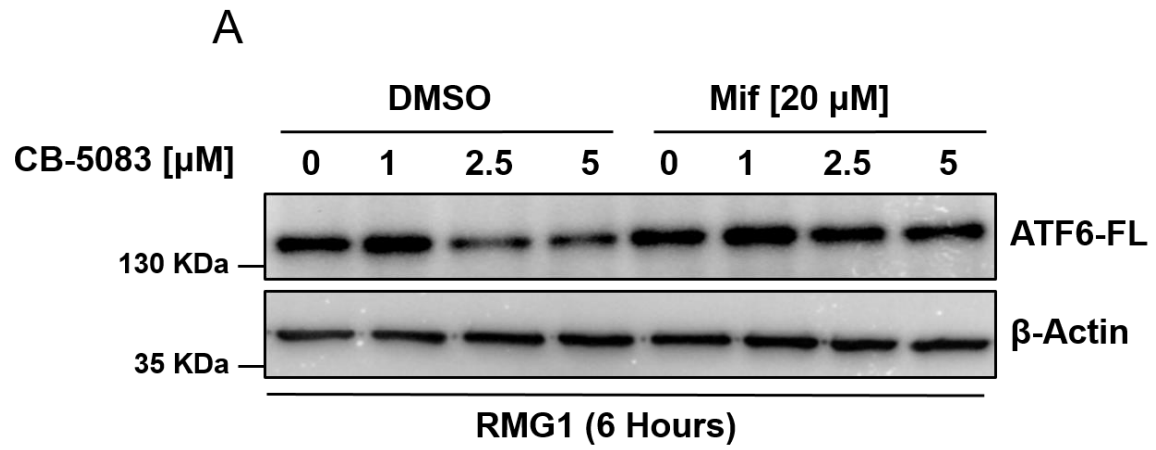

Figure 4.7. Mifepristone treatment inhibit full length ATF6 cleavage. A) RMG1 cells were incubated with increasing doses of CB-5083 (1 μM-5 μM) with or without mifepristone (20 μM) for 6 hours. Cells were harvested and proteins were subjected to immunoblotting to analyze the indicated proteins. β-Actin was used a loading control. Representative blots from three biological replicate experiments.

ATF6, an ER transmembrane protein, undergoes N-linked glycosylation to be functional. Induction of the unfolded protein response results in the translocation of full-length ATF6 (ATF6-FL) to the Golgi. In Golgi, ATF6 is cleaved first by Site-1 Protease (S1P) to intermediate ATF6 (ATF6-I) and subsequently by Site-2 Protease (S2P) to produce nuclear ATF6 (ATF6-N). To further confirm the inhibition of ATF6 cleavage by mifepristone, we expressed 3XFlag-ATF6 plasmid in HEK-293T cells for 24 hours. After 24 hours of transient transfection, we treated the

cells with 20 μM mifepristone for 1, 3, 6, 10 and 24 hours. As positive controls for this experiment, we treated the cells with 2 μM tunicamycin and 2.5 μM CB-5083 for 3 and 10 hours. The untreated sample (D) was collected after 10 hours of vehicle treatment (DMSO). It is important to note that full length ATF6 (ATF6-FL) is detected as two bands representing glycosylated and unglycosylated AFT6 (Figure 4.8). The unglycosylated ATF6 provides a sensing mechanism that regulates unfolded protein response whereby underglycosylation of ATF6 triggers the unfolded protein response (Hong et al., 2004). Consistent with the literature, treatment with tunicamycin for three hours produces relatively more abundant unglycosylated ATF6-FL (Figure 4.8) and induces the active form of cleaved ATF6 (ATF6-N) (Figure 4.8, long exposure). In CB-5083-treated cells at three hours, glycosylated ATF6-FL is more prominent than unglycosylated ATF6-FL. Yet, CB-5083 also induces the active form of cleaved ATF6, suggesting that CB-5083 activates this pathway through a mechanism that is distinct from ATF6 underglycosylation. Interestingly, mifepristone treatment causes higher levels of glycosylated than unglycosylated ATF6. This effect is expected to prevent ATF6 sensing mechanism that is dependent on underglycosylated ATF6 and may limit ATF6 activation.

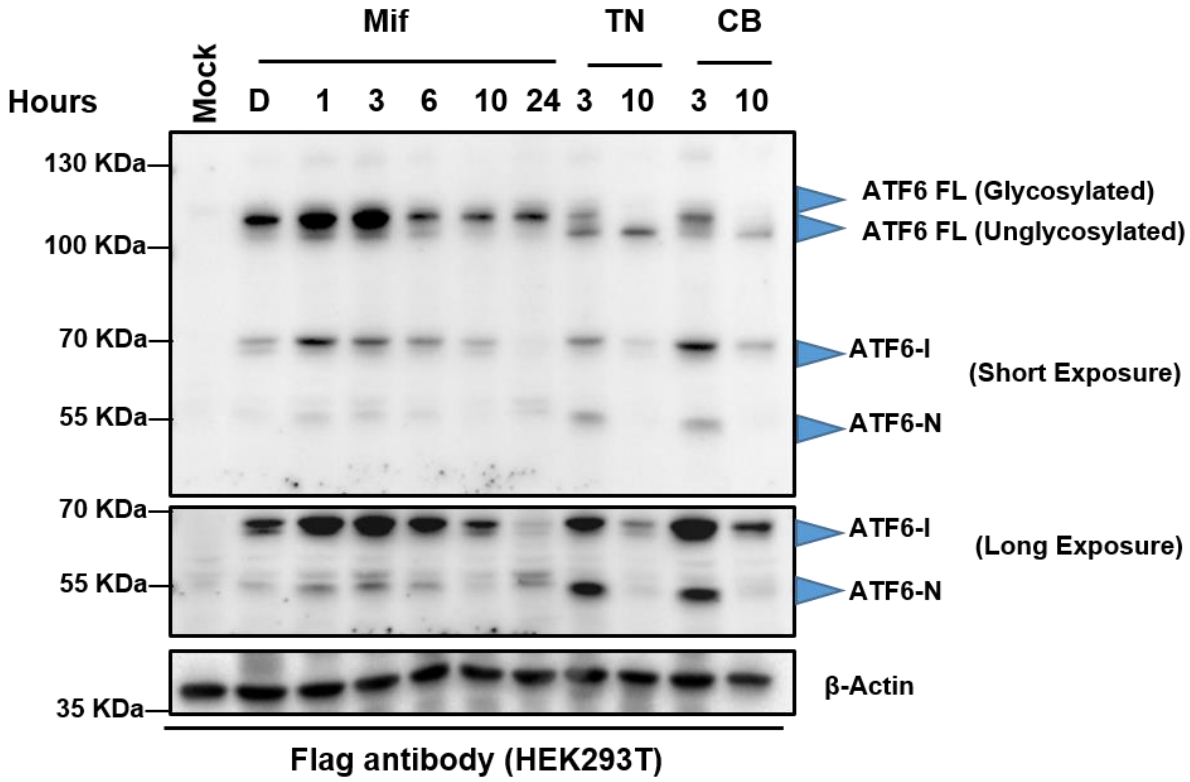

Figure 4.8. Mifepristone treatment promotes glycosylated ATF6. HEK293T cells were transiently transfected with a 3XFlag-ATF6 plasmid for 24 hours and subsequently treated with 20 μM mifepristone for 1,3,6,10 and 24 hours, while D sample was incubated in DMSO for 10 hours. 3XFlag-ATF6 expressing HEK293T cells were treated with 2.5 μM CB-5083 and 2 μM TN (tunicamycin) for 3 hours and 10 hours. Mock indicates the addition of transfection reagents without plasmid. ATF6 FL, ATF6-I and ATF6-N stands for full-length ATF6, intermediate ATF6, and nuclear ATF6 respectively. All lysates were subjected to immunoblotting with Anti-flag antibody. β-actin was used a loading control. Representative images from three biological replicate experiments.

4.2.4 Mifepristone treatment activates heme-regulated inhibitor (HRI) pathway to induce activating transcription factor 4 (ATF4)

Activating transcription factor 4 (ATF4) gets activated upon phosphorylation of eukaryotic initiation factor 2 alpha (eIF2α), which can be phosphorylated by four upstream kinases PERK, GCN2, HRI, and PKR (please see the list of abbreviations for full forms). To investigate the potential involvement of PERK and GCN2 towards ATF4 activation, we incubated mouse embryonic fibroblast generated from PERK knockout mice (PERK-MEF$^{-/-}$) and mouse embryonic fibroblast generated from GCN2 knockout mice (GCN2-MEF$^{-/-}$) with 20 μM of mifepristone and harvested whole cell lysates at 6 and 12 hours. Similarly, we treated both mouse embryonic fibroblasts (MEFs) with 2 μM tunicamycin for 10 hours, which acted as positive controls for the experiment. As expected, 2 μM tunicamycin was unable to induce the expression of ATF4 in PERK-MEF$^{-/-}$; however, in both conditions ATF4 expression was induced with 20 μM mifepristone (Figure 4.9A). These results indicate that mifepristone activated ATF4 independent of PERK or GCN kinases. Next, we analyzed the effect of kinases HRI and PKR towards the activation of ATF4. We transiently transfected small interfering RNAs (siRNAs) targeting HRI and PKR for 48 hours and followed with 20 μM mifepristone treatment for 6 and 10 hours. Our results indicate that siRNA targeting HRI was able to attenuate ATF4 expression (Figure 4.9B). Taken together, these results suggest that ATF4 activation upon mifepristone treatment is mediated through HRI pathway.

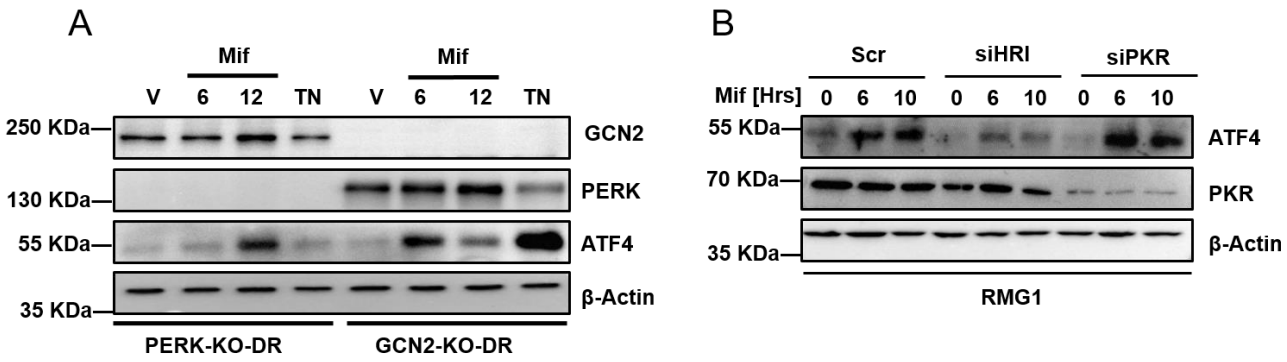

Figure 4.9. Mifepristone activates HRI kinase pathway. A) Mouse embryonic fibroblast generated from PERK knockout mice (PERK-KO-DR) and mouse embryonic fibroblast generated from GCN2 knockout mice (GCN2-KO-DR) were incubated with 20 μM of mifepristone for 6 and 12 hours. Vehicle (V) and TN (2 μM-Tunicamycin) treatments were performed for 12 hours and lysates were probed with indicated antibodies. β-Actin was used a loading control. Representative blots from three replicate experiments. B) RMG1 cells were transiently transfected with scrambled (Scr) and small interfering RNAs (siRNAs) targeting HRI (siHRI) and PKR (siPKR) for 48 hours followed by treatment of 20 μM of mifepristone for 6 and 10 hours. Protein lysates were then subjected to immunoblotting with indicated antibodies. β-Actin was used a loading control. Small interfering RNAs transfections were replicated in OVSAHO ovarian cancer cell line.

4.3. Discussion

Endoplasmic reticulum (ER) consists of interconnected tubules and flattened sacs that extend the entire cytoplasm. The primary functions of endoplasmic reticulum include post-translational modifications of nascent proteins, folding of secretory proteins, synthesis of lipids and storage of calcium. Several physiological insults such as calcium dysregulation, glucose or nutrient deprivation, increased reactive oxygen species and increased burden of misfolded and unfolded proteins in the endoplasmic reticulum can trigger the unfolded protein response. The unfolded protein response is primarily an adaptive response that is manifested through phosphorylation of two transmembrane endoplasmic reticulum kinase IRE1 and PERK and cleavage of endoplasmic reticulum transmembrane protein ATF6. Over the years, several studies have shown that the unfolded protein response can be targeted in multiple human disorders

including cancer. In Chapter 3, we showed that the unfolded protein response pathway can be induced in ovarian cancer by inhibiting VCP. VCP inhibitors induces unrestrained unfolded protein response that eventually initiates caspases-mediated cell death. Furthermore, we showed that VCP inhibitors can be combined with salubrinal potentiating the effect of VCP inhibitors. In this chapter, our primary objective was to identify a clinically relevant agent that could enhance the cytotoxic effect of VCP inhibitors by modulating the unfolded protein response in ovarian cancer cells. Several compounds that modulate several branches of the unfolded protein response have been identified over the year; however, none has been FDA-approved. Through this study, we identified strong synergistic cytotoxicity between mifepristone and several classes of VCP inhibitors at a clinically achievable dose of mifepristone.

Recently, a clinical case report showed that single-agent 200 mg mifepristone (oral/day) resulted in long-term high-quality survival of an 80-year-old female with metastatic lung cancer and a 58-year-old male with metastatic bilateral renal cell carcinoma. The 80-year-old female was reported to have no tumors 5 years after the initial treatment, while the male was reported to have stable disease for 10 years with no new lesion. Neither patients reported any side effect from the long-term treatment of mifepristone (Check et al., 2016). These evidences indicate that mifepristone could be used in cancer therapy even as long-term maintenance therapy. Since oral VCP inhibitors display a pan-cancer cytotoxicity, our results have broad implications in terms of designing future combination clinical trials with VCP inhibitors.

Mifepristone was initially approved as an anti-progesterone receptor inhibitor (Naoki et al., 1988); however, subsequent studies have identified other targets of mifepristone including several reports suggesting that mifepristone treatment display atypical unfolded protein response (Dioufa et al., 2010). We decided to investigate the mechanism of this atypical unfolded protein response

upon mifepristone treatment. Mifepristone treatment resulted in the inhibition of Grp78 expression (endoplasmic reticulum chaperone) as well as induction of ATF4. Although we observed a decrease in phospho-IRE1α and an increase in total IRE1α expression with mifepristone treatment, the endoribonuclease activity of IRE1α was not affected by mifepristone. Next, we analyzed the changes in the ATF6 branch. Our results indicate that unlike tunicamycin and CB-5083, mifepristone inhibits the cleavage of full length ATF6 (ATF6-FL) (Figure 4.10). We also observed an increase in glycosylated ATF6 in mifepristone-treated cells. Given that unglycosylated ATF6 serves as a sensor to induce the unfolded protein response, we speculate that the enhanced glycosylation of ATF6 may prevent full engagement of this branch during the induction of the unfolded protein response by CB-5083. Moreover, previous studies have shown that glycosylation-deficient ATF6 (T645I mutation) results in higher rate of Golgi translocation where S1P and S2P process ATF6 to produce active ATF6 (Hong et al., 2004). In fact, ATF6 translocation to the Golgi is first step in the activation of ATF6 branch in the unfolded protein response. Therefore, increased glycosylation of ATF6 that promoted by mifepristone may hinder the translocation of ATF6 to the Golgi during the unfolded protein response and attenuate the process of ATF6. Consistent with this assertion, our results show that mifepristone prevents the decrease in full length ATF6 that is induced by CB-5083. Collectively, our results suggest that mifepristone promotes glycoslylation of ATF6 and attenuate the activation of ATF6 branch during the induction of the unfolded protein response induced by CB-5083.

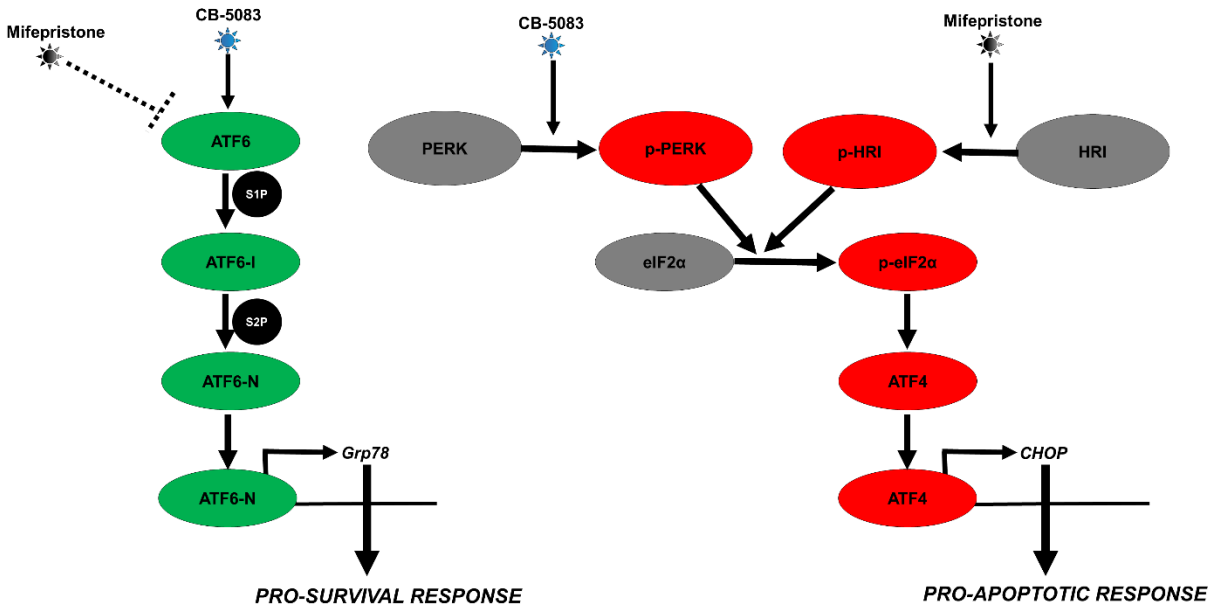

Figure 4.10. Putative mechanism for synergistic cytotoxicity between CB-5083 and mifepristone. Treatment with VCP inhibitor- CB-5083 activates activating transcription factor 6 (ATF6) branch and protein kinase R-like endoplasmic reticulum kinase (PERK) branch. Activation of ATF6 can result in the induction of glucose-regulated protein 78 (Grp78). Induction of Grp78 is considered a pro-survival response. Similarly, PERK activation can ultimately induce CCAAT/Enhancer-binding protein homologous protein (CHOP). Enhanced expression of CHOP can be a pro-apoptotic response. Mifepristone treatment inhibits ATF6 branch and enhances CHOP expression through the activation of heme-regulated inhibitor (HRI) kinase pathway. The combination of these two effects could result in enhanced cytotoxicity seen with CB-5083 and mifepristone combination.

Recently, Gallagher *et al.* used endoplasmic reticulum stress-responsive element (ERSE) to screen compounds that could inhibit ATF6 and showed that Ceapsins could selective inhibit ATF6α. The study showed that Ceapsin-A7 (ATF6α inhibitor) enhanced the cytotoxicity of thapsigargin (unfolded protein response inducer) (Gallagher et al., 2016). Results from our synergy studies between VCP inhibitors (unfolded protein response inducer) and mifepristone (ATF6 branch inhibitor) are therefore in agreement with their observation. However, further studies need to done to confirm that the synergistic effect between mifepristone and VCP inhibitors is mediated via this mechanism.

Through this study, we found that mifepristone treatment activates heme-regulated inhibitor (HRI) pathway resulting in ATF4 activation. Induction of ATF4 increases the expression of CHOP and enhanced CHOP expression has been shown to induce the unfolded protein response mediated cell death (Figure 4.10). This underlines a parallel mechanism of action that could result in potential synergy between mifepristone and VCP inhibitors. It is possible that both the activation of HRI pathway and inhibition of ATF6 branch confers the final synergistic cytotoxicity in our experiments. Subsequent studies need to be done to analyze the effect of each of these targets to conclusively identify the mechanism of cytotoxicity mediated through mifepristone. Similarly, we observed synergistic effect between CB-5083 and mifepristone in IGROV1 (shown to have low GR expression) and triple negative breast cancer (TNBC) cell line-MDA-MB-468. These results suggest that the atypical unfolded protein response via mifepristone is independent of glucocorticoid receptor, estrogen receptor and progesterone receptor inhibition; however, we are unable to rule out a potential role of mifepristone through unknown steroids or growth factors inhibition. In this chapter, we identified exciting and clinically relevant candidates that can be used in the combination chemotherapy. Similarly, we discovered a previously uncharacterized

mechanism of mifepristone in modulating the unfolded protein response. Mifepristone has been shown to be a safe compound even when given over a long interval. We envision mifepristone to be used as a maintenance therapy together with other modulators of the protein quality control pathways such as VCP inhibitors, heat-shock protein 90 (Hsp90) inhibitors, and autophagy modulators.

Chapter 5: Understanding the mechanism of resistance to VCP inhibitors

Portions of this chapter are reproduced from the following publication with permission where required.

- **Bastola P**, Wang F, Schaich M, Gan T, Freudenthal B, Chou TF, Chien J (2017) Specific mutations in D1-D2 linker region of VCP/p97 enhance ATPase activity and confer resistance to VCP inhibitors. Cell Death Discovery 3, 17065. PMID: 29367883

5.1 Introduction

Valosin-containing protein (VCP), also known as p97 or Cdc48 in yeast, belongs to AAA (ATPase Associated with diverse cellular Activities) family of ATPase. The protein has an N terminal domain, two ATPase domains (D1 and D2), followed by a short C terminal extension (Banerjee et al., 2016; DeLaBarre and Brunger, 2003; Meyer et al., 2012; Zhang et al., 2000). These domains are linked via two linker regions between N and D1 as well as D1 and D2 (Please see Figure 1.8) (Banerjee et al., 2016). While the N-terminal domain mostly interacts with substrates and co-factors, both D1 and D2 domains bind and hydrolyze adenosine triphosphate (ATP) (DeLaBarre and Brunger, 2005; Meyer et al., 2012). Mutations in the D2 domain that prevent binding of ATP or abolish ATP hydrolysis result in a dominant-negative phenotype suggesting that D2 domain is responsible for driving most functions associated with VCP, while the ATPase activity in D1 domain provides a supportive function (Song et al., 2003). Recently solved high-resolution cryoelectron microscopy structure of VCP depicted a two-step ATP-driven conformational changes associated with VCP activity (Banerjee et al., 2016). The structure revealed that binding of ATP to the D2 domain brings about a conformational change to D2 and subsequently to D1-D2 linker region. The conformational change at the D1-D2 linker region allows ATP binding at the D1 domain facilitating substrates to bind to the N-terminal region. The structure uncovered the significance of the D1-D2 linker region and demonstrated that D1-D2 inhibitors caused a steric clash, which abolished the function of VCP (Banerjee et al., 2016).

VCP has been linked with various cellular processes including ubiquitin-mediated degradation (Beskow et al., 2009; Bodnar and Rapoport, 2017), endoplasmic reticulum associated degradation (ERAD) (DeLaBarre et al., 2006; Ye et al., 2001), chromatin associated degradation (CAD) (Franz et al., 2011), protein aggregate processing (Ju et al., 2008), endosomal trafficking

(Bug and Meyer, 2012), mitochondria-associated degradation (Kim et al., 2013), and autophagy (Ju et al., 2009). Although VCP has been implicated in a multitude of cellular processes, its function in the ATP-mediated extraction of unfolded proteins from the endoplasmic reticulum (ER) for degradation via proteasome has been extensively studied (Jarosch et al., 2002; Wójcik et al., 2006). Similarly, the role of VCP-mediated ATP hydrolysis in the unfolding of ubiquitinated client proteins that are targeted for degradation by the proteasome is also well established (Dai and Li, 2001). These functions make VCP an essential component in protein quality control (PQC). Protein quality control has emerged as an essential factor in tumor development, and components of protein quality control have been proven to be valid targets for cancer therapeutics. Recent genome-wide short hairpin RNA (shRNA) screens identified various components of protein quality control, such as proteasomal subunits and VCP, as essential genes in cancer cells (Cheung et al., 2011; Marcotte et al., 2012). Therefore, VCP inhibitors may serve as novel cancer therapeutics that exploit unique vulnerabilities or dependencies of cancer cells.

Several studies reported the development of VCP inhibitors and showed that these compounds induce endoplasmic reticulum stress and apoptosis in cancer cells (Anderson et al., 2015; Chou et al., 2011; Magnaghi et al., 2013). High-throughput screening (HTS) of compound libraries from Maybridge Hitfinder Collection and National Institute of Health (NIH) Molecular Libraries Small Molecule Repository yielded in the identification of DBeQ (N^2,N^4-dibenzyl quinazoline-2,4-diamine) as a selective, reversible, ATP-competitive inhibitor of VCP (Chou et al., 2011). Subsequently, a structure-activity relationship (SAR) study was performed using DBeQ and N-benzyl-2-(2-fluorophenyl) quinazoline-4-amine 1 as a starting point. The study resulted in the identification of ML240, which displayed improved potency and inhibited the D2-ATPase activity of VCP (Chou et al., 2013). A derivative of ML240 was later developed into CB-5083,

which displayed better specificity towards VCP and more importantly showed efficacy in several tumor xenograft models when administered orally (Anderson et al., 2015; Zhou et al., 2015). Such promising results allowed for the start of two Phase I clinical trials.

Prompted by the potential application of VCP inhibitors in cancer, several studies have focused on understanding the mechanism of resistance towards VCP inhibitors. Cells resistant to CB-5083 have been shown to harbor mutations in *VCP*, yet details regarding the mechanism of resistance are unknown (Anderson et al., 2015). Similarly, prolonged treatment with an allosteric VCP inhibitor, NMS-873, resulted in a heterozygous A530T mutation in *VCP*. However, these resistant cell lines did not show any cross-resistance towards CB-5083 or other VCP inhibitors (Her et al., 2016). These results suggest that target alterations may represent a molecular mechanism of resistance to VCP inhibitors.

Given that CB-5083 has entered the realm of clinical trials, we set out to understand the mechanism of resistance towards this compound. Here, we established and characterized the *in vitro* mechanism of resistance to CB-5083. Our study indicates target alterations as a potential mechanism of resistance to CB-5083 *in vitro*, thereby providing a critical potentially theranostic marker that should be considered in clinical trial settings. Finally, our studies highlight the relevance for the further development of novel VCP inhibitors that can overcome resistance to existing VCP inhibitors.

5.2 Result

5.2.1 Development of CB-5083 resistant cell lines

With oral VCP inhibitor CB-5083 in two Phase I clinical trials, we set out to understand the potential mechanism of resistance towards CB-5083. Since one of Phase I clinical trials for CB-5083 focuses on advanced solid tumors, we selected a high grade serous ovarian cancer cell

line OVSAHO for our studies. To understand the mechanism of resistance towards CB-5083, we established CB-5083-resistant cell lines as outlined in Figure 5.1A and 5.1C. We incubated OVSAHO cells with 2.5 μM of CB-5083 for 24 hours, which resulted in significant cell death. Cells were allowed to recover in the drug-free medium for 5-10 days. Three more rounds of treatment and recovery were performed with the incremental increase of 0.5 μM CB-5083 per round (Figure 5.1A).

After four rounds of incremental exposures to CB-5083, we observed a small increase in resistance to CB-5083 in the recovered cells (OVSAHO-R) compared to the parental cells (Figure 5.1B). Next, we treated 500 OVSAHO-R cells with either 2 μM CB-5083 or 3 μM CB-5083 continuously for 15 days (Figure 5.1C). Surviving cells were allowed to form colonies and expanded separately to get two separate populations of resistant cells (O-CB-R1 & O-CB-R2). Both O-CB-R1 and O-CB-R2 displayed an elongated cell structure in contrast to rounded cell morphology of the parental OVSAHO cells (Figure 5.1F). More importantly, O-CB-R1 and O-CB-R2 cell lines showed 5.3 and 5.7-fold increase in resistance towards CB-5083, respectively (Figure 5.1D, 5.1E, 5.2C).

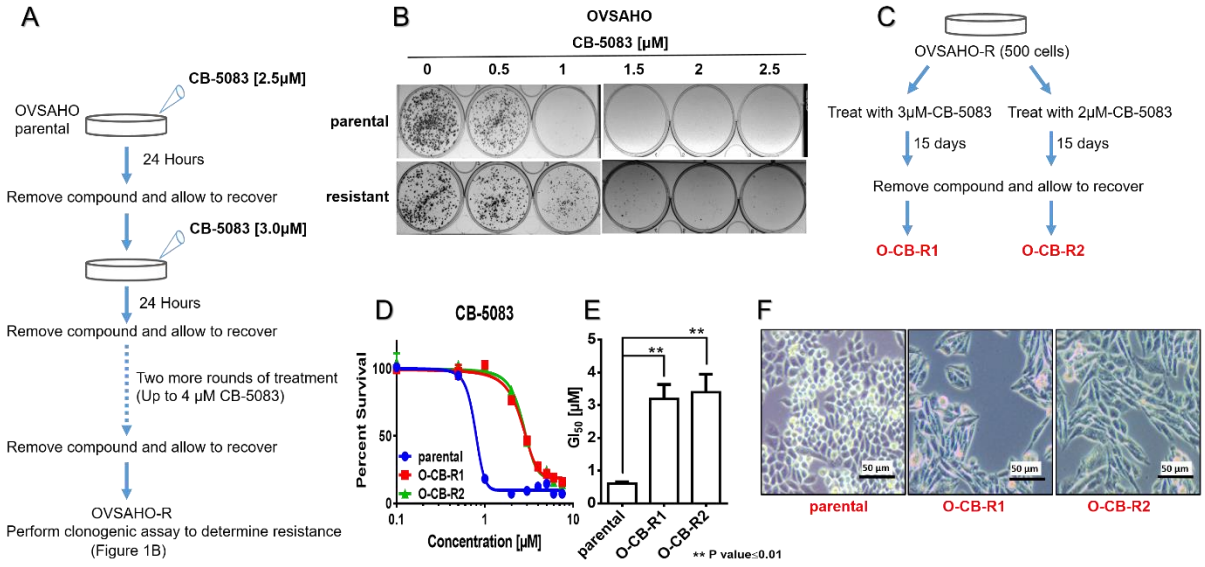

Figure 5.1. Development of CB-5083-resistant cells. A) Experimental setup used to generate the initial OVSAHO resistant cells. B) Colony formation assay was performed on parental OVSAHO cells and OVSAHO-R (resistant) cells. Cells were treated with different concentrations of CB-5083 between 0.5 μM-2.5 μM for 48 hours and then allowed to recover under normal media for 8 additional days. C) Experimental setup used to generate O-CB-R1 and O-CB-R2 from OVSAHO-R. D) OVSAHO parental, O-CB-R1 and O-CB-R2 were incubated with incremental doses of CB-5083 (0.1 μM-10 μM) for 72 hours and cell viability was determined using SRB assay. Dose-response curves were generated via GraphPad Prism using four parameters nonlinear regression and the curves were constrained on top (100%) and bottom (>0%). Every point in the dose-response curve represents Mean± SEM taken from at least two technical replicate samples for all cell lines. (E) The bar graph represents Mean GI_{50} + SEM taken from three biological replicates in all cell lines. P-values were calculated using Student's t-test. F) Images of OVSAHO parental, O-CB-R1 and O-CB-R2 were taken on Zeiss light microscope at 100X magnification.

5.2.2 Molecular characterization of resistance cell lines

In Chapter 3, we showed that VCP knockdown cells were more sensitive to VCP inhibitors than VCP-proficient cells. In contrast, both O-CB-R1 and O-CB-R2 cells showed around 50% reduction in the VCP expression (messenger RNA and protein) compared to the parental cells (Figure 5.2A, 5.2B). Furthermore, we examined the cytotoxicity of several VCP inhibitors and the proteasome inhibitor- bortezomib. Compared to the parental cell line, only NMS-873 displayed cross-resistance in O-CB-R1 and O-CB-R2 (Figure 5.2C). Surprisingly, we were unable to observe cross-resistance towards DBeQ and ML240, which share close chemical structure to CB-5083. We also did not observe cross-resistance to the recently described allosteric VCP inhibitor UPCDC-30425 as well as the proteasome inhibitor- bortezomib (Figure 5.2C).

In Chapter 3, we showed that CB-5083 treatment induced the unfolded protein response (UPR); therefore, we evaluated the induction of the unfolded protein response with two VCP inhibitors- CB-5083 and DBeQ, a proteasome inhibitor- bortezomib, and an endoplasmic reticulum stress inducer- tunicamycin. Based on our cytotoxicity data, we expected CB-5083 treatment to have a reduced activation of the unfolded protein response in the resistance cells. As expected, we observed reduced activation of ATF4 at both 3 hours and 6 hours in the resistant cells (Figure 5.2D). We also observed the reduced induction of ATF4 in the resistant cells with DBeQ, bortezomib, and tunicamycin treatments (Figure 5.2D). Given that tunicamycin and bortezomib were not known to directly affect VCP, the attenuated ATF4 induction in resistant cell lines suggests that these cells might have acquired an increase in the adaptive capacity to handle the endoplasmic reticulum stress response.

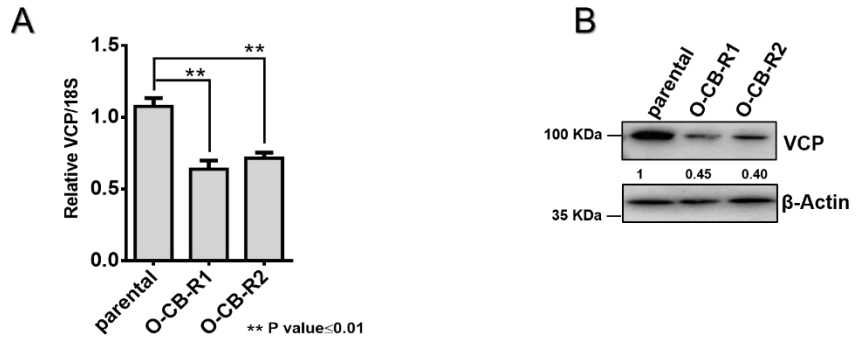

C

Mean GI50±SEM (μM)			
Compound	**Parental**	**O-CB-R1**	**O-CB-R2**
CB-5083	0.6±0.05	3.19±0.45 (5.3)	3.40±0.55 (5.7)
NMS-873	3.3±0.08	12.2±1.55 (3.7)	11.6±1.86 (3.5)
ML240	2.5±0.6	2.5±0.6	2.5±0.6
DBeQ	7.0±0.8	6.4±0.7	7.1±0.9
UPCDC-30245	2.5±0.4	2.6±0.2	2.6±0.5
Bortezomib	0.28±0.08	0.33±0.10	0.33±0.10

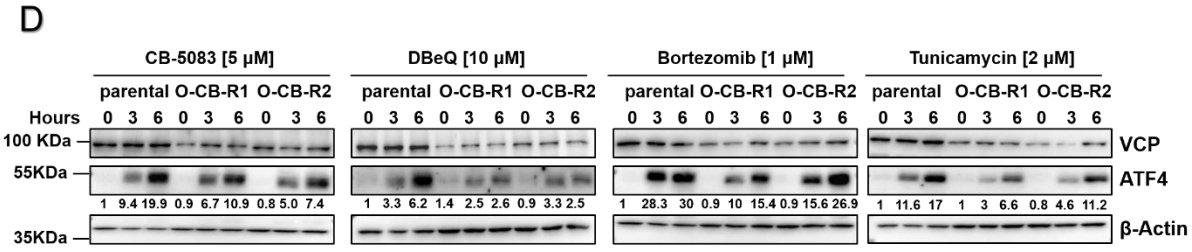

Figure 5.2. Effects on VCP/p97 mRNA and protein expression, cross-resistance and changes in the unfolded protein response (UPR) in resistant cell line. A) Quantitative RT-PCR was performed to evaluate the mRNA expression of VCP in OVSAHO parental, O-CB-R1 and O-CB-R2. Bar graph represents the mean relative mRNA expression + SEM normalized to 18S from three independent q-RT-PCR experiments. P-values were calculated using Student's t-test B) Whole cell lysates were immunoblotted and probed with the antibody against VCP to evaluate the protein expression. β-Actin was used as the loading control. Numbers below the VCP blot indicate relative VCP expression normalized to the β-Actin loading control. C) Table displays Mean GI_{50} ± SEM (μM) with several VCP inhibitors and proteasome inhibitor (Bortezomib) from three independent experiments in parental and resistant cells. Numbers in the bracket for CB-5083 and NMS-873 treatment represent the drug resistance index (DRI) in resistant cells compared to parental cells. D) OVSAHO-parental, O-CB-R1, and O-CB-R2 were treated with CB-5083, DBeQ, bortezomib or tunicamycin at indicated concentrations. Cells were collected at 3- and 6-hour time points and whole cell lysates were subjected to immunoblotting and probed with indicated antibodies. Numbers below the ATF4 blots indicate relative ATF4 protein expression normalized to β-Actin (loading control).

5.2.3 CB-5083 resistant cells harbor missense mutations in the D1-D2 linker region of *VCP*

Based on previous studies indicating that CB-5083 resistant cells harbor mutations in *VCP* (Anderson et al., 2015; Zhou et al., 2015), we decided to sequence-specific regions of the *VCP* gene. CB-5083 has been shown to be a D2 specific inhibitor (Anderson et al., 2015; Zhou et al., 2015); therefore, we sequenced all the exons spanning the D2 domain (exon 13-16). Similarly, homozygous point mutations in the D1-D2 linker region were observed in CB-5083-resistant cells (Anderson et al., 2015). Hence, we decided to sequence the D1-D2 linker region (exon 11 and 12) as well. In O-CB-R2, we identified one heterozygous mutation at codon 470 (E470K, exon 12) and one heterozygous mutation at codon 603 (Q603*, exon 14) (Figure 5.4A). In another resistant cell line, O-CB-R1, we found two heterozygous mutations at codon 470 (E470K and E470D, exon 12), one heterozygous mutation at codon 603 (Q603*, exon 14) and one heterozygous frameshift deletion (N616M fs, exon 14) (Figure 5.4A). Since both O-CB-R1 and O-CB-R2 contained a mixed population of cells and could, therefore, harbor heterogeneous mutations in VCP, we isolated several single clones from both the resistant cell populations. We generated three sub-clones from O-CB-R2, and all three sub-clones harbored a similar heterozygous E470K mutation in *VCP* (data not shown).

We also generated two sub-clones from O-CB-R1 (O-CB-R1.1 and O-CB-R1.2) and observed two separate heterozygous mutations, E470K and E470D, in O-CB-R1.1 and O-CB-R1.2 respectively (Figure 5.4A). O-CB-R1.1 cells also contained a heterozygous nonsense mutation at codon 603 (Q603*, exon 14). In contrast, O-CB-R1.2 cells contained a heterozygous frameshift deletion at codon 616 (N616M fs*63, exon 14) (Figure 5.4A). Similar to O-CB-R1, both O-CB-R1.1 and O-CB-R1.2 displayed a significant increase in the half-maximal growth inhibition (GI_{50})

compared to the parental cell line when treated with CB-5083 (Figure 5.3A). In addition, analysis of somatic mutations in *VCP* in tumor samples from the cancer genome atlas (TCGA) dataset indicated that frameshift mutations at codon 616 in *VCP* are frequently observed in cancer samples, while mutations in E470 and Q603 have not been reported (Figure 5.3B-5.3C). Previous studies identified several homozygous point mutations along the D1-D2 linker region (codons 472, 473, and 474) in CB-5083 resistant cells (Anderson et al., 2015). The clusters of mutations within this region further highlights the importance of D1-D2 linker in the mechanism of resistance to VCP inhibitors.

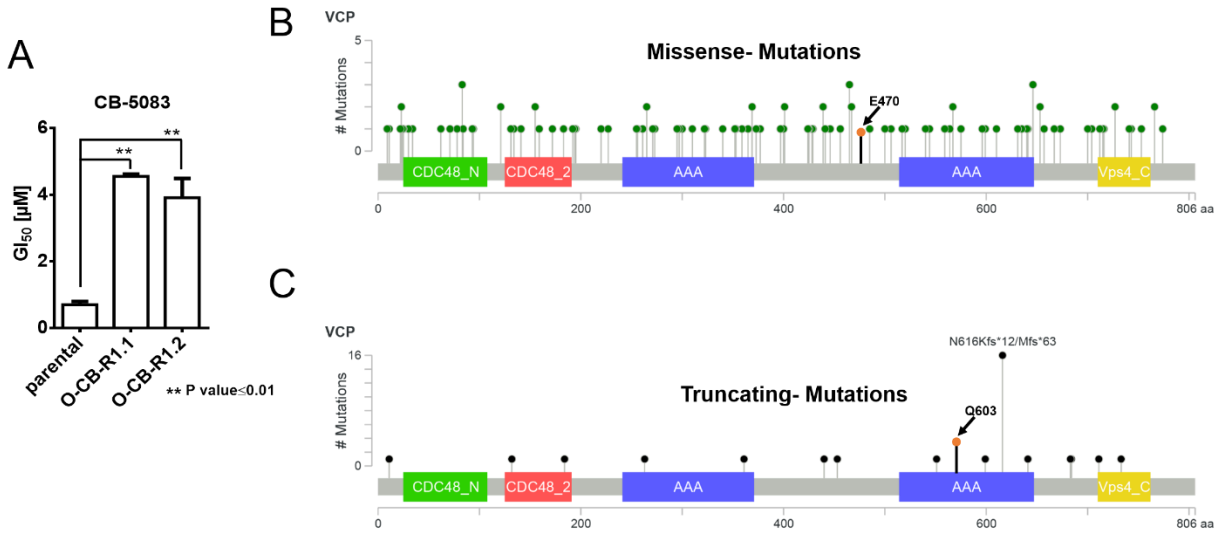

Figure 5.3. Common mutations observed in the cancer genome atlas (TCGA) dataset. A) The bar graph represents Mean GI_{50} + SEM in OVSAHO parental and two sub-clones from O-CB-R1 (O-CB-R1.1 and O-CB-R1.2) taken from three biological replicates. P-values were calculated using the two-tailed student's t-test. Known missense mutations (B) and truncation mutations (C) associated with cancer. Tentative sites for the E470 missense mutations and Q603 truncation mutation are artificially drawn to indicate the mutations observed in the resistant cell lines.

To determine if the heterozygous mutations at codons 470 and 603/616 are compound mutations present in both alleles or two single mutations present separately in two alleles, we decided to sequence the complementary DNA (cDNA). In contrast to genomic DNA sequencing results, we detected homozygous mutations at codon 470, while no mutation was detected at codon 603 or 616 in the cDNA (Figure 5.4B). These results suggest that mutations in codons 470 and 603/616 are not compound mutations present in the same allele. In fact, these results suggest the first set of mutations at codon 470 (E470K or E470D) are present in one *VCP* allele while another set of mutations at codons 603 (Q603*) or 616 (N616Mfs*63) are present in the other *VCP* allele. Although VCP mRNA with E470K or E470D mutations is expressed and can be detected in cDNA sequencing as homozygous mutations, the VCP mRNA with either Q603* or N616Mfs* 63 mutations is not expressed because of nonsense-mediated decay, and therefore they are not detected in the cDNA sequencing.

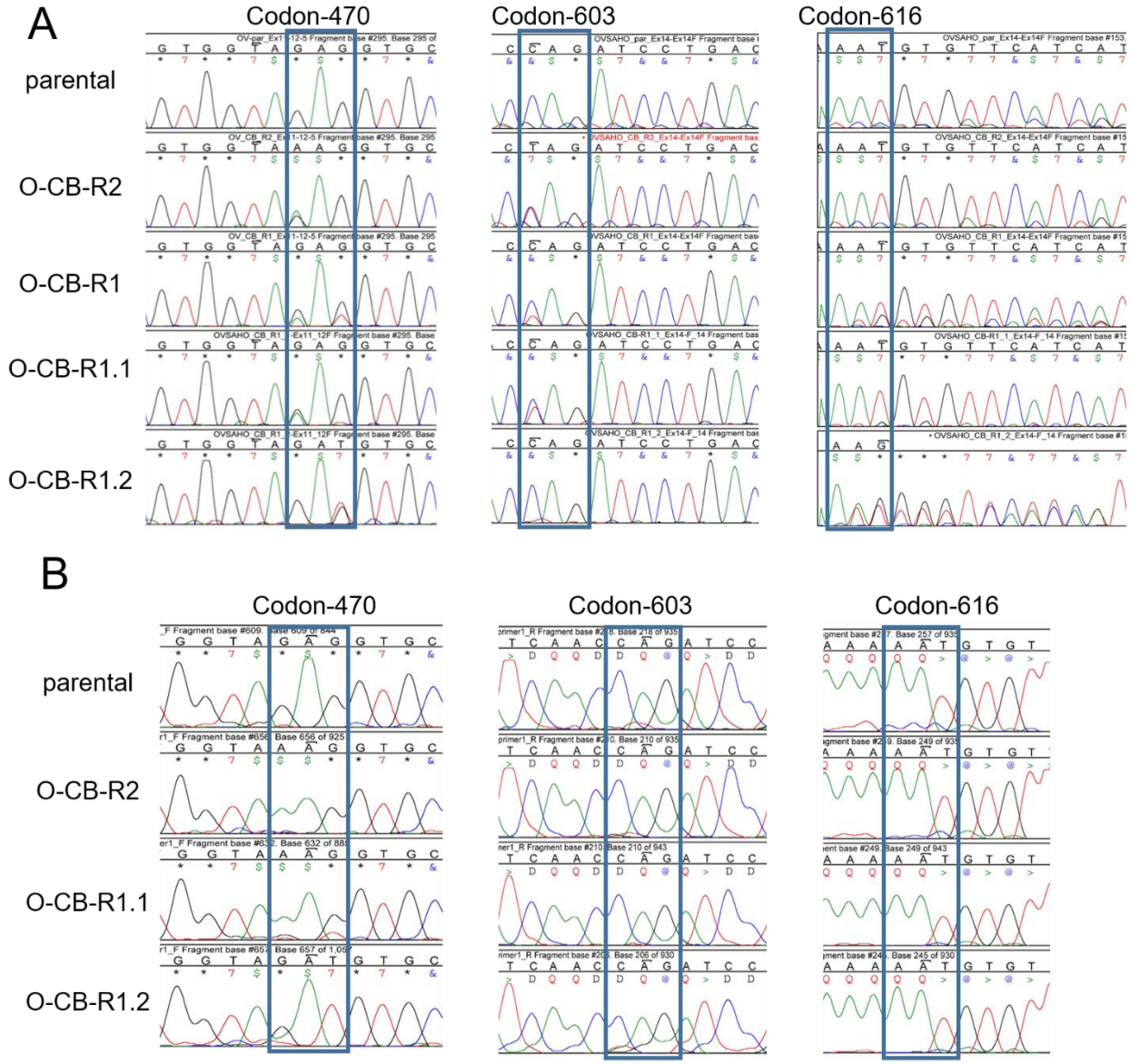

Figure 5.4. CB-5083-resistant cell lines harbor heterozygous mutations at exon 12 and exon 14. A) Chromatograms displaying the region of *VCP* genomic DNA coding sequence at exon 12 and exon 14 in OVSAHO parental, O-CB-R2 and O-CB-R1 as well as two pure sub-clones O-CB-R1.1 and O-CB-R1.2 generated from O-CB-R1. Blue box marks codons 470, 603 and 616 that harbors mutations in the resistant clones. B) Chromatograms displaying the region of *VCP* c-DNA in OVSAHO parental, OVSAHO-CB-R2, OVSAHO-CB-R1.1 and OVSAHO-CB-R1.2. Blue box marks codon 470, 603 and 616.

Previous studies have shown that the mechanisms of action pertaining to drugs can be inferred from the perturbed transcriptomes induced by the drugs (Lamb et al., 2006). To investigate potential molecular mechanisms contributing to CB-5083 resistance, we characterized the transcriptomes perturbed by CB-5083 in parental and resistant cells. We performed RNA sequencing of parental OVSAHO and CB-5803-resistant O-CB-R1 after treatment with vehicle (DMSO) or CB-5083 (5 μM) for 6 hours. We selected 6-hours treatment to limit the perturbation of gene expression to the primary response induced by CB-5083, as previous studies (Lamb et al., 2006). First, we analyzed the mutations in *VCP* in RNA sequencing data from parental and O-CB-R1 treated with DMSO. Consistent with our Sanger sequencing results, we detected both E470K (C→T) and E470D (C→A) missense mutations in VCP transcripts from O-CB-R1 but not in parental cells (Figure 5.5A). Furthermore, we did not detect nonsense mutations at codon 603 or codon 616 in both parental and resistant transcripts (data not shown), which further confirmed that transcripts with nonsense mutations at codon 603 and codon 616 were subjected to nonsense-mediated decay.

Figure 5.5. Nonsynonymous mutations in VCP transcripts. A) OVSAHO parental and OVSAHO resistant (O-CB-R1) transcripts spanning codon 470 of VCP. The arrows in O-CB-R1 transcripts represent two different nonsynonymous mutations in VCP at codon 470 with either C>T (E470K) or C>A (E470D). It should be noted that VCP is transcribed from the negative strand, and codon 470 is read as GAG (a reverse complement of CTC). C>T transition at the first base of the codon in the positive strand is read as AAG, which codes for lysine (K). C>A transversion at the third base of the codon in the positive strand is read as GAU, which codes for aspartic acid (D).

Subsequently, we performed mutational analysis to detect other nonsynonymous mutations in the resistant cell line compared to the parental cell line. We identified 71 unique nonsynonymous substitutions in O-CB-R1. In Table 5.1, we list top 11 nonsynonymous substitutions in O-CB-R1. It should be noted that these mutations are found in the transcripts that are abundant in both parental and resistant cells, and they likely represent true mutations that are not found in parental cells. Next, we investigated perturbed gene expression induced by CB-5083 in both cell lines. A total of 3047 transcripts were differentially expressed in the parental cells after CB-5083 treatment, while only 31 transcripts were differentially expressed in O-CB-R1 after CB-5083 treatment, with an overlap in 19 transcripts between the two cell lines (Figure 5.6A). In Figure 5.6B, we outline the number of transcripts that were differentially expressed (upregulated and downregulated) in both cell lines with CB-5083 treatment.

Top Nonsynonymous substitutions in the resistant cell line			
Gene	**Reference- Amino Acid**	**Substitution**	**Zygosity**
VCP	E470	K	Heterozygous
VCP	E470	D	Heterozygous
FLNA	R484	W	Heterozygous
UQCR10	S8	L	Heterozygous
MCM7	A241	S	Heterozygous
APBB2	T131	S	Homozygous
TNKS1BP1	P602	H	Heterozygous
ADAM10	I385	F	Heterozygous
SLC16A3	D260	A	Heterozygous
TRAK1	N857	S	Heterozygous
ATG4B	V364	D	Heterozygous

Table 5.1. List of Top 11 nonsynonymous gene substitutions in the resistant cell line.

A

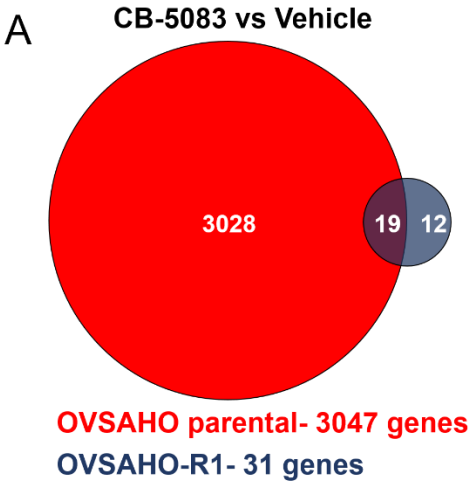

B

	Up by CB-5083 (FDR≤0.001) ≥1.5-Fold	Down by CB-5083 (FDR≤0.001) ≥1.5-Fold
Parental	1666	1381
Resistant (R1)	31	0
Overlap	19	0

Figure 5.6. The number of differentially expressed transcripts with CB-5083 treatment. A) The Venn diagram represents the number of the differentially regulated transcripts in both parental and resistant cell lines upon 6 hours of treatment with CB-5083 (5 μM). Differential expression was calculated based on the false discovery rate ≤ 0.001 and fold change ≥ 1.5. B) The table indicates the number of transcripts that are differentially regulated (upregulated and downregulated) in OVSAHO-parental and O-CB-R1 cells with CB-5083 treatment.

Next, we focused on the 19 shared transcripts that were upregulated with CB-5083 in both cell lines. We plotted the upregulated transcripts based on their maximum mean expression values (Figure 5.7A) and relative fold change values (Figure 5.7B). Based on the maximum mean expression values, DDIT3 (CHOP) was the most highly upregulated transcript in the parental group (Figure 5.7A). Likewise, based on the fold change values, ATF3 was the most highly upregulated transcript among the parental group (Figure 5.7B). Considering that *CHOP* and *ATF3* are upregulated upon the induction of the unfolded protein response, our results indicate that oral VCP inhibitor- CB-5083 induces the unfolded protein response. Although resistant cells show induction of these transcripts, the maximum mean expression values for DDIT3 (CHOP) as well as fold change for ATF3 transcript are lower in the resistant cell line (O-CB-R1) than parental cells, suggesting that the effect of CB-5083 is consistently attenuated in the resistant cells.

Similarly, we analyzed the 12 transcripts that were upregulated only in O-CB-R1. These included transcripts such as IER3IP1_1, EIF3CL, and TIMM23B (Figure 5.7C-5.7D). Upregulation of these transcripts may represent an adaptive response that allows O-CB-R1 to escape CB-5083-mediated cytotoxic effect.

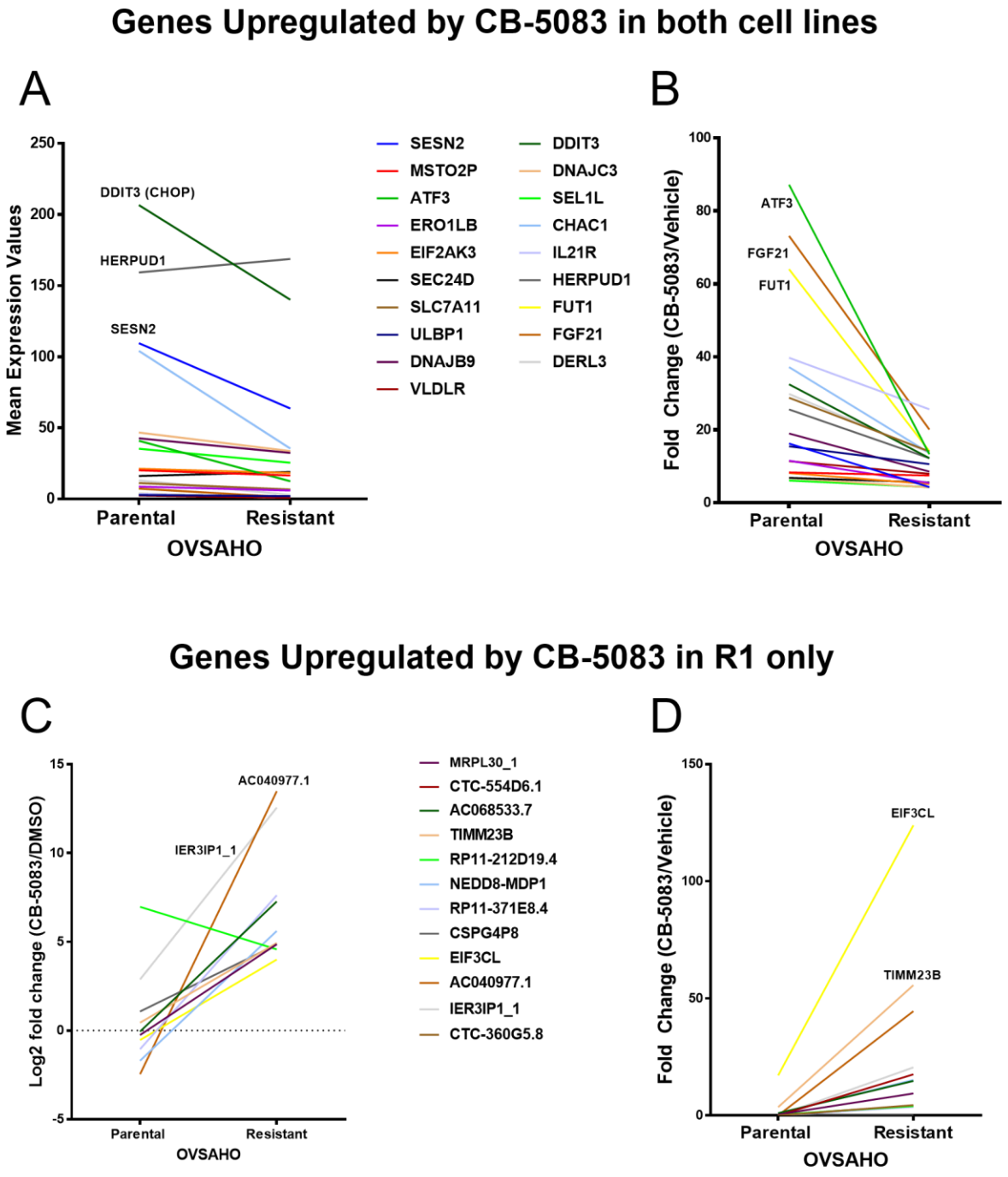

Figure 5.7. Alterations in transcripts related to the unfolded protein response with CB-5083 treatment. Plots represent A) maximum mean expression values and (B) relative fold change values of the 19 shared transcripts that were upregulated with CB-5083 treatment in OVSAHO parental and resistant (O-CB-R1) cells. Each line represents a transcript. C) Plot represents the log2 fold change of the 12 transcripts that were significantly upregulated with CB-5083 treatment only in the resistant cells (FDR<0.001). It should be noted that negative Log2 fold change values in parental cells indicate the corresponding genes are downregulated in parental cells. RP11-

212D19.4, shown in green line, was upregulated by CB-5083 in parental cells. However, this upregulation was not significant. D) Plot represents the relative fold change values of the 12 transcripts that were significantly upregulated by CB-5083 only in the resistant cell line.

Furthermore, we performed pathway analysis identified through ontology term enrichment based on the list of transcripts that were differentially regulated in both cell lines upon CB-5083 treatment using fold change > 1 and false discovery rate (FDR) ≥ 0.01. These new parameters allowed us to capture more transcripts, which were then used to analyze the affected pathways inferred from the ontology terms associated with these genes. In both parental and resistant cells, the "response to endoplasmic reticulum stress (GO:0034976)" pathway was the most significantly associated GO term for genes upregulated by CB-5083 treatment (Figure 5.8A-5.8B). Similarly, when we analyzed the ontology terms associated with the genes downregulated by CB-5083, we observed GO terms associated with the "cell division" in the parental line, however, this was not observed in the resistant cell line (Figure 5.8C-5.8D). In addition to pathways defined by GO terms, other pathways included those defined by the Reactome (R-HSA) database and the Gene Set Enrichment Analysis Gene Sets (M), and Kyoto Encyclopedia of Genes and Genomes (KEGG) pathway database (hsa). These results further confirm that CB-5083 induces the expression of genes associated with the response to endoplasmic reticulum stress in both cell lines.

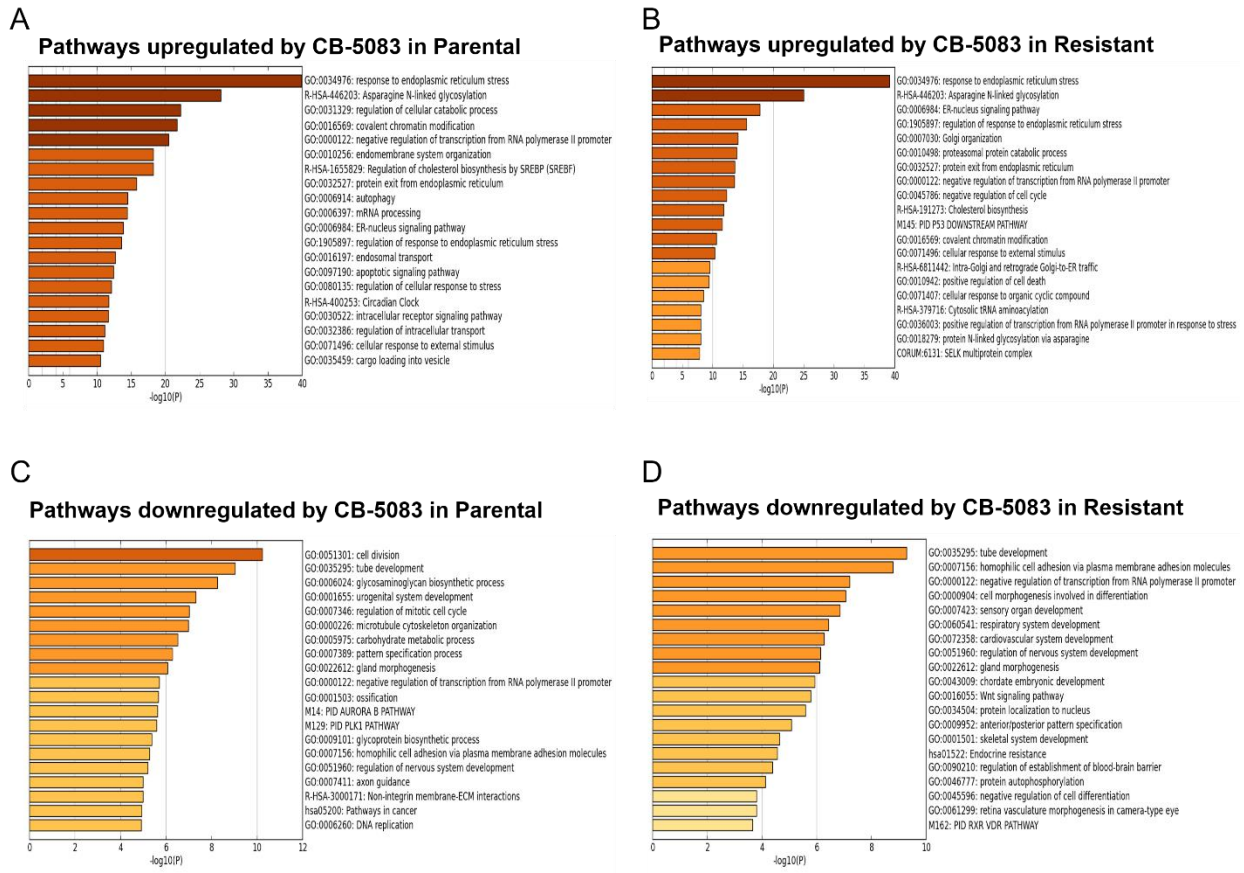

Figure 5.8. Differential regulation of pathways with CB-5083 treatment. A) Inferred pathways upregulated by 5 μM of CB-5083 treatment in the OVSAHO parental cells. B) Inferred pathways upregulated by 5 μM of CB-5083 treatment the resistant (O-CB-R1) cells. C) Inferred pathways associated with genes downregulated by 5 μM of CB-5083 treatment in OVSAHO parental cells. D) Inferred pathways associated with genes downregulated by 5μM of CB-5083 treatment in the resistant (O-CB-R1) cells. Terms with the prefix "GO" are from the Gene Ontology Consortium, the prefix "R-HAS" from the Reactome, the prefix "M" from the Gene Set Enrichment database, and the prefix "has" is from the KEGG database.

5.2.4 E470K and E470D mutants show higher ATPase activity and increased resistance than wild-type VCP

To determine the effect of specific missense mutations on VCP ATPase activity, we performed site-directed mutagenesis of a bacterial expression construct containing VCP as previously described (Chou et al., 2014). The list of plasmids used to purify VCP proteins (wildtype and E470 mutants) is shown in Figure 5.10C. Wildtype and two mutant form of VCP proteins were purified according to the published procedure (Chou et al., 2014) and Biomol Green reagent (a modified Malachite Green assay) was used to determine ATPase activity. Figure 5.9A demonstrated that both E470D and E470K have elevated ATPase activity, about 5.8-fold and 3.4-fold respectively. Next, we determined *in vitro* half-maximal inhibitory concentration (IC_{50}) of CB5083, NMS-873, ML240, ML241, and DBeQ (Figure 5.9B-5.9D, Figure 5.10A-5.10B). Our result indicated that CB-5083 was about 3.4 to 3.8 fold less active in inhibiting the E470 mutants than the wildtype (WT) VCP and interestingly, ML240 was about 15-fold less active (Figure 5.9B, 5.9D). The allosteric inhibitor NMS-873 was about 2.6 to 2.9-fold less active toward the E470 mutants (Figure 5.9C). Increased IC_{50} in the E470 mutants was also observed with ML241 and DBeQ (Figure 5.10A-5.10B). These results show the E470 mutants display increased ATPase activity and resistance to a broad spectrum of VCP inhibitors.

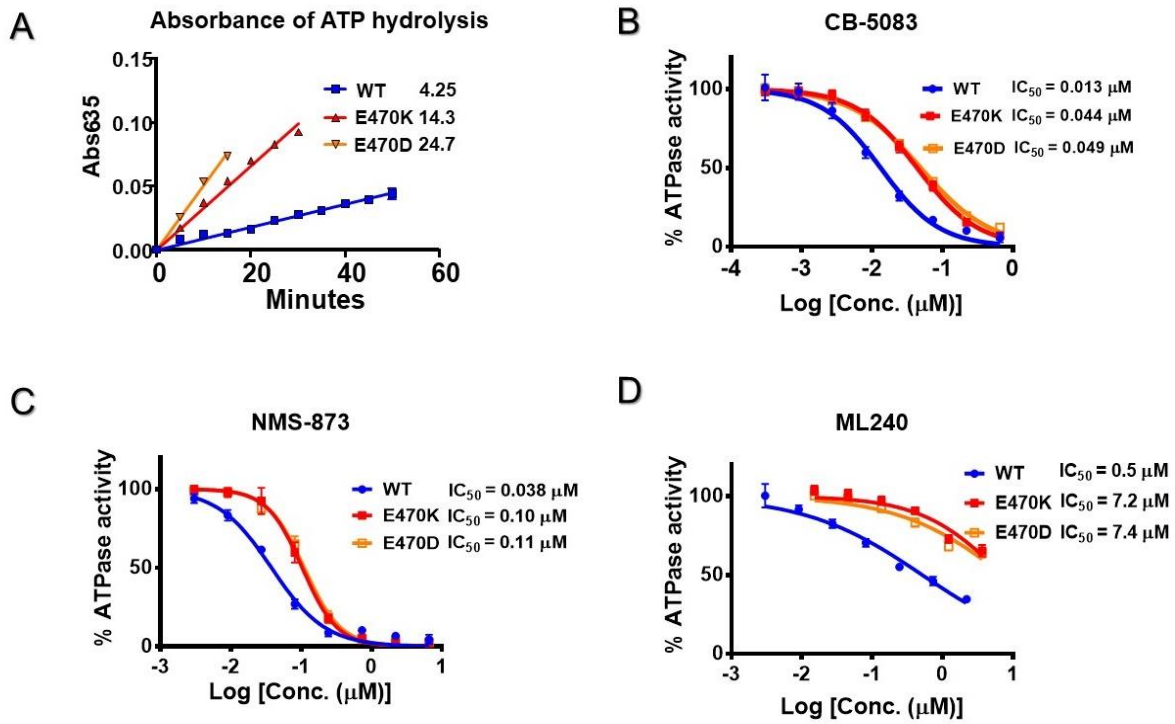

Figure 5.9. Mutations at codon 470 enhance VCP activity and attenuate CB-5083, NMS-873 and ML240 function. (A)Time-dependent experiment with wildtype (WT) VCP/p97 and two E470 mutants to determine their specific ATPase activities. Specific ATPase activity of VCP proteins presented in the figure was measured in nmol/min/nmol. (B)-(D) Titration curves of CB5083, NMS-873, and ML240 for WT, E470K, and E470D VCP proteins. IC_{50} (μM) was calculated using Prism with the equation [log(agonist) vs. response - Variable slope (four parameters)].

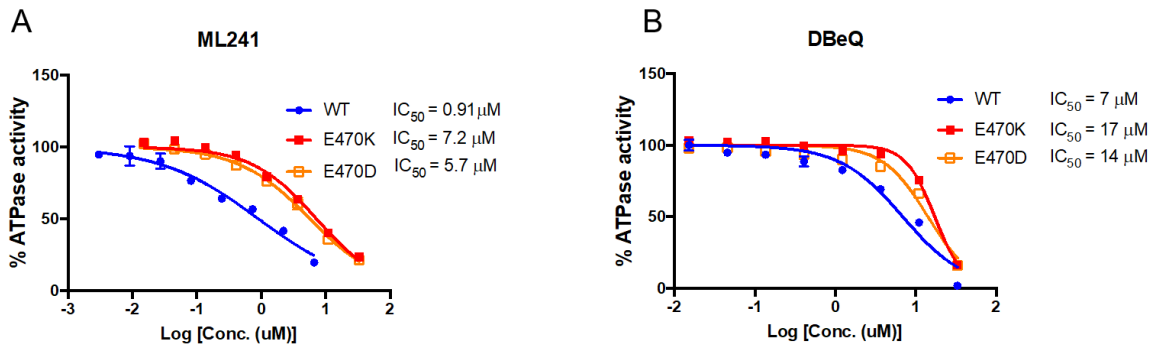

C

Plasmids used in this study

Plasmid Number	Plasmid name	Vector	Source and Reference
TCB-197/ SLB-001	Human p97 pET15_T	pET15b_TEV linker	Chou, 2014*
TCB-499	E470D human p97 pET15_T	pET15b_TEV linker	This study
TCB-490	E470K human p97 pET15_T	pET15b_TEV linker	This study

*Chou, T. F., Bulfer, S. L., Weihl, C. C., Li, K., Lis, L. G., Walters, M. A., Schoenen, F. J., Lin, H. J., Deshaies, R. J., and Arkin, M. R. (2014) Specific inhibition of p97/VCP ATPase and kinetic analysis demonstrate interaction between D1 and D2 ATPase domains. *J. Mol. Biol.* **426**, 2886-2899.

Figure 5.10. Mutations at codon 470 attenuates other VCP inhibitors function. Titration curves of ML241 (A) and DBeQ (B) for WT, E470K and E470D VCP proteins in inhibiting ATPase activity. IC_{50} (uM) was calculated using Prism with the equation [log(agonist) vs. response -- Variable slope (four parameters)].

5.2.5 Mutation at E470 may affect binding to CB-5083 and NMS-873

To determine the binding site of CB-5083, and therefore possible impacts of E470 mutations, we utilized the molecular docking program AutoDock Vina with a 2.4 Å hexameric structure of VCP (PDB code 5FTK) (Figure 5.11A) (Banerjee et al., 2016; Trott and Olson, 2010). A search for binding sites of CB-5083 was performed on a hexameric VCP with a 30 x 30 x 30 $Å^3$ cubic region oriented near the mutation site while keeping the D2 active site of the enzyme within the search box. Two thermodynamically similar binding modes were observed: one was at the D1-D2 interface with the methyl group from the benzimidazole ring in contact with E470. The carbon molecule of the attached methyl group is 4.3 Å from both the carbon two and three of E470 (Figure

5.11B, 5.11C). The calculated free energy for ligand binding of that mode was -8.9 kcal/mol. A previous docking study observed binding of CB-5083 at the ATP binding site of D2 (Zhou et al., 2015). However, the search parameters used were centered on the D2 active site of VCP and did not include the D1-D2 interface region (Zhou et al., 2015).

Similar to the previous study, we also observed an additional binding pocket in the active site of the D2 domain with similar thermodynamic favorability of binding (-9.5 kcal/mol), suggesting CB-5083 can bind at both the D1-D2 linker and the ATP binding site, which may account for its previous characterization as a competitive inhibitor. However, based on our cellular studies the likely mode of action within our experimental design is through interfacial binding near E470, and mutations at E470 would likely alter binding of CB-5083. We also performed docking studies on NMS-873 because our resistant cell lines O-CB-R1 and O-CB-R2 displayed the cross-resistance (Figure 5.2C). NMS-873 has been previously shown to be an allosteric inhibitor of VCP and binds at the interface between the D1 and D2 domains (Magnaghi et al., 2013). Molecular docking of this compound into hexameric VCP with the same search parameters outlined for CB-5083 yielded binding modes at the interface (-9.9 kcal/mol) with direct contacts to E470 (Figure 5.11D-5.11E). This is consistent with mutations at E470 promoting resistance due to disruption of NMS-873 binding.

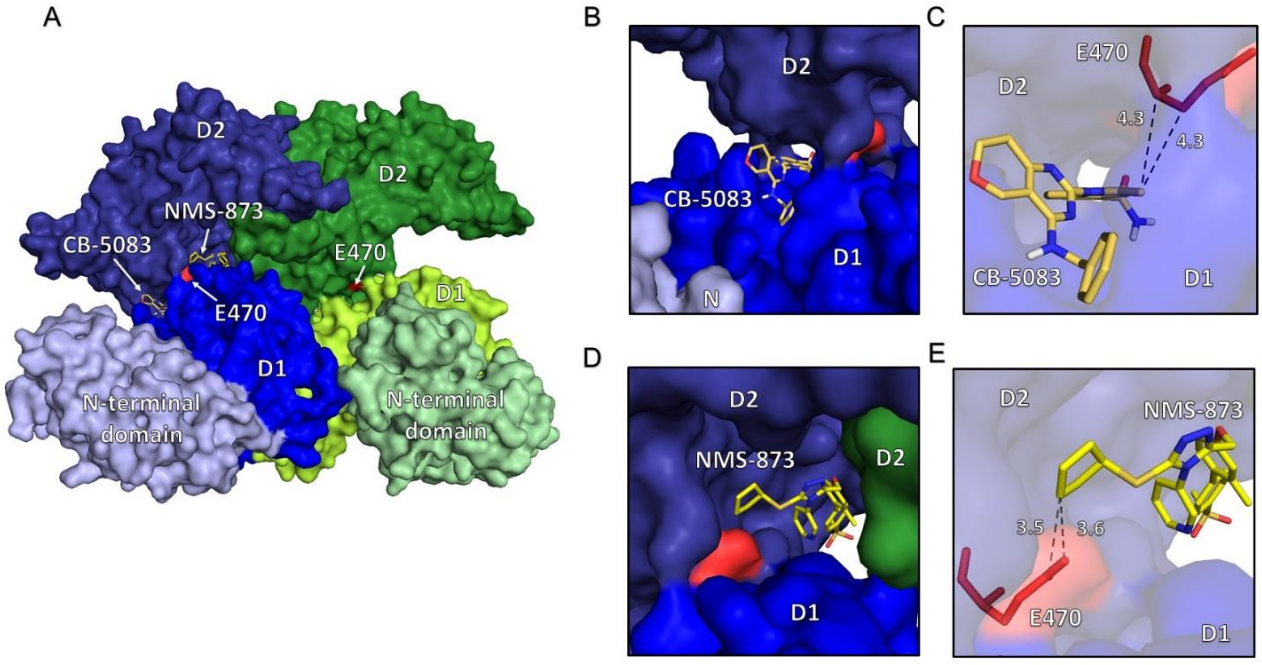

Figure 5.11. Molecular Docking of CB-5083 and NMS-873 into VCP. (A) A structural overview of two subunits of the VCP hexamer, with one in shades of blue and one in shades of green. The lightest shade represents the N terminal domain, the medium shade represents the D1 ATPase domain, and the darkest shade represents the D2 ATPase domain, as labeled. The mutation site E470 is labeled and in red. The binding sites near the D1-D2 linker of CB-5083 and NMS-873 are labeled (B) The primary binding mode of CB-5083, in the interface between the D1 and D2 subdomains. (C) A close-up view of the binding site of CB-5083, with distances to E470 marked. (D) The primary binding mode of NMS-873, at the interface of two VCP subunits and the D1-D2 linker, which is also in close proximity to the mutation site E470. (E) A close-up view of the primary binding mode of NMS-873, with distances to the mutation site marked in angstrom.

5.3 Discussion

We observed acquired mutations in *VCP* in ovarian cancer cells upon the acquisition of *in vitro* resistance to CB-5083. In particular, we consistently observed mutations at E470 in the resistant clones. Our results also indicate that specific substitutions, such as E470K or E470D, enhance the *in vitro* ATPase activity. Consistent with enhanced ATPase activities of these mutants, higher concentrations of CB-5083 were required to inhibit the activities of these mutants. Although these studies highlight the specificity of VCP inhibition by CB-5083 and the cytotoxic effect produced by VCP inhibition, our studies also provide an important cautionary note in the development of novel therapeutics targeting VCP. Cancer cells can rapidly acquire activating mutations in *VCP* that could bypass the effect of CB-5083.

Codon 470 is located in the linker region between D1 and D2 domains of VCP. Utilizing Cryo-EM, previous studies solved the structure of VCP bound to another inhibitor UPCDC-30245, and the results indicate that UPCDC-30245 binds to the linker region between D1 and D2 domains (Banerjee et al., 2016). This interaction interferes with the two-step sequential activation of D2 and D1 by ATP binding. Docking of CB-5083 to the structure, reported by Banerjee *et al*. (2016), suggests that CB-5083 may also associate with the D1-D2 linker region as well as the active site. Therefore, we speculate that the mechanism of inhibition of VCP by CB-5083 may be similar to UPCDC-30245, in which binding of a ligand to the interface of the two domains prevents the ratcheting motion, between D1 and D2 domains, that is required for the function of a full hexamer (Banerjee et al., 2016). Future structural studies investigating the interaction between VCP and CB-5083 are needed to confirm this assertion.

Docking studies suggest that, in addition to binding at the active site of VCP, CB-5083 may bind to the linker region between D1 and D2 and interact with residue 470. E470K substitution

could, therefore, disrupt the hydrophobic interaction between CB-5083 and E470 and interfere with that binding mode. Although the full effect of the mutation cannot be completely understood by docking alone, it is possible that amino acid substitution partially occludes the CB-5083 binding site, making CB-5083 binding less thermodynamically favorable. Therefore, we speculate that E470 substitutions reduce the affinity to CB-5083 and promote resistance to CB-5083.

In addition to the potential direct effect of E470 mutations on the ligand and target interactions, two other indirect mechanisms of inhibition could also be speculated. First, mutations at E470 induce conformation changes that lower binding affinity to VCP inhibitors. Second, mutations at E470 increase the enzymatic activity of VCP, and therefore a higher amount of inhibitors is needed to inhibit VCP mutants. Results from enzymatic *in vitro* ATPase assays indicate VCP mutants are more active than the wildtype VCP. Therefore, activating mutations may contribute to resistance to VCP inhibitors (Figure 5.12). These results are similar to the resistance mechanism associated with kinase inhibitors where target proteins or other components of the targeted pathway became mutated to create a bypass mechanism that produces resistance to kinase inhibitors (Johannessen et al., 2010).

It is interesting to note that although E470K and E470D VCP mutants are resistant to ML240, as indicated by *in vitro* ATPase assays, cells with VCP mutants are still sensitive to ML240. One possible interpretation of the results is that cytotoxicity effect produced by ML240 is not solely dependent on VCP inhibition. These results suggest additional targets of ML240 contribute to cytotoxicity. It will be important to identify these additional targets so that ML240 can be further developed as cancer therapeutics to overcome resistance to CB-5083.

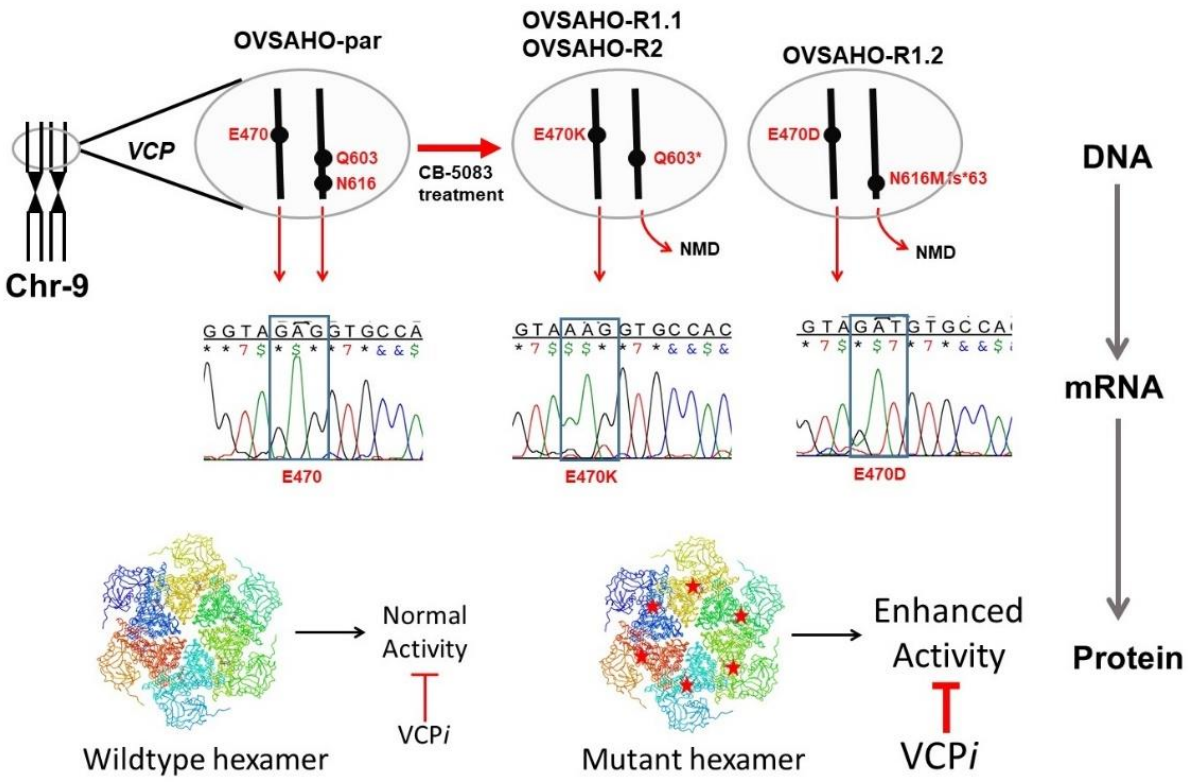

Figure 5.12. Graphical abstract elucidating the in vitro mechanism of resistance to CB-5083. Incremental and prolonged exposure to CB-5083 produced cells that acquired resistance to CB-5058. These cells harbor activating missense mutations at codon 470 (E470K or E470D) of VCP gene in one allele and inactivating nonsense (Q603*) or frameshift stop (N616Mfs*63) mutations in another allele. Although heterozygous mutations in DNA are detected at these sites, only homozygous mutations at codon 470 are detected in cDNA, suggesting that inactivating mutations are subjected to nonsense-mediated decay (NMD). The E470 mutants (E470K/E470D) display enhanced ATPase activity and require higher concentrations of VCP inhibitors to achieve the inhibitory effect.

We also observed that CB-5083-resistant cells harbor two different mutations on separate alleles: (1) activating mutations at E470, and (2) an inactivating nonsense mutation at Q603* or a frameshift deletion at N616. Complementary DNA sequence analysis of expressed VCP transcripts identified the E470 mutant transcripts as the primary transcripts. Transcripts containing Q603* and N616Mfs*63 are undetectable in the cDNA sequence analysis although these mutations are observed in the DNA sequence analysis. These results support our conclusion that nonsense mutations (Q603* and N616Mfs*63) are located in the other *VCP* allele and that transcripts produced from this mutant VCP are subjected to nonsense-mediated decay. Additionally, cells with mutant VCP show reduced expression of VCP, further providing a corroborating evidence that one allele is not expressed. Collectively, these results suggest a co-selection of activating and inactivating mutations in *VCP* under *in vitro* CB-5083 selection pressure.

With the RNA sequencing analysis, we validated our Sanger sequencing results and showed that resistant cells harbored two different mutations. Interestingly, we observed 69 other nonsynonymous mutations in the resistance cells. These include genes such *as UQCR10, MCM7, SLC16A3,* and *ATG4B.* Some of these nonsynonymous mutations could be passenger mutations that were present in a very small population of cells later acquired fitness-conferring mutations in VCP during the multiple rounds of CB-5083 treatment. However, some of these mutations could be associated with fitness-conferring traits that work in concert with or independently from the VCP mutations. Independent drug selection studies with CB-5083 should help in answering this question. Upon pathway analysis of differentially regulated genes, we observed the most significant association between genes upregulated by CB-5083 and the response to endoplasmic reticulum stress in both parental and resistant cells, while downregulated genes by CB-5083 in parental cells were associated with the pathway for cell division as defined by the GO term. Given

that the response to endoplasmic reticulum stress was the most significant GO term associated with genes upregulated by CB-5083 in resistant cells, our results suggest CB-5083 treatment can still target mutant VCP to affect protein quality control pathway, albeit the magnitude of the effect may be small compared to parental cells. Our assertion is supported by gene expression analysis indicating that only 31 genes were upregulated by CB-5083 by at least 1.5-fold in resistant cells whereas 1666 genes were upregulated by CB-5083 by at least 1.5-fold in parental cells.

Finally, we observed inactivating mutations in *VCP* in tumor samples reported by the Cancer Genome Atlas (TCGA) sequencing studies. In particular, truncating mutations at codon 616 are the most frequent hotspot mutations in *VCP* in TCGA database. Given that our *in vitro* selection with CB-5083 resulted in co-selection of activating and inactivating mutations in separate *VCP* alleles, the pre-existence of truncating mutations at codon 616 may portend acquired resistance to CB-5083. Therefore, ongoing clinical trials investigating the therapeutic effect of CB-5083 in cancer should investigate the theranostic potential of these mutations in cancer patients enrolled in the clinical trials.

Chapter 6: Overall discussion and future directions

Portions of this chapter are reproduced from the following publications with permission where required.

- **Bastola P** and Chien J (2018) Co-selected mutations in VCP: a novel mechanism of resistance to VCP inhibitors. Cell Death & Disease 9, 35. PMID: 29348605

6.1. Significance

The combination of cisplatin (or carboplatin) and paclitaxel (or docetaxel) are the primary standard-of-care chemotherapeutic agents for ovarian cancer. Cisplatin became the mainstay of ovarian cancer treatment after a series of studies carried out in the 1970s that showed a response rate between 25%-30% in ovarian cancer patients resistant to conventional therapy (Wiltshaw and Kroner, 1976; Young et al., 1979). In 1992, paclitaxel (Taxol) was FDA approved for the treatment of ovarian cancer. In the 1990s, two randomized controlled clinical trials investigated the efficacy of cisplatin and taxol combination in ovarian cancer patients. Both trials reported significant improvement in the progression-free survival and overall survival with the combination (McGuire et al., 1996; Piccart et al., 2000). Over the last two decades, however, the treatment regimen and the survival rates for ovarian cancer have not changed significantly. Recently, several targeted therapies have been granted FDA approval in ovarian cancer. These include the VEGF inhibitor bevacizumab and PARP inhibitors olaparib, rucaparib and niraparib. In 2014, olaparib became the first targeted agent to be FDA approved for ovarian cancer treatment. Olaparib was approved as maintenance therapy for the treatment of advanced ovarian cancer in patients with germline *BRCA1* or *BRCA2* mutations who have received three or more prior lines of chemotherapy. Subsequently, rucaparib was FDA approved in 2016 for treating ovarian cancer patients with germline and/or somatic mutations in *BRCA1* or *BRCA2*, while niraparib was FDA approved in 2017 as maintenance therapy in patients with recurrent platinum-sensitive ovarian cancer. Similarly, the VEGF inhibitor bevacizumab was FDA approved in 2014 for the treatment of platinum-resistant epithelial ovarian cancer. The FDA approval of these agents lends support to the idea that targeted therapies can be used to treat ovarian cancer. However, the paucity of

clinically approved molecularly targeted agents against ovarian cancer outlines the significance of identifying newer targets or therapeutic agents for this disease.

For this dissertation, I set out to identify vulnerabilities in high-grade serous ovarian cancer. A malignant genome harbors copy number alterations, aneuploidy, and mutations, which can be seen as inherent vulnerabilities. These alterations increase the transcriptomic stress and subsequently increase the proteotoxic stress. Proteotoxic stress can manifest itself as endoplasmic reticulum stress response resulting in the induction of the unfolded protein response. Mild unfolded protein response restores protein homeostasis by upregulating endoplasmic reticulum resident chaperone and downregulating protein synthesis. However, prolonged induction of the unfolded protein response (terminal UPR) can trigger cell death (Figure 6.1). I rationalized that increased copy number alterations in high-grade serous ovarian cancer create transcriptomic stress and subsequently result in proteotoxic stress in these tumors. Therefore, I decided to identify components in the protein quality control that can be targeted in ovarian cancer.

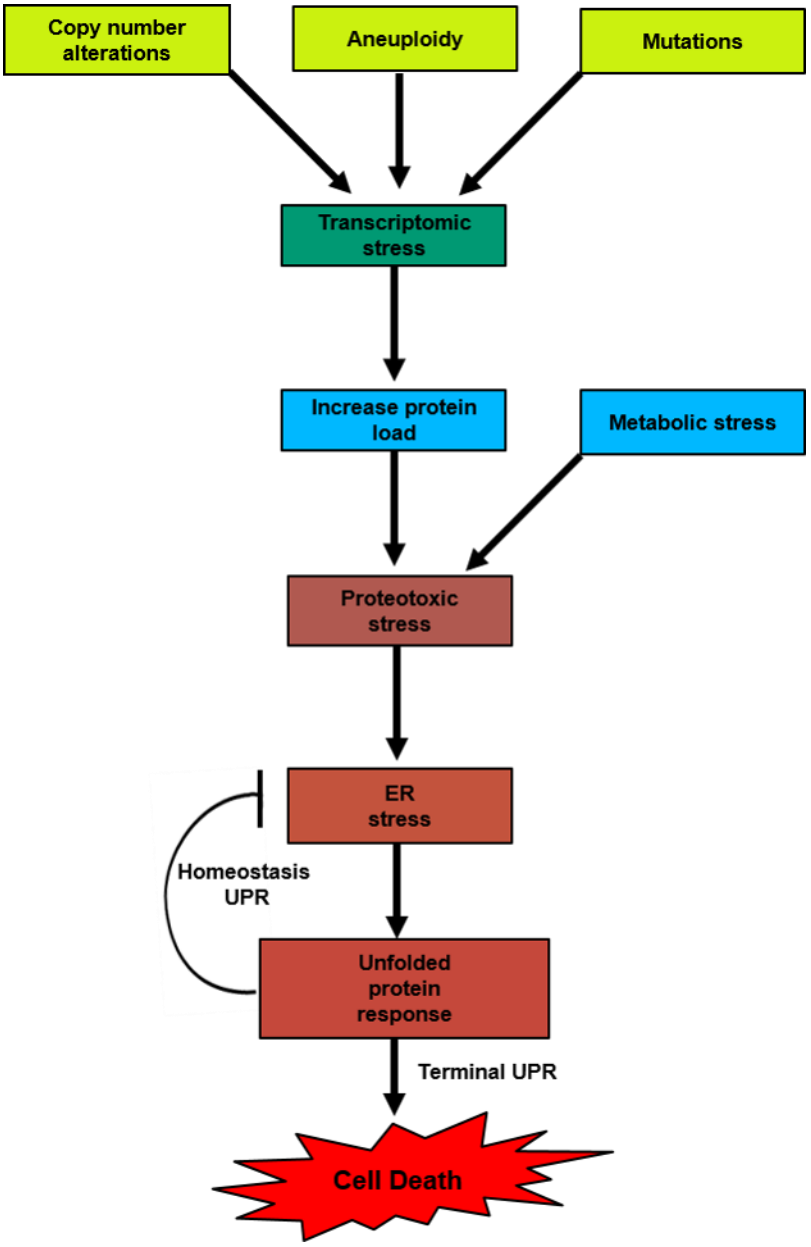

Figure 6.1. Inducing terminal unfolded protein response in cancer cells. Cancer genomes harbor numerous alterations that result in the increased transcriptomic stress. This in combination with metabolic stress in cancer causes proteotoxic stress. The increase in proteotoxic stress triggers endoplasmic reticulum stress resulting in the induction of the unfolded protein response. Mild induction of the unfolded protein response helps to mitigate the upstream endoplasmic reticulum stress. Such induction of the unfolded protein response is considered to be a homeostatic (homeostasis UPR). However, a prolonged induction of the unfolded protein response (terminal UPR) can trigger cell death. Adapted from: Oakes and Papa, Annual Review Pathology. 2015 (Oakes and Papa, 2015).

The protein quality control is a pro-survival response, which consists of (1) chaperones that allow the folding of nascent peptides during protein synthesis or refolding of denatured proteins induced by cellular stresses, (2) endoplasmic reticulum-associated degradation and the unfolded protein response that are involved in the adaptive response to endoplasmic reticulum stress, (3) the ubiquitin proteasome system that degrades misfolded, unfolded, unwanted, or damaged proteins to maintain proteostasis, and (4) autophagy that can remove unfolded protein aggregates through lysosomal degradation pathway. Cells ensure protein homeostasis by maintaining a balance in the rate of protein synthesis and degradation. Dysfunction in protein homeostasis can trigger abnormal the cellular functions and result in various human disorders. Similarly, cancer cells harbor a host of genomic alterations which can result in the dysregulation of protein expression and the aberrant expression of dysfunctional proteins. Such proteins must be efficiently recycled/degraded through cellular degradation machinery to maintain protein homeostasis. Cancer cells are heavily reliant on protein quality control pathways for survival and proliferation, a process known as the non-oncogenic addiction. Hence, targeting components of the protein quality control pathways has been shown to be effective in cancer therapeutics. The FDA approval of proteasome inhibitors such as bortezomib and carfilzomib has provided support to the idea that the ubiquitin proteasome system, a component of protein homeostasis, could be targeted in cancer (Chen et al., 2011; Kuhn et al., 2007). Likewise, the effectiveness of compounds such as Hsp90 inhibitors (Sidera and Patsavoudi, 2014), autophagy modulators (Boulay et al., 2004), and HDAC inhibitors (Santo et al., 2012) in several cancer types further support this idea.

Multiple genome-wide short hairpin RNAs (shRNAs)-based loss-of-function screening studies identified components of the protein quality control pathway, such as protease subunits in the proteasome system or VCP, as vulnerable targets in cancer (Etemadmoghadam et al., 2013;

Marcotte et al., 2012). Based on these studies, I decided to target VCP in ovarian cancer. Next, I identified candidate compounds to inhibit VCP *in vitro*. Based on their specificity towards targeting VCP, I decided to use the quinazoline-based VCP inhibitors DBeQ and ML240. During the course of this dissertation, another VCP inhibitor, CB-5083, became the first-in-class VCP inhibitor to show favorable pharmacokinetics and pharmacodynamics when administered orally in tumor-bearing mice. Based on these results, I decided to include CB-5083 in my studies. Upon identifying the therapeutic target and compounds, I started this dissertation project with the following questions:

1) Does inhibiting VCP through genetic or pharmacological agents result in cytotoxicity in ovarian cancer cells?
2) Can VCP inhibitors be combined with other agents that modulate the protein quality control pathway?
3) What are some of the mechanisms of resistance towards VCP inhibitors?

Through this dissertation, I was able to answer these questions. In the subsequent sections, I will summarize our results while outlining future directions.

6.2. Summary and future directions for Chapter 3

In Chapter 3, we showed a dose-dependent *in vitro* cytotoxicity induced by VCP inhibitors DBeQ and ML240 in several ovarian cancer cells (Figure 3.1). Similarly, small interfering RNA (siRNA)-mediated knockdown of VCP in ovarian cancer cells attenuated cell growth (Figure 3.2). These results provided a proof-of-concept that VCP can be targeted in ovarian cancer. Additionally, we characterized cellular responses, such as the cell cycle arrest (Figure 3.4), induction of the unfolded protein response (Figure 3.6), increased proteasomal inhibition (Figure

3.7), and the activation of apoptosis (Figure 3.5) upon the treatment of VCP inhibitors. VCP has been shown to mediate diverse cellular functions including endoplasmic reticulum-associated degradation, the ubiquitin proteasome system, mitochondria-mediated degradation, chromatin-associated degradation, stress granules formation, and autophagy. So far, our studies have primarily been focused on the endoplasmic reticulum-associated degradation and the ubiquitin proteasome system. It is likely that VCP inhibitors have effects on other cellular processes, and these inhibitors could be used to study their effects on other VCP-mediated functions.

VCP has been linked to several molecular functions pertaining to protein quality control. However, one of the primary questions is how VCP mediates such diverse functions. With scores of studies illuminating its function in several biological processes, a pattern has emerged. VCP is able to mediate such diverse functions through a set of approximately 30 different cofactor proteins. Unique sets of cofactor proteins have been associated with separate VCP functions. Major cofactors that regulate VCP function include Ufd1-Npl4, p47, and UBXD1 (van den Boom and Meyer, 2017). This presents a new avenue to expand the development of function-specific VCP inhibitors, where a particular function pertaining to VCP can be targeted by inhibiting VCP interaction with a specific cofactor. In fact, some preliminary studies have identified compounds that display increased potency against the VCP-p47 complex (Fang et al., 2015).

Furthermore, we showed that VCP inhibitors can be combined with the GADD34 inhibitor, salubrinal, to induce synergistic cytotoxicity (Figure 3.8-3.10). The rationale for a combination therapy is to use drugs that work by different mechanisms and can display increased effects when used together. Chemotherapeutic agents are often associated with drug-related toxicities. Identifying compounds that are synergistic allows lowering the dose of these agents, which could lower the drug-related toxicities. Additionally, targeting tumor cells with a combination of

compounds can avoid the development of drug resistance. Our results have implications not just for ovarian cancer therapy, but results from our studies are relevant for designing combination therapies for other tumors. Since VCP inhibitors display cytotoxicity towards multiple different cancer types, the combination of VCP inhibitors and salubrinal should show efficacy in other cancer types.

Similarly, we showed that cytotoxicity mediated through VCP inhibitors can be enhanced by modulating the unfolded protein response. With scores of compounds that modulate the unfolded protein response in the drug development pipeline, our studies provide a rationale for combining the compounds that induce terminal unfolded protein response with the compounds that inhibit ubiquitin proteasome system. In future, synergistic cytotoxicity can be assessed between VCP inhibitors and compounds that have been shown to modulate the unfolded protein response using the sulforhodamine B (SRB) assays and drug synergy studies protocol outlined in Chapter 2.3.

Finally, we showed that VCP inhibitors can be combined with other compounds to enhance the cytotoxic effect. In future, high-throughput drug screening can be performed to identify possible FDA approved compounds that display synergistic cytotoxicity with VCP inhibitors. Identifying FDA approved drug candidates that enhance the synergistic cytotoxicity with VCP inhibitors will allow to enhance the efficacy of VCP inhibitors as well as negate the possible occurrence of drug resistance.

6.3. Summary and future directions for Chapter 4

In Chapter 4, we showed synergy between mifepristone and VCP inhibitors. In this chapter, our primary focus was to identify a clinically relevant drug combination with VCP inhibitors. We were able to establish that a clinically achievable dose of mifepristone was synergistic with the oral VCP inhibitor CB-5083 *in vitro*. Pursuing this drug combination in the clinic can be the most

direct application of this dissertation towards providing greater therapeutic benefits in cancer patients. Before pursuing this combination in patients, synergistic cytotoxicity towards VCP inhibitors and mifepristone need to be assessed in rodent cancer models. For assessing the effective on ovarian tumors, ovarian cancer xenografts will be injected intraperitoneally to immune compromised mice. Before performing the combination treatment, effective individual dose will be established by treating these mice with different doses of CB-5083 and mifepristone using oral gavage. Effectiveness with a single agent will be determined by comparing the decrease in tumor burden in drug treated mice to the vehicle treated mice. After establishing effective single dose for both drugs, experiments will be performed to analyze the effectiveness of the combination compared to the single agents. This will be assessed first by examining the tumor burden, and second by performing long term survival studies.

After the establishment of synergy between VCP inhibitors and mifepristone *in vitro*, we investigated the mechanism that contributed to the drug synergy. Mifepristone has been shown to modulate the unfolded protein response, but the mechanism was largely unknown. Our results point to the activation of the heme-regulated inhibitor (HRI) kinase pathway, and the inhibition of the activation transcription factor 6 (ATF6) pathway as two possible mechanisms for the mifepristone-induced unfolded protein response. Although we were able to narrow down to two potential mediators of the mifepristone-induced unfolded protein response, further studies are needed to confirm whether both proteins are necessary for the synergistic cytotoxicity induced by the combination of VCP inhibitors with mifepristone.

To further dissect the involvement of the HRI kinase pathway towards the synergistic cytotoxicity, it would be necessary to perform the synergy experiment following the knockdown of HRI protein using small interfering RNAs. Additionally, we could perform synergistic studies

between VCP inhibitors and specific HRI activators (Chen et al., 2013). Results from these studies will allow us to identify the involvement of HRI kinase pathway in providing the synergy between VCP inhibitors and mifepristone.

Similarly, to verify the role of the ATF6 branch in the synergy between VCP inhibitors and mifepristone, it would be important to investigate the effects of ATF6 knockdown or knockout in several ovarian cancer cell lines treated with VCP inhibitors. The increased sensitivity towards VCP inhibitors upon the ATF6 knockdown or knockout will allow us to further implicate ATF6 in the drug synergy. More importantly, the rescue experiments with the enforced expression of transcriptionally active ATF6 should further define the role of ATF6 in the drug synergy between VCP inhibitors and mifepristone.

Our synergy studies show that compounds targeting various components of the protein quality control pathway can be combined to enhance the cytotoxicity. During the course of this study, first-in-class selective histone deacetylase 6 (HDAC6) inhibitors ACY-241 and ACY-1215 have entered clinical trials for several cancer types. HDAC6, a cytoplasmic deacetylase, has gained a significant attention as a therapeutic target due to its role in microtubule association and aggresome clearance, making it an important mediator of the protein quality control (Dallavalle et al., 2012). Additionally, HDAC6 has been shown to associate with Hsp90 (Kovacs et al., 2005) and VCP (Boyault et al., 2006) during aggresome formation. These features make HDAC6 inhibitors ideal candidates to perform synergistic studies with VCP inhibitors.

In this dissertation, I used VCP inhibitors to target the protein quality control in ovarian cancer. The protein quality control pathway is important for other essential cellular processes such as cell cycle regulation, DNA repair, and cell division. Given that DNA repair genes, such as *BRCA1* and *BRCA2*, are clients of heat shock proteins (Johnson et al., 2013; Noguchi et al., 2006; Stecklein et

al., 2012) that are involved in protein homeostasis and given that VCP is directly involved in the recruitment of P53BP1 in the initial steps of DNA damaging signaling (Acs et al., 2011; Meerang et al., 2011), it is possible that VCP inhibitors may enhance sensitivity to DNA-targeted chemotherapies, such as carboplatin, cisplatin, and inhibitors of poly (ADP)-ribosylation polymerases (PARP inhibitors).

6.4. Summary and future directions for Chapter 5

In Chapter 5, we employed a combination of incremental and continuous dosing scheme to establish CB-5083 resistant ovarian cancer cell lines. We identified two heterozygous mutations, E470D and E470K, in the D1-D2 linker region (Figure 5.4). This amino acid position is close to previously identified point mutations in CB-5083-resistant cell lines (Anderson et al., 2015), which further underlines the importance of the D1-D2 linker region in the development of resistance to CB-5083. Furthermore, the *in vitro* VCP ATPase activity assay showed an increase in basal ATPase activity and a higher IC_{50} towards several classes of VCP inhibitors in these VCP-mutant cells compared to parental counterparts (Figure 5.9). Additionally, we performed unbiased docking to show that E470 is located in a putative CB-5083 binding site (Figure 5.11). Our results in combination with mutations observed by Anderson *et al*., suggest D1-D2 linker region as an additional putative binding site for CB-5083.

Besides the discovery of missense mutations in the D1-D2 linker region, we also found heterozygous nonsense mutations at Q603 and N616. Furthermore, these nonsense mutations were identified only in genomic DNA sequencing and not in the cDNA sequencing of CB-5083-resistant cells. These results suggest nonsense mutations at Q603 and N616 are subjected to nonsense-mediated decay. Consequently, mutant cell lines showed reduced expression of VCP mRNA and protein, which is consistent with the effect of nonsense-mediated decay. Nonsense mutation at

N616 is one of the most reported alterations of VCP in several cancer subtypes, making it a relevant theranostic marker in selecting patients in clinical trials. Our studies suggest that the co-selection of an activating mutation (such as E470K) and an inactivating mutation (such as Q603*) is necessary for the development of resistance to CB-5083 (Bastola and Chien, 2018). Therefore, tumors with preexisting somatic mutations at N616 are expected to quickly develop resistance to CB-5083, and these patients may not benefit from the treatment.

VCP forms hexameric complexes, and our results suggest that inhibition of a wildtype VCP subunit by CB-5083 in a hexameric complex is sufficient for cytotoxicity. Hence, activating mutation in one VCP allele that escapes inhibition by CB-5083 is not sufficient to generate resistance to CB-5083, and the other VCP allele is also subjected to either activating mutation or truncation mutation. In our studies, we observed that the second VCP allele is lost through nonsense mutations (Figure 6.2A). Furthermore, previous studies have shown a correlation between gene copy number and mRNA level of VCP with resistance to VCP inhibitors (Anderson et al., 2015); however, the correlation values were low. Our results indicate that mutations in *VCP* should also be taken into consideration when performing such analyses.

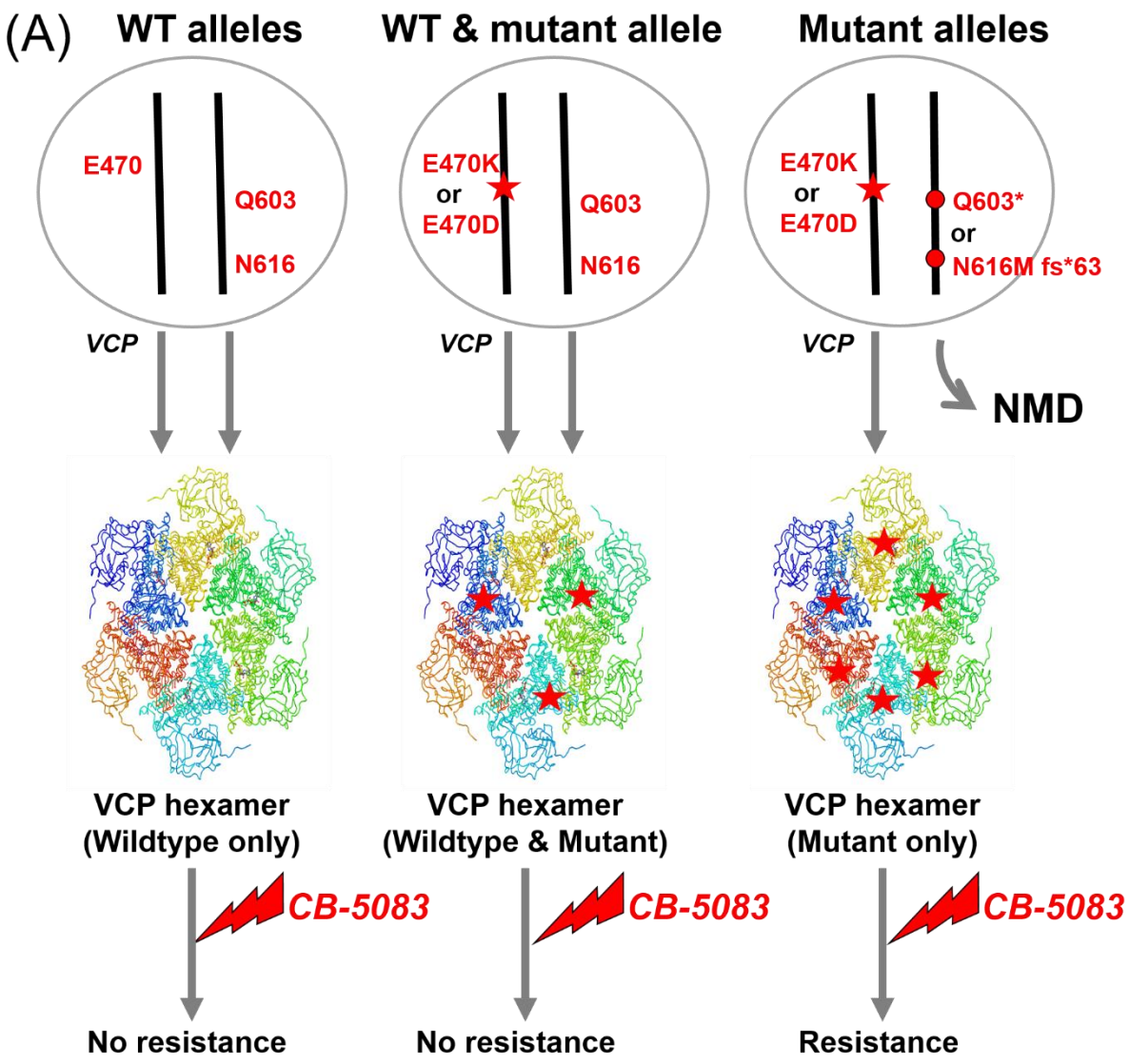

Figure 6.2. Co-selected mutations in VCP confers resistance to CB-5083. A) Presence of both wildtype VCP alleles results in wildtype VCP protein hexamer, which can be inhibited by CB-5083. Similarly, the presence of one mutant allele (E470K or E470D) results in VCP protein hexamers with mixed VCP proteins (wildtype and mutant). However, inhibition of wildtype protein in the complex upon CB-5083 treatment is sufficient for cytotoxicity. Loss of wildtype copy is required for resistance towards CB-5083.

Our study identified a unique pattern of co-selected mutations with CB-5083 treatment, whereby prolonged treatment allowed for the selection of activating missense mutations at D1-D2 linker region and inactivating nonsense mutations at the D2 domain. This co-selection could occur in one of three scenarios as outlined in Figure 6.2B. Both mutations may appear synchronously or asynchronously in a sequential manner. We observed a progressive establishment of resistance towards CB-5083 which allows us to favor the asynchronous model of resistance; however, the definitive study needs to be done to confirm this model of resistance. Similarly, further studies are required to identify exact sequence of asynchronous mutations that lead to resistance (scenario 2 or scenario 3). Nonetheless, given that truncation mutation at N616 is found in tumor samples, it is conceivable to suggest that these tumor cells could acquire asynchronous activating mutations in the second allele to become resistant to CB-5083.

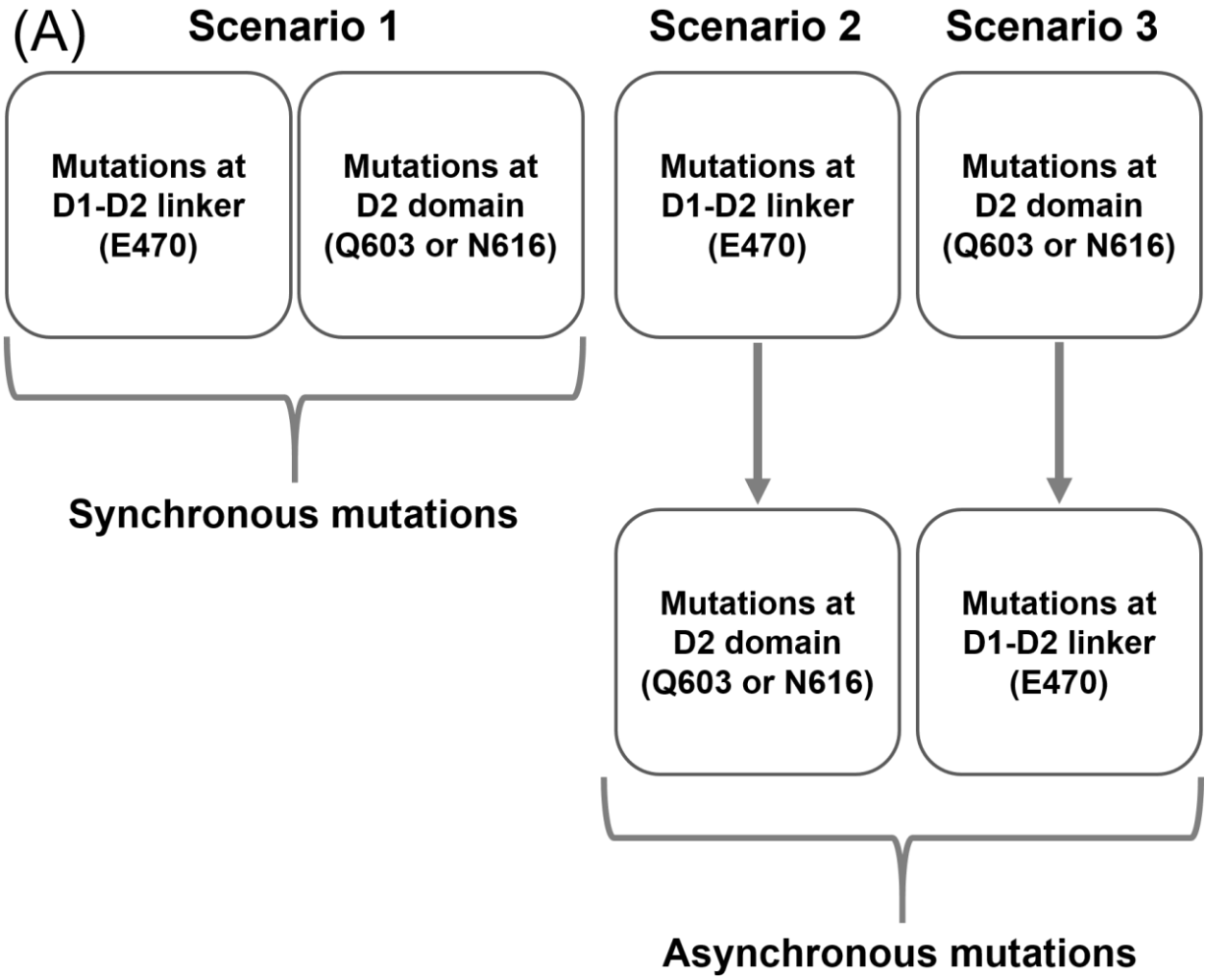

Figure 6.3. Putative scenarios of co-selected mutations. A) Co-selected mutations observed upon CB-5083 treatment can occur via three scenarios. Scenario 1 outlines the chance of two different mutations occurring simultaneously; whereas scenario 2 and 3 outline the occurrence of serial mutations whereby mutations at D1-D2 linker is then followed by mutations at the D2 domain or *vice versa*.

In order to study the progression of VCP resistance, we can take the drug resistance study performed in Chapter 5 as a template. In Figure 5.1A & 5.1C, we outline a combination of intermittent and continuous dosing scheme to generate CB-5083 resistant cell lines. We could apply this dosing scheme while collecting cells after each round of drug treatment. Tumor cells should gradually develop resistance towards CB-5083. Sequencing VCP gene and complementary DNA at various time points during the selection process should help us track the sequence of activating and inactivating mutations in the development of resistance in the tumor cells.

In Chapter 5, we showed that recombinant E470D and E470K proteins display increased ATPase activity and resistance to VCP inhibitors using VCP-ATPase assay; however, we have not shown if the introduction of these missense mutations results in resistance to CB-5083 in cell lines. Clustered regularly interspaced short palindromic repeats-Cas9 (CRISPR-Cas9) genome editing can be used to introduce these mutations in OVSAHO parental cell lines.

Although *in vitro* ATPase assay suggests VCP mutant proteins (E470K and E470D) are cross-resistant to other VCP inhibitors, such as ML240 and DBeQ, CB-5083-resistant cells carrying these mutations retain their sensitivity towards ML240 and DBeQ. These results suggest that off-target effects of ML240 and DBeQ contribute to cytotoxicity. It would be important to define additional targets of ML240 and DBeQ, as these cellular targets may be important for further development of therapeutics to overcome resistance to CB-5083.

Lastly, our results in Chapter 5 show that target alternation can be a potential route to resistance towards VCP inhibitors. Establishment of resistance cell lines and creation of novel VCP mutant proteins should aid in the development of novel VCP inhibitors as well as provide insight into the understanding of VCP protein which displays such diverse cellular functions.

6.5. Overall conclusion

In conclusion, our studies provide a proof-of-concept that VCP can be targeted in ovarian cancer. Likewise, we identified clinically relevant drug combinations (CB-5083 and mifepristone) that should be investigated further. Importantly, we showed that VCP inhibitors can be synergistic with other compounds that modulate the unfolded protein response. Lastly, we showed that prolonged treatment with VCP inhibitor- CB-5083 can result in the development of resistance through a series of missense and nonsense mutations in the *VCP* gene.

Chapter 7: References

Acs, K., Luijsterburg, M.S., Ackermann, L., Salomons, F.A., Hoppe, T., Dantuma, N.P., 2011. The AAA-ATPase VCP/p97 promotes 53BP1 recruitment by removing L3MBTL1 from DNA double-strand breaks. Nature Structural & Molecular Biology 18, 1345-1350.

Adams, P.D., Afonine, P.V., Bunkoczi, G., Chen, V.B., Davis, I.W., Echols, N., Headd, J.J., Hung, L.W., Kapral, G.J., Grosse-Kunstleve, R.W., McCoy, A.J., Moriarty, N.W., Oeffner, R., Read, R.J., Richardson, D.C., Richardson, J.S., Terwilliger, T.C., Zwart, P.H., 2010. PHENIX: a comprehensive Python-based system for macromolecular structure solution. Acta crystallographica Section D Structural Biology 66, 213-221.

Aghajanian, C., Blessing, J.A., Darcy, K.M., Reid, G., DeGeest, K., Rubin, S.C., Mannel, R.S., Rotmensch, J., Schilder, R.J., Riordan, W., 2009. A phase II evaluation of bortezomib in the treatment of recurrent platinum-sensitive ovarian or primary peritoneal cancer: a Gynecologic Oncology Group study. Gynecologic Oncology 115, 215-220.

Aghajanian, C., Dizon, D.S., Sabbatini, P., Raizer, J.J., Dupont, J., Spriggs, D.R., 2005. Phase I Trial of Bortezomib and Carboplatin in Recurrent Ovarian or Primary Peritoneal Cancer. Journal of Clinical Oncology 23, 5943-5949.

Akin, J.M., Waddell, J.A., Solimando, D.A., 2014. Paclitaxel and Carboplatin (TC) Regimen for Ovarian Cancer. Hospital Pharmacy 49, 425-431.

Altman, A.D., Nelson, G., Chu, P., Nation, J., Ghatage, P., 2012. Optimal debulking targets in women with advanced stage ovarian cancer: a retrospective study of immediate versus interval debulking surgery. Journal of Obstetrics and Gynaecology Canada 34, 558-566.

Alverez, C., Arkin, M.R., Bulfer, S.L., Colombo, R., Kovaliov, M., LaPorte, M.G., Lim, C., Liang, M., Moore, W.J., Neitz, R.J., Yan, Y., Yue, Z., Huryn, D.M., Wipf, P., 2015. Structure-Activity Study of Bioisosteric Trifluoromethyl and Pentafluorosulfanyl Indole Inhibitors of the AAA ATPase p97. ACS Medicinal Chemistry Letters 6, 1225-1230.

Alverez, C., Bulfer, S.L., Chakrasali, R., Chimenti, M.S., Deshaies, R.J., Green, N., Kelly, M., LaPorte, M.G., Lewis, T.S., Liang, M., Moore, W.J., Neitz, R.J., Peshkov, V.A., Walters, M.A., Zhang, F., Arkin, M.R., Wipf, P., Huryn, D.M., 2016. Allosteric Indole Amide Inhibitors of p97: Identification of a Novel Probe of the Ubiquitin Pathway. ACS Medicinal Chemistry Letters 7, 182-187.

Anderson, D.J., Le Moigne, R., Djakovic, S., Kumar, B., Rice, J., Wong, S., Wang, J., Yao, B., Valle, E., von Soly, S.K., Madriaga, A., Soriano, F., Menon, M.-K., Wu, Z.Y., Kampmann, M., Chen, Y., Weissman, J.S., Aftab, B.T., Yakes, F.M., Shawver, L., Zhou, H.-J., Wustrow, D., Rolfe, M., 2015. Targeting the AAA ATPase p97 as an approach to treat cancer through disruption of protein homeostasis. Cancer Cell 28, 653-665.

Anuncibay-Soto, B., Perez-Rodriguez, D., Santos-Galdiano, M., Font, E., Regueiro-Purrinos, M., Fernandez-Lopez, A., 2016. Post-ischemic salubrinal treatment results in a neuroprotective role in global cerebral ischemia. Journal of Neurochemistry 138, 295-306.

Armstrong, D.K., 2002. Relapsed ovarian cancer: challenges and management strategies for a chronic disease. The Oncologist 7, 20-28.

Atkins, C., Liu, Q., Minthorn, E., Zhang, S.Y., Figueroa, D.J., Moss, K., Stanley, T.B., Sanders, B., Goetz, A., Gaul, N., Choudhry, A.E., Alsaid, H., Jucker, B.M., Axten, J.M., Kumar, R., 2013. Characterization of a novel PERK kinase inhibitor with antitumor and antiangiogenic activity. Cancer Research 73, 1993-2002.

Auner, H.W., Moody, A.M., Ward, T.H., Kraus, M., Milan, E., May, P., Chaidos, A., Driessen, C., Cenci, S., Dazzi, F., Rahemtulla, A., Apperley, J.F., Karadimitris, A., Dillon, N., 2013. Combined inhibition of p97 and the proteasome causes lethal disruption of the secretory apparatus in multiple myeloma cells. PLoS One 8, e74415.

Axten, J.M., Medina, J.R., Feng, Y., Shu, A., Romeril, S.P., Grant, S.W., Li, W.H., Heerding, D.A., Minthorn, E., Mencken, T., Atkins, C., Liu, Q., Rabindran, S., Kumar, R., Hong, X., Goetz, A., Stanley, T., Taylor, J.D., Sigethy, S.D., Tomberlin, G.H., Hassell, A.M., Kahler, K.M., Shewchuk, L.M., Gampe, R.T., 2012. Discovery of 7-methyl-5-(1-{[3-(trifluoromethyl)phenyl]acetyl}-2,3-dihydro-1H-indol-5-yl)-7H-p yrrolo[2,3-d]pyrimidin-4-amine (GSK2606414), a potent and selective first-in-class inhibitor of protein kinase R (PKR)-like endoplasmic reticulum kinase (PERK). Journal of Medicinal Chemistry 55, 7193-7207.

Bamford, J., Webster, R.M., 2017. The ovarian cancer drug market. Nature Review Drug Discovery 16, 451-452.

Banerjee, S., Bartesaghi, A., Merk, A., Rao, P., Bulfer, S.L., Yan, Y., Green, N., Mroczkowski, B., Neitz, R.J., Wipf, P., Falconieri, V., Deshaies, R.J., Milne, J.L., Huryn, D., Arkin, M., Subramaniam, S., 2016. 2.3 A resolution cryo-EM structure of human p97 and mechanism of allosteric inhibition. Science 351, 871-875.

Barrott, J.J., Haystead, T.A.J., 2013. Hsp90, an unlikely ally in the war on cancer. The FEBS journal 280, 1381-1396.

Bastola, P., Chien, J., 2018. Co-selected mutations in VCP: a novel mechanism of resistance to VCP inhibitors. Cell Death & Disease 9, 35.

Baulieu, E.E., 1989. Contragestion and other clinical applications of RU 486, an antiprogesterone at the receptor. Science 245, 1351-1357.

Baumeister, P., Luo, S., Skarnes, W.C., Sui, G., Seto, E., Shi, Y., Lee, A.S., 2005. Endoplasmic reticulum stress induction of the Grp78/BiP promoter: activating mechanisms mediated by YY1 and its interactive chromatin modifiers. Molecular and Cellular Biology 25, 4529-4540.

Berkenblit, A., Cannistra, S.A., 2005. Advances in the management of epithelial ovarian cancer. The Journal of Reproductive Medicine 50, 426-438.

Beskow, A., Grimberg, K.B., Bott, L.C., Salomons, F.A., Dantuma, N.P., Young, P., 2009. A Conserved Unfoldase Activity for the p97 AAA-ATPase in Proteasomal Degradation. Journal of Molecular Biology 394, 732-746.

Bodnar, N.O., Rapoport, T.A., 2017. Molecular Mechanism of Substrate Processing by the Cdc48 ATPase Complex. Cell 169, 722-735.

Boulay, A., Zumstein-Mecker, S., Stephan, C., Beuvink, I., Zilbermann, F., Haller, R., Tobler, S., Heusser, C., O'Reilly, T., Stolz, B., Marti, A., Thomas, G., Lane, H.A., 2004. Antitumor efficacy of intermittent treatment schedules with the rapamycin derivative RAD001 correlates with prolonged inactivation of ribosomal protein S6 kinase 1 in peripheral blood mononuclear cells. Cancer Research 64, 252-261.

Boyault, C., Gilquin, B., Zhang, Y., Rybin, V., Garman, E., Meyer-Klaucke, W., Matthias, P., Müller, C.W., Khochbin, S., 2006. HDAC6–p97/VCP controlled polyubiquitin chain turnover. The EMBO Journal 25, 3357-3366.

Boyce, M., Bryant, K.F., Jousse, C., Long, K., Harding, H.P., Scheuner, D., Kaufman, R.J., Ma, D., Coen, D.M., Ron, D., Yuan, J., 2005. A selective inhibitor of eIF2alpha dephosphorylation protects cells from ER stress. Science 307, 935-939.

Bryant, H.E., Schultz, N., Thomas, H.D., Parker, K.M., Flower, D., Lopez, E., Kyle, S., Meuth, M., Curtin, N.J., Helleday, T., 2005. Specific killing of BRCA2-deficient tumours with inhibitors of poly(ADP-ribose) polymerase. Nature 434, 913-917.

Buchan, J.R., Kolaitis, R.-M., Taylor, J.P., Parker, R., 2013. Eukaryotic stress granules are cleared by granulophagy and Cdc48/VCP function. Cell 153, 1461-1474.

Bug, M., Meyer, H., 2012. Expanding into new markets--VCP/p97 in endocytosis and autophagy. Journal of Structural Biology 179, 78-82.

Bursavich, M.G., Parker, D.P., Willardsen, J.A., Gao, Z.H., Davis, T., Ostanin, K., Robinson, R., Peterson, A., Cimbora, D.M., Zhu, J.F., Richards, B., 2010. 2-Anilino-4-aryl-1,3-thiazole

inhibitors of valosin-containing protein (VCP or p97). Bioorganic & Medicinal Chemistry Letters 20, 1677-1679.

Butler, L.M., Ferraldeschi, R., Armstrong, H.K., Centenera, M.M., Workman, P., 2015. Maximizing the Therapeutic Potential of Hsp90 Inhibitors. Molecular Cancer Research 13, 1445-1451.

Buys, S.S., Partridge, E., Black, A., Johnson, C.C., Lamerato, L., Isaacs, C., Reding, D.J., Greenlee, R.T., Yokochi, L.A., Kessel, B., Crawford, E.D., Church, T.R., Andriole, G.L., Weissfeld, J.L., Fouad, M.N., Chia, D., O'Brien, B., Ragard, L.R., Clapp, J.D., Rathmell, J.M., Riley, T.L., Hartge, P., Pinsky, P.F., Zhu, C.S., Izmirlian, G., Kramer, B.S., Miller, A.B., Xu, J.L., Prorok, P.C., Gohagan, J.K., Berg, C.D., 2011. Effect of screening on ovarian cancer mortality: the Prostate, Lung, Colorectal and Ovarian (PLCO) Cancer Screening Randomized Controlled Trial. Jama 305, 2295-2303.

Cancer Genome Atlas Research Network, 2011. Integrated genomic analyses of ovarian carcinoma. Nature 474, 609-615.

Cao, K., Nakajima, R., Meyer, H.H., Zheng, Y., 2003. The AAA-ATPase Cdc48/p97 regulates spindle disassembly at the end of mitosis. Cell 115, 355-367.

Caravita, T., de Fabritiis, P., Palumbo, A., Amadori, S., Boccadoro, M., 2006. Bortezomib: efficacy comparisons in solid tumors and hematologic malignancies. Nature Clinical Practice. Oncology 3, 374-387.

Cazanave, S.C., Elmi, N.A., Akazawa, Y., Bronk, S.F., Mott, J.L., Gores, G.J., 2010. CHOP and AP-1 cooperatively mediate PUMA expression during lipoapoptosis. American Journal of Physiology-Gastrointestinal and Liver Physiology 299, G236-243.

Chapman, E., Maksim, N., de la Cruz, F., La Clair, J.J., 2015. Inhibitors of the AAA+ chaperone p97. Molecules 20, 3027-3049.

Cheaib, B., Auguste, A., Leary, A., 2015. The PI3K/Akt/mTOR pathway in ovarian cancer: therapeutic opportunities and challenges. Chinese Journal of Cancer 34, 4-16.

Check, J.H., Check, D., Wilson, C., Lofberg, P., 2016. Long-term High-quality Survival with Single-agent Mifepristone Treatment Despite Advanced Cancer. Anticancer Research 36, 6511-6513.

Chen, D., Frezza, M., Schmitt, S., Kanwar, J., Dou, Q.P., 2011. Bortezomib as the First Proteasome Inhibitor Anticancer Drug: Current Status and Future Perspectives. Current Cancer Drug Targets 11, 239-253.

Chen, T., Takrouri, K., Hee-Hwang, S., Rana, S., Yefidoff-Freedman, R., Halperin, J., Natarajan, A., Morisseau, C., Hammock, B., Chorev, M., Aktas, B.H., 2013. Explorations of substituted urea functionality for the discovery of new activators of the heme-regulated inhibitor kinase. Journal of Medicinal Chemistry 56, 9457-9470.

Chen, X., Shen, J., Prywes, R., 2002. The luminal domain of ATF6 senses endoplasmic reticulum (ER) stress and causes translocation of ATF6 from the ER to the Golgi. The Journal of Biological Chemistry 277, 13045-13052.

Cheung, H.W., Cowley, G.S., Weir, B.A., Boehm, J.S., Rusin, S., Scott, J.A., East, A., Ali, L.D., Lizotte, P.H., Wong, T.C., Jiang, G., Hsiao, J., Mermel, C.H., Getz, G., Barretina, J., Gopal, S., Tamayo, P., Gould, J., Tsherniak, A., Stransky, N., Luo, B., Ren, Y., Drapkin, R., Bhatia, S.N., Mesirov, J.P., Garraway, L.A., Meyerson, M., Lander, E.S., Root, D.E., Hahn, W.C., 2011. Systematic investigation of genetic vulnerabilities across cancer cell lines reveals lineage-specific dependencies in ovarian cancer. Proceedings of the National Academy of Sciences 108, 12372-12377.

Chien, J., Kuang, R., Landen, C., Shridhar, V., 2013. Platinum-Sensitive Recurrence in Ovarian Cancer: The Role of Tumor Microenvironment. Frontiers in Oncology 3, 251.

Chien, W., Ding, L.W., Sun, Q.Y., Torres-Fernandez, L.A., Tan, S.Z., Xiao, J., Lim, S.L., Garg, M., Lee, K.L., Kitajima, S., Takao, S., Leong, W.Z., Sun, H., Tokatly, I., Poellinger, L., Gery, S., Koeffler, P.H., 2014. Selective inhibition of unfolded protein response induces apoptosis in pancreatic cancer cells. Oncotarget 5, 4881-4894.

Chou, T.-F., Deshaies, R.J., 2011. Quantitative Cell-based Protein Degradation Assays to Identify and Classify Drugs That Target the Ubiquitin-Proteasome System. The Journal of Biological Chemistry 286, 16546-16554.

Chou, T.F., Brown, S.J., Minond, D., Nordin, B.E., Li, K., Jones, A.C., Chase, P., Porubsky, P.R., Stoltz, B.M., Schoenen, F.J., Patricelli, M.P., Hodder, P., Rosen, H., Deshaies, R.J., 2011. Reversible inhibitor of p97, DBeQ, impairs both ubiquitin-dependent and autophagic protein clearance pathways. Proceedings of the National Academy of Sciences 108, 4834-4839.

Chou, T.F., Bulfer, S.L., Weihl, C.C., Li, K., Lis, L.G., Walters, M.A., Schoenen, F.J., Lin, H.J., Deshaies, R.J., Arkin, M.R., 2014. Specific inhibition of p97/VCP ATPase and kinetic analysis demonstrate interaction between D1 and D2 ATPase domains. Journal of Molecular Biology 426, 2886-2899.

Chou, T.F., Li, K., Frankowski, K.J., Schoenen, F.J., Deshaies, R.J., 2013. Structure-activity relationship study reveals ML240 and ML241 as potent and selective inhibitors of p97 ATPase. ChemMedChem 8, 297-312.

Ciriello, G., Miller, M.L., Aksoy, B.A., Senbabaoglu, Y., Schultz, N., Sander, C., 2013. Emerging landscape of oncogenic signatures across human cancers. Nature Genetics 45, 1127-1133.

Dai, R.M., Li, C.-C.H., 2001. Valosin-containing protein is a multi-ubiquitin chain-targeting factor required in ubiquitin-proteasome degradation. Nature Cell Biology 3, 740-744.

Dallavalle, S., Pisano, C., Zunino, F., 2012. Development and therapeutic impact of HDAC6-selective inhibitors. Biochemical Pharmacology 84, 756-765.

DeLaBarre, B., Brunger, A.T., 2003. Complete structure of p97/valosin-containing protein reveals communication between nucleotide domains. Nature Structural Biology 10, 856-863.

DeLaBarre, B., Brunger, A.T., 2005. Nucleotide Dependent Motion and Mechanism of Action of p97/VCP. Journal of Molecular Biology 347, 437-452.

DeLaBarre, B., Christianson, J.C., Kopito, R.R., Brunger, A.T., 2006. Central pore residues mediate the p97/VCP activity required for ERAD. Molecular Cell 22, 451-462.

Deshaies, R.J., 2014. Proteotoxic crisis, the ubiquitin-proteasome system, and cancer therapy. BMC Biology 12, 94.

Dimopoulos, M.A., Moreau, P., Palumbo, A., Joshua, D., Pour, L., Hajek, R., Facon, T., Ludwig, H., Oriol, A., Goldschmidt, H., Rosinol, L., Straub, J., Suvorov, A., Araujo, C., Rimashevskaya, E., Pika, T., Gaidano, G., Weisel, K., Goranova-Marinova, V., Schwarer, A., Minuk, L., Masszi, T., Karamanesht, I., Offidani, M., Hungria, V., Spencer, A., Orlowski, R.Z., Gillenwater, H.H., Mohamed, N., Feng, S., Chng, W.J., 2016. Carfilzomib and dexamethasone versus bortezomib and dexamethasone for patients with relapsed or refractory multiple myeloma (ENDEAVOR): a randomised, phase 3, open-label, multicentre study. The Lancet Oncology 17, 27-38.

Dioufa, N., Kassi, E., Papavassiliou, A.G., Kiaris, H., 2010. Atypical induction of the unfolded protein response by mifepristone. Endocrine 38, 167-173.

Dittmer, D., Pati, S., Zambetti, G., Chu, S., Teresky, A.K., Moore, M., Finlay, C., Levine, A.J., 1993. Gain of function mutations in p53. Nature Genetics 4, 42-46.

Drexler, H.C., Risau, W., Konerding, M.A., 2000. Inhibition of proteasome function induces programmed cell death in proliferating endothelial cells. The FASEB Journal 14, 65-77.

Du, W., Mei, Q.-b., 2013. Ubiquitin-proteasome system, a new anti-tumor target. Acta Pharmacologica Sinica 34, 187-188.

Dunlop, E.A., Tee, A.R., 2009. Mammalian target of rapamycin complex 1: Signalling inputs, substrates and feedback mechanisms. Cellular Signalling 21, 827-835.

Etemadmoghadam, D., George, J., Cowin, P.A., Cullinane, C., Kansara, M., Gorringe, K.L., Smyth, G.K., Bowtell, D.D., 2010. Amplicon-dependent CCNE1 expression is critical for clonogenic survival after cisplatin treatment and is correlated with 20q11 gain in ovarian cancer. PLoS One 5, e15498.

Etemadmoghadam, D., Weir, B.A., Au-Yeung, G., Alsop, K., Mitchell, G., George, J., Australian Ovarian Cancer Study, G., Davis, S., D'Andrea, A.D., Simpson, K., Hahn, W.C., Bowtell, D.D.L., 2013. Synthetic lethality between CCNE1 amplification and loss of BRCA1. Proceedings of the National Academy of Sciences 110, 19489-19494.

Fang, C.J., Gui, L., Zhang, X., Moen, D.R., Li, K., Frankowski, K.J., Lin, H.J., Schoenen, F.J., Chou, T.F., 2015. Evaluating p97 inhibitor analogues for their domain selectivity and potency against the p97-p47 complex. ChemMedChem 10, 52-56.

Farmer, H., McCabe, N., Lord, C.J., Tutt, A.N., Johnson, D.A., Richardson, T.B., Santarosa, M., Dillon, K.J., Hickson, I., Knights, C., Martin, N.M., Jackson, S.P., Smith, G.C., Ashworth, A., 2005. Targeting the DNA repair defect in BRCA mutant cells as a therapeutic strategy. Nature 434, 917-921.

Ferlay, J., Soerjomataram, I., Dikshit, R., Eser, S., Mathers, C., Rebelo, M., Parkin, D.M., Forman, D., Bray, F., 2015. Cancer incidence and mortality worldwide: sources, methods and major patterns in GLOBOCAN 2012. International Journal of Cancer 136, E359-E386.

Franz, A., Orth, M., Pirson, P.A., Sonneville, R., Blow, J.J., Gartner, A., Stemmann, O., Hoppe, T., 2011. CDC-48/p97 coordinates CDT-1 degradation with GINS chromatin dissociation to ensure faithful DNA replication. Molecular Cell 44, 85-96.

Fribley, A., Wang, C.Y., 2006. Proteasome inhibitor induces apoptosis through induction of endoplasmic reticulum stress. Cancer Biology & Therapy 5, 745-748.

Gallagher, C.M., Garri, C., Cain, E.L., Ang, K.K.-H., Wilson, C.G., Chen, S., Hearn, B.R., Jaishankar, P., Aranda-Diaz, A., Arkin, M.R., Renslo, A.R., Walter, P., 2016. Ceapins are a new class of unfolded protein response inhibitors, selectively targeting the ATF6α branch. eLife 5, e11878.

Gao, J., Aksoy, B.A., Dogrusoz, U., Dresdner, G., Gross, B., Sumer, S.O., Sun, Y., Jacobsen, A., Sinha, R., Larsson, E., Cerami, E., Sander, C., Schultz, N., 2013. Integrative analysis of complex cancer genomics and clinical profiles using the cBioPortal. Science Signaling 6, pl1.

Gentile, M., Offidani, M., Vigna, E., Corvatta, L., Recchia, A.G., Morabito, L., Morabito, F., Gentili, S., 2015. Ixazomib for the treatment of multiple myeloma. Expert opinion on Investigational Drugs 24, 1287-1298.

Ghosh, A.P., Klocke, B.J., Ballestas, M.E., Roth, K.A., 2012. CHOP potentially co-operates with FOXO3a in neuronal cells to regulate PUMA and BIM expression in response to ER stress. PloS One 7, e39586.

Goyeneche, A.A., Caron, R.W., Telleria, C.M., 2007. Mifepristone inhibits ovarian cancer cell growth in vitro and in vivo. Clinical Cancer Research 13, 3370-3379.

Grunberg, S.M., Weiss, M.H., Russell, C.A., Spitz, I.M., Ahmadi, J., Sadun, A., Sitruk-Ware, R., 2006. Long-term administration of mifepristone (RU486): clinical tolerance during extended treatment of meningioma. Cancer Investigation 24, 727-733.

Gui, L., Zhang, X., Li, K., Frankowski, K.J., Li, S., Wong, D.E., Moen, D.R., Porubsky, P.R., Lin, H.J., Schoenen, F.J., Chou, T.F., 2016. Evaluating p97 Inhibitor Analogues for Potency against p97-p37 and p97-Npl4-Ufd1 Complexes. ChemMedChem 11, 953-957.

Gyorffy, B., Lanczky, A., Szallasi, Z., 2012. Implementing an online tool for genome-wide validation of survival-associated biomarkers in ovarian-cancer using microarray data from 1287 patients. Endocrine-related cancer 19, 197-208.

Halliday, M., Radford, H., Sekine, Y., Moreno, J., Verity, N., le Quesne, J., Ortori, C.A., Barrett, D.A., Fromont, C., Fischer, P.M., Harding, H.P., Ron, D., Mallucci, G.R., 2015. Partial restoration of protein synthesis rates by the small molecule ISRIB prevents neurodegeneration without pancreatic toxicity. Cell Death & Disease 6, e1672.

Hanahan, D., Weinberg, R.A., 2000. The Hallmarks of Cancer. Cell 100, 57-70.

Hanahan, D., Weinberg, R.A., 2011. Hallmarks of cancer: the next generation. Cell 144, 646-674.

Hänzelmann, P., Schindelin, H., 2017. The Interplay of Cofactor Interactions and Post-translational Modifications in the Regulation of the AAA+ ATPase p97. Frontiers in Molecular Biosciences 4, 21.

Harding, H.P., Novoa, I., Zhang, Y., Zeng, H., Wek, R., Schapira, M., Ron, D., 2000. Regulated translation initiation controls stress-induced gene expression in mammalian cells. Molecular Cell 6, 1099-1108.

Harding, H.P., Zhang, Y., Ron, D., 1999. Protein translation and folding are coupled by an endoplasmic-reticulum-resident kinase. Nature 397, 271-274.

He, L., Lee, J., Jang, J.H., Sakchaisri, K., Hwang, J., Cha-Molstad, H.J., Kim, K.A., Ryoo, I.J., Lee, H.G., Kim, S.O., Soung, N.K., Lee, K.S., Kwon, Y.T., Erikson, R.L., Ahn, J.S., Kim, B.Y., 2013. Osteoporosis regulation by salubrinal through eIF2alpha mediated differentiation of osteoclast and osteoblast. Cellular Signalling 25, 552-560.

Her, N.G., Toth, J.I., Ma, C.T., Wei, Y., Motamedchaboki, K., Sergienko, E., Petroski, M.D., 2016. p97 Composition Changes Caused by Allosteric Inhibition Are Suppressed by an On-Target Mechanism that Increases the Enzyme's ATPase Activity. Cell Chemical Biology 23, 517-528.

Hideshima, T., Chauhan, D., Richardson, P., Mitsiades, C., Mitsiades, N., Hayashi, T., Munshi, N., Dang, L., Castro, A., Palombella, V., Adams, J., Anderson, K.C., 2002. NF-kappa B as a therapeutic target in multiple myeloma. The Journal of Biological Chemistry 277, 16639-16647.

Ho, N., Li, A., Li, S., Zhang, H., 2012. Heat Shock Protein 90 and Role of Its Chemical Inhibitors in Treatment of Hematologic Malignancies. Pharmaceuticals 5, 779-801.

Hong, M., Luo, S., Baumeister, P., Huang, J.M., Gogia, R.K., Li, M., Lee, A.S., 2004. Underglycosylation of ATF6 as a novel sensing mechanism for activation of the unfolded protein response. The Journal of Biological Chemistry 279, 11354-11363.

Huang, Z., Wu, Y., Zhou, X., Xu, J., Zhu, W., Shu, Y., Liu, P., 2014. Efficacy of therapy with bortezomib in solid tumors: a review based on 32 clinical trials. Future Oncology 10, 1795-1807.

Husain, A., Wang, Y., Hanker, L.C., Ojeda, B., Anttila, M., Breda, E., Vuylsteke, P., Pujade-Lauraine, E., 2016. Independent radiologic review of AURELIA, a phase 3 trial of bevacizumab plus chemotherapy for platinum-resistant recurrent ovarian cancer. Gynecologic Oncology 142, 465-470.

Jacobs, I.J., Menon, U., Ryan, A., Gentry-Maharaj, A., Burnell, M., Kalsi, J.K., Amso, N.N., Apostolidou, S., Benjamin, E., Cruickshank, D., Crump, D.N., Davies, S.K., Dawnay, A., Dobbs, S., Fletcher, G., Ford, J., Godfrey, K., Gunu, R., Habib, M., Hallett, R., Herod, J., Jenkins, H., Karpinskyj, C., Leeson, S., Lewis, S.J., Liston, W.R., Lopes, A., Mould, T., Murdoch, J., Oram, D., Rabideau, D.J., Reynolds, K., Scott, I., Seif, M.W., Sharma, A., Singh, N., Taylor, J., Warburton, F., Widschwendter, M., Williamson, K., Woolas, R., Fallowfield, L., McGuire, A.J., Campbell, S., Parmar, M., Skates, S.J., 2016. Ovarian cancer screening and mortality in the UK Collaborative Trial of Ovarian Cancer Screening (UKCTOCS): a randomised controlled trial. The Lancet 387, 945-956.

Jafari, R., Almqvist, H., Axelsson, H., Ignatushchenko, M., Lundback, T., Nordlund, P., Martinez Molina, D., 2014. The cellular thermal shift assay for evaluating drug target interactions in cells. Nature Protocols 9, 2100-2122.

Jarosch, E., Taxis, C., Volkwein, C., Bordallo, J., Finley, D., Wolf, D.H., Sommer, T., 2002. Protein dislocation from the ER requires polyubiquitination and the AAA-ATPase Cdc48. Nature Cell Biology 4, 134-139.

Jarosz, D.F., Lindquist, S., 2010. Hsp90 and environmental stress transform the adaptive value of natural genetic variation. Science 330, 1820-1824.

Johannessen, C.M., Boehm, J.S., Kim, S.Y., Thomas, S.R., Wardwell, L., Johnson, L.A., Emery, C.M., Stransky, N., Cogdill, A.P., Barretina, J., Caponigro, G., Hieronymus, H., Murray, R.R., Salehi-Ashtiani, K., Hill, D.E., Vidal, M., Zhao, J.J., Yang, X., Alkan, O., Kim, S., Harris, J.L., Wilson, C.J., Myer, V.E., Finan, P.M., Root, D.E., Roberts, T.M., Golub, T., Flaherty, K.T., Dummer, R., Weber, B.L., Sellers, W.R., Schlegel, R., Wargo, J.A., Hahn, W.C., Garraway, L.A., 2010. COT drives resistance to RAF inhibition through MAP kinase pathway reactivation. Nature 468, 968-972.

Johnson, N., Johnson, S.F., Yao, W., Li, Y.C., Choi, Y.E., Bernhardy, A.J., Wang, Y., Capelletti, M., Sarosiek, K.A., Moreau, L.A., Chowdhury, D., Wickramanayake, A., Harrell, M.I., Liu, J.F., D'Andrea, A.D., Miron, A., Swisher, E.M., Shapiro, G.I., 2013. Stabilization of mutant BRCA1 protein confers PARP inhibitor and platinum resistance. Proceedings of the National Academy of Sciences 110, 17041-17046.

Ju, J.S., Fuentealba, R.A., Miller, S.E., Jackson, E., Piwnica-Worms, D., Baloh, R.H., Weihl, C.C., 2009. Valosin-containing protein (VCP) is required for autophagy and is disrupted in VCP disease. Journal of Cell Biology 187, 875-888.

Ju, J.S., Miller, S.E., Hanson, P.I., Weihl, C.C., 2008. Impaired protein aggregate handling and clearance underlie the pathogenesis of p97/VCP-associated disease. Journal of Bioliogical Chemistry 283, 30289-30299.

Kane, R.C., Bross, P.F., Farrell, A.T., Pazdur, R., 2003. Velcade: U.S. FDA approval for the treatment of multiple myeloma progressing on prior therapy. The Oncologist 8, 508-513.

Kang, M.J., Wu, T., Wijeratne, E.M., Lau, E.C., Mason, D.J., Mesa, C., Tillotson, J., Zhang, D.D., Gunatilaka, A.A., La Clair, J.J., Chapman, E., 2014. Functional chromatography reveals three natural products that target the same protein with distinct mechanisms of action. Chembiochem 15, 2125-2131.

Kang, S.A., Pacold, M.E., Cervantes, C.L., Lim, D., Lou, H.J., Ottina, K., Gray, N.S., Turk, B.E., Yaffe, M.B., Sabatini, D.M., 2013. mTORC1 phosphorylation sites encode their sensitivity to starvation and rapamycin. Science 341, 1236566.

Kim, N.C., Tresse, E., Kolaitis, R.M., Molliex, A., Thomas, R.E., Alami, N.H., Wang, B., Joshi, A., Smith, R.B., Ritson, G.P., Winborn, B.J., Moore, J., Lee, J.Y., Yao, T.P., Pallanck, L., Kundu, M., Taylor, J.P., 2013. VCP is essential for mitochondrial quality control by PINK1/Parkin and this function is impaired by VCP mutations. Neuron 78, 65-80.

Koizumi, M., Tanjung, N.G., Chen, A., Dynlacht, J.R., Garrett, J., Yoshioka, Y., Ogawa, K., Teshima, T., Yokota, H., 2012. Administration of salubrinal enhances radiation-induced cell death of SW1353 chondrosarcoma cells. Anticancer Research 32, 3667-3673.

Konstantinopoulos, P.A., Ceccaldi, R., Shapiro, G.I., D'Andrea, A.D., 2015. Homologous Recombination Deficiency: Exploiting the Fundamental Vulnerability of Ovarian Cancer. Cancer Discovery 5, 1137-1154.

Kovacs, J.J., Murphy, P.J., Gaillard, S., Zhao, X., Wu, J.T., Nicchitta, C.V., Yoshida, M., Toft, D.O., Pratt, W.B., Yao, T.P., 2005. HDAC6 regulates Hsp90 acetylation and chaperone-dependent activation of glucocorticoid receptor. Molecular Cell 18, 601-607.

Kretschmer, X.C., Baldwin, W.S., 2005. CAR and PXR: xenosensors of endocrine disrupters? Chemico-Biological Interactions 155, 111-128.

Kuhn, D.J., Chen, Q., Voorhees, P.M., Strader, J.S., Shenk, K.D., Sun, C.M., Demo, S.D., Bennett, M.K., van Leeuwen, F.W., Chanan-Khan, A.A., Orlowski, R.Z., 2007. Potent activity of carfilzomib, a novel, irreversible inhibitor of the ubiquitin-proteasome pathway, against preclinical models of multiple myeloma. Blood 110, 3281-3290.

Kuo, K.-T., Guan, B., Feng, Y., Mao, T.-L., Chen, X., Jinawath, N., Wang, Y., Kurman, R.J., Shih, I.-M., Wang, T.-L., 2009. Analysis of DNA Copy Number Alterations in Ovarian Serous Tumors Identifies New Molecular Genetic Changes in Low-grade and High-grade Carcinomas. Cancer Research 69, 4036-4042.

Lamb, J., Crawford, E.D., Peck, D., Modell, J.W., Blat, I.C., Wrobel, M.J., Lerner, J., Brunet, J.P., Subramanian, A., Ross, K.N., Reich, M., Hieronymus, H., Wei, G., Armstrong, S.A., Haggarty, S.J., Clemons, P.A., Wei, R., Carr, S.A., Lander, E.S., Golub, T.R., 2006. The Connectivity Map: using gene-expression signatures to connect small molecules, genes, and disease. Science 313, 1929-1935.

Lambrechts, S., Smeets, D., Moisse, M., Braicu, E.I., Vanderstichele, A., Zhao, H., Van Nieuwenhuysen, E., Berns, E., Sehouli, J., Zeillinger, R., Darb-Esfahani, S., Cacsire Castillo-Tong, D., Lambrechts, D., Vergote, I., 2016. Genetic heterogeneity after first-line chemotherapy in high-grade serous ovarian cancer. European Journal of Cancer 53, 51-64.

Ledermann, J., Harter, P., Gourley, C., Friedlander, M., Vergote, I., Rustin, G., Scott, C.L., Meier, W., Shapira-Frommer, R., Safra, T., Matei, D., Fielding, A., Spencer, S., Dougherty, B., Orr, M., Hodgson, D., Barrett, J.C., Matulonis, U., 2014. Olaparib maintenance therapy in patients with platinum-sensitive relapsed serous ovarian cancer: a preplanned retrospective analysis of outcomes by BRCA status in a randomised phase 2 trial. The Lancet Oncology 15, 852-861.

Ledermann, J.A., 2016. PARP inhibitors in ovarian cancer. Annals of oncology 27 Suppl 1, i40-i44.

Lee, M.J., Lee, B.-H., Hanna, J., King, R.W., Finley, D., 2011. Trimming of Ubiquitin Chains by Proteasome-associated Deubiquitinating Enzymes. Molecular & Cellular Proteomics 10, R110.003871.

Levanon, K., Crum, C., Drapkin, R., 2008. New insights into the pathogenesis of serous ovarian cancer and its clinical impact. Journal of Clinical Oncology 26, 5284-5293.

Lilienbaum, A., 2013. Relationship between the proteasomal system and autophagy. International Journal of Biochemistry and Molecular Biology 4, 1-26.

Liu, R., Shi, P., Nie, Z., Liang, H., Zhou, Z., Chen, W., Chen, H., Dong, C., Yang, R., Liu, S., Chen, C., 2016. Mifepristone Suppresses Basal Triple-Negative Breast Cancer Stem Cells by Down-regulating KLF5 Expression. Theranostics 6, 533-544.

Lopes, U.G., Erhardt, P., Yao, R., Cooper, G.M., 1997. p53-dependent induction of apoptosis by proteasome inhibitors. The Journal of Biological Chemistry 272, 12893-12896.

Mackenzie, R.W.A., Elliott, B.T., 2014. Akt/PKB activation and insulin signaling: a novel insulin signaling pathway in the treatment of type 2 diabetes. Diabetes, Metabolic Syndrome and Obesity: Targets and Therapy 7, 55-64.

Magnaghi, P., D'Alessio, R., Valsasina, B., Avanzi, N., Rizzi, S., Asa, D., Gasparri, F., Cozzi, L., Cucchi, U., Orrenius, C., Polucci, P., Ballinari, D., Perrera, C., Leone, A., Cervi, G., Casale, E., Xiao, Y., Wong, C., Anderson, D.J., Galvani, A., Donati, D., O'Brien, T., Jackson, P.K., Isacchi, A., 2013. Covalent and allosteric inhibitors of the ATPase VCP/p97 induce cancer cell death. Nature Chemical Biology 9, 548-556.

Marciniak, S.J., Yun, C.Y., Oyadomari, S., Novoa, I., Zhang, Y., Jungreis, R., Nagata, K., Harding, H.P., Ron, D., 2004. CHOP induces death by promoting protein synthesis and oxidation in the stressed endoplasmic reticulum. Genes & Development 18, 3066-3077.

Marcotte, R., Brown, K.R., Suarez, F., Sayad, A., Karamboulas, K., Krzyzanowski, P.M., Sircoulomb, F., Medrano, M., Fedyshyn, Y., Koh, J.L., van Dyk, D., Fedyshyn, B., Luhova, M., Brito, G.C., Vizeacoumar, F.J., Vizeacoumar, F.S., Datti, A., Kasimer, D., Buzina, A., Mero, P., Misquitta, C., Normand, J., Haider, M., Ketela, T., Wrana, J.L., Rottapel, R., Neel, B.G., Moffat, J., 2012. Essential gene profiles in breast, pancreatic, and ovarian cancer cells. Cancer Discovery 2, 172-189.

Maurel, M., Chevet, E., Tavernier, J., Gerlo, S., 2014. Getting RIDD of RNA: IRE1 in cell fate regulation. Trends in biochemical sciences 39, 245-254.

McClung, E.C., Wenham, R.M., 2016. Profile of bevacizumab in the treatment of platinum-resistant ovarian cancer: current perspectives. International Journal of Women's Health 8, 59-75.

McCullough, K.D., Martindale, J.L., Klotz, L.O., Aw, T.Y., Holbrook, N.J., 2001. Gadd153 sensitizes cells to endoplasmic reticulum stress by down-regulating Bcl2 and perturbing the cellular redox state. Molecular and Cellular Biology 21, 1249-1259.

McGuire, W.P., Hoskins, W.J., Brady, M.F., Kucera, P.R., Partridge, E.E., Look, K.Y., Clarke-Pearson, D.L., Davidson, M., 1996. Cyclophosphamide and cisplatin compared with paclitaxel and cisplatin in patients with stage III and stage IV ovarian cancer. The New England Journal of Medicine 334, 1-6.

Meerang, M., Ritz, D., Paliwal, S., Garajova, Z., Bosshard, M., Mailand, N., Janscak, P., Hubscher, U., Meyer, H., Ramadan, K., 2011. The ubiquitin-selective segregase VCP/p97 orchestrates the response to DNA double-strand breaks. Nature Cell Biology 13, 1376-1382.

Meng, L.-h., Zheng, X.F.S., 2015. Toward rapamycin analog (rapalog)-based precision cancer therapy. Acta Pharmacologica Sinica 36, 1163-1169.

Meyer, H., Bug, M., Bremer, S., 2012. Emerging functions of the VCP/p97 AAA-ATPase in the ubiquitin system. Nature Cell Biology 14, 117-123.

Meyer, H.H., Wang, Y., Warren, G., 2002. Direct binding of ubiquitin conjugates by the mammalian p97 adaptor complexes, p47 and Ufd1-Npl4. The Embo Journal 21, 5645-5652.

Mimura, N., Fulciniti, M., Gorgun, G., Tai, Y.T., Cirstea, D., Santo, L., Hu, Y., Fabre, C., Minami, J., Ohguchi, H., Kiziltepe, T., Ikeda, H., Kawano, Y., French, M., Blumenthal, M., Tam, V., Kertesz, N.L., Malyankar, U.M., Hokenson, M., Pham, T., Zeng, Q., Patterson, J.B., Richardson, P.G., Munshi, N.C., Anderson, K.C., 2012. Blockade of XBP1 splicing by inhibition of IRE1alpha is a promising therapeutic option in multiple myeloma. Blood 119, 5772-5781.

Mirza, M.R., Monk, B.J., Herrstedt, J., Oza, A.M., Mahner, S., Redondo, A., Fabbro, M., Ledermann, J.A., Lorusso, D., Vergote, I., Ben-Baruch, N.E., Marth, C., Mądry, R., Christensen, R.D., Berek, J.S., Dørum, A., Tinker, A.V., du Bois, A., González-Martín, A., Follana, P., Benigno, B., Rosenberg, P., Gilbert, L., Rimel, B.J., Buscema, J., Balser, J.P., Agarwal, S., Matulonis, U.A., 2016. Niraparib Maintenance Therapy in Platinum-Sensitive, Recurrent Ovarian Cancer. The New England Journal of Medicine 375, 2154-2164.

Miyamoto, Y., Nakagawa, S., Wada-Hiraike, O., Seiki, T., Tanikawa, M., Hiraike, H., Sone, K., Nagasaka, K., Oda, K., Kawana, K., Nakagawa, K., Fujii, T., Yano, T., Kozuma, S., Taketani, Y., 2013. Sequential effects of the proteasome inhibitor bortezomib and chemotherapeutic agents in uterine cervical cancer cell lines. Oncology Reports 29, 51-57.

Morris, G.M., Huey, R., Lindstrom, W., Sanner, M.F., Belew, R.K., Goodsell, D.S., Olson, A.J., 2009. AutoDock4 and AutoDockTools4: Automated docking with selective receptor flexibility. Journal of Computional Chemistry 30, 2785-2791.

Mukhopadhyay, A., Elattar, A., Cerbinskaite, A., Wilkinson, S.J., Drew, Y., Kyle, S., Los, G., Hostomsky, Z., Edmondson, R.J., Curtin, N.J., 2010. Development of a functional assay for homologous recombination status in primary cultures of epithelial ovarian tumor and correlation with sensitivity to poly(ADP-ribose) polymerase inhibitors. Clinical Cancer Research 16, 2344-2351.

Muller, Patricia A., Vousden, Karen H., 2014. Mutant p53 in Cancer: New Functions and Therapeutic Opportunities. Cancer Cell 25, 304-317.

Nagel, R., Semenova, E.A., Berns, A., 2016. Drugging the addict: non-oncogene addiction as a target for cancer therapy. EMBO Reports 17, 1516-1531.

Naoki, T., Ikuya, S., Osamu, T., Keishi, M., 1988. RU486, a progestin antagonist, binds to progesterone receptors in a human endometrial cancer cell line and reverses the growth inhibition by progestins. Journal of Steroid Biochemistry 31, 161-166.

Neckers, L., Workman, P., 2012. Hsp90 molecular chaperone inhibitors: are we there yet? Clinical Cancer Research 18, 64-76.

Neri, P., Ren, L., Gratton, K., Stebner, E., Johnson, J., Klimowicz, A., Duggan, P., Tassone, P., Mansoor, A., Stewart, D.A., Lonial, S., Boise, L.H., Bahlis, N.J., 2011. Bortezomib-induced "BRCAness" sensitizes multiple myeloma cells to PARP inhibitors. Blood 118, 6368-6379.

Nijhawan, D., Zack, T.I., Ren, Y., Strickland, M.R., Lamothe, R., Schumacher, S.E., Tsherniak, A., Besche, H.C., Rosenbluh, J., Shehata, S., Cowley, G.S., Weir, B.A., Goldberg, A.L., Mesirov, J.P., Root, D.E., Bhatia, S.N., Beroukhim, R., Hahn, W.C., 2012. Cancer vulnerabilities unveiled by genomic loss. Cell 150, 842-854.

Nijman, S.M., 2011. Synthetic lethality: general principles, utility and detection using genetic screens in human cells. FEBS Letters 585, 1-6.

Nikawa, J., Yamashita, S., 1992. IRE1 encodes a putative protein kinase containing a membrane-spanning domain and is required for inositol phototrophy in Saccharomyces cerevisiae. Molecular Microbiology 6, 1441-1446.

Noguchi, M., Yu, D., Hirayama, R., Ninomiya, Y., Sekine, E., Kubota, N., Ando, K., Okayasu, R., 2006. Inhibition of homologous recombination repair in irradiated tumor cells pretreated with Hsp90 inhibitor 17-allylamino-17-demethoxygeldanamycin. Biochemical and biophysical research communications 351, 658-663.

Oakes, S.A., Papa, F.R., 2015. The Role of Endoplasmic Reticulum Stress in Human Pathology. Annual Review of Pathology 10, 173-194.

Oren, M., Rotter, V., 2010. Mutant p53 gain-of-function in cancer. Cold Spring Harbor perspectives in biology 2, a001107.

Oslowski, C.M., Urano, F., 2011. Measuring ER stress and the unfolded protein response using mammalian tissue culture system. Methods in Enzymology 490, 71-92.

Papandreou, C.N., Daliani, D.D., Nix, D., Yang, H., Madden, T., Wang, X., Pien, C.S., Millikan, R.E., Tu, S.-M., Pagliaro, L., Kim, J., Adams, J., Elliott, P., Esseltine, D., Petrusich, A., Dieringer, P., Perez, C., Logothetis, C.J., 2004. Phase I Trial of the Proteasome Inhibitor Bortezomib in Patients With Advanced Solid Tumors With Observations in Androgen-Independent Prostate Cancer. Journal of Clinical Oncology 22, 2108-2121.

Papandreou, I., Denko, N.C., Olson, M., Van Melckebeke, H., Lust, S., Tam, A., Solow-Cordero, D.E., Bouley, D.M., Offner, F., Niwa, M., Koong, A.C., 2011. Identification of an Ire1alpha

endonuclease specific inhibitor with cytotoxic activity against human multiple myeloma. Blood 117, 1311-1314.

Parrales, A., Iwakuma, T., 2015. Targeting Oncogenic Mutant p53 for Cancer Therapy. Frontiers in Oncology 5, 288.

Parrales, A., Ranjan, A., Iyer, S.V., Padhye, S., Weir, S.J., Roy, A., Iwakuma, T., 2016. DNAJA1 controls the fate of misfolded mutant p53 through the mevalonate pathway. Nature Cell Biology 18, 1233-1243.

Parzych, K., Chinn, T.M., Chen, Z., Loaiza, S., Porsch, F., Valbuena, G.N., Kleijnen, M.F., Karadimitris, A., Gentleman, E., Keun, H.C., Auner, H.W., 2015. Inadequate fine-tuning of protein synthesis and failure of amino acid homeostasis following inhibition of the ATPase VCP/p97. Cell Death & Disease 6, e2031.

Piccart, M.J., Bertelsen, K., James, K., Cassidy, J., Mangioni, C., Simonsen, E., Stuart, G., Kaye, S., Vergote, I., Blom, R., Grimshaw, R., Atkinson, R.J., Swenerton, K.D., Trope, C., Nardi, M., Kaern, J., Tumolo, S., Timmers, P., Roy, J.A., Lhoas, F., Lindvall, B., Bacon, M., Birt, A., Andersen, J.E., Zee, B., Paul, J., Baron, B., Pecorelli, S., 2000. Randomized intergroup trial of cisplatin-paclitaxel versus cisplatin-cyclophosphamide in women with advanced epithelial ovarian cancer: three-year results. Journal of the National Cancer Institute 92, 699-708.

Pick, E., Kluger, Y., Giltnane, J.M., Moeder, C., Camp, R.L., Rimm, D.L., Kluger, H.M., 2007. High HSP90 expression is associated with decreased survival in breast cancer. Cancer Research 67, 2932-2937.

Plate, L., Cooley, C.B., Chen, J.J., Paxman, R.J., Gallagher, C.M., Madoux, F., Genereux, J.C., Dobbs, W., Garza, D., Spicer, T.P., Scampavia, L., Brown, S.J., Rosen, H., Powers, E.T., Walter, P., Hodder, P., Wiseman, R.L., Kelly, J.W., 2016. Small molecule proteostasis regulators that reprogram the ER to reduce extracellular protein aggregation. eLife 5, e15550.

Polucci, P., Magnaghi, P., Angiolini, M., Asa, D., Avanzi, N., Badari, A., Bertrand, J., Casale, E., Cauteruccio, S., Cirla, A., Cozzi, L., Galvani, A., Jackson, P.K., Liu, Y., Magnuson, S., Malgesini, B., Nuvoloni, S., Orrenius, C., Sirtori, F.R., Riceputi, L., Rizzi, S., Trucchi, B., O'Brien, T., Isacchi, A., Donati, D., D'Alessio, R., 2013. Alkylsulfanyl-1,2,4-triazoles, a new class of allosteric valosine containing protein inhibitors. Synthesis and structure-activity relationships. Journal of Medicinal Chemistry 56, 437-450.

Prat, J., Oncology, F.C.o.G., 2015. FIGO's staging classification for cancer of the ovary, fallopian tube, and peritoneum: abridged republication. Journal of Gynecologic Oncology 26, 87-89.

Pujade-Lauraine, E., Hilpert, F., Weber, B., Reuss, A., Poveda, A., Kristensen, G., Sorio, R., Vergote, I., Witteveen, P., Bamias, A., Pereira, D., Wimberger, P., Oaknin, A., Mirza, M.R., Follana, P., Bollag, D., Ray-Coquard, I., 2014. Bevacizumab combined with chemotherapy for platinum-resistant recurrent ovarian cancer: The AURELIA open-label randomized phase III trial. Journal of Clinical Oncology 32, 1302-1308.

Queitsch, C., Sangster, T.A., Lindquist, S., 2002. Hsp90 as a capacitor of phenotypic variation. Nature 417, 618-624.

Raedler, L., 2015. Velcade (Bortezomib) Receives 2 New FDA Indications: For Retreatment of Patients with Multiple Myeloma and for First-Line Treatment of Patients with Mantle-Cell Lymphoma. American Health & Drug Benefits 8, 135-140.

Ramirez, P.T., Landen, C.N., Jr., Coleman, R.L., Milam, M.R., Levenback, C., Johnston, T.A., Gershenson, D.M., 2008. Phase I trial of the proteasome inhibitor bortezomib in combination with carboplatin in patients with platinum- and taxane-resistant ovarian cancer. Gynecologic Oncology 108, 68-71.

Ri, M., Tashiro, E., Oikawa, D., Shinjo, S., Tokuda, M., Yokouchi, Y., Narita, T., Masaki, A., Ito, A., Ding, J., Kusumoto, S., Ishida, T., Komatsu, H., Shiotsu, Y., Ueda, R., Iwawaki, T., Imoto, M., Iida, S., 2012. Identification of Toyocamycin, an agent cytotoxic for multiple myeloma cells, as a potent inhibitor of ER stress-induced XBP1 mRNA splicing. Blood Cancer Journal 2, e79.

Rojas-Rivera, D., Delvaeye, T., Roelandt, R., Nerinckx, W., Augustyns, K., Vandenabeele, P., Bertrand, M.J.M., 2017. When PERK inhibitors turn out to be new potent RIPK1 inhibitors: critical issues on the specificity and use of GSK2606414 and GSK2656157. Cell Death and Differentiation 24, 1100-1110.

Rubin, S.C., Randall, T.C., Armstrong, K.A., Chi, D.S., Hoskins, W.J., 1999. Ten-year follow-up of ovarian cancer patients after second-look laparotomy with negative findings. Obstetrics and Gynecology 93, 21-24.

Rutherford, S.L., Lindquist, S., 1998. Hsp90 as a capacitor for morphological evolution. Nature 396, 336-342.

Rutkowski, D.T., Kaufman, R.J., 2004. A trip to the ER: coping with stress. Trends in Cell Biology 14, 20-28.

Sano, R., Reed, J.C., 2013. ER stress-induced cell death mechanisms. Biochima et Biophysica Acta 1833, 3460-3470.

Santo, L., Hideshima, T., Kung, A.L., Tseng, J.-C., Tamang, D., Yang, M., Jarpe, M., van Duzer, J.H., Mazitschek, R., Ogier, W.C., Cirstea, D., Rodig, S., Eda, H., Scullen, T., Canavese, M., Bradner, J., Anderson, K.C., Jones, S.S., Raje, N., 2012. Preclinical activity, pharmacodynamic, and pharmacokinetic properties of a selective HDAC6 inhibitor, ACY-1215, in combination with bortezomib in multiple myeloma. Blood 119, 2579-2589.

Sarbassov, D.D., Guertin, D.A., Ali, S.M., Sabatini, D.M., 2005. Phosphorylation and regulation of Akt/PKB by the rictor-mTOR complex. Science 307, 1098-1101.

Saxton, R.A., Sabatini, D.M., 2017. mTOR Signaling in Growth, Metabolism, and Disease. Cell 168, 960-976.

Schmidt, E.K., Clavarino, G., Ceppi, M., Pierre, P., 2009. SUnSET, a nonradioactive method to monitor protein synthesis. Nature Methods 6, 275-277.

Schrodinger, LLC, 2015. The PyMOL Molecular Graphics System, Version 1.8.
Seguin, S.J., Morelli, F.F., Vinet, J., Amore, D., De Biasi, S., Poletti, A., Rubinsztein, D.C., Carra, S., 2014. Inhibition of autophagy, lysosome and VCP function impairs stress granule assembly. Cell Death and Differentiation 21, 1838-1851.

Shamu, C.E., Walter, P., 1996. Oligomerization and phosphorylation of the Ire1p kinase during intracellular signaling from the endoplasmic reticulum to the nucleus. The EMBO Journal 15, 3028-3039.

Sharma, R., Graham, J., Mitchell, H., Brooks, A., Blagden, S., Gabra, H., 2009. Extended weekly dose-dense paclitaxel/carboplatin is feasible and active in heavily pre-treated platinum-resistant recurrent ovarian cancer. British Journal of Cancer 100, 707-712.

Sidera, K., Patsavoudi, E., 2014. HSP90 inhibitors: current development and potential in cancer therapy. Recent patents on anti-cancer drug discovery 9, 1-20.

Sidrauski, C., Tsai, J.C., Kampmann, M., Hearn, B.R., Vedantham, P., Jaishankar, P., Sokabe, M., Mendez, A.S., Newton, B.W., Tang, E.L., Verschueren, E., Johnson, J.R., Krogan, N.J., Fraser, C.S., Weissman, J.S., Renslo, A.R., Walter, P., 2015. Pharmacological dimerization and activation of the exchange factor eIF2B antagonizes the integrated stress response. eLife 4, e07314.

Siegel, R.L., Miller, K.D., Jemal, A., 2018. Cancer statistics, 2018. CA: A Cancer Journal for Clinicians 68, 7-30.

Skrott, Z., Mistrik, M., Andersen, K.K., Friis, S., Majera, D., Gursky, J., Ozdian, T., Bartkova, J., Turi, Z., Moudry, P., Kraus, M., Michalova, M., Vaclavkova, J., Dzubak, P., Vrobel, I., Pouckova, P., Sedlacek, J., Miklovicova, A., Kutt, A., Li, J., Mattova, J., Driessen, C., Dou, Q.P., Olsen, J., Hajduch, M., Cvek, B., Deshaies, R.J., Bartek, J., 2017. Alcohol-abuse drug disulfiram targets cancer via p97 segregase adaptor NPL4. Nature 552, 194-199.

Song, C., Wang, Q., Li, C.C., 2003. ATPase activity of p97-valosin-containing protein (VCP). D2 mediates the major enzyme activity, and D1 contributes to the heat-induced activity. The Journal Biological Chemistry 278, 3648-3655.

Soucy, T.A., Smith, P.G., Milhollen, M.A., Berger, A.J., Gavin, J.M., Adhikari, S., Brownell, J.E., Burke, K.E., Cardin, D.P., Critchley, S., Cullis, C.A., Doucette, A., Garnsey, J.J., Gaulin, J.L., Gershman, R.E., Lublinsky, A.R., McDonald, A., Mizutani, H., Narayanan, U., Olhava, E.J., Peluso, S., Rezaei, M., Sintchak, M.D., Talreja, T., Thomas, M.P., Traore, T., Vyskocil, S., Weatherhead, G.S., Yu, J., Zhang, J., Dick, L.R., Claiborne, C.F., Rolfe, M., Bolen, J.B., Langston, S.P., 2009. An inhibitor of NEDD8-activating enzyme as a new approach to treat cancer. Nature 458, 732-736.

Stecklein, S.R., Kumaraswamy, E., Behbod, F., Wang, W., Chaguturu, V., Harlan-Williams, L.M., Jensen, R.A., 2012. BRCA1 and HSP90 cooperate in homologous and non-homologous DNA double-strand-break repair and G2/M checkpoint activation. Proceedings of the National Academy of Sciences 109, 13650-13655.

Stringer-Reasor, E.M., Baker, G.M., Skor, M.N., Kocherginsky, M., Lengyel, E., Fleming, G.F., Conzen, S.D., 2015. Glucocorticoid Receptor Activation Inhibits Chemotherapy-induced Cell Death in High-grade Serous Ovarian Carcinoma. Gynecologic Oncology 138, 656-662.

Subik, K., Lee, J.F., Baxter, L., Strzepek, T., Costello, D., Crowley, P., Xing, L., Hung, M.C., Bonfiglio, T., Hicks, D.G., Tang, P., 2010. The Expression Patterns of ER, PR, HER2, CK5/6, EGFR, Ki-67 and AR by Immunohistochemical Analysis in Breast Cancer Cell Lines. Breast Cancer (Auckl) 4, 35-41.

Supko, J.G., Hickman, R.L., Grever, M.R., Malspeis, L., 1995. Preclinical pharmacologic evaluation of geldanamycin as an antitumor agent. Cancer Chemotherapy and Pharmacology 36, 305-315.

TCGA, 2011. Integrated genomic analyses of ovarian carcinoma. Nature 474, 609-615.

Teng, Y., Gao, M., Wang, J., Kong, Q., Hua, H., Luo, T., Jiang, Y., 2014. Inhibition of eIF2alpha dephosphorylation enhances TRAIL-induced apoptosis in hepatoma cells. Cell Death & Disease 5, e1060.

Trott, O., Olson, A.J., 2010. AutoDock Vina: improving the speed and accuracy of docking with a new scoring function, efficient optimization, and multithreading. Journal of Computational Chemistry 31, 455-461.

Tsujimoto, Y., Tomita, Y., Hoshida, Y., Kono, T., Oka, T., Yamamoto, S., Nonomura, N., Okuyama, A., Aozasa, K., 2004a. Elevated Expression of Valosin-Containing Protein (p97) Is Associated with Poor Prognosis of Prostate Cancer. Clinical Cancer Research 10, 3007-3012.

Tsujimoto, Y., Tomita, Y., Hoshida, Y., Kono, T., Oka, T., Yamamoto, S., Nonomura, N., Okuyama, A., Aozasa, K., 2004b. Elevated expression of valosin-containing protein (p97) is associated with poor prognosis of prostate cancer. Clinical Cancer Research 10, 3007-3012.

Underhill, C., Toulmonde, M., Bonnefoi, H., 2011. A review of PARP inhibitors: from bench to bedside. Annals of Oncology 22, 268-279.

Valle, C.W., Min, T., Bodas, M., Mazur, S., Begum, S., Tang, D., Vij, N., 2011. Critical role of VCP/p97 in the pathogenesis and progression of non-small cell lung carcinoma. PLoS One 6, e29073.

van den Boom, J., Meyer, H., 2017. VCP/p97-Mediated Unfolding as a Principle in Protein Homeostasis and Signaling. Molecular Cell 69, 182-194.

Vichai, V., Kirtikara, K., 2006. Sulforhodamine B colorimetric assay for cytotoxicity screening. Nature Protocols 1, 1112-1116.

Volkmann, K., Lucas, J.L., Vuga, D., Wang, X., Brumm, D., Stiles, C., Kriebel, D., Der-Sarkissian, A., Krishnan, K., Schweitzer, C., Liu, Z., Malyankar, U.M., Chiovitti, D., Canny, M., Durocher, D., Sicheri, F., Patterson, J.B., 2011. Potent and selective inhibitors of the inositol-requiring enzyme 1 endoribonuclease. The Journal of Biological Chemistry 286, 12743-12755.

Walter, P., Ron, D., 2011. The Unfolded Protein Response: From Stress Pathway to Homeostatic Regulation. Science 334, 1081.

Wang, G., Yang, Z.-Q., Zhang, K., 2010a. Endoplasmic reticulum stress response in cancer: molecular mechanism and therapeutic potential. American Journal of Translational Research 2, 65-74.

Wang, Q., Li, L., Ye, Y., 2008. Inhibition of p97-dependent protein degradation by Eeyarestatin I. The Journal of Biological Chemistry 283, 7445-7454.

Wang, Q., Shinkre, B.A., Lee, J.G., Weniger, M.A., Liu, Y., Chen, W., Wiestner, A., Trenkle, W.C., Ye, Y., 2010b. The ERAD inhibitor Eeyarestatin I is a bifunctional compound with a membrane-binding domain and a p97/VCP inhibitory group. PloS One 5, e15479.

Whitesell, L., Mimnaugh, E.G., De Costa, B., Myers, C.E., Neckers, L.M., 1994. Inhibition of heat shock protein HSP90-pp60v-src heteroprotein complex formation by benzoquinone ansamycins: essential role for stress proteins in oncogenic transformation. Proceedings of the National Academy of Sciences 91, 8324-8328.

Wijeratne, E.M., Gunaherath, G.M., Chapla, V.M., Tillotson, J., de la Cruz, F., Kang, M., JM, U.R., Araujo, A.R., Arnold, A.E., Chapman, E., Gunatilaka, A.A., 2016. Oxaspirol B with p97 Inhibitory Activity and Other Oxaspirols from Lecythophora sp. FL1375 and FL1031, Endolichenic Fungi Inhabiting Parmotrema tinctorum and Cladonia evansii. Journal of Natural Products 79, 340-352.

Wiltshaw, E., Kroner, T., 1976. Phase II study of cis-dichlorodiammineplatinum(II) (NSC-119875) in advanced adenocarcinoma of the ovary. Cancer Treatment Reports 60, 55-60.

Winter, M.B., La Greca, F., Arastu-Kapur, S., Caiazza, F., Cimermancic, P., Buchholz, T.J., Anderl, J.L., Ravalin, M., Bohn, M.F., Sali, A., O'Donoghue, A.J., Craik, C.S., 2017. Immunoproteasome functions explained by divergence in cleavage specificity and regulation. eLife 6, e27364.

Wójcik, C., Rowicka, M., Kudlicki, A., Nowis, D., McConnell, E., Kujawa, M., DeMartino, G.N., 2006. Valosin-containing Protein (p97) Is a Regulator of Endoplasmic Reticulum Stress and of the Degradation of N-End Rule and Ubiquitin-Fusion Degradation Pathway Substrates in Mammalian Cells. Molecular Biology of the Cell 17, 4606-4618.

Yamaguchi, H., Wang, H.G., 2004. CHOP is involved in endoplasmic reticulum stress-induced apoptosis by enhancing DR5 expression in human carcinoma cells. The Journal of Biological Chemistry 279, 45495-45502.

Yamamoto, S., Tomita, Y., Hoshida, Y., Toyosawa, S., Inohara, H., Kishino, M., Kogo, M., Nakazawa, M., Murakami, S., Iizuka, N., Kidogami, S., Monden, M., Kubo, T., Ijuhin, N., Aozasa, K., 2004. Expression level of valosin-containing protein (VCP) as a prognostic marker for gingival squamous cell carcinoma. Annals of Oncology 15, 1432-1438.

Yamamoto, S., Tomita, Y., Nakamori, S., Hoshida, Y., Nagano, H., Dono, K., Umeshita, K., Sakon, M., Monden, M., Aozasa, K., 2003. Elevated expression of valosin-containing protein (p97) in hepatocellular carcinoma is correlated with increased incidence of tumor recurrence. Journal of Clinical Oncology 21, 447-452.

Yamanaka, K., Sasagawa, Y., Ogura, T., 2012. Recent advances in p97/VCP/Cdc48 cellular functions. Biochimica et Biophysica Acta 1823, 130-137.

Ye, Y., Meyer, H.H., Rapoport, T.A., 2001. The AAA ATPase Cdc48/p97 and its partners transport proteins from the ER into the cytosol. Nature 414, 652.

Yi, P., Higa, A., Taouji, S., Bexiga, M.G., Marza, E., Arma, D., Castain, C., Le Bail, B., Simpson, J.C., Rosenbaum, J., Balabaud, C., Bioulac-Sage, P., Blanc, J.F., Chevet, E., 2012. Sorafenib-mediated targeting of the AAA(+) ATPase p97/VCP leads to disruption of the secretory pathway, endoplasmic reticulum stress, and hepatocellular cancer cell death. Molecular Cancer Therapeutics 11, 2610-2620.

Young, R.C., Von Hoff, D.D., Gormley, P., Makuch, R., Cassidy, J., Howser, D., Bull, J.M., 1979. cis-Dichlorodiammineplatinum(II) for the treatment of advanced ovarian cancer. Cancer Treatment Reports 63, 1539-1544.

Zagouri, F., Bournakis, E., Koutsoukos, K., Papadimitriou, C.A., 2012. Heat Shock Protein 90 (Hsp90) Expression and Breast Cancer. Pharmaceuticals 5, 1008-1020.

Zarogoulidis, P., Lampaki, S., Turner, J.F., Huang, H., Kakolyris, S., Syrigos, K., Zarogoulidis, K., 2014. mTOR pathway: A current, up-to-date mini-review (Review). Oncology Letters 8, 2367-2370.

Zhang, L., Hapon, M.B., Goyeneche, A.A., Srinivasan, R., Gamarra-Luques, C.D., Callegari, E.A., Drappeau, D.D., Terpstra, E.J., Pan, B., Knapp, J.R., Chien, J., Wang, X., Eyster, K.M., Telleria, C.M., 2016. Mifepristone increases mRNA translation rate, triggers the unfolded protein response, increases autophagic flux, and kills ovarian cancer cells in combination with proteasome or lysosome inhibitors. Molecular Oncology 10, 1099-1117.

Zhang, S.H., Liu, J., Kobayashi, R., Tonks, N.K., 1999. Identification of the cell cycle regulator VCP (p97/CDC48) as a substrate of the band 4.1-related protein-tyrosine phosphatase PTPH1. The Journal of Biological Chemistry 274, 17806-17812.

Zhang, X., Cheng, L., Minn, K., Madan, R., Godwin, A.K., Shridhar, V., Chien, J., 2014. Targeting of mutant p53-induced FoxM1 with thiostrepton induces cytotoxicity and enhances carboplatin sensitivity in cancer cells. Oncotarget 5, 11365-11380.

Zhang, X., Shaw, A., Bates, P.A., Newman, R.H., Gowen, B., Orlova, E., Gorman, M.A., Kondo, H., Dokurno, P., Lally, J., Leonard, G., Meyer, H., van Heel, M., Freemont, P.S., 2000. Structure of the AAA ATPase p97. Molecular Cell 6, 1473-1484.

Zhou, H.-Y., Huang, S.-L., 2012. Current development of the second generation of mTOR inhibitors as anticancer agents. Chinese Journal of Cancer 31, 8-18.

Zhou, H.J., Wang, J., Yao, B., Wong, S., Djakovic, S., Kumar, B., Rice, J., Valle, E., Soriano, F., Menon, M.K., Madriaga, A., Kiss von Soly, S., Kumar, A., Parlati, F., Yakes, F.M., Shawver, L., Le Moigne, R., Anderson, D.J., Rolfe, M., Wustrow, D., 2015. Discovery of a First-in-Class, Potent, Selective, and Orally Bioavailable Inhibitor of the p97 AAA ATPase (CB-5083). Journal of Medicinal Chemistry 58, 9480-9497.